DESIGN AND ANALYSIS OF A DUAL AXIS, ARTICULATED, ANKLE-FOOT ORTHOSIS

by

ELIZABETH L LAWRENCE

A dissertation submitted to the Graduate Faculty in Engineering in partial fulfillment of the requirements for the degree of Doctor of Philosophy, The City University of New York

2004

INFORMATION TO USERS

The quality of this reproduction is dependent upon the quality of the copy submitted. Broken or indistinct print, colored or poor quality illustrations and photographs, print bleed-through, substandard margins, and improper alignment can adversely affect reproduction.

In the unlikely event that the author did not send a complete manuscript and there are missing pages, these will be noted. Also, if unauthorized copyright material had to be removed, a note will indicate the deletion.

ProQuest Information and Learning Company
300 North Zeeb Road
P.O. Box 1346
Ann Arbor, MI 48106-1346

This manuscript has been read and accepted for the Graduate Faculty in Engineering in satisfaction of the dissertation requirement for the degree of Doctor of Philosophy.

April 29, 2004
Date

Glenn L. Houston
Chair of Examining Committee

April 29, 2004
Date

Mumtaz K. Kassir
Executive Officer

Professor Weinbaum

Professor Ganatos

Professor Fritton

Professor Delale
Supervisory Committee

THE CITY UNIVERSITY OF NEW YORK

ABSTRACT

DESIGN AND ANALYSIS OF A DUAL AXIS,

ARTICULATED, ANKLE-FOOT ORTHOSIS

by

Elizabeth L Lawrence

Advisor: Dr. Vern Houston

The prescription of an ankle-foot orthosis (AFO) often entails a time-consuming, labor intensive, trial and error, design, fabrication, and fitting process before a patient is provided with an adequately comfortable and acceptably functional orthosis. Many different types of AFO's have been developed, however few of them take into consideration the fact that the ankle and subtalar joints of the foot rotate about separate axes. Thus, patients usually must endure the effects of limited degree of freedom orthoses with misaligned axes of rotation. This causes unbalanced forces and moments on the patients' anatomical joint axes, and often produces discomfort and pain because of motion of the orthosis on the leg.

For this project, a **JOINT AXIS DIRECTION AND LOCATION** method of determining the effective orientations and locations of the ankle and subtalar axes was developed using motion measurements acquired with a five CCD video camera MacReflex Qualisys Motion Analysis System, data from which was analyzed with custom MATLAB programs, which were written as part of the thesis work. The joint

axes were then projected onto scans of the foot and lower leg. The intersections of the calculated axes with the scans were determined and used to design a dual axis ankle foot orthosis (AFO), which allowed controlled motion about the ankle and subtalar joints. A prototype dual axis orthosis was then fabricated, and a series of comparative gait trials was performed without an orthosis, with a conventional plastic, nonarticulated, posterior leaf spring AFO, and a single degree of freedom, articulated AFO.

The tests showed that the dual axis AFO allowed gait to proceed naturally, without imposition of large, extraneous stresses and moments, as had been incurred with the other orthoses.

ACKNOWLEDGEMENTS

I would like to thank my mentor, Dr Vern Houston for his expert guidance, over the past few years. His willingness and ability to impart knowledge will always be appreciated. I would also like to thank Professor Weinbaum for inviting me to join the PhD program here at CCNY several years ago. In addition, thanks to the faculty members, Professor Weinbaum, Professor Sadegh, Professor Ganatos, Professor Fritton, and Professor Delale, who all contributed immensely as members of the supervisory committee.

I would like to thank my family for their steadfast and unwavering support throughout the experience. Special thanks to Mr Kevin Chen in the Physical Therapy Laboratory at the NYU School of Medicine. I am also grateful to Mr John Milani for use of the Prosthetics and Orthostics fabrication facilites at the NYUSM/VA NYHHCS. Additionally, the support offered by Mr Aaron Beattie, Dr. Gangming Luo, and Carl Mason in the NYUSM/VA NYHHCS Research Department was greatly appreciated.

TABLE OF CONTENTS

LIST OF TABLES

LIST OF ILLUSTRATIONS

I. INTRODUCTION

1.1). *What is an orthosis?*

As defined by the Merriam Webster's Medical Dictionary,[52] an ***orthosis*** is 'a support or brace for weak or ineffective joints or muscles'. The term 'orthosis' is derived from the Greek words 'orth' or 'orthos' which indicates its straightening or corrective goal, and 'osis' which indicates a process or action. Thus, literally, use of an orthosis indicates that corrective action for the purpose of support and straightening has been taken. In addition to possible corrective use, orthoses are commonly used to control, supplement, and/or limit movement, and maintain prescribed alignment of body segments.

Orthoses used as corrective and supportive splints first appeared in prehistoric times. With the progression of time, orthoses were further developed as a by-product of war. As an alternative use for armor, it was described as a 'steel support for the twisted body'. With the use of metal, the importance of weight distribution became critical. Orthotics has thus evolved from the production and use of simple supporting or immobilizing splints to the design, manufacture, and fitting of a wide range of simple to complex, sophisticated, computer controlled devices in use today. Orthoses used to support and/or control the movement of the ankle-foot complex are called ankle-foot orthoses (AFO's).

1.2). *Lower limb orthotics*

An ankle-foot orthosis (AFO) is designed with the goal of providing support, and/or controlling the alignment and/or rate and range of motion of the joints of the foot and ankle by the application of forces and counterforces. Wearers of AFO's generally have specific needs regarding function, comfort, and cosmesis. As far as cosmesis is concerned, it is a general requirement that the orthosis not be visually detracting, and that, in some cases, it should fit easily into a shoe. The orthotist is also required to ensure that the mechanical ankle joint is aligned with the anatomical ankle joint, and that the orthosis is as lightweight and as visually appealing as possible.[100] This is particularly problematic for plastic AFO's, as the effective ankle joint does not come close to the anatomical joint. Moreover, in order to make the patients' gait as stable and efficient as possible, the orthosis must allow the wearer to achieve a gait, which is as near normal as possible. Orthoses also serve to transfer forces from sensitive stress intolerant regions to more stress tolerant regions of the body, reducing friction and shear on sensitive areas, modifying weight transfer patterns, correcting flexible deformities, accommodating fixed deformities, and limiting motion of painful, inflamed, or unstable joints.[7]

1.3). *The human foot*

The human foot is a complex mechanism, both in terms of structure and function, Figure 1.1.[95] It is strong enough to bear several times the weight of the entire body, and yet exhibits the fluid movements necessary for walking, running, and other dynamic activities, with minimal strength and energy requirements.

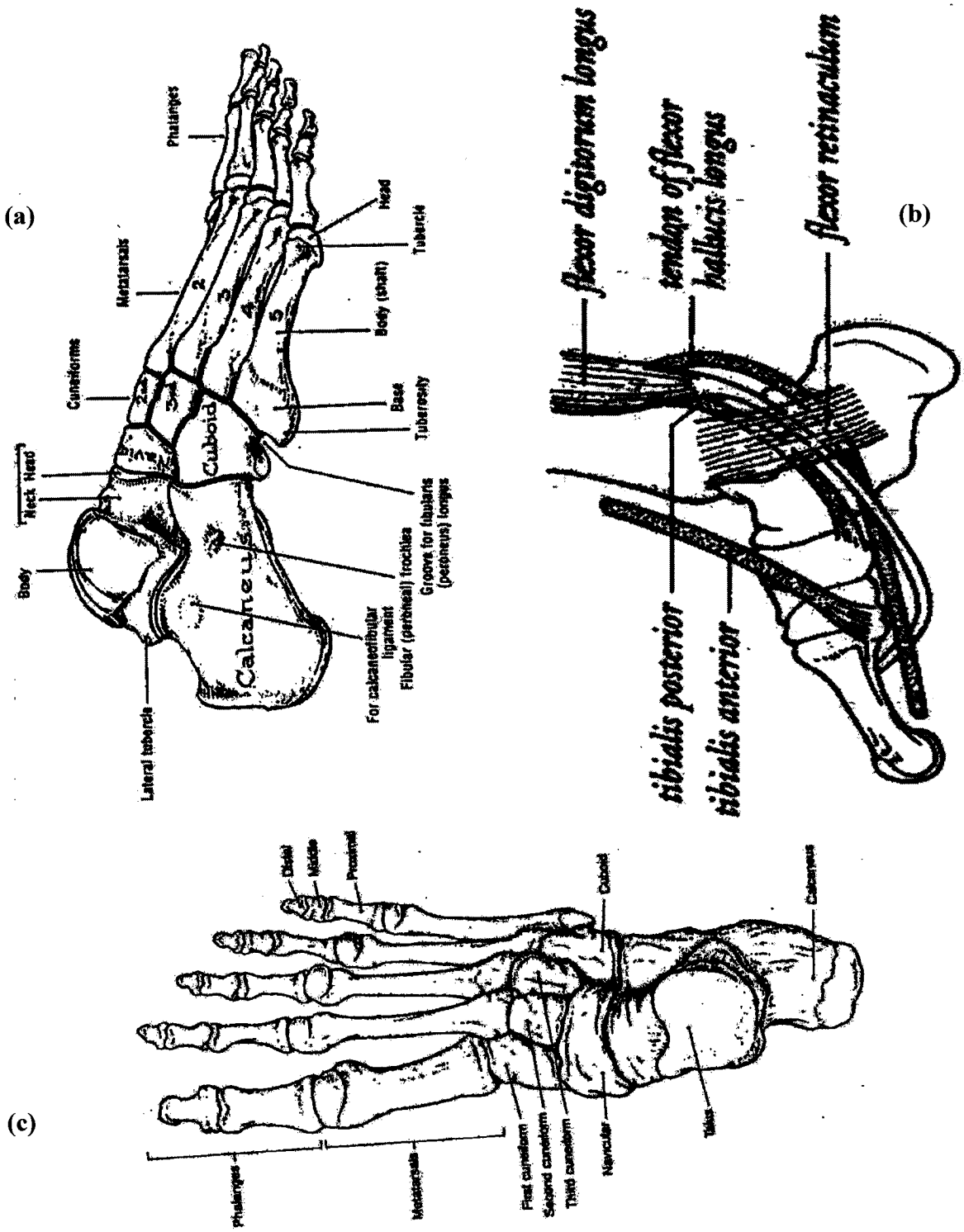

Figure 1.1 *The human foot*[95] *a) lateral; b) medial; c) transverse* views*

***Median plane is the plane dividing the body into symmetrical right and left portions**
***Sagittal plane is a plane parallel to the median plane**
***Coronal (frontal) plane is a vertical plane perpendicular to the median plane, dividing the body into anterior and posterior parts**
***Transverse (horizontal) plane divides the body into upper and lower parts**

The foot is commonly considered to consist of three principal compartments (regions) – the rearfoot, midfoot, and forefoot. The ***rearfoot*** is composed of the talus and calcaneus and is responsible for converting the torque of the lower leg into sagittal, frontal, and anteroposterior movements. The talus and calcaneus are the largest and most posterior of the tarsal bones. They articulate with each other, with the anterior tarsals (navicular, cuneiforms, and cuboid), and with the tibia and fibula. The ***talus*** is made up of a more posterior body and an anterior head connected by a neck. The body of the talus has three facets, which allow articulation with the fibula and tibia, while the head articulates anteriorly with the navicular and inferiorly with the calcaneus. The talus itself is not connected to any muscles, but moves as a result of the movement of the surrounding bones, and is secured to them by ligaments and the retinacular sheath. The ***calcaneus*** is the large 'heel bone'. It has a posterior tuberosity, which serves as the 'point of first contact' with the ground during walking. It constitutes the 'heel lever' arm of the foot, and articulates supereriorly with the talus and anteriorly with the talus and cuboid.

The ***midfoot*** is composed of the cuneiforms, navicular, and cuboid bones. It transmits movement from the rearfoot to the forefoot. The ***navicular*** is concave on its proximal end where it articulates with the talus and has three facets for articulation with the cuneiforms on the distal end. The ***cuboid*** articulates with the calcaneus, navicular, lateral cuneiform, and metatarsals IV and V. The ***cuneiforms*** are three small bones that articulate proximally with the navicular and distally with metatarsals I-III, and help to make up the transverse arch of the foot.

The ***forefoot*** is made up of the metatarsals and phalanges, and adapts to the ground as the surface changes. Each metatarsal has three distal regions - the **proximal**

head, which is approximately quadrangular with facets for articulation with the tarsals and other metatarsals. The body or shaft is long **body** with a roughly triangular cross-section. The**distal head** is round and articulates with the proximal phalanx. Each toe has three phalanges – proximal, middle, and distal – except the hallux (big toe), which has two. The distal phalanx supports the toenail superiorly.

Transversely, the foot may be thought of as being composed of two parts or beams – the ***lateral*** foot and the ***medial*** foot, which are linked to the hind foot. The lateral beam consists of the calcaneus, cuboid, metatarsals, and phalanges IV-V (sometimes III-V depending on the function of the patient). The beams are arched and are responsible for receiving and supporting the body's weight during standing, walking and running. The medial beam is composed of the talus, navicular, cuneiforms, and metatarsals and phalanges I-III. It creates the medial arch and is essential for propulsion and derotation of the lower limb during walking and running.

The momentum and active energy of the body is transferred through the legs to the feet via the tibia and fibula, the distal ends of which form the medial and lateral **malleoli**. The inner aspects of the malleoli and the distal end of the tibia form a mortise, which embraces the talus*. The tibia and fibula are connected by an interosseous membrane, along their length, for added structural integrity.

***a mortise is a cavity prepared to receive a similarly shaped projection of another piece to hold the two together[57]**

1.4). ***The joints of the ankle-foot complex***

Two of the joints crucial to the function of the foot are the ankle and subtalar joints. Although the motion of the ***ankle*** is quite complex, it functions reasonably like a hinge joint, providing dorsiflexion and plantar flexion of the foot. The ankle joint is formed by the articulation of the talus with the tibia and fibula.[53] The ***talar body*** has three facets for enhanced fit and articulation in the mortise formed by the tibia and fibula. The lateral malleolus of the fibula extends obliquely and more distally downward than the medial malleolus, thus providing a snug fit. The superior talus is wider anteriorly than posteriorly. Therefore, its fit into the mortise during dorsiflexion is snugger than in plantar flexion, Figure 1.2.

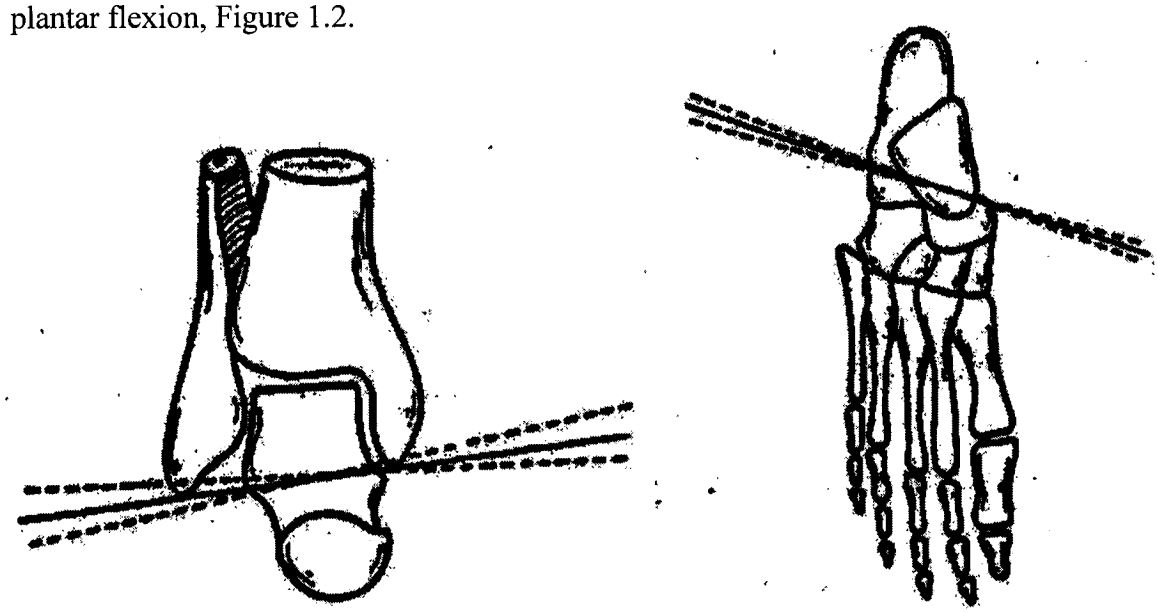

(a) **(b)**

Figure 1.2 *(a) Coronal* and (b) transverse* views of the foot showing the ankle joint axis*[53]

***Median plane is the plane dividing the body into symmetrical right and left portions**
***Sagittal plane is a plane parallel to the median plane**
***Coronal (frontal) plane is a vertical plane perpendicular to the median plane, dividing the body into anterior and posterior parts**
***Transverse (horizontal) plane divides the body into upper and lower part**

It has been postulated that the shape of the tibiotalar mortise is changed by the action of four muscles, which tend to pull down the fibula and tibia. These are the peroneous longus, peroneous brevis, extensor hallucis longus, and the tibialis posterior. Additionally, the mortise is tightened by the extensor hallucis longus and tibialis posterior, which tend to pull medially. As the fibula is lowered, the distal tibiofibular ligaments become taut, furthering tightening the mortise.[10]

Lundberg, et al.,[46], carried out an experiment to investigate the nature of the ankle axis using roentgen stereophotogrammetry, by implanting the fibula, calcaneus, navicular, medial cuneiform and first metatarsal bones with three beads of tantalum each. The beads measured 0.8 mm in diameter. Exposures were then made from 30° of plantar flexion to 30° of dorsiflexion, from 20° of pronation to 20° of supination and from 20° of medial rotation to 10° of lateral rotation of the leg, all in increments of 10°. The joint axes were then projected onto the coronal, transverse, and sagittal planes, with the angle of inclination determined from kinematic calculations, Figure 1.3.

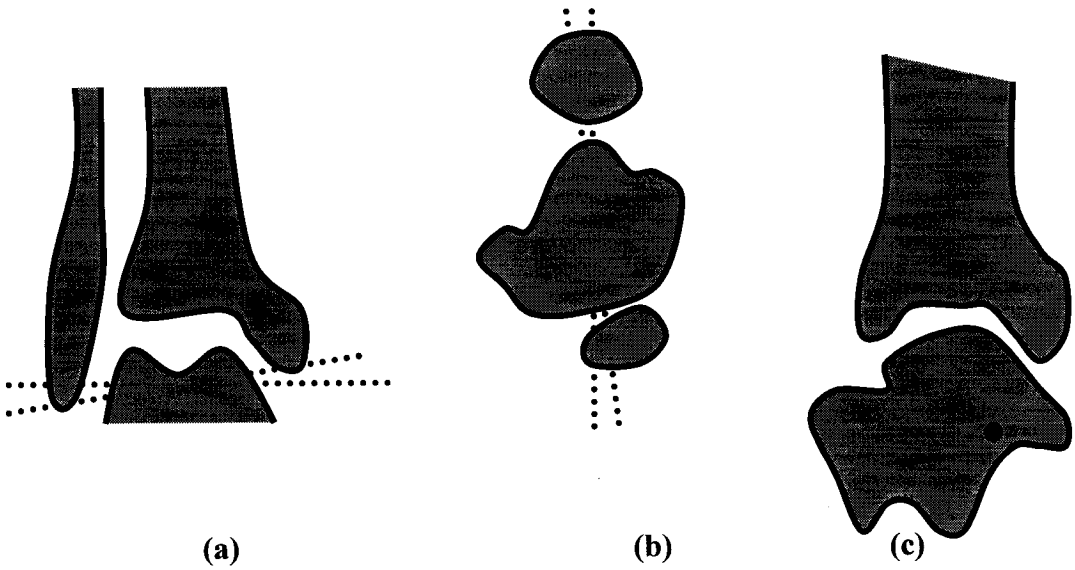

Figure 1.3 *Ankle joint axis projected onto the (a) coronal; (b) transverse; (c) sagittal planes*

It was determined that when the ankle moved from 30° of dorsiflexion to 30° of plantar flexion, the ankle axis rotated from a downward and medial position (or a horizontal position) to a downward and lateral inclination. When the angle changed from 10° to 30° of dorsiflexion, the axis appeared to be located between the tips of the malleoli. Supination and pronation resulted in an inclination of up to 90° in the frontal plane, while projection onto the horizontal plane showed an axis that went from one malleoli to the other. Medial rotation between 0° and 20°, caused inclinations of 1° to 88° in the horizontal plane. Superimposing all of the rotations in all the planes on each other, it was found that there was what appeared to be a central point in the trochlea at which all the axes intersected.

The joints distal to the talus have been shown to play a role in rotation about the transverse axis, when the ankle is plantar flexed or dorsiflexed. According to Lundberg, et al.,[47] although the contribution of the joints of the arch to dorsiflexion is small, it is observed that all of the joints of the arch rotate about axes that also contribute, to some degree, to dorsiflexion and plantar flexion. It was also shown that plantar flexion results in some pronation of the ankle and the joints around the medial cuneiform, in addition to internal rotation of the ankle and external rotation of the talonavicular joint. All of the joints of the foot that are distal to the ankle played a part in pronation and supination, with the talonavicular joint being the largest contributor.[48] Internal rotation of the leg was also observed to be transformed into pronation and supination of the foot as a result of movement of the ankle joint and the first tarsometatarsal joint in addition to the action of the subtalar joint, with large amounts of rotation taking place in the talonavicular joint in external rotation.[49]

The ***subtalar joint*** is principally created by the articulation of the calcaneus with the talus. The distal convex surface of the talus fits against the concave surface of the calcaneus anteriorly, while posteriorly, the opposite is true. It allows dorsiflexion, plantar flexion, adduction, and abduction. The subtalar joint rotates about an imaginary line, the ***axis of Henke***, which enters the posterolateral tuberosity of the calcaneus and runs anterosuperomedially, exiting through the medial neck of talus.[53] It is inclined at about 42° from the horizontal and 16° from the long axis of the transverse plane, Figure 1.4. Although the nature of the articulation between the talus and the calcaneus has not been defined clearly, it is generally thought that the rotation is screw-like.

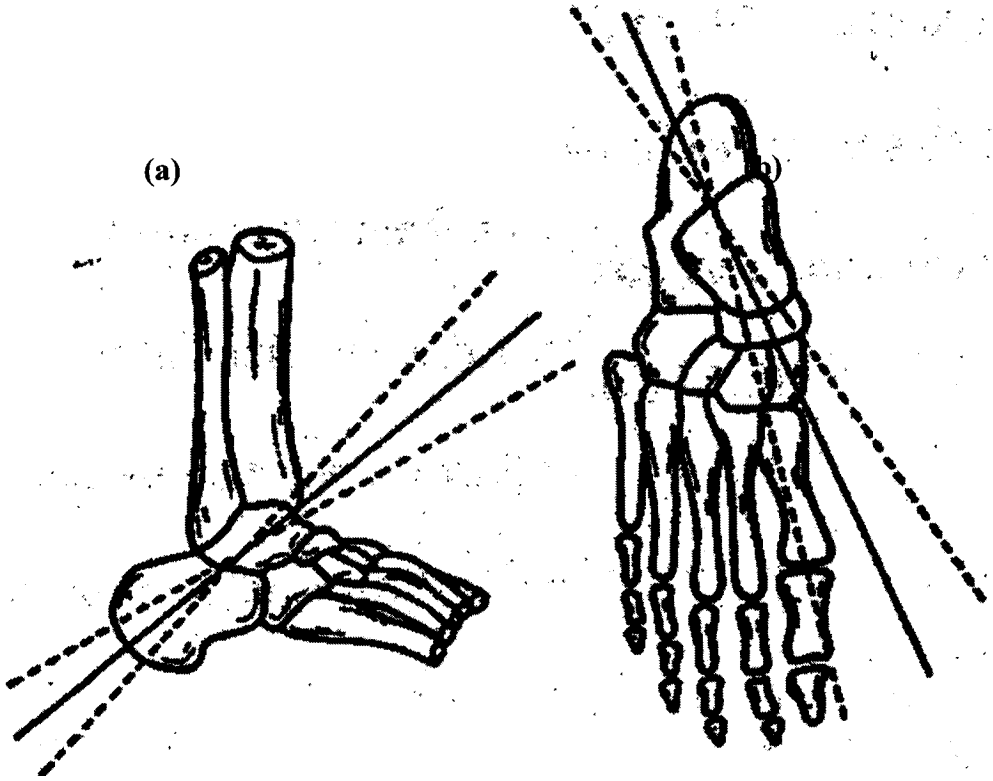

Figure 1.4 *(a) Coronal and (b) transverse views of the foot showing the subtalar joint axis*[53]

The orientation of the subtalar joint actually varies from person to person. The more the axis is aligned with the long axis of the foot, the more it contributes to eversion and inversion. Generally, the range of motion of the subtalar joint varies from 5° to 50° of inversion and 5° to 26° of eversion. The more the subtalar joint is aligned with the long axis of the leg, the more it contributes to abduction and adduction.[63]

The greatest contact area of the talus with the surrounding bones has been found to exist in the posterior facet of the subtalar joint, followed by the talonavicular joint, the anteromedial facet of the subtalar joint, and finally the talocalcaneonavicular ligament articulation.[72]

According to Inman et al.,[27] the average ankle joint, on the medial side, was found to pass 5±3 mm distal to the distal tip of the medial malleollus, with a range of 0 to 11 mm. On the lateral side, it was found to pass 3±2 mm distal to the distal tip of the lateral malleolus, with a range of 0 to 12 mm. Also on the lateral side, it was also found to pass 8±5 mm anterior to the distal tip of the lateral malleolus. That is, the ankle axis lies obliquely in the coronal plane, and runs a little distal to each of the malleoli. Thus its location can be found by palpation of the malleoli (under the tips) or by viewing a anteroposterior x-ray of the malleoli. Inman et al.,[27] also state that, on average, the projection of the subtalar joint onto a vertical plane is 42°±9°, with a deviation from the midline of the foot of 23°±11°.

The subtalar joint center may also be located using the methods described by Sell.[78] With these methods, the position and motion of the subtalar joint may be estimated by measuring the frontal position of the calcaneus relative to the tibia with a goniometer,

thereby determining the degree of inversion or eversion of the calcaneus. It may also be determined by measuring the weight-bearing height of the navicular tuberosity.

To accomplish the first of these tasks, having ensured that the subjects have consistent foot position during walking, a dynamic gait template is made by having the subjects dip their feet in oil and walk on a strip of butcher paper. The middle four footfalls are outlined and a straight line constructed connecting the two right heels and then the two left heels on the medial side. From this template, the base of gait and the toe-out position are ascertained. This data (base of gait and toe-out position) may also be determined by using the Gait-Rite System, described in chapter 4.

To find the orientation of the subtalar joint using the calcaneal position technique, the subjects are asked to stand on the edge of a block, with the front sections of their feet hanging over the edge. The locations of both calcanei are then detected by hand and a dot used to mark the position of their superior and inferior border centers. The neutral position of the joint is found by rotating the lower leg internally and externally, while examining the anteroposterior and anterolateral sides of the tali manually until the talar heads are felt equally, that is until the medial head of the talus is no longer prominent when moving the foot from an inverted to an everted position. The calcaneal position is recorded by using an inclinometer held parallel to the two dots on the calcaneus. The difference between the angle of inclination in the resting position and the neutral position is then determined to be the degree of calcaneal motion.

The navicular height technique entails pinpointing the most prominent area of the navicular tuberosity and marking it with a dot. Their subtalar joints are then positioned in the neutral position once again and using a rectangular card positioned vertically on the

medial side of the foot, slightly in front of the navicular, the distance between the top surface of the table and the mark previously made is marked on the card. This is repeated with the patient in a relaxed position and the difference recorded as the navicular height.

Also to be considered in analyzing the biomechanics of the foot, are the transverse tarsal, cuneiform, tarsometatarsal joints, and the metatarsophalangeal and interphalangeal joints. The transverse tarsal joint is the joint between the posterior and anterior tarsals and is made up of the medial talocalcaneonavicular joint (a convex surface of the talar head fitting against a convex surface of the navicular) and the lateral calcaneocuboid joint (an S-shaped surface of the calcaneus, fitting against a corresponding surface of the cuboid). The transverse tarsal joint is crucial in inversion and eversion, and in adjustment to uneven surfaces. It is reinforced by the talonavicular and calcaneocuboidal ligaments. Its motion in supination has been described as resulting from the navicular gliding medially and inferiorly on the head of the talus, while the cuboid follows the navicular through medial and inferior motion on the talus. The reverse is true for pronation. A longitudinal axis that allows eversion, inversion, adduction, and abduction has been identified in addition to an oblique axis that allows dorsiflexion and plantar flexion. The motion of this joint contributes to the motion of the ankle and subtalar joint and may even compensate for them when an injury or pathomechanical disorder is sustained.[63] The normal transverse tarsal joint has been observed to have a range of motion from 0° to 20° in inversion and 0° to 10° in eversion. It has also been noted that as the subtalar joint pronates, the transverse tarsal joint follows along resulting in flattening of the medial longitudinal arch, while supination of both of these joints results in elevation of the arch.

The cuneiforms articulate with the cuboid, navicular, and each other and are connected by dorsal and plantar ligaments and interosseous ligaments. The tarsometatarsal joints are described as gliding joints between the cuneiforms, cuboid and the bases of the metatarsals, although they have also been compared to rotatory joints. The articulation between the base of the first metatarsal and the medial cuneiform is about an axis that has an anterior, lateral, and downward orientation and almost lies in the transverse plane between the frontal and sagittal planes. It combines dorsiflexion and inversion/plantar flexion and eversion with very small amounts of abduction and adduction, resulting in uniaxial pronation and supination. The second metatarsal and middle cuneiform rotate about their own axis, as do the third metatarsal and lateral cuneiform, while the fourth metatarsal rotates about its own axis. The fifth metatarsal rotates about an axis that allows pronation and supination to occur between the metatarsal and cuboid.

The metatarsophalangeal joints are biaxial with flexion and extension occurring in the sagittal plane, and adduction and abduction in the transverse planes.[63] The range of motion of the big toe in extension at the metatarsophalangeal joint has been recorded as varying between 0° and 70° while the other four toes exhibit a range of extension varying between 0° and 90°. A range of flexion of 0° to 50° has been recorded for all of the toes. The interphalangeal joints, on the other hand, are uniaxial and allow flexion and extension in the sagittal plane. They have been observed to have a range of flexion of 0° to 35° and a range of extension of 0° to 60°.

1.5). ***Range of motion of the normal foot***

Medical-biomechanical diagnostics as well as engineering modeling, analysis, and design involving the ankle-foot complex requires that the range of motion of the ankle and subtalar joints be determined. Investigators have shown that the normal ankle joint has an effective range of dorsiflexion of at least 10°. Generally, the range of dorsiflexion achievable lies between 10° and 23°. Similarly, effective plantar flexion of the ankle joint lies between 23° and 48°. With the use of a three-bar, three-dimensional model of the ankle-joint complex, van den Bogert, et al.,[8] showed that the effective subtalar joint was inclined at 37.4° ± 2.7° from the horizontal plane, and had a medial deviation of 18° ± 16.2°. Van den Bogert also demonstrated that the lateral side of the ankle joint axis was oriented posteriorly at 6.8° ± 8.1° and was inclined downward at 7° ± 5.4°. Bahr, et al., [4] found that from 10° to 20° of plantar flexion, all motion occurred in the tibiotalar joint, while the ratio of subtalar motion to tibiotalar motion during supination was 3:1 and 4:1 during internal-external rotation.

The work of Le Damany, et al.,[17] showed an average value of 22°± 20° of tibial rotation about the long axis of the tibia, facilitated by the raising and lowering of the arch of the foot, with a range of 0° to 56° of external rotation. Von Lanz, et al.,[36] reported an average value of 23° of external tibial rotation, with a range of 7° to 48°, while Hutter, et al.,[26] reported an average value of 21° ± 10° with a range of 4° to 40°. Experiments by Hinterman, et al., [24] showed that 10° of dorsiflexion resulted in 0.1° of eversion and 2.1° of internal rotation of the tibia, whereas 10° of plantar flexion resulted in 1.6° of inversion and 1.3° of external rotation of the tibia. MuCullough, et al.,[51] reported external and internal rotation of the talus relative to the tibia to have a maximum value of

7.5° ± 1.5° in both directions, while Lundberg, et al.,[49] reported values of 8.9° of external rotation and 1.4° of internal rotation in dorsiflexion, while plantar flexion resulted in 0.6° of external rotation.

The position of the ankle axis in the transverse plane in relation to the midline of the foot was found to be 84° ± 7° with a range of 69° to 99°, by Inman, et al.[27] Inman, et al., also studied the orientation of the ankle axis in the frontal plane and found it to be 93.3° ± 3.2° to the horizontal, with a range of 88° to 100°. Lundberg, et al.,[46] determined that the ankle moved from 30° of dorsiflexion to 30° of plantar flexion, as its axis rotated from a downward and medial or horizontal position to a downward and lateral inclination. When the angle changed from 10° to 30° of dorsiflexion, the axis appeared to be located between the tips of the malleoli. Supination and pronation resulted in an inclination of up to 90° in the frontal plane, while projection onto the horizontal plane showed an axis that went from one malleoli to the other. Medial rotation of the ankle joint between 0° and 20° caused inclinations of 1° to 88° in the horizontal plane. Murray, et al., found that the maximum total amount of total ankle motion in normal men was about 10° in dorsiflexion and 20° in plantar flexion. Winter, et al.,[96] reported a mean range of ankle motion of 35°, while Lamoreaux, et al.,[35] reported a total ankle motion of 30°. Lundberg, et al., also found that the orientation of the ankle joint varied from – 12° in extreme plantar flexion to 22.5° at maximum dorsiflexion. Bagget, et al.,[3] determined that the range of motion of the normal nonweightbearing ankle joint in dorsiflexion was 0° through 16.5°, with an average of 8.25° ± 4.13°, and for the weightbearing ankle was 7.1° through 34.7°, with an average of 20.90° ± 6.79°. Marsh, et al.,[50] concluded that the optimum length of the tibialis anterior corresponded to about 10° of dorsiflexion, and

maximum voluntary torque developed at about 10° of plantar flexion and decreased as the ankle dorsiflexed past 5°. In investigating the subtalar joint, Inman, et al., reported an average of 42° ± 9° in the sagittal plane, and an average of 23° ± 11° in the horizontal plane, Figure 1.5.[27]

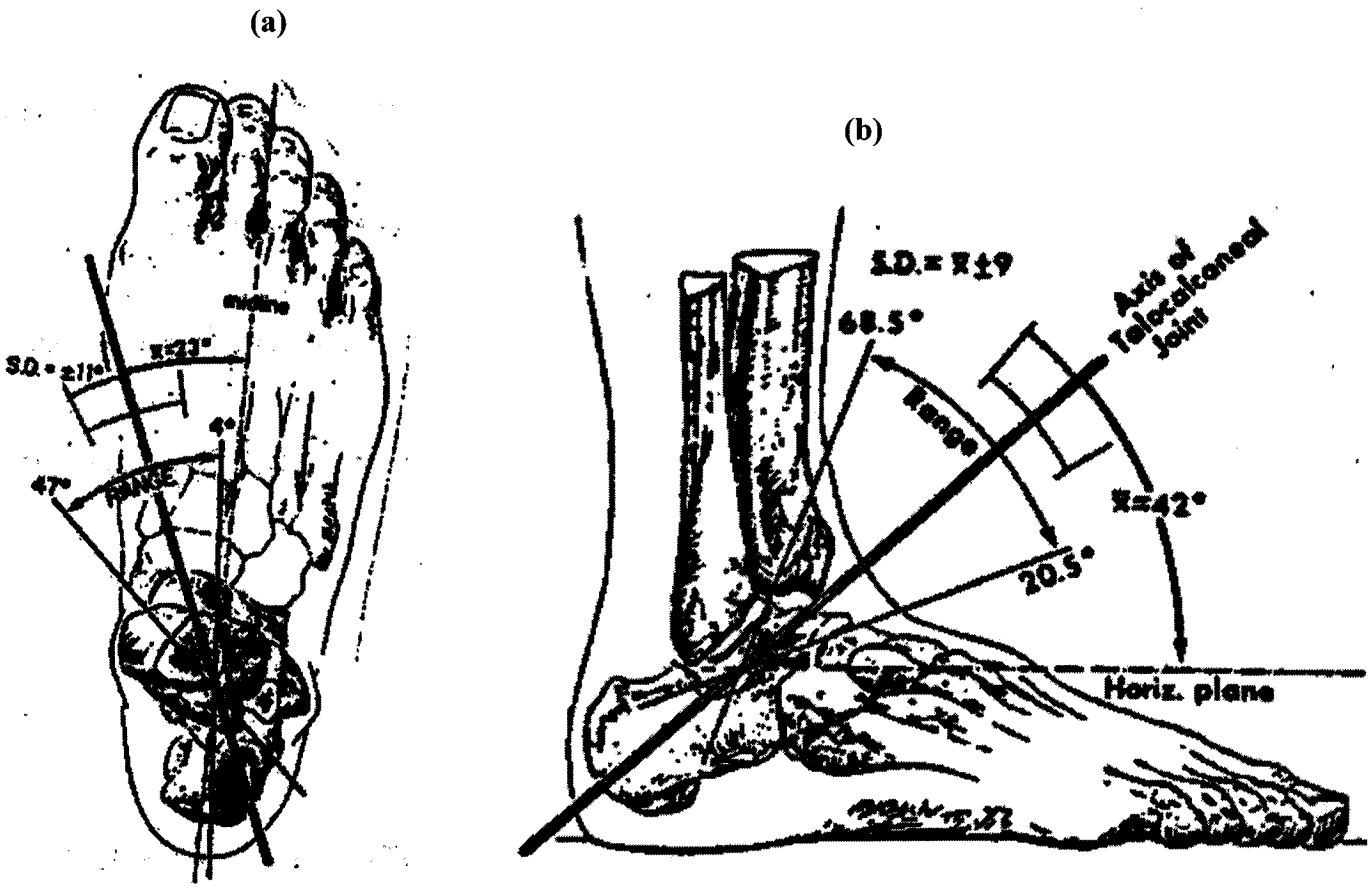

Figure 1.5 *The orientation of the subtalar joint (from Inman[27]); a) transverse; b) lateral views*

Wang, et al.,[94] found that the average excursion in the sagittal plane of the calcaneus was 58.6° ± 5.4° while that of the talus was 51.5° ± 4.8°, and that of the navicular was 69.2° ± 6.4° as the ankle went through its entire range. Roaas, et al.,[74] determined the mean range of motion of the normal foot to be 15.3° in dorsiflexion, 39.7° in plantar flexion, 27.6° in valgus, and 27.7° in varus. The American Academy[2] of Orthopaedic Surgeons reported that the range of motion was 18° in dorsiflexion, 48° in plantar flexion, 18° (forefoot) + 5° (hindfoot) in eversion, and 33° (forefoot) + 5° (hindfoot) in varus. Boone and Azen[9] gave values of 12.2° in dorsiflexion, 54.3° in plantar flexion, 19.2° in valgus, and 36.2° in varus. Allinger, et al.,[1] carried out in vivo experiments that found the total range of motion of abduction to adduction to be 21.4° in the young and 22.2° in the elderly, while eversion was found to have a maximum of 92.2° from maximum dorsiflexion to maximum plantar flexion. The passive range of motion was also documented as 5° to 50° in inversion and 5° to 26° in eversion.

Tables 1.1 – 1.5 below summarize some of the work done thus far to determine the orientation and range of these joints. In vitro results are presented separately from in vivo results, as it is expected that the range of motion and orientation of the axis of rotation of the joints would be different for live subjects and cadaveric specimens. Also to be taken into consideration, is the fact that differences in experimental setups may also account for differences in results. It must also be observed that some of the cadavers may have had conditions or diseases affecting their motility, which were unknown to the investigators.

It must also be noted that the information available on the location and orientation of the joint axes is too sparse and inadequate to allow physicians and therapists to

sufficiently prescribe orthoses, without a considerable amount of time spent on the fitting process. Aside from the time wasted, there are also the factors of discomfort, inconvenience to be considered. Therefore it is would be considerably helpful if there were some method to eliminate this period of fitting by trial and error.

Table 1.1. *Ankle Joint Biomechanical Studies – in vivo*

Ref. No.	Investigator(s)	Date of Study	No. of Subjects	Ankle Joint											
				Dorsiflexion (deg)				Plantarflexion (deg)				Axis Orientation (deg)			
				Average	Std. Dev.	Max	Min	Average	Std. Dev.	Max	Min	Average	Std. Dev.	Max	Min
2	AAOS*	1965		18				48							
1	Allinger et al.	1993	7	21.4	~	~	~								
			10	22.2	~	~	~								
3	Bagget et al.	1993	20	8.25 nonweightbearing	4.13	16.5	0								
				20.90 weightbearing	6.79	34.7	7.1								
8	Van den Bogert et al.	1994	14	~	~	~	~	~	~	~	~	6.8 (posteriorly, lateral side)	8.1	~	~
												7.0 (downward, lateral side)	5.4		
9	Boone et al.	1979	109	12.6	4.4	~	~	56.2	6.1	~	~	~	~	~	~
45	Lindsjo et al.	1985	317	33.6 (male, standing with weightbearing)	6.5	~	~	43.0	7.3	~	~	~	~	~	~
				31.4 (female, standing with weightbearing)	7.1			46.4	7.5						
60	Nigg et al.	1992		25.6	1.9										
74	Roaas et al.	1982	192	15.3	5.8	40	5	39.6	7.5	55	10	~	~	~	~
88	Stefanyshyn	1994		21.8	4,7										
98	Woodburn et al.	1991		25.7	6.7										

Table 1.2. *Ankle Joint Biomechanical Studies – in vitro*

Ref. No.	Investigator(s)	Date of Study	No. of Specimens	Ankle Joint											
				Dorsiflexion (deg)				Plantarflexion (deg)				Axis Orientation			
				Average	Std. Dev.	Max	Min	Average	Std. Dev.	Max	Min	Average	Std. Dev.	Max	Min
27	Inman et al.	1976	46									84 (between ankle axis and midline of foot)	7	99	69
			107									82.7 (between ankle axis and midline of tibia)	3.7	94	74
												11.3 (average angular difference between ankle axis and tibia plafond)	4.1	21	2
65	Parenteau et al	1998		-44°	10.9°				71.6°	5.7					

Table 1.3. *Subtalar Joint Biomechanical Studies – in vivo*

Ref No.	Investigator(s)	Date of Study	No. of Sub-jects	Subtalar Joint											
				Inversion (deg)				Eversion (deg)				Axis Orientation			
				Av	Std. Dev	Max	Min	Av	Std. Dev.	Max	Min	Av	Std. Dev.	Max	Min
2	AAOS	1969		33(fore foot) + 5 (hind foot)				18 (fore foot) + 5 (hind foot)							
8	Van den Bogert	1994	14									37.4 (inclination from horizontal plane) 18.0 (medial deviation)	2.7 16.2		
9	Boone et al.	1979	109	36.2 (fore foot)	4.2			19.2 (fore foot)	4.9						
74	Roaas et al.	1982	192	27.7	6.9	50	15	27.6	4.6	50	15				

Table 1.4. *Subtalar joint biomechanical studies – in vivo*

Ref No.	Investigator(s)	Date of Study	No. of Speci-mens	Subtalar Joint											
				Inversion (deg)				Eversion (deg)				Axis Orientation			
				Av	Std. Dev.	Max	Min	Av	Std. Dev.	Max	Min	Av	Std. Dev.	Max	Min
27	Inman et al.	1976	56									42 (as projected onto sagittal plane)	9	68	20
												23 (deviation from midline of foot in horizontal plane)	11	47	4

Table 1.5. *Tibial rotation biomechanical studies – in vitro*

Ref No.	Investigator(s)	Date of Study	No. of Specimens	Finding
24	Hinterman et al.	1995	14	10° of dorsiflexion resulted in 2.1° of internal rotation 10° of plantarflexion resulted in 1.3° of external rotation Axis location independent of load Different axes for dorsiflexion and plantarflexion
26	Hutter et al.	1949	40	Average external tibial rotation, 21°± 10° (-4° to 40° range)
17	Le Damany	1909	200	Average tibial rotation, 22°±20° (0° to 56° range)
51	McCullough et al.	1980	8	25° of rotation in unloaded state, with 1 kg load Linear decrease in range of rotation with increasing load
55	Michelsen et al.	1996	13	1.9°± 4.12° of internal rotation, at maximum plantarflexion 7.2°± 3.88° of external rotation, at maximum dorsiflexion
36	Von Lanz et al.	1938		Average external tibial rotation, 23° (7° to 48° range)

1.6). ***Stability of the foot***

The morphology of the foot can be envisioned as three arches, the ***medial***, ***transverse***, and ***lateral*** arches. An arch is a structure forming a curved, pointed, or flat upper edge of an open space that supports the weight above it. In the case of the foot, the arches support the weight of the body, however, the ends of the arches are forced apart, and the restraining forces are required in order to prevent the arches of the foot from falling flat. This induces tensile forces in the upper portion of the arch and compressive forces in the lower portion. The heel and heads of the metatarsals act as the ends of the arches and in this case the restricting force is provided by the plantar aponeurosis, which ties them together, Figure 1.6.

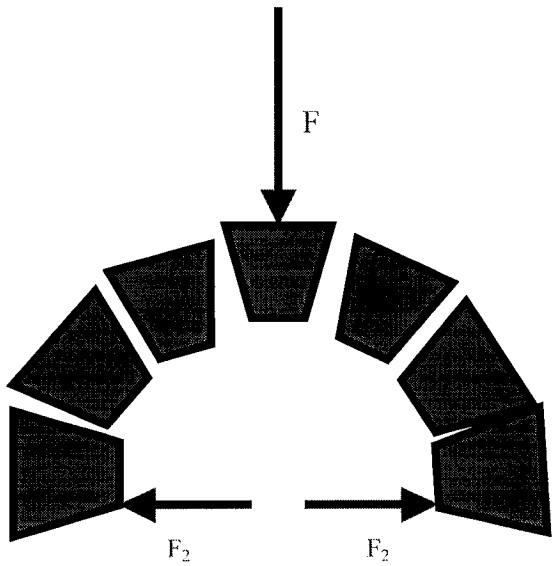

Figure 1.6 *Forces acting on an arch*[7]

The arches allow the foot to absorb shock, adapt to the walking surface, to be flexible, and to distribute the weight of the body. Their principle function is to rotate and derotate the body and leg during gait, which in turn allows for a longer step length

without excessive excursion of the body's center of gravity, thus conserving energy. The body's weight is mainly distributed amongst the posteroinferior tuberosity of the calcaneus, which bears the most weight during heel strike to late mid-stance phase, and the metatarsal heads which pick up an equal amount of load from heel rise to toe-off.

The ***medial*** arch is formed by five bones (calcaneus, talus, navicular, medial cuneiform, and metatarsal I), four ligaments (including the talocalaneal and calcaneonavicular) and four muscles (abductor hallucis, tibialis posterior, peroneus longus, and flexor hallucis longus). The flexor hallucis longus stretches the arch, supports the calcaneus, and supports the talus. The ***lateral*** arch is lower than the medial arch, and is covered by muscles underneath, thus allowing the lateral side of the foot to touch the ground. Therefore, the medial arch is involved in propulsion, while the lateral arch aids in weight-bearing. The lateral arch is formed by three bones (calcaneus, cuboid, and metatarsal V), three ligaments (short plantar, long plantar, and plantar aponeurosis), and two muscles (peroneus brevis and peroneus longus). The peroneus longus serves to support the calcaneus and the cuboid. The ***transverse*** arch is highest around the middle of the metatarsals and is higher on the medial side than on the lateral side. It is supported by the adductor hallucis, peroneus longus, tibialis posterior, and the interossei. These arches provide supporting mechanisms that allow each leg to bear the weight of half of the body. Problems may arise, however, if for example, the forces are too high, exceeding the structural integrity of the arch components as in the case of obese patients, or if the ligaments become too loose, or too tight, leading to pathomechanical conditions.

1.7). ***The gait cycle***

The gait cycle, Figure 1.7, has two major components – ***swing*** phase and ***stance*** phase.[7] Stance phase (60% of cycle) occurs when the limb is in contact with the ground, while the swing phase (40% of cycle) occurs when the limb is not in contact with the ground. Stance phase may be further subdivided into five events (1) ***heel contact*** (the instant the heel touches the ground); (2) ***foot-flat*** (initial contact of the foot with the floor); (3) ***mid-stance*** (when the greater trochanter is in vertical alignment with the vertical bisector of the foot, as viewed in the sagittal plane; (4) ***heel-off*** (when the heel rises from the floor); (5) ***toe-off*** (when the toe leaves the floor).

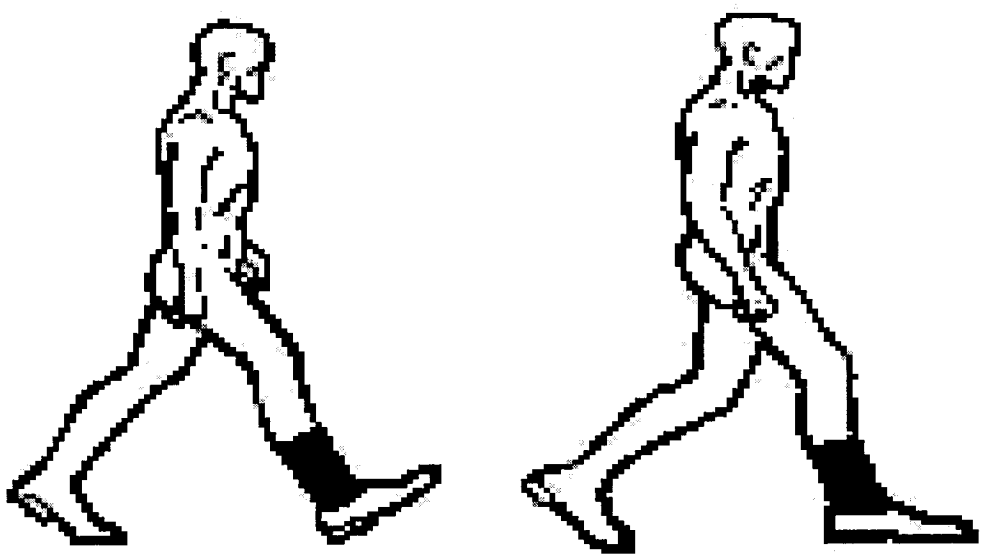

(1) heel contact ***(2) foot-flat***

Figure 1.7 *The gait cycle*[7]

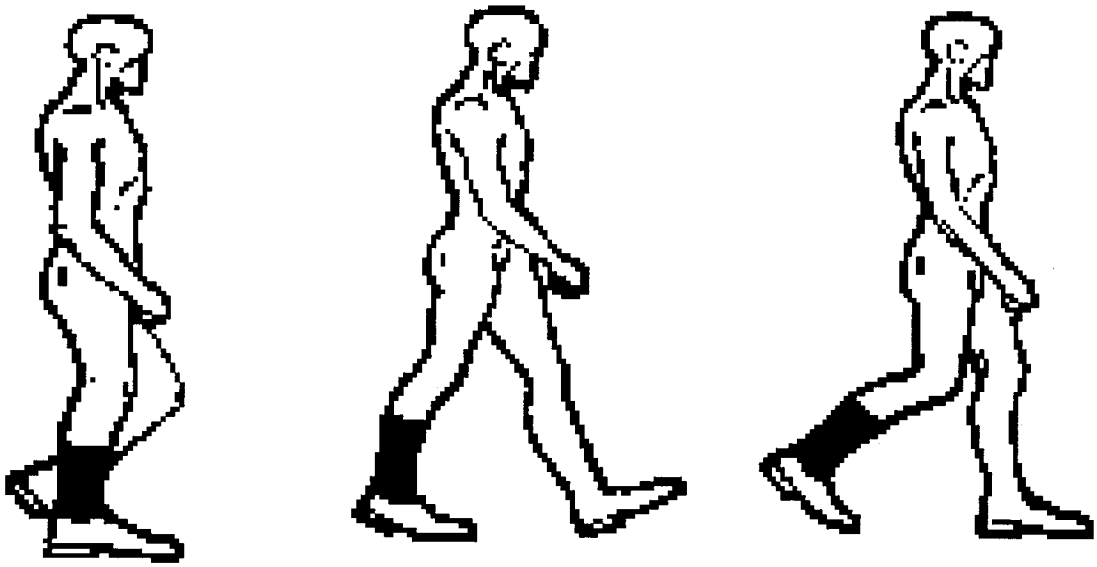

(3) mid-stance *(4) heel-off* *(5) toe-off*

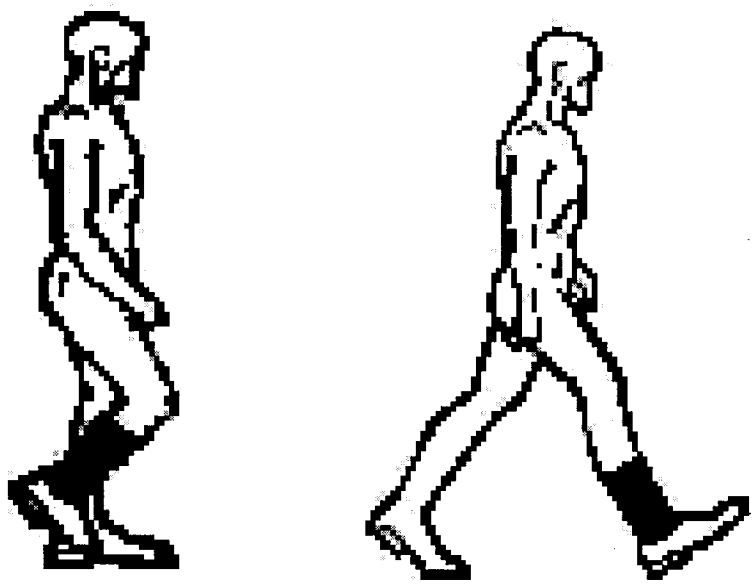

(6) swing *(7) heel contact*

Figure 1.7 *The gait cycle*[7]

At heel contact, the tibialis anterior, extensor digitorum longus, and extensor hallucis longus provide the forces necessary to cause dorsiflexion of the ankle. The dorsiflexors then continue to act as antagonists controlling the amount of plantar flexion and preventing the foot from slapping the ground as a result of inertial forces and gravity. At foot flat, the dorsiflexors become inactive, and the calf muscles - gastrocnemius, soleus, tibialis posterior, flexor digitorum longus, and peroneus longus - together with the knee extensors, act to move the tibia and body center of gravity forward over the foot. From midstance to heel off, the calf muscles work to control the amount of dorsiflexion of the ankle. A sudden burst of energy is generated by the plantar flexors at toe off (push off) during active, vigorous walking and running. The plantar flexors remain active until toe-off, when they become inactive. As the toe leaves the ground, the pretibial muscles contract, holding the foot in a neutral or slightly dorsiflexed position through midswing. This neutral position is maintained until heel contact once again occurs.

In early stance, there is a ground reaction force, $\boldsymbol{R}$, which is equal and opposite to the combined weight of the body and body inertia force, **W**. The reaction force exerts a moment about the ankle joint, Figure 1.8. This moment is equal to the ground reaction force multiplied by the perpendicular distance from the ankle joint to the line of action of the ground reaction force, $\boldsymbol{a}$, and is opposed by the force produced by the dorsiflexors, $\boldsymbol{F_D}$, which may be considered to act at a distance, $\boldsymbol{b}$, from the ankle. When the foot is in equilibrium, these moments are equal, that is, $\boldsymbol{F_D * b = R * a}$.

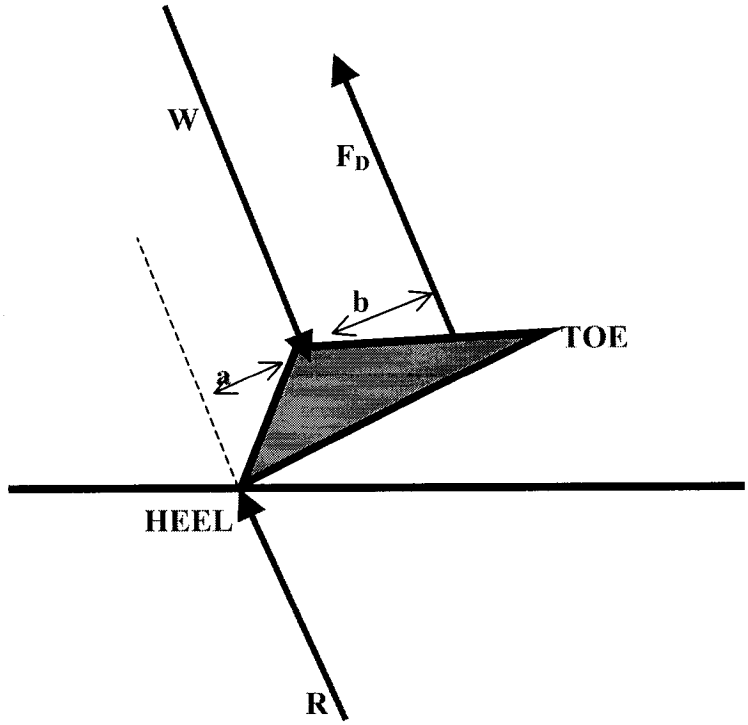

Figure 1.8 *Forces on normal foot in early stance*

During late stance, the gastrocnemius and soleus contract generating a force, $\mathbf{F_P}$, that plantar flexes the foot in a normal healthy individual, Figure 1.9.

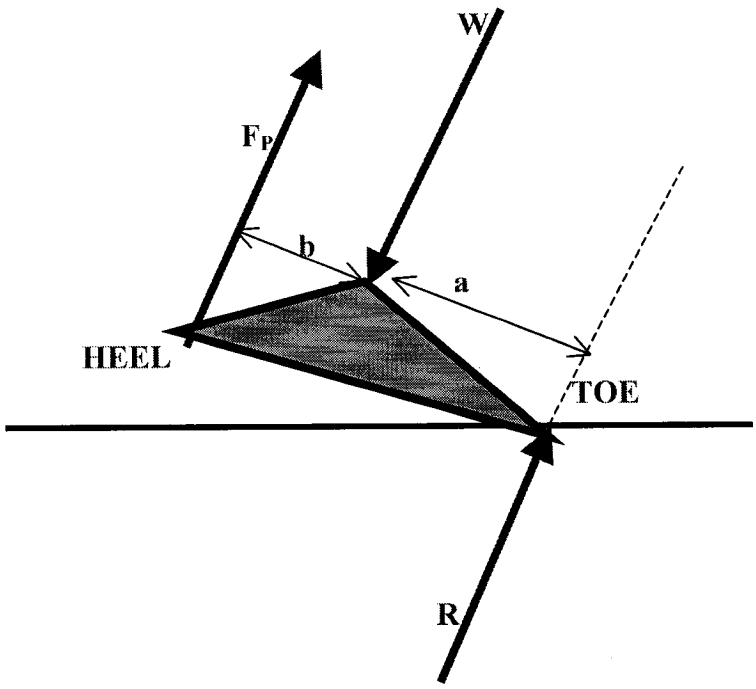

Figure 1.9 *Forces on normal foot in late stance*

During swing phase, a force due to the weight of the foot acts at a distance, x, from the ankle joint and is opposed by the dorsiflexors, Figure 1.10.

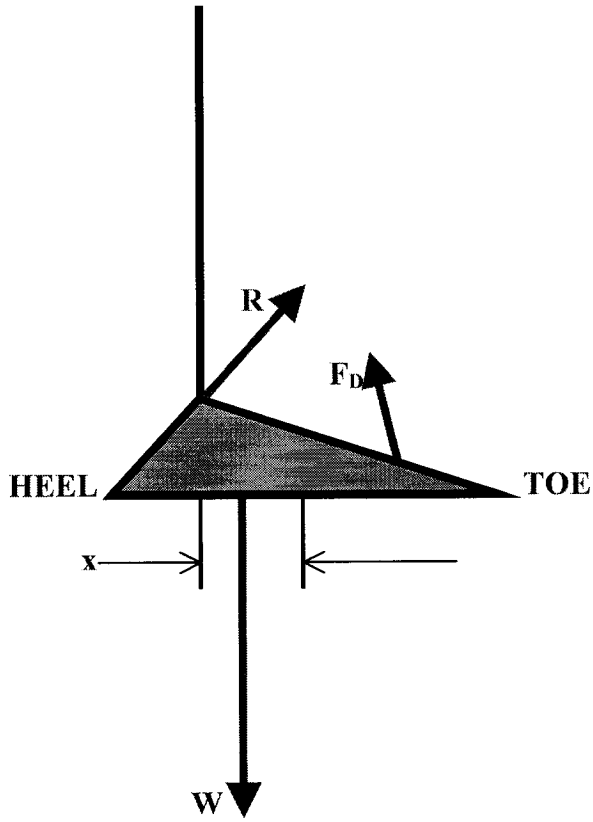

Figure 1.10 *Forces acting on the foot in normal swing*

The gait cycle is also sometimes subdivided into eight phases[69] – ***initial contact*** (when the foot makes contact the ground), ***loading response*** (begins with initial contact with the ground and continues until the opposite foot is lifted for swing), ***mid stance*** (starts with the contralateral foot being lifted and continues until the weight of the body is aligned over the fore-foot), ***terminal stance*** (starts with heel rise and continues until the other foot makes contact with the ground), ***pre-swing*** (starts with initial contact of the contralateral foot with the ground and ends with ipsilateral toe-off), ***initial swing*** (begins

with the foot leaving the floor and continues until the contralateral foot is opposite it), ***mid swing*** (starts with both feet opposite each other and ends with the tibia vertical and the swinging foot forward), and ***terminal swing*** (begins with the tibia vertical and continues until the foot makes contact with the ground).

Dorsiflexion is produced by the action of (1) the ***tibialis anterior*** which originates from the lateral condyle and superolateral shaft of the tibia and inserts on the medial cuneiform and base of metatarsal I; (2) the ***extensor digitorum longus*** which originates from the lateral tibial condyle and interosseous membrane and inserts on toes II-V and is involved in dorsiflexion of the foot and extension of toes II-V; (3) the ***extensor hallucis longus*** which originates from the central medial fibula and interosseous membrane and inserts dorsally on distal phalanx I; (4) the ***peroneus tertius*** which helps in dorsiflexion and eversion, although it is sometimes absent. The dorsiflexor muscles become active during pre-swing, starting with the extensor hallucis longus, which remains active during pre-swing, followed by the tibialis anterior which becomes active in initial swing, and the extensor digitorum longus, which become active in mid-swing. All of the dorsiflexors are active at initial contact, but their action is terminated by the end of loading response.

There are seven muscles that are involved in plantarflexion, however, most of the torque is provided by the ***gastrocnemius*** (which arises by two heads on the posterior femoral condyles, and inserts on the posteroinferior calcaneus) and the ***soleus*** (which arises from the posterosuperior tibia and fibula and merges with the gastrocnemius to insert on the posterodistal calcaneus by the Achilles tendon). Together, these muscles make up the ***triceps surae***. The soleus becomes active near the end of the loading response phase and continues at a constant level through midstance. Activitiy increases

with terminal stance, but subsequently decreases and becomes inactive with the onset of pre-swing. The gastrocnemius becomes active during loading response and activity increases through the middle of terminal stance, and becomes inactive by the end of this phase.

The other five muscles are collectively called the ***perimalleolar*** muscles. These are (1) the ***tibialis posterior*** which is the deepest calf muscle, arising from the posterosuperior tibial and fibular shafts and interosseous membrane and inserting primarily on the prominent medial tubercle of the navicular; (2) the ***flexor digitorum longus*** which originates from the posteromedial tibial shaft and inserts on distal phalanges II-V; (3) the ***flexor hallucis longus*** which arises from the posteroinferior fibula and interosseous membrane and inserts on distal phalanx I.; (4) the ***peroneus longus*** which arises from the head of the superolateral shaft of the fibula and inserts on the medial cuneiform and base of metatarsal I via a long tendon; (5) the ***peroneus brevis*** which arises from the inferolateral fibular shaft and inserts on the lateral tubercle of metatarsal V. The tibialis anterior becomes active at initial contact and activity continues through single stance, followed by the flexor digitorum longus at 10% of the gait cycle, followed by the flexor hallucis longus at 25% of the gait cycle, which both remain active into pre-swing. The peroneal muscles become active during midstance, and while activity of the peroneous brevis continues until the start of pre-swing, the peroneous brevis becomes inactive towards the end of terminal stance.

2. LITERATURE REVIEW

In order to understand the nature of the ankle-joint complex, several models have been created by various investigators. These models may be categorized as either static (or quasi-static) or dynamic.

2.1). *Static Models of the foot*

Several static models of the ankle-joint complex have been proposed, most of which have been in vitro (experimental) or computerized models. Leardini, et al.,[38] observed that the unloaded ankle may in fact follow a preferred kinematic trajectory that is guided by articulating surfaces and ligamentous tethers during passive motion. This path was thought to be the same for dorsiflexion as well as for plantar flexion. In cadaveric studies, loads were applied to seven skeleto-ligamentous lower leg preparations obtained from lower leg amputations, and their path of motion subsequently tracked. With joint capsules and ligaments left intact, all of the skin and subcutaneous and muscle tissue were removed, leaving specimens composed of the tibia, fibula, talus, and calcaneus. Upon removal of the loads, it was observed that the foot reverted to the path of motion that it had followed before the external loads were applied. Moreover, the motion of the articulating surfaces was found to be guided by isometric rotation of fascicles within particular ligaments.

Parenteau, et al.,[65] performed in vitro quasi-static tests with the purpose of determining the moment-angle characteristics of the ankle-subtalar joint about a fixed angle of rotation. A leg-foot specimen was placed in the apparatus shown below, Figure 2.1, in which it was constrained to rotate about the lateral x-axis in dorsiflexion and plantar flexion, and about the longitudinal y-axis in inversion and eversion.

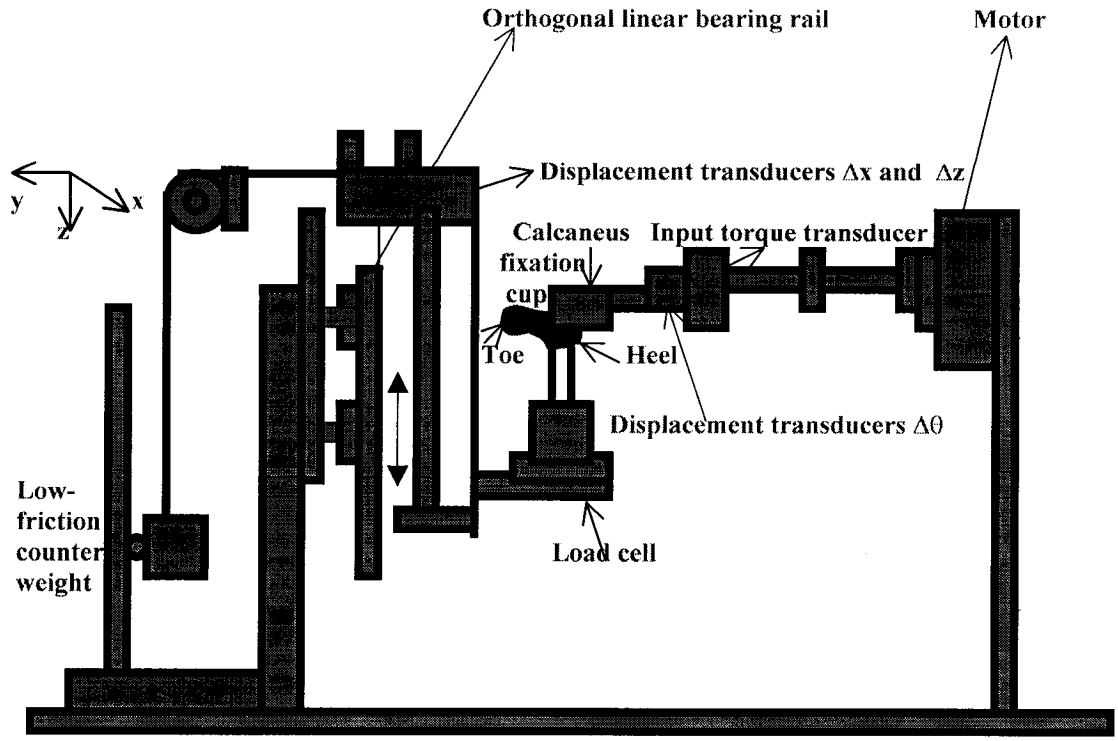

Figure 2.1 *Apparatus to locate the center of rotation (following Parenteau, et al.[65])*

It was discovered that it required an average moment of –33.1 ± 16.5 Nm in dorsiflexion and 40.1 ± 9.2 Nm in plantar flexion in order to cause failure in the ankle-subtalar joint complex. Failure was defined as the point at which there was tissue damage, fracture, joint popping or –(45°-50°) of dorsiflexion, 65°-75° of plantar flexion, -(40°-45°) of inversion and 40°-45° of eversion. The average angle at which failure occurred was –44 ±10.9° in dorsiflexion and 71.6 ±5.7° in plantar flexion. It was also discovered that inversion had a failure moment of –34.1 ± 14.5 Nm and inversion a failure moment of 48.1 ± 12.2 Nm. Additionally, the maximum angle of inversion at failure was 34.3 ± 7.5° and the maximum eversion angle was 32.4 ± 7.3°. It was noted that the tests to failure involving dorsiflexion caused fractures of the lateral malleolus and

rupture of the calcaneofibular ligament, while plantar flexion resulted in tearing of the interosseous talocalcaneal ligament. Extended inversion caused the rupture of the calcaneofibular ligament and eversion, the tearing of the deltoid ligament and the fracture of the medial malleolus.

Metz-Schimmerl, et al.,[53] studied the three-dimensional characteristics of the foot and ankle, by performing computerized tomography (CT) examinations, while the foot was held in a neutral position, a dorsiflexed positon, and in a plantar flexed position. Tomography is the process whereby pictures of a predetermined plane section of a solid object are made by blurring out the images of other planes.[57] Using rigid body motion theory, the relative angular orientation, translation, and rotation of the tibia, talus, and calcaneus were determined and transformation matrices used to determine the degree of rotation and translation that the tibia and calcaneus had undergone. The results showed that plantar flexion occurred primarily in the ankle joint, and was transmitted to the subtalar joint while 75% of dorsiflexion occurred in the ankle joint.

In order to predict the response of the foot to static and dynamic forces while dorsiflexed, inverted, and everted, a three-dimensional finite element model of the human ankle-foot complex was created by Tannous, et al.,[90] IGES files were used to define the surface geometry of the bones of the foot along with the tibia and fibula. The fit of the bones with respect to each other and the location of the demarcating lines between the bones were distinguished through the use of radiographic scans. Using PATRAN/P3,[67] the fibula, tibia, talus, calcaneus, and plantar tissue were modeled using 8-noded hexagonal solid elements, while ligaments, interosseous membrane, and retinacula were represented by 4-noded membrane elements, and the remainder of the bones were

modeled as rigid bodies. The resulting model was processed with LSDYNA3D software and was validated by applying conditions that reflected the tests performed on cadaveric specimens.

The model showed a dorsiflexion rotation of 20° and an external rotation of 7°, when exposed to dorsiflexion at 5 mph, which were values similar to the experimental results. When subjected to various input velocities, the calcaneus showed the highest principle shear and tensile stresses, followed by the talus, tibia, and fibula. The talus had the highest shear strain, followed by the tibia, calcaneus, and fibula, while the tibia had the highest maximum principal strain, followed by the talus, calcaneus, and fibula. The initial input velocities of 5 and 7.5 mph resulted in similar patterns of maximum principal and maximum shear strain. Additionally, the stress patterns of the foot in 20° of dorsiflexion were different from the patterns of the foot in the neutral position.

In addition to geometric models, finite element models of the foot of varying levels of complexity have also been developed. One such model was discussed by Jacob, et al.,[28] in which a comparison was made between a three-dimensional, two-arch model of a normal foot and another of the foot of a patient with Hansen's Disease (commonly known as leprosy). The heel-strike phase of gait was represented with the foot at an angle of 30°, an ankle force of 2.25 times body weight, and muscle forces, which acted at strategic locations.

For the normal foot, the mid-stance phase of gait included a vertical ankle joint force of 2,100 N, muscle forces from the tibialis anterior of 516 N, extensor hallucis longus of 50 N, and extensor digitorum longus of 114 N, and was comprised of 3,292 brick elements and 116 spring elements. The muscles included in the model were the

triceps surae with a force of 550 N, peroneous longus of 132 N, peroneous brevis of 64 N, tibialis posterior of 290 N, flexor hallucis longus of 143 N, flexor digitorum longus of 68 N, and adductor hallucis. The model for the subject with Hansen's Disease incorporated an ankle-joint force of 2,100 N, and forces due to the tibialis posterior of 232 N, flexor hallucis longus of 143 N, and flexor digitorum longus of 68 N. As a result of paralysis, forces resulting from action of the peroneous longus and peroneous brevis were not included, but the forces from the flexor digitorum longus, flexor hallucis longus, and triceps surae were the same as in the model of the normal foot. The boundary conditions were the same as those for the normal foot.

Having carried out the analysis, it was concluded that the areas of high stress in the push-off phase were the dorsal and plantar central regions of the lateral metatarsals, the dorsal junctions of the calcaneus, the dorsal junction of calcaneus and cuboid, the dorsal central area of medial metatarsals, the neck of talus, and the dorsal sides of the navicular and cuneiforms. Moreover, there was also increased stress during push-off in the Hansen's disease model.

A computational foot-ankle model was developed by Ledoux, et al.,[40] in which transverse CT images of a cadaveric foot were obtained at intervals of 1 mm. The aim was to be able to predict the response of a foot to tibial forces. It was concluded that it was indeed possible to use the model to predict the response of the foot to specifically applied forces, to examine the effect of injury to specific muscles and ligaments, to study the roles of particular structures within the foot, and to produce orthoses and footwear with specific design parameters.

Using the apparatus shown below, Siegler, et al.,[81] studied the three-dimensional kinematics of the ankle and subtalar joints using a joint coordinate system and a finite helical axis representation, Figure 2.2.

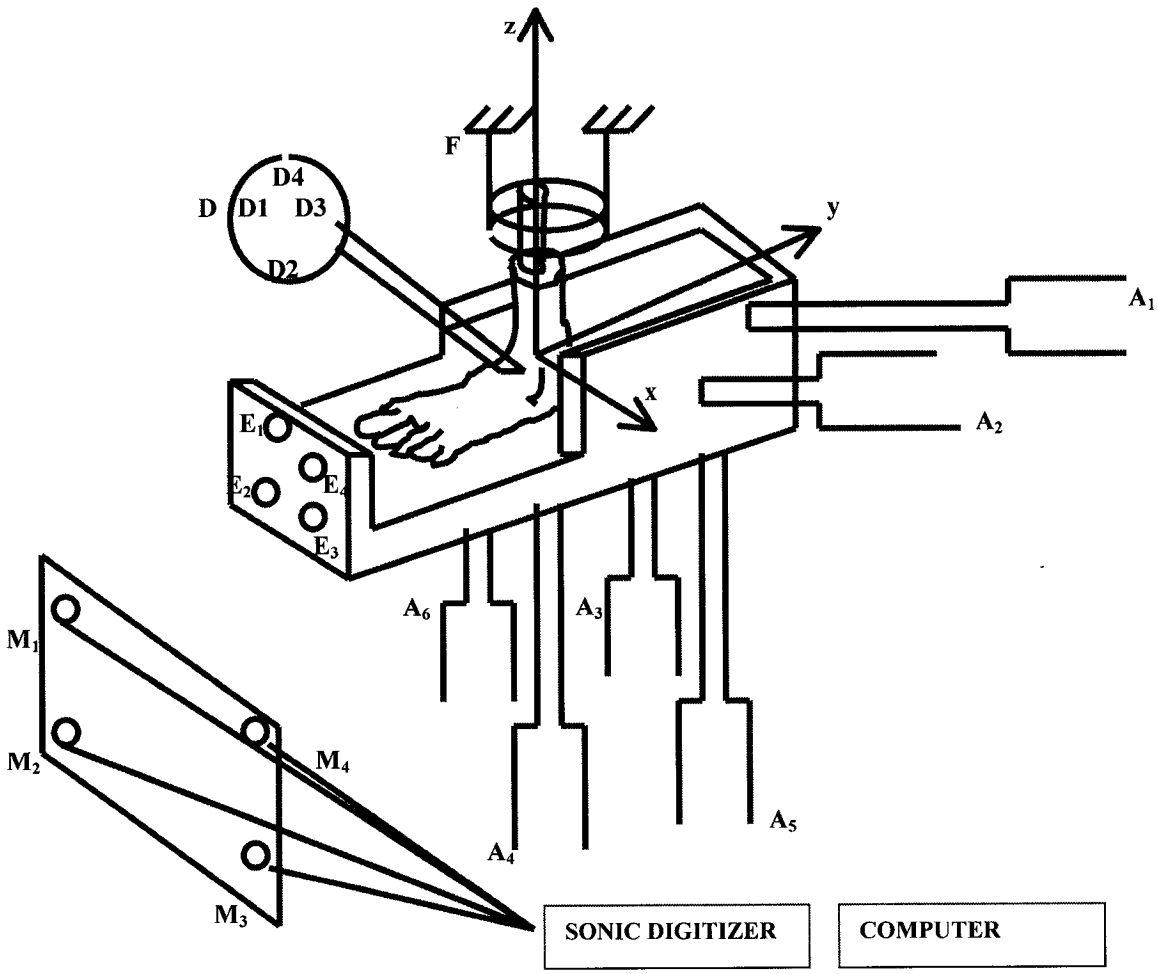

F = Test frame; E = Calcaneus fixture; D=Talus plate;
M_1-M_4 = Microphones measuring coordinates of sonic emitters
D_1-D_4 = Sonic emitters recording postion and orientation of talus
E_1-E_4 = Sonic emitters recording postion and orientation of calcaneus
A_1-A_6 = Actuators applying moment to calcaneus about z-axis
A_1-A_6 = Actuators applying moment to calcaneus about x-axis
A_5-A_6 = Actuators applying moment to calcaneus about y-axis

Figure 2.2 *Apparatus used to study three-dimensional kinetics (following Siegler, et al.[81])*

Three joint coordinate systems were then defined, thereby allowing the relative position between the tibia and talus, tibia and calcaneus, and talus and calcaneus to be established for each increment. The relative positions of the bones were established using homogeneous transformation matrices derived from measured points. Using this information it was concluded that (1) the range of motion of the foot-shank complex is larger than for any single joint within it; (2) the ankle and subtalar joints do not act as ideal hinge joints with a fixed axis of rotation; (3) dorsiflexion/plantar flexion is coupled with inversion/eversion and internal/external rotation to a small extent, but inversion/eversion and internal/external rotation are coupled to a large extent; (4) internal/external rotation are essentially contributed to equally by both the ankle and subtalar joints; (5) the ankle joint contributes more to dorsiflexion/plantar flexion than the subtalar joint, while the latter contributes more to inversion/eversion than the former; (6) translational movements of the tibia with respect to the calcaneus are very small during inversion/eversion and internal/external rotation, however, dorsiflexion causes forward motion of the calcaneus, while plantar flexion results in posterior displacement of the calcaneus.

2.2). *Dynamic models of the foot*

Several dynamic models of the foot have been created and studied in order to further understand the ankle-joint complex, while in motion. Some of these models were theoretical, experimental (in vitro), while others were computer generated.

A two-dimensional, four-bar geometric reproduction of the ankle joint was created by Leardini, et al.,[37] with the purpose of modeling passive rotation and to determine the role played by the articulating surfaces and ligaments in determining the preferred path of motion. For the model, the tibia and fibula as well as the calcaneus and talus were considered to be two rigid bone segments and the calcaneofibular and tibiocalcalneal ligaments considered to be inextensible ligaments that rotated as pin joints, without resistance, on the sagittal plane.

The model was analyzed using kinematic equations and was constructed in such a way so as to accommodate the assumption that the bones remained in contact with each other and that the length of the ligaments joining them remained constant. That is to say, the shape of one articular surface dictated that of the other. In constructing the conjugate surface, the fact that the normal common to the two articulating surfaces at their point of contact passed through the instantaneous center of rotation was taken into consideration, thereby circumventing the problem of interpenetration or separation of the bones. In this way, the shape of the talus-mortise interface and the position of the contact point on both surfaces were ascertained.

This single degree of freedom model has several uses including the prediction of calcaneus landmark trajectories, ligament orientations, instantaneous centers of rotation, and conjugate talus surface profiles.

Wang, et al.,[94] performed experiments in which the kinematics of the ankle and subtalar joints while in continuous motion were examined using computerized radiocinematography. In this study, nineteen subjects were asked to flex their knee at 30° and were subsequently examined under a roentgenographic tube, while the ankle was allowed to move freely in a plane parallel to the examination table. As the ankle moved through its entire range of plantar flexion and dorsiflexion, the images appearing on the fluoroscopy monitor were recorded synchronously with a video-recorder, transferred to a computer via a video digitizer, and analyzed with a program designed for pictorial use. In order to determine the center of rotation of the ankle joint, the displacements of two points of a link were tracked as it moved and were subsequently graphed using. The intersection of the perpendicular bisectors of the lines connecting points on the graph was the instantaneous center. The images of greatest points of extreme flexion, both dorsiflexion and plantar flexion were superimposed upon each other in order to establish the range of motion of the ankle. As a matter of interest, the change in the positions of the bones relative to each other was also observed.

The centers of rotation of the ankle joint were found to lie near to each other, within the body of the talus, close to the subtalar joint, and was within the area covered by the lateral process of the talus in the lateral view. It was also noted that the longitudinal axis of the lower tibia pointed towards the instantaneous center of rotation. The average excursion in the sagital plane of the calcaneus was 58.6 ± 5.4° while that of the talus was 51.5 ± 4.8° , and the navicular was 69.2 ± 6.4° as the ankle went through its entire range. Also of interest was the fact that the distance between the fibula and the posterior tibia did not change as the lower leg was fixed and the foot was flexed. The

distance between the middle and posterior facets of the subtalar joint increased as the foot was dorsiflexed and plantar flexed, indicating that there was inversion in the frontal plane during plantar flexion. Additionally, the distance between the fibula and posterior tibia margin increased as the ankle moved from plantar flexion to dorsiflexion and the internal rotation of the lower leg was indicated by the anterior displacement of the fibula with respect to the tibia.

Stahelin, et al.,[87] built an apparatus in order to quantify the motion of bones in the ankle joint complex in vitro. The positioning of the horizontal axis was altered to simulate flexion as well as inversion and eversion. The tibia was fixed at its proximal end with an adjustable rod placed down the medullary channel and aligned with the longitudinal axis of the tibia. The tendons were attached to wires and the muscles stimulated by applying pulling forces to the wires. The weight of the body was represented with vertical loads and a moment applied to represent rotational torques. Bone movement was quantified using a three-dimensional motion acquisition system, which was comprised of three cameras that viewed markers placed on the anterior, medial, and lateral sides and another that recorded the top view. The rotation of the foot plate was induced with a manual lever causing the foot to rotate 15° through 25° of dorsiflexion, plantar flexion, pronation, supination, inversion and eversion and 15° through 20° of dorsal extension and inversion/plantar flexion and eversion. The axes were defined from visible bone structures.

The motion of the bones was quantified using a three-dimensional motion acquisition system and the intersegmental rotation in defined joint coordinate systems calculated using Kintrak motion analysis software.

A two-part, viscoelastic model of the foot that incorporated springs and dampers was created by Gilchrist and Winter, using ADAMS dynamic software, to be used in predicting foot motion during stance phase of gait.[21] To achieve this, the foot was considered to be two segments connected by a revolute joint joining the metartarsals and phalanges. Its movement throughout the gait cycle was defined by analyzing a three-dimensional gait analysis of one subject. The resultant joint forces and moments were found by employing inverse dynamics methods and determining the ground reaction forces and specific kinematic data.

The sole of the foot was modeled with viscoelastic spring/damper elements to reflect the movement of the bones relative to each other and the deformation of the soft tissue of the foot as it was loaded. Three of these vertically positioned elements were placed under the toes, while six were placed under the remaining areas of the foot along its midline. A non-linear damping coefficient was used in order to control how quickly the value of the force increased as the spring underwent increasing degrees of compression and was represented by a Heaviside step function.

$$\begin{cases} x \le x_0 & c = c_0 \\ x_0 \le x \le x_1 & c = c_0 + (c_1 - c_0)*\{(x-x_0)^2/(x_1-x_0)\}^2*[3-2\{(x-x_0))/(x_1-x_0)\}] \\ x \ge x_1 & c = c_1 \end{cases} \qquad (2.1)$$

where c_0 and x_0 were zero and x_1 symbolized the value of the displacement when the damping coefficient became constant and c_1 symbolized the greatest value of the damping coefficient. Horizontal frictional forces at the contact elements were considered

to be linear functions of velocity and, once again, the step change in force was modeled with a Heaviside function, with the damping a function of the vertical spring force. As rotation in the sagittal plane was a result of the ground reaction forces, a torsional damper was used to maintain control of the rotation about the anterior/posterior and vertical axes of the foot, although large degrees of damping tended to prevent this type of rotation.

The model was validated using measured forces and the forces in both models were found to be in relative agreement. It was noted that small adjustments in the damping coefficients, and changes in the spring constants and distribution of the contact elements resulted in considerable error generation.

Recently, methods have been proposed to estimate the axis and center of rotation of joints. Halvorsen et al.[23] present models which feature a rotational joint with a fixed axis of rotation (hinge joint) and a ball and socket joint (spherical joint). The method uses three non-parallel and non-planar displacements to find the center of rotation, while the axis of rotation is found, using the Reuleaux method, which uses two non-parallel displacements, Figure 2.3, through P1, P2, and P3.[73]

This method utilizes two non-parallel displacements, as defined by the positions and displacements of three non-collinear points on a body, to determine the axis of rotation (defined by the intersection of two planes through the midpoints of the displacements and normal to the displacements).

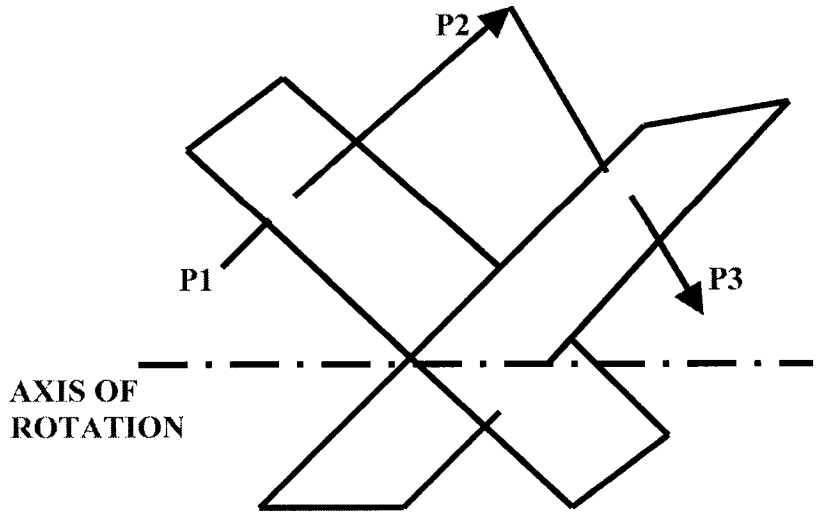

Figure 2.3 *The axis of rotation by Reuleaux method*[73]

However, unlike the Reuleaux method, which utilizes motion at only two distinct instants in time and two-dimensional motion, Halvorsen's method utilizes the whole data set, and does not assume rigid body motion.[23] Cost functions are defined based on the following assumptions: (1) the axis of rotation is defined by the intersection of two planes through the midpoints of the displacements and normal to the displacements; (2) all points on a body rotating about a hinge joint without translation, have paths of circles or circle segments; (3) each point on the rotating body follows a path which lies on the surface of a sphere, the radius of which is equal to the distance from that point to the center of rotation (that is, the set of planes of rotation of all points on the body, intersect at the center of rotation), Figure 2.4.

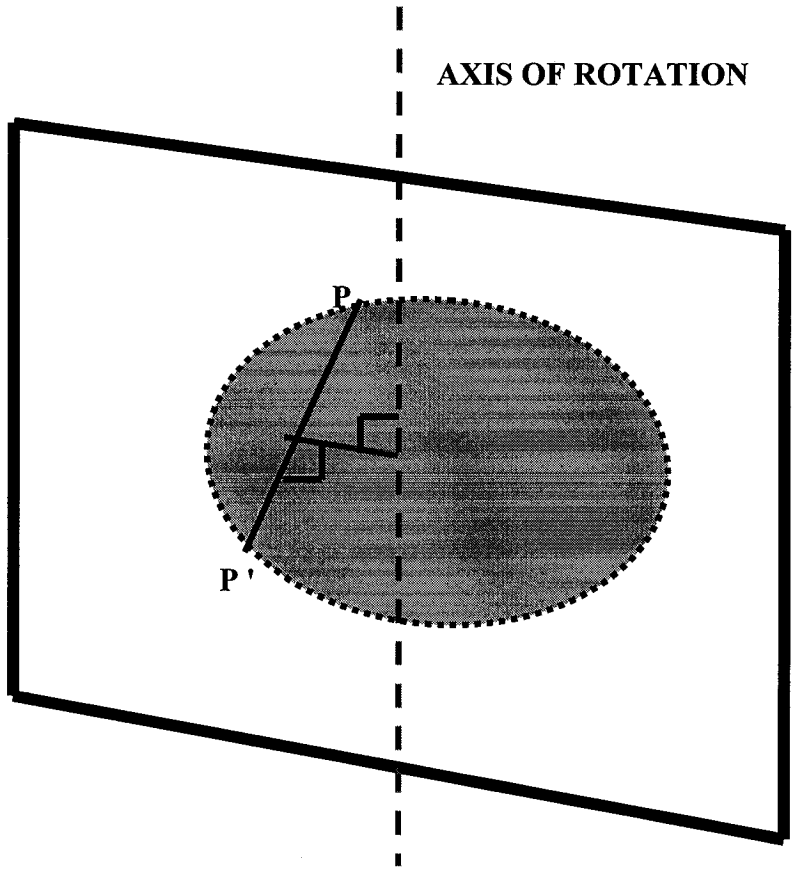

Figure 2.4 *(1) The point paths as circle segments and (2) the displacements normal to the plane of the axis of rotation and midpoint of displacement*

Assuming that the solution to the first condition is a unit vector, ω, which is normal to the plane spanned by all displacements, $\Delta\mathbf{p}$, the following simple quadratic optimization problem is formulated:

$$s_1 = \sum_i (\Delta\mathbf{p}_i^T\omega)(\Delta\mathbf{p}_i^T\omega) = \omega^T(\Sigma(\Delta\mathbf{p}_i\Delta\mathbf{p}_i^T))\omega = \omega^T C\omega \qquad (2.2)$$

where $|\omega| = 1$ *and C is the smallest eigenvalue of the 3X3 matrix, C.*

The second condition allows the formulation of the following least-squares problem:

$$S_2 = \sum_i (\Delta\mathbf{p}_i^T(((\mathbf{p}_i + \mathbf{p}_i')/2) - \mathbf{q}))^2 \qquad (2.3)$$

where $\mathbf{p}_i$ *and* $\mathbf{p}_i'$ *are the start and endpoints of the displacement and q is the position vector of any point on the axis (of the rotational joint), or the center of rotation (of the spherical joint).*

When tested with simulated data, the model was found to give good results when there were skin position artifacts, while the estimates were reasonable when random measurement errors were introduced to the data set.

Gamage et al.,[20] also proposed models to determine the axis and center of rotation of a limb segment. The first model assumed that a set of vectors on a body rotates about a time varying axis of rotation, with a fixed center of rotation, Figure 2.5.

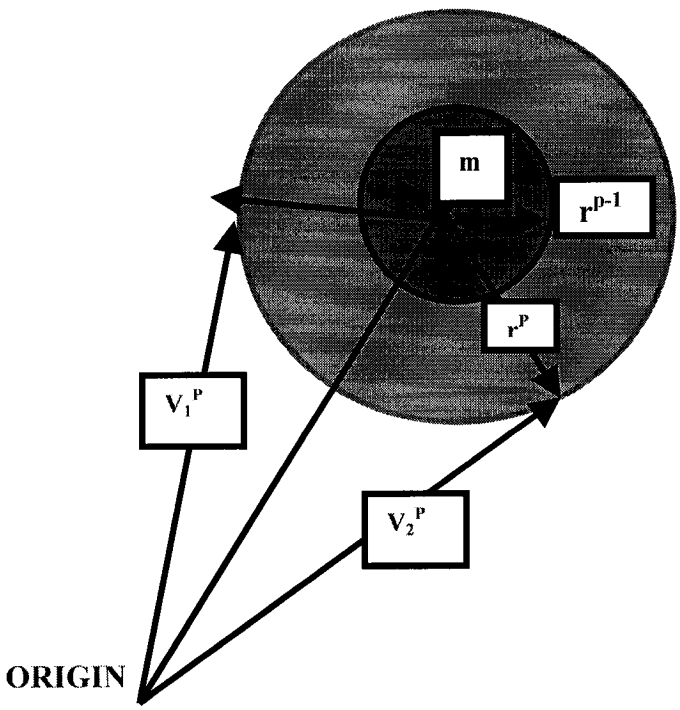

Figure 2.5 *Set of vectors on a body rotating about time varying axis of rotation*

It was given that each individual vector, v^k in the k'th time frame marked out a sphere as it rotated about the center of rotation. A cost function was derived and minimized to determine the radius of rotation and the center of rotation.

$$\sum_{p=1}^{P} \sum_{k=1}^{N} [(v_k^p - m)\{(v_k^p - m)^2 - (r^p)^2\}] = 0 \qquad (2.4)$$

The joint was also modeled as a hinge joint, with a fixed axis of rotation and moving center of rotation. It was assumed that the minimum distances from each point on the body to the axis of rotation, was fixed, Figure 2.6.

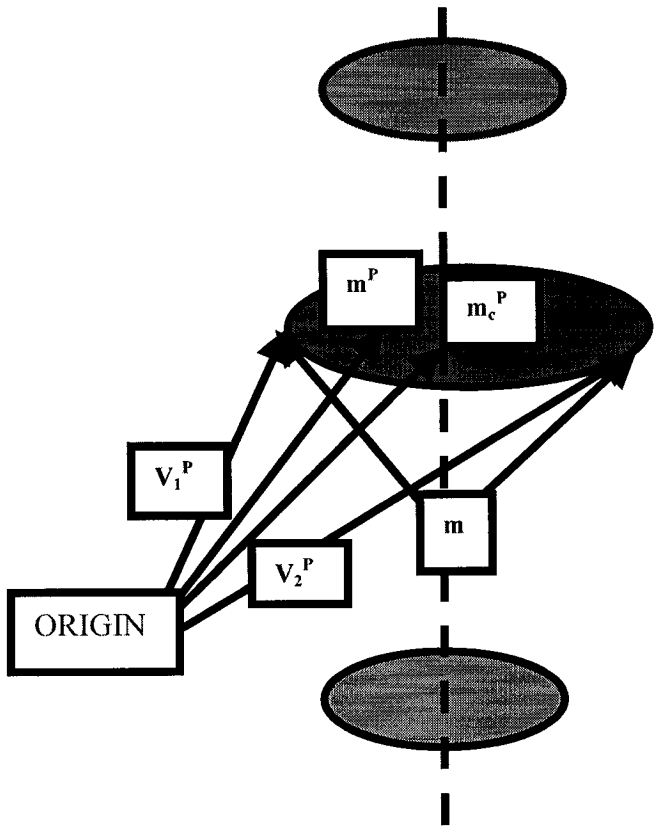

Figure 2.6 *Joint modeled as hinge joint, with fixed axis of rotation and moving center of rotation*

Cost functions were defined to find a single point on the axis of rotation and the direction of the axis of rotation. The basis of the theory is that the vector components, $\mathbf{v}_k^p - \mathbf{m}^p$, ideally, are on a plane perpendicular to the axis of rotation.

$$\mathbf{C} = \sum_{p=1}^{P} \sum_{k=1}^{N} [(\mathbf{v}_k^p - \mathbf{m}^p)*\mathbf{n}]^2 \qquad (2.5)$$

Taking any point, m, on the axis and the distance from the point to the circular arc, the following cost function is obtained and used to find m:

$$\mathbf{C} = \sum_{p=1}^{P} \sum_{k=1}^{N} [(\mathbf{v}_k^p - \mathbf{m})^2 - (r^p)^2]^2 \qquad (2.6)$$

This method may be adapted to joints with translational movement, that is, the joints of the body.

2.3). *Pathomechanics of the foot and ankle*

If the forces applied to the foot cannot be sustained or if the leg is incapable of producing the motions and/or forces necessary for proper function, then a pathomechanical condition is said to be present. Such conditions may result from congenital malformation, trauma, muscular imbalance, neurological disorders, skeletal pathologies, or vascular disorders. Bones may be abnormally shaped because of traumatic injuries or faulty development. Weak muscles cause ligaments and bones to undergo abnormally high stresses or simply may not provide enough resistance to stronger muscles, thus upsetting the dynamic equilibrium of the joints. The reverse is true in that unusually strong muscles may also cause imbalance of forces around a joint or joints. Moreover, problems may arise if the muscles fire at the wrong time, so that the actions become uncoordinated and hinder function. Basic deformities of the foot include cavus, equinovarus, equinus, pes planus (flatfoot), and tibiotalar arthritis. These and other conditions cause the development of ***antalgic gait*** - a gait or posture that an individual assumes with the aim of lessening or stopping pain which may result from one of several conditions, including arthritis, tendon rupture, bone fracture, gout, etc. A gait pattern is assumed that reduces the amount of loading applied to the affected limb.

Paralytic dysfunction is caused by disruption of the ***motor system***, which controls locomotion and fine movement. The motor system is composed of the spinal cord, brain stem, and motor cortex and acts on motor neurons in the spinal cord, allowing the body to perform many functions including the maintenance of body posture and equilibrium by innervating skeletal muscles causing them to relax or contract. Brain stem inputs to the spinal cord carry out the maintenance of posture and balance. Locomotor generators in

the spinal cord are driven by the cortex (the locomotor command center in the brain), creating controlled movements, which are modified by sensory feedback. As each component of the motor system has a different role, pathology or deficits in specific parts result in characteristic biomechanical disorders.

Complex motor behaviors require inputs from (1) the ***motor cortex*** (responsible for fine movements, instructing the motor neurons to activate their respective skeletal muscles); (2) ***supplemental and premotor cortices*** (involved in the planning of movements, transmitting information to the cortex); (3) the ***posterior cortex*** (involved in the processing of sensory information leading to purposeful movement); (4) the ***cerebellum*** (which initiates and plans movement, coordinates limb movement, and maintains posture and equilibrium); (5) the ***basal ganglia*** (involved in cognition and movement).

Pathomechanical conditions of the ankle-foot complex may also be classified as either ***excessive plantarflexion*** or ***excessive dorsiflexion***. Excessive plantarflexion is a result of pretibial muscle weakness, plantar-flexion contracture, soleus overactivity, and voluntary posturing for weak quadriceps. When the pretibial muscles do not produce an adequate dorsiflexion force, the foot hits the ground inadequately controlled. This is observed mostly during the mid swing, initial contact, and loading transfer phases of gait. Plantar flexion contracture may be rigid, caused by stiffness of the fibrous tissues, or elastic, which results from the stretching of dense tissues under the force of body weight. Rigid contracture results in low heel mode of initial contact, early foot flat in loading response, and insufficient tibial advancement during mid stance. It may also cause a plantar flexed foot during mid swing, which results in subsequent toe drag, as well as

premature terminal stance. Elastic contracture causes the ankle to give under the weight of the body and causes excessive plantar flexion during mid swing due to insufficient force being generated by the dorsiflexors. The soleus and gastrocnemius may also contribute when they experience spasticity, causing them to be constantly active, which has an effect similar to plantar flexion contracture. The effects of voluntary excessive ankle plantar flexion are seen in patients with weak quadriceps, as a reaction to the knee flexion thrust experienced during loading response.

Excessive dorsiflexion of the ankle may be caused by soleus weakness, which results in the loss of tibial stability during the weight-bearing period, thus disrupting the mechanism of complementary roles of agonist and antagonists. Since there is insufficient soleus action during mid stance, as the tibia advances over the foot the ankle is inadequately constrained and goes into excessive dorsiflexion. Action of the gastrocnemius can further exacerbate the problem, as the combination of its action with the weak soleus causes accelerated tibial advancement. Fixation of the ankle at the neutral position, as a result of fusion, or an orthosis with a plantarflexion stop also leads to excessive dorsiflexion from heel contact to midstance as the normal plantar flexion that occurs during limb loading is obstructed. This occurs as the foot and tibia are locked at right angles to each other, causing a plantar flexion moment at the heel that translates to a knee flexion moment. Patients compensate for this by taking smaller steps and walking more flat footed.

Cerebral palsy is a term used to refer to movement and posture disorders that result from defects or lesions of the immature brain. These disorders may be either dynamic, which occur as a result of muscle imbalance about the ankle joint, or fixed,

which is secondary to muscular contracture or bone and joint malalignment. ***Equinus*** is an example of a static and/or dynamic deformity that occurs in patients with cerebral palsy, and is defined as a limitation of passive ankle dorsiflexion beyond the neutral point. It results from premature or prolonged activity or contracture of the gastrocnemius and/or soleus. Equinus patients exhibit a lack of normal heel strike, and therefore loss of first ankle rocker. In less severe cases, the patient can achieve flatfoot, although this is often accompanied by secondary deformities such as genu recurvatum or midfoot break. In more severe cases, the knee is maintained in flexion, as the functional limbs are not equal in length. In order to determine whether the deformity is static or dynamic, the hindfoot is inverted to lock the subtalar joint. If the foot stays in plantarflexion, the deformity is static, however if it is passively correctible past 90°, the deformity is dynamic. Dynamic deformity is sometimes treated by therapy along with plaster casts, however the effects are sometimes temporary. If the deformity is static, the ankle is stretched and a well-molded short leg cast or a long leg cast (if knee flexion contracture or hamstring tightness are also present) is applied and changed weekly for at least three weeks or until a plantigrade position of the foot is achieved. Following removal of the cast, the foot is stretched daily and an AFO is worn at all times. Dynamic deformity is generally treated with a brace (sometimes an articulated AFO with a 90° plantar flexion stop), which has been found to reduce ankle excursion, increase ankle dorsiflexion at foot strike, and increase the plantarflexion moment at push off. If the patient has a persistent fixed contracture of the gastrocnemius/soleus, an obligate toe-toe gait, genurecurvatum in stance phase, or a development of a midfoot break, surgical intervention is indicated. For patients with dynamic deformity, the Achilles tendon is anteriorly advanced, and a short

leg cast is then worn for 6 weeks. Following this, the patient wears an AFO for up to 6 months. This method has been found to be highly effective, with gait being greatly improved in 98% of patients. For patients with fixed deformity, the Achilles tendon is lengthened, followed by wearing a short leg cast for 6 weeks, then an AFO for 3 months. This method has also been shown to have excellent results.

Valgus causes the foot to turn outward, forcing the individual to walk on the inner border of the foot. It results from unbalanced forces rotating the foot about the subtalar axis in pronation, causing the medial arch to be lowered and the forefoot to abduct. In some patients, spasticity and overactivity of the peroneal muscles play a part in the development of the deformity, however patients with the deformity show an inactive posterior tibialis muscle. Adduction of the hip, a valgus knee, and external tibial torsion often occur during gait, while during stance, patients exhibit hindfoot valgus, midfoot break, and abduction of the forefoot. A valgus prevention AFO may be used, however it does not have any permanent corrective effects. When the problem is not helped with the aid of an orthosis, surgery is indicated. Procedures used include extraarticular subtalar arthrodesis, which has been found to be effective in 97% of patients. Another alternative is to place a screw through the superior neck of talus into the calcaneus so the hindfoot remains in place.

At the other extreme, ***Varus***, causes the individual to walk on the outer border of the foot, as the foot is turned inward by unbalanced forces that supinate and adduct the foot about the subtalar joint. It seldom occurs alone, and is often associated with ankle equinus deformity and is most commonly caused by overactivity of the posterior tibialis muscle, and sometimes the anterior tibialis muscle. The deformity may be treated with a

varus prevention AFO (a custom-molded plastic orthosis that uses three-point fixation to correct the hindfoot position passively). Surgical intervention entails the release of specific tissues and tendon transfer and is performed on patients who are developing pain or callosities or for whom orthoses are not effective. The decision as to which procedure should be used is based on dynamic gait electromyography. For example, if it shows inappropriate activity of the posterior tibialis tendon, a split posterior tibial tendon transfer is performed, with excellent results.

With ***Pes cavus*** deformity, the longitudinal arch is excessively elevated and does not flatten with weightbearing. The forefoot is also commonly plantar flexed in the cavus foot, which results from an imbalance between the long extensors and the long flexors of the foot. The higher the cavus arch, the more the toes are pulled into a hyperextended position at the metatarsophalangeal joint, as the plantar fascia is contracted and the situation is gradually worsened. The most common causes of pes cavus have been found to be Charcot-Marie-Tooth disease; poliomyelitis (a viral disease characterized by involvement of the central nervous system, stiff neck, and sometimes atrophy of groups of muscles, resulting in contraction and permanent deformity and/or paralysis); meningomyelocele, a hernial protrusion of a part of the meninges (the three membranes that envelop the brain and spinal cord) and substance of the spinal cord through a defect in the vertebral column); traumatic nerve injury; and spinocerebellar degeneration (degeneration of the spinal cord and cerebellum). AFO's are used to provide stability, however, bony prominences on the foot are taken into consideration, with molded reliefs incorporated into the AFO. Additionally, surgical plantar fascia release is used to reduce forefoot plantar flexion and calcaneal varus. In cases where the great toe is elevated, the

interphalangeal joint is fused and the extensor hallucis is released from its insertionon on the distal phalanx and inserted onto the neck of the first metatarsal, thus allowing it to aid in correcting plantar flexion. In cases where the peroneous longus is preserved, but the peroneous brevis is weak, tenodesis of the peroneous longus to the peroneous brevis allows the patient to evert the hindfoot and stabilize the hindfoot. In other cases, peroneous longus to peroneous brevis transfer are used along with calcaneal osteotomies. Fixed forefoot plantar flexion is usually corrected with a metatarsal osteotomy along with a plantar fascia release to correct a forefoot valgus. If equinus is also present, osteotomy of the second and third metatarsals is also required.

Hemiplegia is total or partial paralysis of one side of the body caused by disease or injury to the corticospinal tracts of the central nervous system, which along with the associated motor tracts extend from the cerebral cortex to the lower end of the spinal cord. Causes of injury include blood vessel disease, wounds, tumors, or abscesses. The location of the injury/lesion generally indicates the body segments that are affected.

Hemiplegia involves difficulty speaking, understanding, or recognizing words, an alteration of sensation on the affected side of the body (often with pain and some anesthesia, and may involve incontinence, blurred vision, and difficulty self-feeding. Hemiparesis causes the patient to have muscular weakness or partial paralysis on one side of the body, while the other side of the body in completely intact. The most common cause of both of these conditions is stroke, which results from bleeding in the brain or from an obstruction of a blood vessel to the brain, such as a blood clot. Every year about 550,000 Americans experience a stroke, killing about 150,000 people. Of the 400,000 that survive, 14% will have another within one year. Hemiplegia causes patients to

exhibit drop foot with motor weakness at the knee and hip, in addition to impaired balance, and sometimes even pain, which contribute to susceptibility to falls because of loss of motor control and strength. The muscles of the foot and lower leg are shown in Figure 2.7, and their functions summarized in Table 2.1.

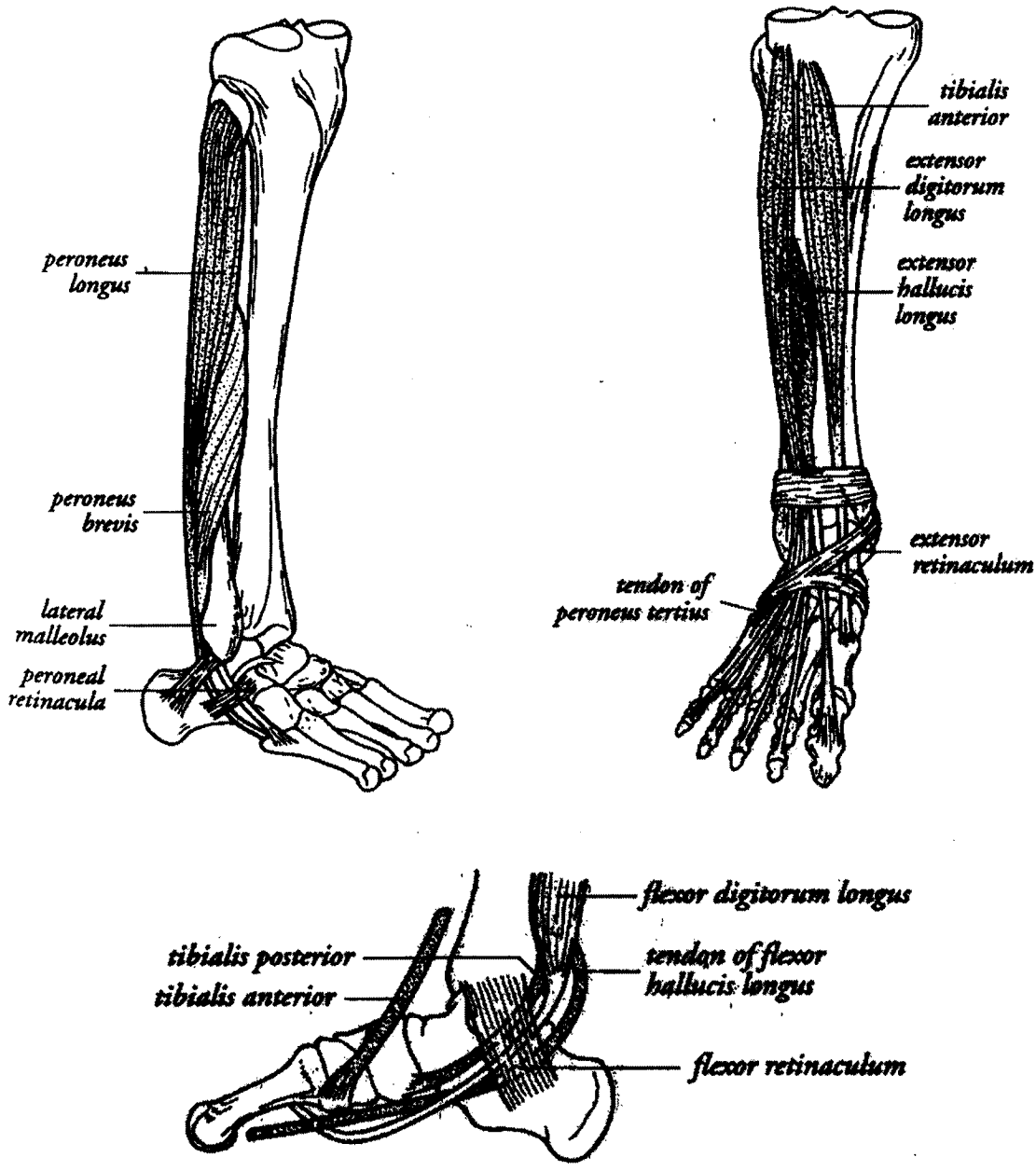

Figure 2.7. *The muscles of the foot and lower leg*[10]
a) anterior; b) lateral; c) medial views

Table 2.1 *The biomechanical function of the muscles of the foot and ankle*

Function	Muscles
Plantar flexors	**tibialis posterior, flexor digitorum longus, flexor hallucis longus, peroneus longus, peroneus brevis, gasrocsoleus**
Dorsiflexors	**tibialis anterior, extensor hallucis longus, extensor digitorum longus**
Evertors	**tibialis anterior, tibialis posterior, flexor digitorum longus, flexor hallucis longus**
Invertors	**extensor hallucis longus, extensor digitorum longus, peroneus longus, peroneus brevis**

Thilman, et al.,[91] showed that the ankle of a hemiplegic patient exhibited increased stiffness after the foot is dorsiflexed beyond 70°. In plantar flexion and between 95° and 110°, there was no difference in stiffness the two ankles, however, as the ankle was dorsiflexed, the ankle contralateral to the cerebral lesion was found to be much stiffer. Radtka, et al.,[71] demonstrated that the use of dynamic ankle-foot orthoses with a plantar flexion stop or polypropylene solid ankle-foot orthoses were both suitable for hemiplegic patients with excessive plantar flexion during stance, however the type prescribed depended on the specific characteristics of the patients disability. Use of orthoses showed increased stride length, decreased cadence, and reduced excessive ankle plantar flexion when compared with no orthoses. Lehmann, et al.,[42] evaluated five palstic ankle-foot orthoses to compare their effective when used by patients with varying degrees of plantar flexor spasticity. The models that enclosed the malleoli were the least flexible and provided the greatest plantar flexion resistance to prevent toe drag during swing when worn by patients with severe plantar flexion spasticity. They also provided the

greatest dorsiflexion resistance, substituting for the action of the gastrocnemiussoleus during the latter part of stance. They also produced large flexion moments at the knee at the initial foot contact. Models that were trimmed in the region of the malleoli were more flexible and did not provide a pushoff substitute, but did allow for toe clearance during swing. It was concluded that patients with mild plantar flexor spasticity would benefit from the use of the more flexible orthoses. It has also been shown by Lehmann, et al.,[43] that hemiplegic patients exhibit asymmetry in both stance and swing phases, with stance phase becoming shorter, and swing phase becoming longer that the unaffected side. The use of an AFO allowed the walking speed to be increased, the duration of midstance phase to be shortened, the duration of pushoff phase to be increased, and that of heel strike phase to be increased.

2.4). *Range of motion of the pathological foot*

Yamamoto, et al. [99], studied the subtalar instability after lateral ligament injury of the ankle was sustained. They found that the subtalar tilt angle was 9.7° ± 3.2° in acute injuries, 10.3°± 2.9° in chronic injuries, and 5.2°± 2.6° in normal ankles. Michelson, et al.,[54] investigated the alteration in ankle motion as a result of a medial sliding calcaneal osteotomy. It was found that there was 4.4° ± 2.5° of internal rotation at maximum dorsiflexion as opposed of 2.5° ± 1.7° for healthy cadaveric ankles. It was also found that there was an increase of varus from 0.42°± 0.56° versus 0.08° ± 0.34° for intact ankles. The effect of supination-external rotation type of fracture on motion was examined by Michelsen, et al.,[55] who found that for intact cadaveric specimens, there was a mean of 1.9° ± 4.12° of internal rotation of the talus at maximum plantarflexion, and a mean rotation of 7.2° ± 3.88° of external rotation at maximum dorsiflexion. In fractured specimens varus increased from 2.4° ± 2.4° at plantar flexion as opposed to 0.3° ± 1.96° at dorsiflexion. Cass et al.,[13] studied the effects of hindfoot instability on kinematics. External rotation of the leg resulted in 11.1° of inversion in the intact ankle. After releasing the anterior talofibular ligament, an additional external rotation of 4.9° was obtained, while additional release of the calcaneofibular ligament resulted in 12.8° more of rotation than with the intact joint. Talar tilt of 20.6° occurred after both of the ligaments were released.

2.5). ***Ankle-foot orthoses***

Historically, orthoses were made of wood, leather, and/or metal. Metal designs of orthoses usually consist of two metal uprights proximally connected to a metal calf band, and distally forming a connection to an ankle mechanism, which is connected to a shoe or insert. In either case, it is necessary for the shoe worn to be very sturdy with a spring steel or similar shank. This is especially true if the uprights are attached to the shoe by stirrups or a caliper. A stirrup is a U-shaped structure that is riveted to the sole and shank of the shoe under the malleoli. It is sometimes split distally to allow the user to wear different shoes as it may be detached from the shoe, although this does compromise its strength and appearance. Additionally, the split stirrup allows more congruence to be experienced between the mechanical and anatomical joint.

A caliper is an insert placed into a tube in the heel of the shoe, which allows the wearer to remove the uprights and interchange shoes. However, in this case, the mechanical joint is at the level of the heel, rather than at the level of the anatomical joint. This causes counterforces from incongruous alignment, which makes it less comfortable than the stirrup, as the calf band moves during dorsiflexion and plantar flexion. The shoe insert, which can be shaped to the contours the foot, provides an alternative to direct shoe attachment of the orthosis. It also provides more control and support and is comfortable, as the joints are more congruent. The insert allows the user to interchange shoes, although these too must be bigger than the original size in order to accommodate the bulk of the insert.

Ankle stops and flexion/extension assists, which prevent mediolateral motion and help to control dorsiflexion and/or plantar flexion by mechanical stops or springs are also

incorporated into AFO's. If a patient has weak dorsiflexors, as in the case of the drop foot, then plantar flexion stops are used to restrict plantar flexion, but allow unlimited dorsiflexion. A spring may be used in order to assist in dorsiflexion, as it is compressed after heel strike, which controls plantar flexion, and recoils in the swing phase aiding dorsiflexion. A second spring may also be used to help to control plantar flexion. It is compressed during mid-stance and plantar flexes the ankle by recoiling. These are commercially available in orthotic joints, such as the Klenzak joint, which provides a dorsiflexion moment for toe pickup during swing phase and mimics the contraction of the dorsiflexors at heel strike.[41] The reverse is true for persons with weak plantar flexors. Movement in both directions may also be restricted by incorporation of joint stops to limit motion. In this case, the front and back of the ankle joint are adjusted, allowing specific ranges of motion. In some cases, only mediolateral control is required, thus unlimited dorsiflexion and plantar flexion are allowed.

Plastic AFO designs may be formed from a single piece of thermoplastic material. Plastic AFO's have three identifiable sections – the calf strap, calf shell, and the shoe insert. The ***posterior leaf spring*** is the most common type of thermoplastic AFO, Figure 2.8. Its purpose is to compensate for weak dorsiflexors by resisting plantar flexion. However, it provides minimal mediolateral control and may move on the leg both proximally and distally, if not held in place by a well-fitting, laced shoe, as the effective centers of rotation during walking do not coincide with the axis of motion of the anatomical ankle. This may result in large stresses and strains in the foot and calf soft tissues. Plastic AFO's therefore require carefully fitting.

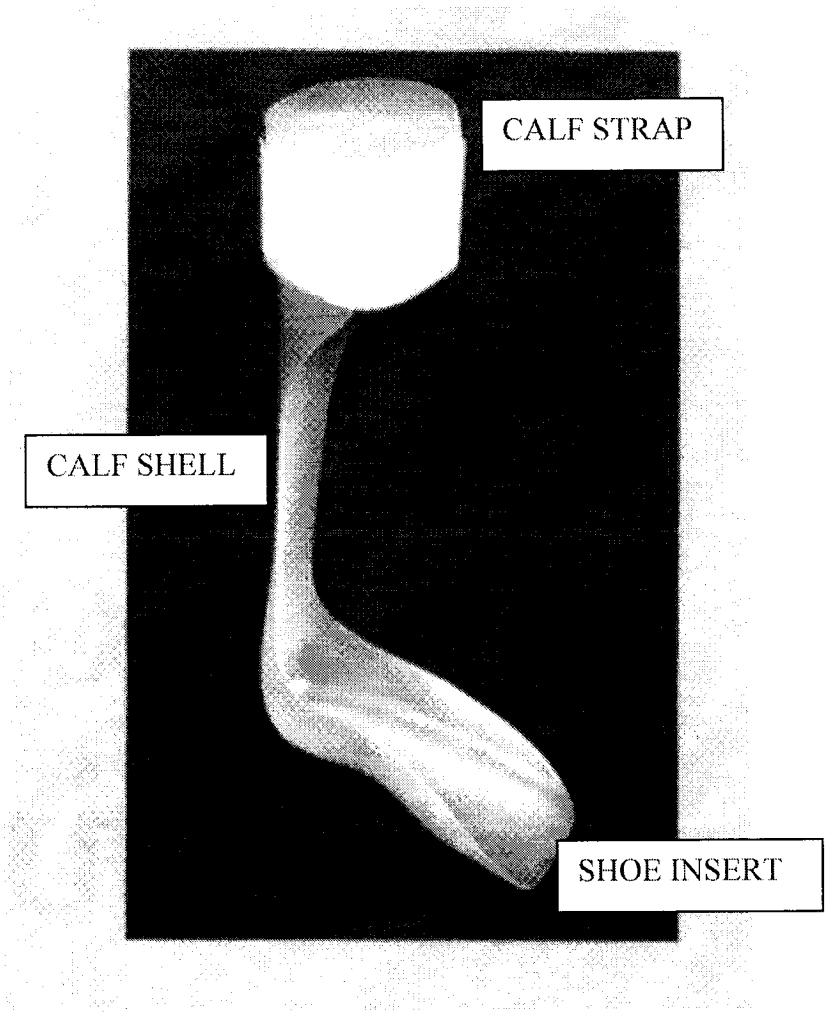

Figure 2.8 *The posterior leaf spring*

The posterior leaf spring orthosis is indicated for patients with peripheral nerve injuries, which cause flaccid foot drop, and has been found to improve ankle function of patients with cerebral palsy.

Despite the fact that plastic AFO's are available commercially as preformed stock items, they may be adjusted to some extent for individual patients, by heating and cutting the plastic during the fitting process. Ounpuu, et al.,[64] have shown that the posterior leaf

spring orthosis, when used to aid patients with excessive equinus or drop foot in swing, reduces equinus and allows ankle dorsiflexion in midstance.

Recently, the DACS (dorsiflexion assist controlled by springs) orthosis was developed by Yamamoto, et al.[100] with the aim of allowing the dorsiflexion assist moment to be easily changed and to prevent the generation of a plantar flexion assist moment, Figure 2.9. It also consists of a shoe insert and calf shell, but these parts are in fact separate and are connected at the ankle joint. There is an assist device located at the back of the ankle region that generates a corrective dorsiflexion assist moment, through the implementation of a compressive spring force. As the foot plantar flexes, the spring is compressed by a piston and an assist moment, proportional to the angle of plantar flexion, is generated. This angle of plantar flexion may actually range from 0° to 10°. When the foot dorsiflexes, a slider in the piston allows the ankle joint to rotate freely. The initial angle is predetermined by changing the length of the assist device, thus allowing control of the point at which the dorsiflexion moment begins to develop.

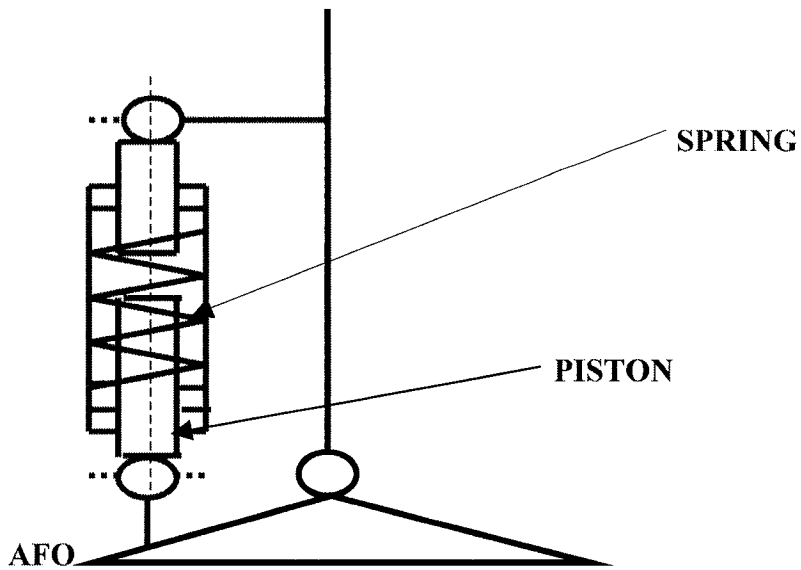

Figure 2.9 *DACS AFO in neutral position (following Yamamoto, et al.[100])*

The investigators found that dorsiflexion of the ankle joint was greatly improved when wearing all of the AFO's except for the posterior AFO. However, it was realized that the degree of hyperextension throughout the entire cycle and external rotation at toe off were much less when the patient wore the DACS AFO. They also claimed that the walking velocity was also much higher when using this AFO.

Hachisuka, et al.,[22] tested the DACS ankle-foot orthosis on hemiplegic patients. However, they found that it did not significantly improve their gait, nor did it improve their walking speed when compared with their gait when wearing their regular orthosis. However, it was recognized that the results of the experiment may have been caused by the patients being accustomed to a specific gait that allowed them to walk comfortable in their regular orthosis.

Lehmann, et al.,[43] found that hemiparetic patients exhibited shorter step length, longer stance duration, and subsequently, shorter swing duration that healthy subjects. They also found that AFO's increased walking speed. Wiley, et al.,[97] found that, before exercise, the use of an orthosis reduced active inversion by 11°, active plantar flexion by 6°, active eversion by 3°. After exercise, active inversion was reduced by 9°, active plantar flexion by 4°, active eversion by 2°, while there was no effect on active dorsiflexion.

The thermoplastic AFO, commonly referred to as the ***modified leaf spring***, gives increased mediolateral control, as the trim lines are more anterior. There is also more resistance to dorsiflexion and plantar flexion. The rigid, solid ankle-foot orthosis is used to treat patients with traumatic arthritis and other conditions for which the foot must be

completely immobilized. Thus, it is used by stroke patients and other patients with severe spasticity.[84]

To determine the axis about which dorsiflexion and plantar flexion occur with the use of a plastic AFO (PAFO), and to evaluate the fit during ambulation, Sumiya, et al.,[89] performed a study in which thirty hingeless plastic ankle-foot orthoses were flexed about a fixed ankle axis which was defined as being located at lateral malleolus height. The orthoses had varying trim lines about the ankle region that consisted of circles and their tangents. The centers of the circles were considered to be located at fixed ankle axis. Curves of radii of 20%, 40%, and 60% of the lateral malleolus height (the height from the bottom of the orthosis and the ankle axis) were trimmed from the orthoses, which were then bent to determine their flexibility. The orthoses were plantar flexed and dorsiflexed up to 16° in both directions, using still cameras to record lateral views. It was concluded that the instantaneous centers of rotation were focused on the junction between the calf shell and the shoe insert. The vertical movement of the calf-strap experienced by the subject during ambulation, was caused by the centers of the movement being deviated backwards from the ankle axis of the orthosis. This was a result of the 'effective' joint axis being malaligned with the ankle and subtalar joints. They recommended that in order to limit this effect, the straps should be fastened loosely or the shoe should be not be laced too tightly.

The ***spiral AFO*** consists of a shoe insert joined to a spiral that originates at the mediodistal aspect of the insert, passes around the leg posteriorly, traverses across the anterior aspect, and terminates in a calf band with a lateral opening, at the level of the medial epicondyle. It also has a calf band with a lateral opening. The goal of the design

of this orthosis is to allow some degree of rotation of the leg with respect to the foot in the transverse plane, yet ensure control of plantar flexion, dorsiflexion, inversion, and eversion.

The ***hemispiral AFO*** is similar to the spiral but differs in that the upright makes only a half turn around the leg. It offers more control for persons with equinus or varus foot. The orthosis may be twisted mediolaterally, thus allowing it to resist moderate forces and would therefore be prescribed for patients with flaccid paralysis or upper motor neuron lesions, which causes some spasticity and foot inversion. Additionally, dorsiflexion and plantar flexion result in the development of forces in the AFO causing improved toe pickup.

As previously mentioned, when the foot is in equilibrium, the moments about the ankle are equal, that is, $F_D * b = R * a$, where F_D is the force due to the dorsiflexor muscles, b is the distance of the dorsiflexors from the center of rotation of the ankle joint, R is the ground reaction force, and a is the distance of R from the center of rotation of the ankle joint. When $F_D * b < R * a$, as is the case of patients with weak dorsiflexors, the foot accelerates and hits the ground with a slap.

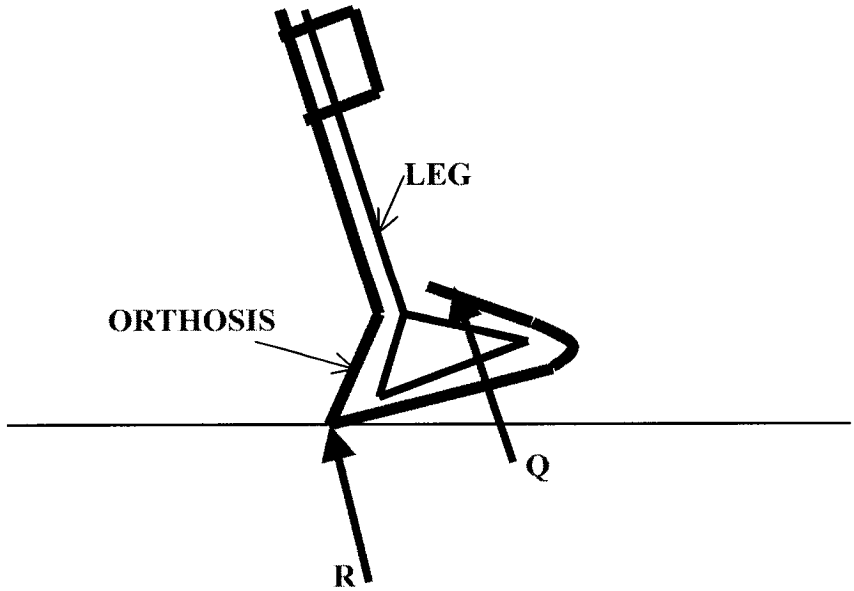

Figure 2.10 *Forces on AFO in early stance*

When an AFO is used, the ground reaction force acts on the heel of the AFO, which then exerts a supporting force, **Q**, on the foot. When this force acts behind the ankle joint, it causes the joint to plantar flex until there is no further action of a plantar flexion moment, that is, when its line of action passes through the ankle joint, Figure 2.10.

For patients with weak or inactive plantar flexors, an orthosis is used to prevent too much dorsiflexion during late stance, as the foot dorsiflexes passively until the line of action of **Q** passes through the ankle joint, Figure 2.11.

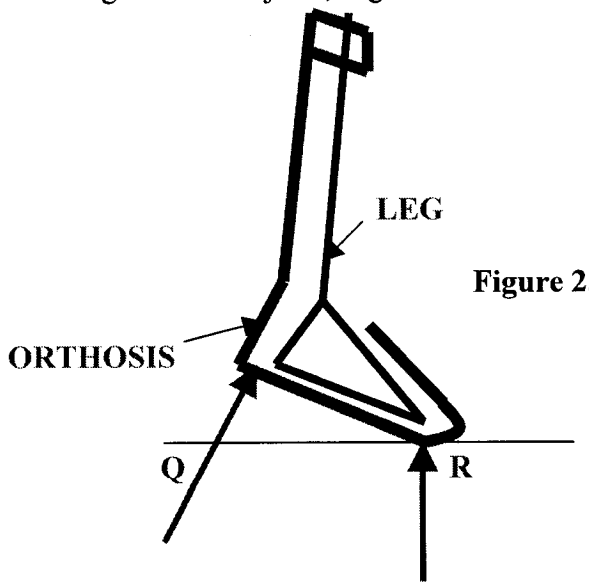

Figure 2.11 *Forces on AFO in late stance*

For patients with weak dorsiflexors, the force due to the foot weight opposed by the dorsiflexors is insufficient to allow ground clearance during swing. An AFO is used to compensate for this, Figure 2.12.

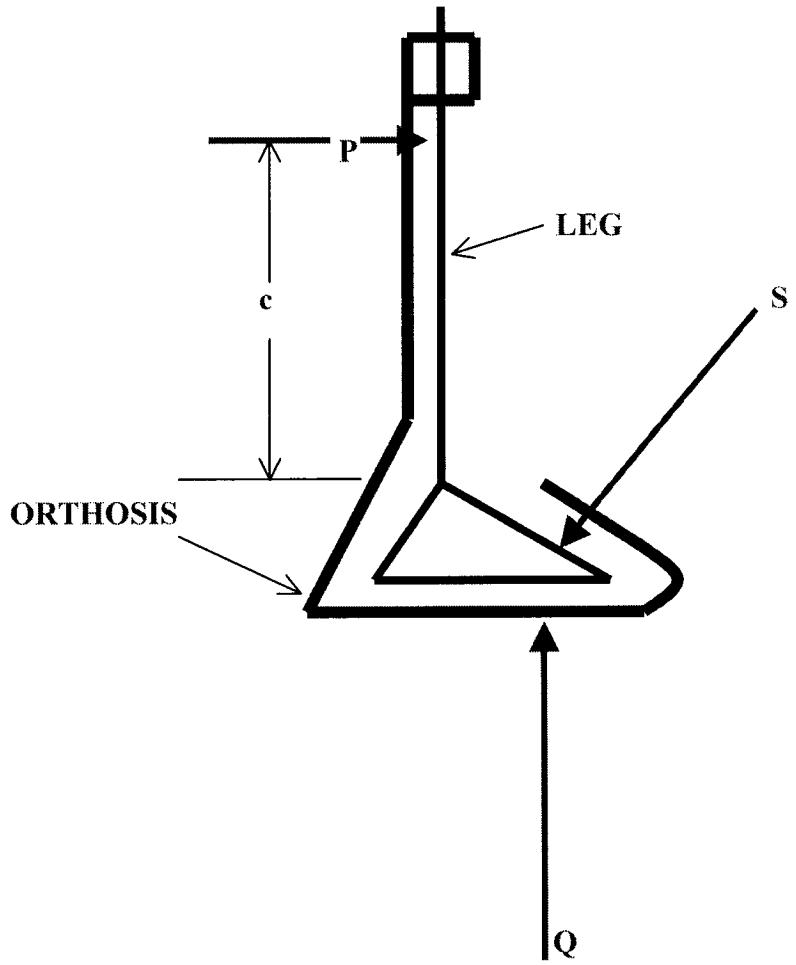

Figure 2.12 *Forces on the foot due to AFO*

The foot exerts the force, ***Q***, on the AFO, but downward motion is prevented by the force, ***S***, applied by the dorsal surface of the foot. As the foot plantar flexes, a force **P*c** is created about the ankle, equal to ***W*x***, which opposes the moment due to the weight of the foot.

The stress distribution in these different types of orthoses varies remarkably, as predicted by Chu, et al.,[15] through experimental stress analysis. Eight strain gauges, which measured horizontal and vertical deformation, were attached to five different models of AFO's at strategic locations, Figure 2.13.

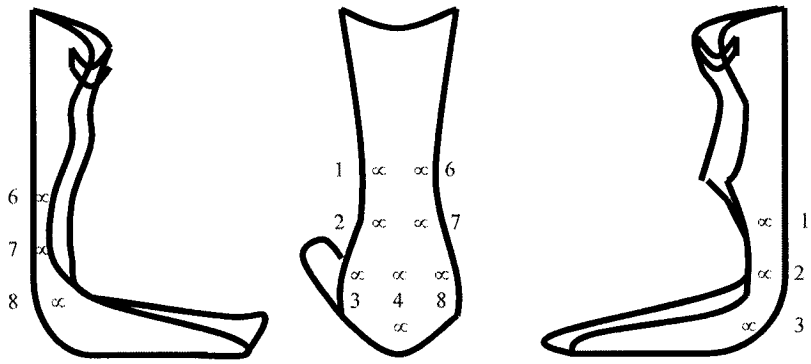

Figure 2.13 *The points of attachment of the strain gauges following Chu, et al.*[15]

These models, in order of increasing neck width, were the: (1) Flex (4.9 cm), which provides minimal support; (2) Standard (7.6 cm), which limited support; (3) Moderate (9.9 cm), which limits flexion, but provides more support; (4) Solid (11.8 cm), which does not allow any flexion, but still more support; and (5) Varus (11.8 cm), which has the widest neck, thus providing maximum support and allowing no flexion. The material thickness also varied between 0.39 cm and 0.41 cm. All of the AFO's were subsequently worn while the subject walked forwards at a slow and then fast pace, while running, while walking backwards, and during the acts of jumping, standing up, and lifting an object of 25 lbs. It was shown that the location and magnitude of the stresses incurred depended on both the activity of the patient was performing, and the type of orthosis worn. For example, it was found that the average peak stress increased with the flexibility of the orthosis, and was generally found to be located in lateral side of the

orthosis near the region of the ankle. As the width of the orthosis ankle region decreased, the stress concentration moved from the upper ankle to the lower ankle region. It was also noted that in all except the Varus orthosis, which had the widest ankle region, faster walking caused the peak stress concentration in the ankle region to move from both sides of the ankle region as seen in slow walking, to the lower lateral side of the ankle. This effect was explained by the increased magnitude of the loading forces that resulted with the increased velocity in addition to the shift in position of the resultant ground reaction force contact point. Running was noted to cause high stresses in the middle of the lower ankle region as well as the middle of the calf support section at heel strike. Backward walking appeared to have the same effect as slow walking on the orthosis whereas fast walking caused similar effects.

Jumping resulted in the generation of high stresses in the lower ankle and heel regions, and caused shear failure after a few successive trials. Standing up and sitting down did not create significant changes in the stress distribution in the neck region, but was influenced by the speed at which the maneuver was carried out. Additionally, object lifting seemed to create stress distributions similar to those found in standing. In general, it was found that each orthosis generated its own specific stress distributions with the peak stresses located at specific locations. For example, the Varus orthosis showed peak stresses at the ankle region lateral side, while the Flex orthosis exhibited peak stresses at the ankle and the lower lateral side of the ankle region. Peak stresses in both the Solid and the Moderate orthoses were generated at the ankle and upper ankle regions on both sides, while the Standard orthosis showed its peak stresses at the ankle and the upper ankle region on the lateral side.

The effect of the forces of walking on orthoses can also be illustrated using static element analysis. A quasi-static, 3-D finite element model of the ankle-foot complex and an ankle-foot orthosis was created using PATRAN[67] and analyzed using ADINA[92] by Chu, et al.,[14] to simulate the effect of a stroke patient with drop foot. The top of the model, about one-third of the height of an average lower leg (above the ankle joint), was considered to be fixed in all planes. It was also assumed that there was no slippage between the soft tissue and bones of the foot or between the orthosis and foot and that the upper portion of the leg was secured with a calf strap.

Toe drag, which occurred as a result of the drop foot, as well as toe off, were also described with concentrated nodal forces. Additionally, material properties were assumed to be linear, perfectly elastic, and isotropic and the velocity of the ground contact point was taken as 0.45 m/s at 78° with respect to the x-axis in the sagittal plane. Heel strike and toe drag were simulated by moving the ground upwards and toe-off by giving it negative velocity.

The model showed high stress concentrations in the heel and ankle regions of the orthosis and a maximum compressive stress at the center of the heel during heel contact. The peak tensile and shear stresses were found in the ankle region of the orthosis model during terminal stance at toe-off, at which time the compressive stress was found to be highest at the medial side arc of the AFO, in the neck region just above the shoe insert. Simulation of toe drag was not found to have much effect on the stress distribution. However, in general, predicted peak stresses in the increased with soft tissue stiffness and decreased with decreased AFO stiffness during heel contact.

In order to predict the behavior of a thermoplastic AFO, a mathematical model that incorporated beam theory was developed by Leone.[44] Three forces were applied to an idealized model of an AFO - a vertical force, a horizontal force in the direction of walking progression, and another perpendicular to the first horizontal force. The displacements and rotations at the location of the strap were assumed to be zero and a force in the y direction was applied to the sole of the orthosis to represent the weight of the foot and the area of contact at the base of the foot was assumed to be a distributed force in the metatarsal region, but was modeled as a concentrated force.

Assuming that the calf region and the plantar aspect area up to a specified distance were C-shaped, and the remainder resembled a flat plate, the moments of inertia for each portion were calculated accordingly. After determining section properties at a few points, the bending slopes and displacements were calculated using a computer program, the inputs of which were geometric parameters, load magnitude, and material properties. The displacements that resulted from the loads were calculated using twenty equal segments in numerical integrals. The results were checked using a GTSTRUDL finite element model. In addition, dial gauges to measure displacements were placed at points of interest on a posterior leaf spring[7] (PLS AFO), its calf strap clamped to the ground via a mold, and the portion of the ankle region not reproducible with beam theory firmly fastened to the ground. Assuming that the brace was unloaded during swing phase, and that the only forces acting on the brace were those that determined the angle of the foot with respect to the calf, loads were then applied in the y-direction only. The test values for P_x and P_y=4.45 N were found to be in close agreement with the theoretical values, and after applying a correction to the twist angle calculation, theoretical values of

P_z was also shown to agree with test values. It was therefore concluded that it was theoretically possible to predict the effect of an AFO on the human leg, and to use this prediction to custom-design AFO's.

The interface pressures between the molded AFO's and the foot were studied by Nowak, et al.,[62] while subjects performed several activities of daily living, including walking, standing up from a seated position, walking up stairs, and turning. The surfaces of the orthoses were each covered with 4 F-Scan sensors (see page 114 for discussion on F-Scan system). Each of these foot-shaped F-Scan sensors, which were made up of 960 sensing elements, were trimmed to fit the orthosis - 2 were placed in the calf area, 1 was placed in the heel and ankle area, and 1 covered the inner surface of the insert. 1 more sensor was then placed in the inner surface of the shoe and used as a control, and the last was placed underneath the calf strap. The motions typically mentioned above were then performed and the data recorded at a rate of 20 frames per second for 30 seconds. In addition, the temperature dependence of the sensor was studied by placing a static load on it while it was submerged in room temperature water, for 30 minutes. The temperature of the water was then raised to 7° above room temperature. The pressure on the sensor was recorded under both conditions.

It was discovered that the pressure at the shoe-AFO interface was higher than that at the foot/AFO interface, showing that the plantar foot pressures are indeed lowered. It was also noted that the calf shell experienced very little pressure, but that the strap moved substantially during walking, as a result of mismatch of the anatomical and orthosis ankle joint axes. The greatest forces occurred during mid-stance and stair–climbing. However, the pressure distribution was similar for the various activities performed. Furthermore, it

was discovered that the readings of the sensor did not change after being loaded for thirty minutes, but there was a slight change (3%) as the temperature was raised by 5°C and even more (11.7%) as it was raised by 7°C.

In order to analyze the effects of AFO design on ground reaction forces, the position of the center of pressure, and the timing of the stance phase events while walking were measured by Balmaseda, et al.[5] It was observed that using a thermoplastic AFO caused the stance phase to be shortened as a result of shortening of the midstance phase. There has been interest expressed in the effect that wearing shoes has on the distribution of pressure on the plantar surface of the foot. Experimental results have shown that the peak pressures under the heel are more uniform and heel contact time increases in shod gait compared to barefoot gait.[83] In addition, the peak pressure under the fifth to the first metatarsal heads increases and the medial side of the foot is loaded more when shoes are worn. When barefoot, however, the pressure distribution under the metatarsals is essentially more uniform.

Use of a prescribed rigid foot AFO has also been observed to have a significant effect on the duration and amount of pronation exhibited by patients, when compared to barefoot running.[6] Pronation was noted to begin later and end sooner with the use of an orthosis, as a result of the reorientation of the heel relative to the surface, while the maximum angle of dorsiflexion occurred later in the stance phase of the gait cycle. Additionally, an increase in running speed caused the maximum amount of pronation of the foot to increase. The orthosis wearers were also noted to exhibit greater flexion of the knee. Rao, et al.,[70] have also shown that balance and stability are affected by wearing an orthosis. In their study, a patient with diabetic sensory neuropathy (a result of peroneal

nerve palsy) who was unable to stand on either foot without falling and had impaired sensations of the hands and feet was asked to walk with and without the use of orthoses. It was observed that he fell less when wearing the orthoses. This may have been a result of the increased somatosensory stimulation of the feet with the supporting surface of the orthosis and the ensuing feedback.

A quasi-linear structural model of the plantar soft tissue was developed by Ledoux, et al.,[39] that provided a constitutive relationship for the non-linear viscoelastic characteristics of tissue. Using data derived from experiments involving loading of the foot, the model was shown to reflect a constant dissipation of load frequencies across a broad frequency range. With the assumtion of linear elastic behavior, and incorporating a linear elastic function and a frequency reduced relaxation function, the following equations were used to predict the frequency–sensitive behavior of the plantar soft tissue.

$$F(t) = \int G(t-\tau)(\delta F^e[\varepsilon(t)]/\delta\tau)dt \qquad (2.7)$$

$$F(\varepsilon) = A(e^{B\varepsilon} - 1) \qquad (2.8)$$

$$G(\tau) = 1+(\int S(\tau)e^{-t/\tau}\, d\tau)/(1+\int S(\tau)d\tau) \qquad (2.9)$$

$$S(\tau) = \begin{bmatrix} c_1/\tau + c_2/\tau^2, & \tau_1 \le \tau \le \tau_2 \\ 0, \tau < \tau_1, \textit{ and } \tau > \tau_2 \end{bmatrix} \qquad (2.10)$$

where parameter A was determined by the peak forces, and c_1 represented a damping constant. B represented the elastic and reduced relaxation constants, and c_2 damping

constant. The areas modeled included the subcalcaneal and submetatarsal regions of the foot.

To compare peak stresses and deformation patterns of the foot of a normal individual with those of an individual wearing an AFO, two (the first static and the other dynamic) two-dimensional finite element models were created using ADINA[92] finite element program by Lam, et al.[33]. The model were comprised of bones, tendons, and an orthosis, created using two-dimensional quadrilateral finite elements with four nodes in addition to ligaments, created using truss elements. Neglecting inversion and eversion and assuming that motion of the ankle joint occurred solely in the sagittal plane and that the subtalar joint was considered to be rigid in this same plane, models of the foot with and without the orthosis were created and used to determine deformation, flexion angle, as well as ligament and critical stresses. In the first model, the orthosis was closely attached to the foot, while in the second it fit loosely.

In the static model, a muscle force of 182 N was applied to the Achilles tendon, forces of 712 N applied to the heel and toe regions, and a uniformly distributed load applied to the base of the foot. It was also designed to indicate that the leg was fixed while the foot, attached with ligaments, rotated freely with respect to it, that the upper part of the orthosis was fixed to the leg, while the base of it supported the foot, and that the soft tissues were allowed to slip freely over the tibia.

The dynamic model differed in that an initial velocity of 0.45 m/s was applied to the model, a force of 184 N was applied to the Achilles tendon, while the heel force and forces at the base of the foot remained the same as in the static model.

Upon completion of the analysis, it was concluded that the orthosis reduces the planar flexion motion and peak stresses of the ankle-foot complex and that the maximum stresses, occurring at the top of the orthisis and at the base of the heel, were basically the same for the static and dynamic models. Additionally, slight changes in the shape of the orthosis resulted in a smaller planar flexion angle as well as smaller peak stresses.

A dual-axis ankle-control system was created by Campbell et al.[12], in order to allow the foot to rotate about the ankle and subtalar joints during ambulation, Figure 2.14.

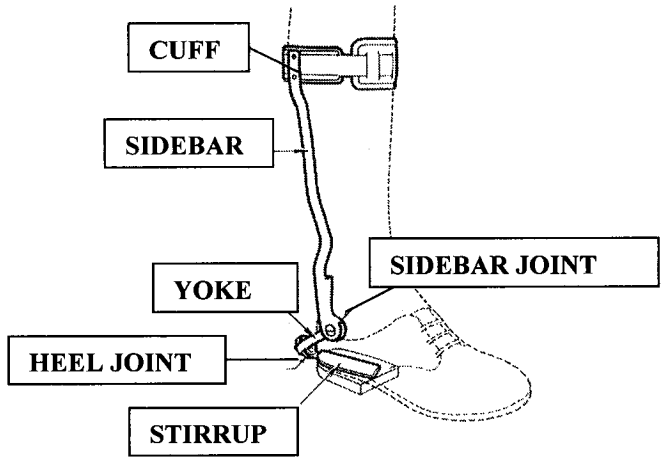

Figure 2.14 *The UC-BL Dual-Axis Ankle-Control Unit*[12]

The goal was to document a method to determine the locations of the anatomical axes and to fabricate an orthosis based upon the determined locations. This orthosis has three basic components – the stirrup and yoke (which are used together with the parts of an adjustable brace and an alignment transfer jig), and sidebar assemblies. The stirrup assembly is comprised of a channel and the stirrup, which attaches the shoe to the end of the subtalar joint that emerges from the heel (heel joint). The subtalar joint is taken as the line drawn 15° laterally off another line drawn along the longitudinal length of the shoe, and intersecting a line drawn across the base of the shoe between the projections of the

ankle joint intersections with foot. In order to allow the patient to wear more than one pair of shoes with the assembly, the shoe can be disconnected from the assembly by sliding the stirrup into and out of the channel. A flanged nut, a flanged screw, a locking screw, and Nylatron washers connect the stirrup to the yoke, and the yoke and sidebar are attached by a sidebar-joint pivot nut and screw. The sidebar is composed of a standard aluminum or steel sidebar and a cuff, which attaches the brace to the lower leg. Rubber bands, between the heel and yoke prevent eversion. The adjustable yoke is then attached to the shoe, to the channel at the base, and to the medial end of the ankle joint, by a pin through a previously taken cast of the leg/shoe, upon which the locations of the medial and lateral ends of the ankle had been marked, Figure 2.15.

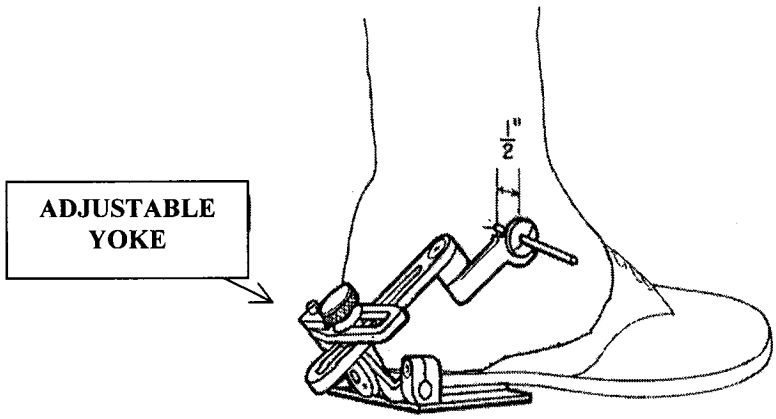

Figure 2.15 *The yoke attached to the shoe*[12]

The adjustable yoke is then adjusted until the pin can pass freely through the yoke, and then locked. A strip of lead is then bent to follow the contour of the shoe form the heel to the ankle joint, at about a distance of about 0.5 inches. The angle between the surface of the heel joint of the adjustable stirrup and the base of the adjustable stirrup, and a stirrup blank is bent to the angle measured, Figure 2.16.

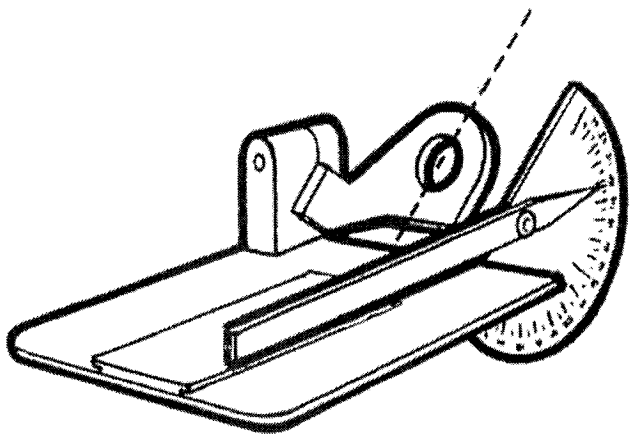

Figure 2.16 *Measuring the angle between the heel joint surface and the adjustable stirrup base*[12]

The transfer jig is then fit to the adjustable yoke and locked, the yoke removed from the jig and a yoke tang (heel joint) and tongue (sidebar joint) placed into the transfer jig, Figure 2.17.

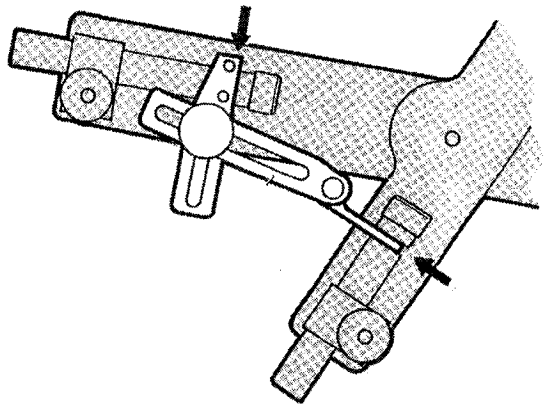

Figure 2.17 *Transferring the alignment of the yoke to the jig*[12]

The tang is first bent to an angle of 45° for convenience. The surfaces of the tang and tongue are then aligned (mated), with an overlap of about half an inch, Figure 2.18.

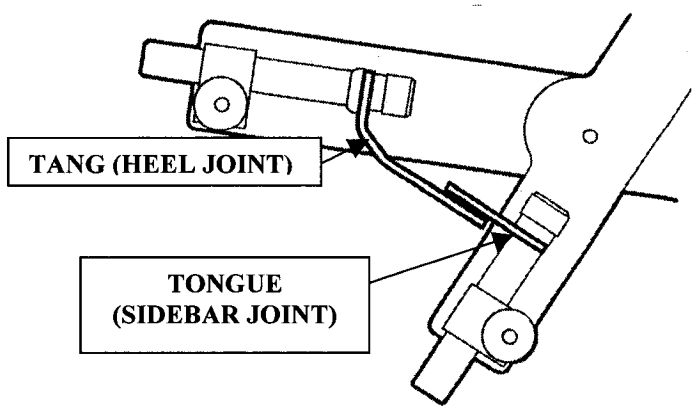

Figure 2.18 *Bending the tang and tongue*[12]

The stirrup and yoke are then assembled, and the stirrup installed into the channel, and the cuff attached. (Further details of the procedure can be found in the papers by Lamareaux[34] or Campbell[12]). The adjustable yoke is then removed and the yoke of the brace is made in the fixture, by bending the yoke and attaching it to the sidebar (ankle) joint.

The yoke alignment transfer jig may also be used to connect the ankle and subtalar joints, which are skew axes, using[34]; (1) the fact that any two non-intersecting and non-parallel (skew) axes have a unique, mutual perpendicular, the lengths of which is the minimum distance between the axes (L); (2) the angle between the two axes, when they are viewed along the mutual perpendicular (A); (3) the distance of the face of each joint from the mutual perpendicular (D_1 and D_2), Figure 2.19.

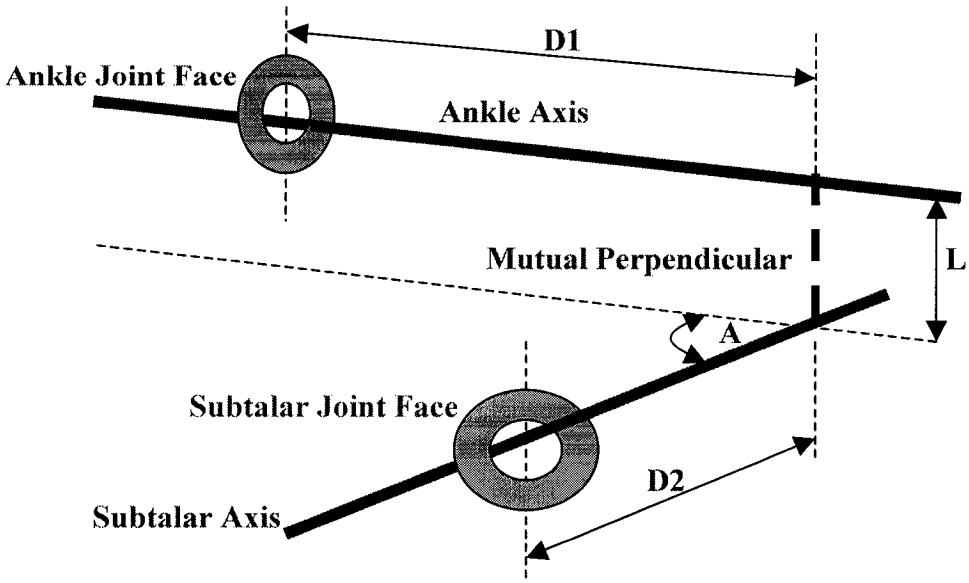

Figure 2.19 *The relationship between the joint axes and the defining parameters*[34]

L is first set and remains constant while the other parameters are set interdependently. The adjustable yoke is then placed in the yoke alignment transfer jig, and adjusted to match the yoke, then locked. The procedure then continues as before.

Lamoreux proposed that the ankle joint be initially defined as passing approximately through the extreme distal tips of the lateral and medial malleoli, and the subtalar joint as 15° of internal rotation of the heel joint. The foot is then moved about the ankle joint, with little or no motion about the subtalar joint, and if there is any linear misalignment of the ankle axes of the foot or orthosis, the calf band will move along the calf and the sidebar may move anteroposteriorly relative to the leg. Adjustments are then to eliminate these motions. The foot is then moved about the subtalar joint only, the calf band will rotate or move proximodistally on the leg, and the sidebar will swing

mediolaterally if there is any misalignment. The alignment is adjusted until there is little or no such motion.

The first models described in this chapter were either quasi static or static, however as was also detailed, the motion of the ankle-foot complex has also been studied with dynamic models. These models were not created with the same methods as the static or quasi-static models, as software that analyzes motion does not analyze models that are composed of thousands of elements, such as brick elements, but models that are composed of specific two-dimensional or three-dimensional geometric shapes. This is considered to be a reasonable approximation as, after the data describing the location and size of the thousands of elements of the static models has been entered into the system used to analyze it, rigid bodies are subsequently created. In some cases, groups of bones that are adjacent to each other are combined to create one body. One such model was the model created by Ledoux, et al., which utilized 8-, 4-, and 2-noded elements to create a mesh, but later simplified the model by creating one body out of several groups of bones that were close to each other. The motion was also prescribed by the application of forces, rather than specifying the actual angular displacements of the components with respect to each other. In addition to these models, other dynamic models are also based solely upon mathematical relationships between the components. The model of the orthosis created by Leone was intended for use in the design phase by specifying the corrective forces required by the patient. On the other hand, the model detailed by Leardini, et al., was created to study the characteristics of passive motion of the ankle-foot complex, suggesting that the foot follows a preferred kinematic trajectory. It did not predict forces that were generated due to the motion. The viscoelastic model created by

Gilchrist, did take into consideration the driving inputs of resultant ankle joint forces and moments. Some dynamic models were even created using the cadaveric foot, as in the case of Stahelin, et al., thus allowing the investigators to visualize the movement of the bones with respect to each other. Of particular interest here, however, are the models proposed by Halvorsen et al.,[23] and Gamage et al,.[20] which estimated the axis and center of rotation of a hinge joint. The methods utilized the assumption that each point on the rotating body has a circular path, and lies on the surface of a sphere, with a radius equal to the distance from the point to the center of the sphere.

Although the orthoses currently in use are effective to some degree, they do not take into consideration the needs of patients on an individual basis. For example, off-the-shelf models, such as the posterior leaf spring orthosis, help patients with drop foot, however the muscles of different patients are impaired to varying degrees. Thus, whereas the AFO may be very effective in some patients, it may not be very effective at all in others. Moreover, most models do not take into consideration the motion of the axis of the anatomical ankle or of the subtalar joint axis, leading to varying degrees of discomfort in different patients. As demonstrated by Sumiya et al.,[89] the results of such malalignment include the vertical movement of the calf-strap during ambulation. Therefore, patients are often required to return for several fitting sessions. The same would apply for the other orthoses, such as the spiral and hemispiral orthoses, as they might offer more flexibility, but once again do not take into consideration the individual patient's needs.

3. METHODS

3.1). *Objectives*

The purpose of this work was to create a design for a dual axis ankle-foot orthosis (AFO), permitting as near normal as possible ankle flexion-extension and subtalar inversion-eversion, during stance and gait. This was accomplished by developing a **JOINT AXIS DIRECTION AND LOCATION** method. The orthosis developed allows inclusion of rotation limits to constrain motion about each axis, as required by a given patient. This enables the orthosis to accommodate the biomechanical requirements of a broad range of patients, optimizing their biomechanical function, minimizing their strength and energy expenditure for stable stance and gait, improving their comfort and eliminating adverse effects from intrusive stresses and moments that arise during stance and gait, from mismatched or nonexistent orthotic joints that hinder the patients' natural movement about their anatomical joints.

3.2). ***Methodology***

To accomplish the proposed objectives, the following protocol and constituent tasks, were developed:

(1) Derive design specifications for an articulated dual axis (ankle and subtalar joint) AFO.

(2) Derive a defining set of equations that spans the solution space (R^3) and can be used to calculate joint centers and respective axis orientations.

(3) Develop an accurate, expeditious, and numerically robust method for solving the defining equation set, and implement the respective algorithm in MATLAB.

(4) Compute the respective joint axes and joint centers relative to a designated local reference frame for a set of measurement data from: (a) a mechanical model with known axes and joint centers: and (b) a human experimental subject.

(5) Design and construct a dual axis AFO from the respective measurements of the project experimental subject.

(6) Test and analyze the performance of the dual axis AFO in comparison with the subjects': (1) normal gait without an orthosis; (2) gait with a conventional articulated, plastic, posterior leaf spring AFO; and (3) gait with a conventional one degree of freedom, articulated, dorsiflexion assist AFO.

Work on each of these respective tasks included the following subtasks.

3.2.1). ***Derivation of mechanical specifications***

In order to obtain the information needed to determine the orientation and location of the subtalar and ankle joint axes of rotation, the ***MacReflex Qualisys Motion Analysis System (Qualisys, Inc., East Winsor, CT, USA)*** was utilized. The system was used to measure and track the spatial trajectories of the fiduciary anatomical landmarks, pre-selected and marked with photoreflective markers.

The Qualisys system consisted of: (1) five CCD video cameras, with high intensity infrared strobes to illuminate and capture the spatial location and photoreflective markers on the tibia/fibula, heel, metatarsals, and navicular; (2) a video processor, which detects and triangulates the spatial location of the markers; and (3) computer-controller, to synchronize camera output, and process and store the measurements. The cameras, which record at 60 frames per second with an exposure time of 0.25 ms, and uses optical filters to remove visible light, are placed around the space containing the object/subject to be studied, so as to capture a maximum number of markers throughout as much of the trial as possible, Figure 3.1.

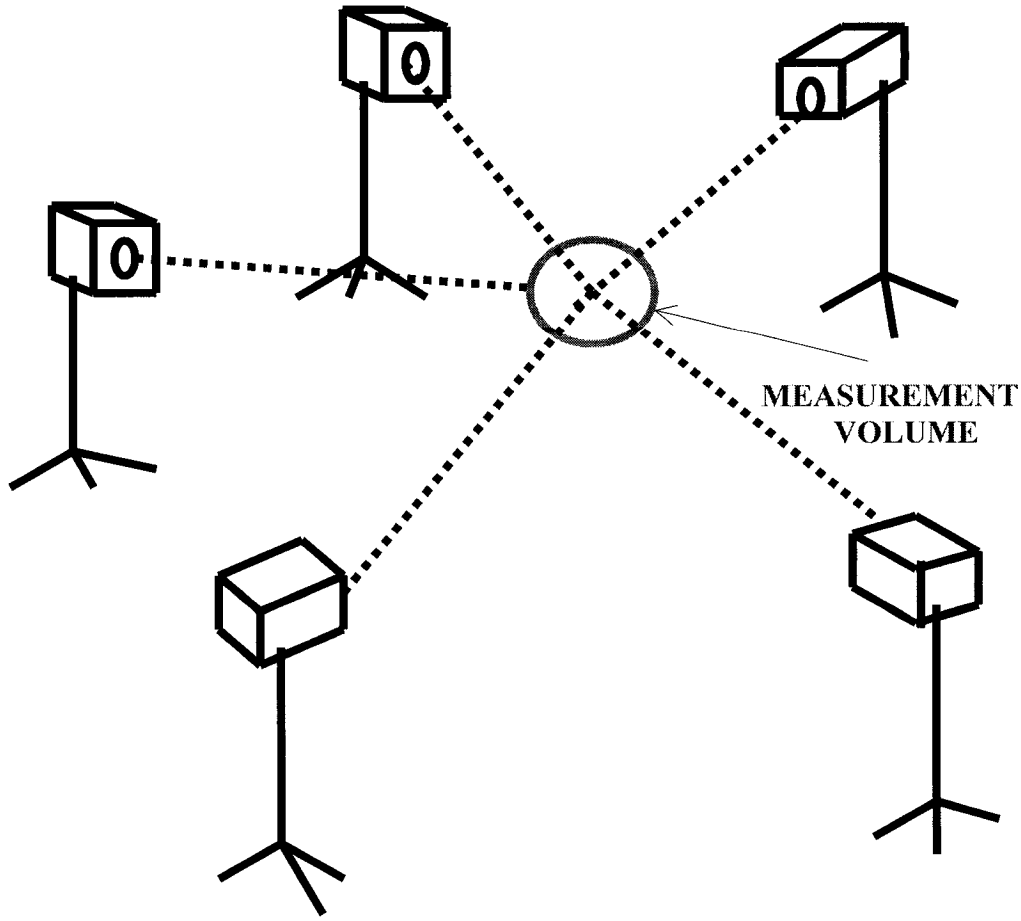

Figure 3.1 *The placement of the cameras of the Qualisys System*

The Qualisys video processor locates the center of each marker by scanning each of the recorded video frames of each of the cameras to detect bright spots corresponding to markers and calculating their optical centers. The two-dimensional coordinates of each detected marker, along with their horizontal and vertical size, are stored for each camera by the computer. The MacReflex software is then used to process the resulting data triangulating the locations of the markers from each frame of each camera in relation to their pixel location, and compared to known distances on a calibrated machined test frame. The resulting output from the MacReflex system can be read into a Microsoft Excel spreadsheet, where the data can be analyzed in a variety of forms including position versus, velocity versus time, and angle versus time. Data from at least two

cameras is necessary to determine the three-dimensional position of each marker. This information may be viewed in the transverse, coronal, and sagittal planes.

The ***Vicon Motion Analysis System (Vicon Motion Systems Inc., 9 Spectrum Pointe, Lake Forest, California, USA)*** is another video motion capture and analysis system. Eight high-resolution cameras, each with a ring of LED strobe lights fixed around the lens, are positioned around the perimeter of the space – the ***capture volume*** – to be studied. The cameras and system are calibrated, and photoreflective markers attached to the subject. All are detected and their position in space analyzed and recorded in the system Datastation/Workstation.

3.2.2). *Derivation of a set of equations used to calculate ankle and subtalar joint centers and joint axis directions*

In order to define the ankle and subtalar joint axes of rotation, it was necessary to find the orientation of each axis, as well as the location of a point on each axis, by using the **JOINT AXIS DIRECTION AND LOCATION** method, which was developed as part of the thesis work. The process was first carried out to define the ankle axis. To derive an equation set, the solution of which would give the location of the ankle joint center (that is, a point which lies along the axis of rotation), it was assumed that all points on the medial tibial plateau (MTP) were equidistant from the joint center of rotation, Figure 3.2. That is,

$$L1 = L2 = L3 = L4 = L \qquad (3.1)$$

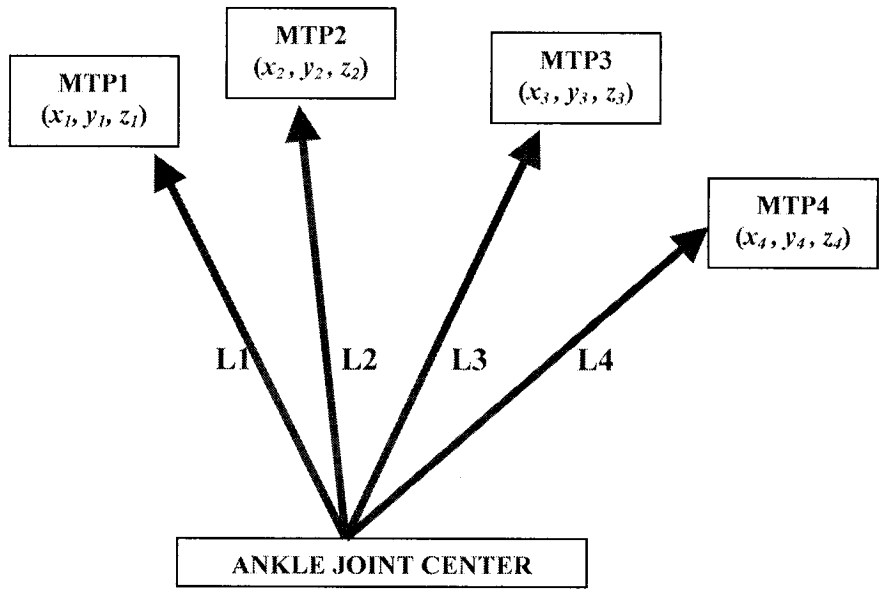

Figure 3.2 *The distances from the four MTP locations to the equivalent ankle joint axis*

The following equation was utilized:

$$[MTP_i(x) - AJL\ (x)]^2 +$$
$$[MTP_i(y) - AJL\ (y)]^2 +$$
$$[MTP_i(z) - AJL\ (z)]^2 - L^2 = 0 \qquad (3.2)$$

For i = 1, 2, 3,4

where,
(1) AJL is the equivalent ankle joint location; (2) MTP is the medial tibial plateau;
(3) L is the distance from each of the MTP locations to the ankle joint, which are assumed to be equal.

The same equation was used for four of the MTP locations, forming a set of four equations, with four unknowns, *x, y, z*, and *L*.

A similar method was used by Silaghi,[82] however it incorporated a weighted average of the center of rotations of the markers. The method used by Gamage, et al.,[20] also assumed that vectors on a rotating body lie on concentric spheres. However, Gamage's solution was reached through the use of geometry and algebraic manipulation.

The direction of the ankle joint axis was found by recording the motion of the tibial section of the leg (MTP) relative to the foot with the Qualisys system, with no (or as little as possible) motion about the subtalar and other joints of the foot. The direction of the joint was found by taking the cross product of the direction vectors of three points (MTP_1, MTP_2, and MTP_3) along the path of the MTP, as shown below, Figure 3.3. This technique is similar to that of Reuleaux.[73]

The entire process was then repeated for the subtalar joint, allowing little or no motion about the ankle or other joints. Inaccuracies in the results obtained by the method

were limited, by constraining the range of motion of the leg (MTP), over which measurements were used for the calculations. This helped to ensure that the motion at the respective joint was limited to one degree of freedom.

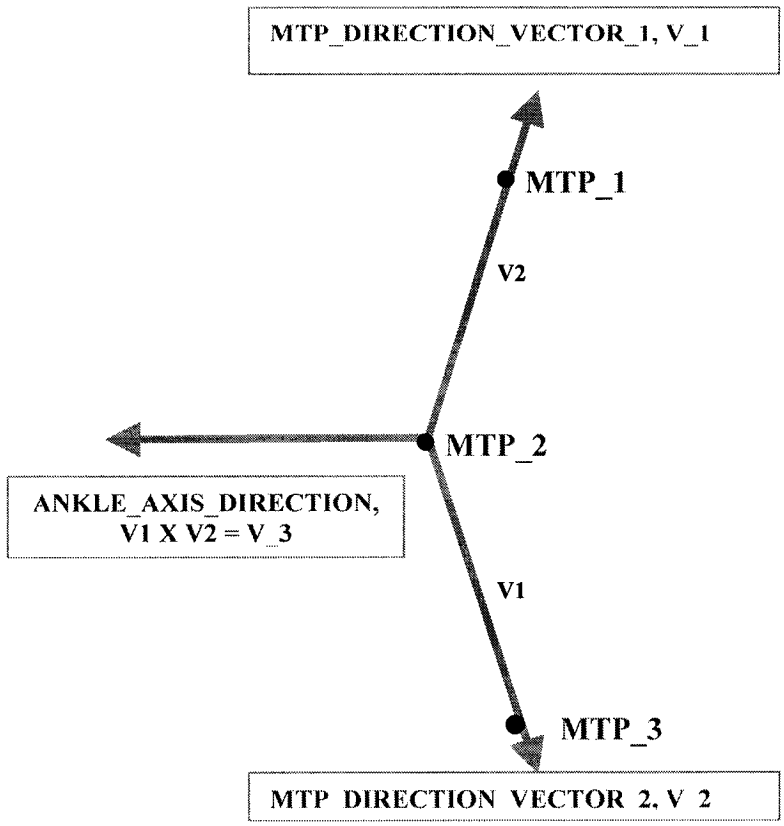

Figure 3.3 *MTP direction vector and ankle joint axis direction (top view)*

The calculations were carried out using data sets such that the lengths of the vectors V1 and V2 were nearly equal. It was found that, regardless of the actual distance between the MTP points used, the results were more accurate when the datasets were chosen so that respective distances were equal in magnitude. The process of finding the joint axis and directions was carried out on each of the data sets, and the axes (directions and locations) plotted.

3.2.3). ***Determination of an accurate, expeditious, numerically robust method, solving the equation set.***

In the method developed in this work, the equations were solved using numeric computational nonlinear optimization methods, as the measurement data from the Qualisys system was not exact, that is; the ankle and subtalar joints are not perfect hinge joints; the photoreflective markers move on the body; there is optical and electrical noise in the system, as well as round off error. In particular, Davidon's 'Variable metric method for minimization,[18] was used, Appendix A. A number of non-linear optimization methods were investigated, but Davidon's method was found to consistently afford the most accurate solutions with the fewest computational iterations.

In creating the program to solve the system of equations defining the location and orientation for the "best" equivalent ankle joint/subtalar joint axes, the main concern was to find a computational method that would solve the system of equations and converge to a value with minimum "cost". The major factors to be considered were: (1) the system of equations was non-linear; (2) new iterations would not necessarily bring more accurate answers, as the distances between the MTP and the ankle joint center could vary without getting closer to a solution with smaller "cost"; and (3) the three unknowns were quite different, that is, x, y, and z were relative spatial coordinates, and the fourth variable was distance, all of which could (and did) have values with different orders of magnitude. Several methods for solving nonlinear systems of equations were considered initially, including Newton's method, Broyden's method, the Steepest Descent method, and the Continuation method, Section 4.3. The MATLAB programs that were written to solve the system of equations were considered to be accurate, as they were validated by solving

several systems of equations (linear and non-linear), with known solutions, prior to being used to solve the system of equations, defining the respective ankle axis location and direction.

The first method considered was Newton's method, that updates the estimate of the root, x_i, using the Jacobian, $J(x_i)$, with the following equation:

$$x_{i+1} = x_i - J(x_i)^{-1} f'(x_i) \qquad (3.3)$$

which converges quadratically.

The next method considered was Broyden's method, which is a generalization of the Secant method, requiring n scalar functional evaluations per iteration. The Jacobian of Newton's method is replaced with an approximation matrix, which is updated with each iteration. However, unlike Newton's method, it does not converge quadratically. At best, it converges superlinearly. It is a quasi-Newton's method, with the derivative of the function to be solved being replaced with the corresponding difference value:

$$f'(x_1) = [f(x_1) - f(x_0)]/(x_1 - x_0) \qquad (3.4)$$

The Steepest Descent method is often used when there is no known good first approximation, however, it lacks the speed of the Newton and quasi-Newton methods. Although it converges linearly, it will generally converge to an acceptable first estimate. It entails approximating an initial value for the function, h, where:

$$h(x_1, x_2, x_3, x_4) = \Sigma [f_i(x_1, x_2, x_3, x_4]^2 \qquad (3.5)$$

The goal is to find h such, where:

$$f_1(x_1, x_2, x_3, x_4) = 0 \qquad (3.6)$$

$$\vdots$$

$$f_4(x_1, x_2, x_3, x_4) = 0$$

A direction from the initial value of x is then found so that the value of h decreases, and a new value of x is found by moving in this new direction. The process is repeated until h is sufficiently close to or equal to zero.

The Continuation method uses a parameter, μ, which is assigned a value between 0 and 1, to solve a problem of the form $\mathbf{F(x) = 0}$. If there exists a nonsingular Jacobian and a constant **W** with $\| \mathbf{J(x)^{-1}} \| \leq \mathbf{W}$ for all of real values of **x**, then for any initial value of x, there is a unique function, $\mathbf{x(\mu)}$, so that

$$\mathbf{Z(\mu, x(\mu)) = 0,} \qquad (3.7)$$

for all values of μ between 0 and . Additionally, if $x(\mu)$ is continuously differentiable and

$$\mathbf{x'(\mu) = -J(x(\mu))^{-1}F(x(0))} \qquad (3.8)$$

for all real values of μ between and including 0 and 1. It determines four constants:

$$\mathbf{k_1 = \lambda[-J(w_j)]^{-1}F\{x(0)\}} \qquad (3.9.1)$$

$$\mathbf{k_2 = \lambda\,[-J(w_j+0.5*\,k_1)]^{-1}F\{x(0)\}} \qquad (3.9.2)$$

$$\mathbf{k_3 = \lambda[-J(w_j+0.5*\,k_2)]^{-1}F\{x(0)\}} \qquad (3.9.3)$$

$$\mathbf{k_4 = \lambda\,[w_j+\,k_3)]^{-1}F\{x(0)\}} \qquad (3.9.4)$$

where the interval [0, 1] is divided into **N** parts with mesh points

$\mu_j = j*\lambda$ for j = 0.....N (3.9.5)

and, $\lambda = (1-0)/N$ ***(3.9.6)***

Then, $x(\mu_j+1) = x(\mu_j) +(1/6)(k_1+2 k_2+2 k_3+ k_4)$

$= w_j + (1/6)[k_1+2 k_2+2 k_3+ k_4]$ ***(3.9.7)***

where, w_{ij} is an approximation to $x_i(\mu_j)$

and, $x(\mu_n) = x(1)$ is the solution. ***(3.9.8)***

Davidon's method utilizes a non-negative symmetric matrix or metric, which is improved upon with each consecutive iteration, Appendix A. The rate of convergence and accuracy of the method was enhanced by defining the initial matrix as a diagonal matrix, whose components were the squares of the uncertainties of the unknowns (the coordinates of the joint center and equal distance from the markers, *x, y, z, and L*). The matrix linearly mapped all changes in the gradient onto changes in position. Rather than use a unit diagonal matrix, the unknowns were then immediately updated using a modified initial matrix, **U**:

$$\mathbf{U} = \begin{bmatrix} \mathbf{1, 0, 0, 0} \\ \mathbf{0, 1, 0, 0} \\ \mathbf{0, 0, 1, 0} \\ \mathbf{0, 0, 0, 5000} \end{bmatrix}$$

The final value of 5000 was used to indicate the expected difference in the rate of change of the last of the four unknowns, the distance between the MTP and the joint center. This adjusted matrix changed the speed with which the program solved the equation set, as the first guess was closer to the actual answer than the unit matrix would have brought it.

3.2.4). *Determination of the location of the axes and joint centers in a local coordinate reference system*

Having calculated the axes' location and direction vectors relative to the Qualisys measurement global reference frame, a new, local coordinate system relative to fiduciary landmarks on the subject' leg was selected, and the transformation matrix, between the local and global coordinate systems, was calculated. The local coordinate system was then located on an optically digitized model of the leg, as well as on a plaster cast of the subject's leg, as the locations of the landmarks were transferred to the cast, by marking their positions on the leg with indelible ink. By utilizing the transformation matrix, the locations of the calculated ankle and subtalar joint axes were then located on the cast and the optically digitized model, relative to the preserved locations of the Qualisys landmarks.

To determine the accuracy of the method proposed, three wooden models of the tibia and foot were fabricated. The first model consisted of a single wooden foot-piece, connected by a hinge joint, obliquely oriented to the XZ plane, Figures 3.4 (a) and (b), to a wooden leg piece. A rod (7 inches long), the ends of which extended a few inches from the hinge itself, was placed within the hinge joint, in order to allow markers from the Qualisys system to be attached to the ends. The tibial and pedal segments of the model could thus rotate freely without bumping into the markers. Markers were also placed on the left and right sides at the proximal end of the tibial segment of the model. This first model was then used to simulate the motion about the ankle joint alone.

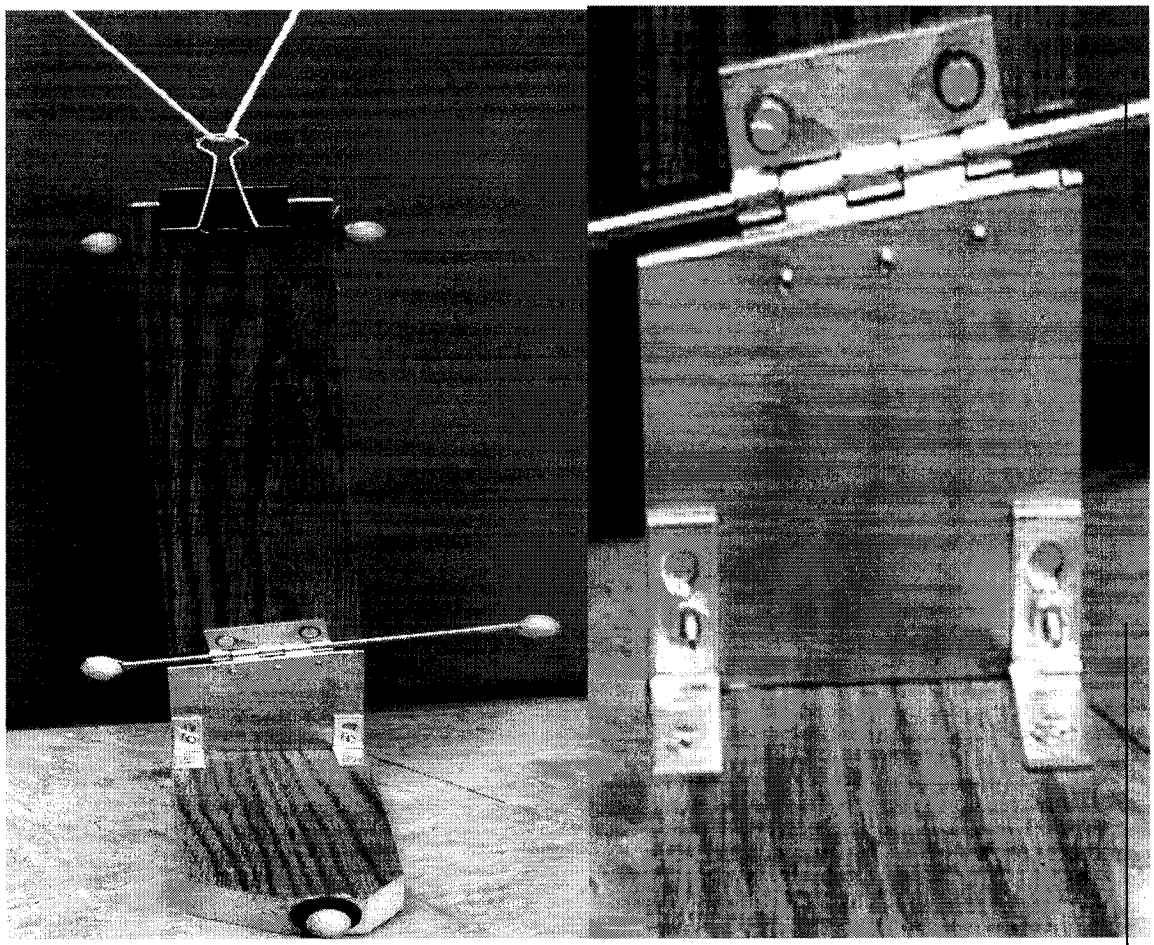

(a) **(b)**

Figure 3.4 *(a) Model with ankle joint; (b) Model enlarged*

The second model was made similar to the first, but with a subtalar joint instead of an ankle joint, Figure 3.5. A rod was also placed through the axis of this joint to facilitate dynamic measurement without interfering with the optical markers. However, in addition to ensuring that the markers, again placed at the ends of the rods, did not come into contact with the model during rotation, it was also crucial to ensure that the marker at the heel end of the joint never contacted the ground - a seemingly obvious, but easy to overlook factor, Figure, 3.5 (a) and (b). Markers were also placed on the proximolateral and medial sides. This model was then used to investigate motion about the subtalar joint axis alone.

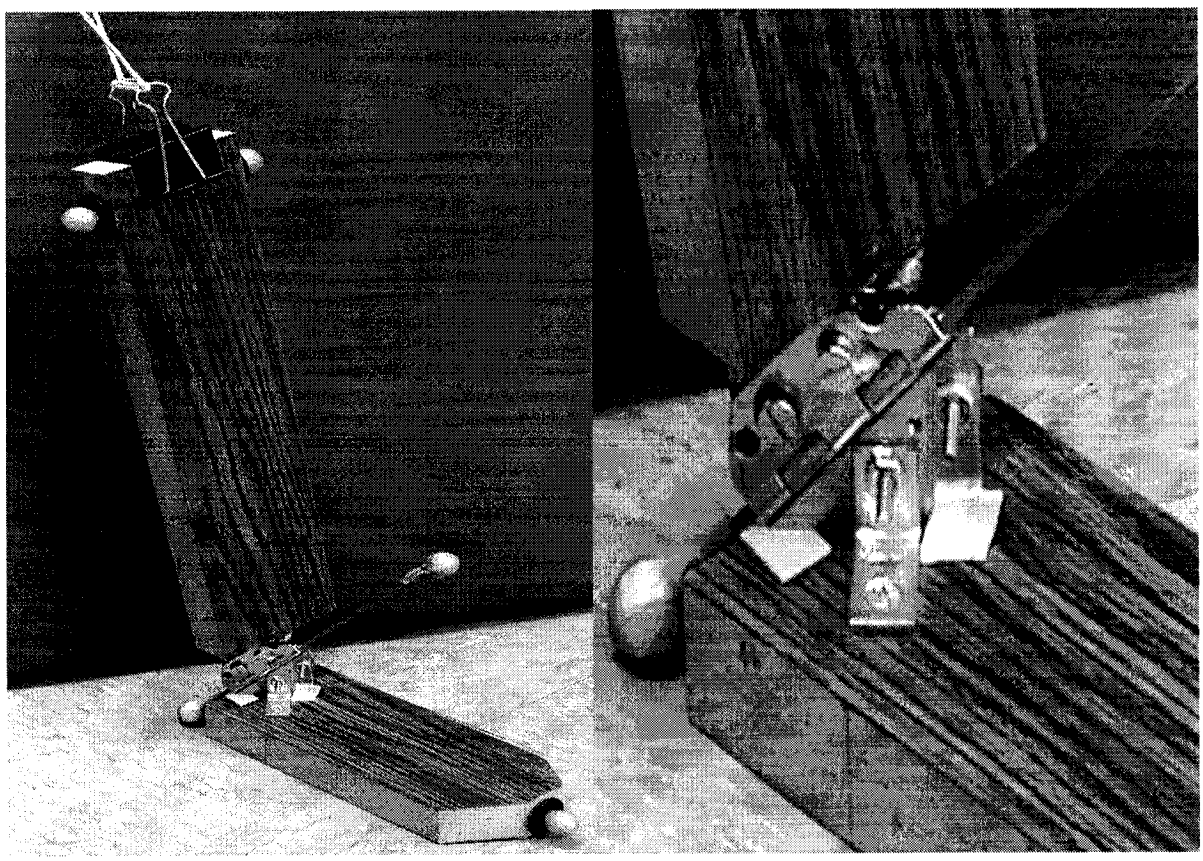

Figure 3.5 (a) *Model with subtalar joint only; (b) Model enlarged*

The third, and most important, model had both an ankle and a subtalar joint. This allowed rotation about either the ankle or subtalar axes, or about both of the axes simultaneously. To achieve this, the joints were modified so that they could be locked, by screwing in removable, metal plates, Figures 3.6 (a) and (b). When using the procedure with patients, they too would be asked to move their feet with as much joint independence as possible. Metal rods, with markers, were placed in the axes of the ankle and subtalar joints. Markers were also placed on the proximolateral and medial sides. The third model was more realistic, as it had both joints.

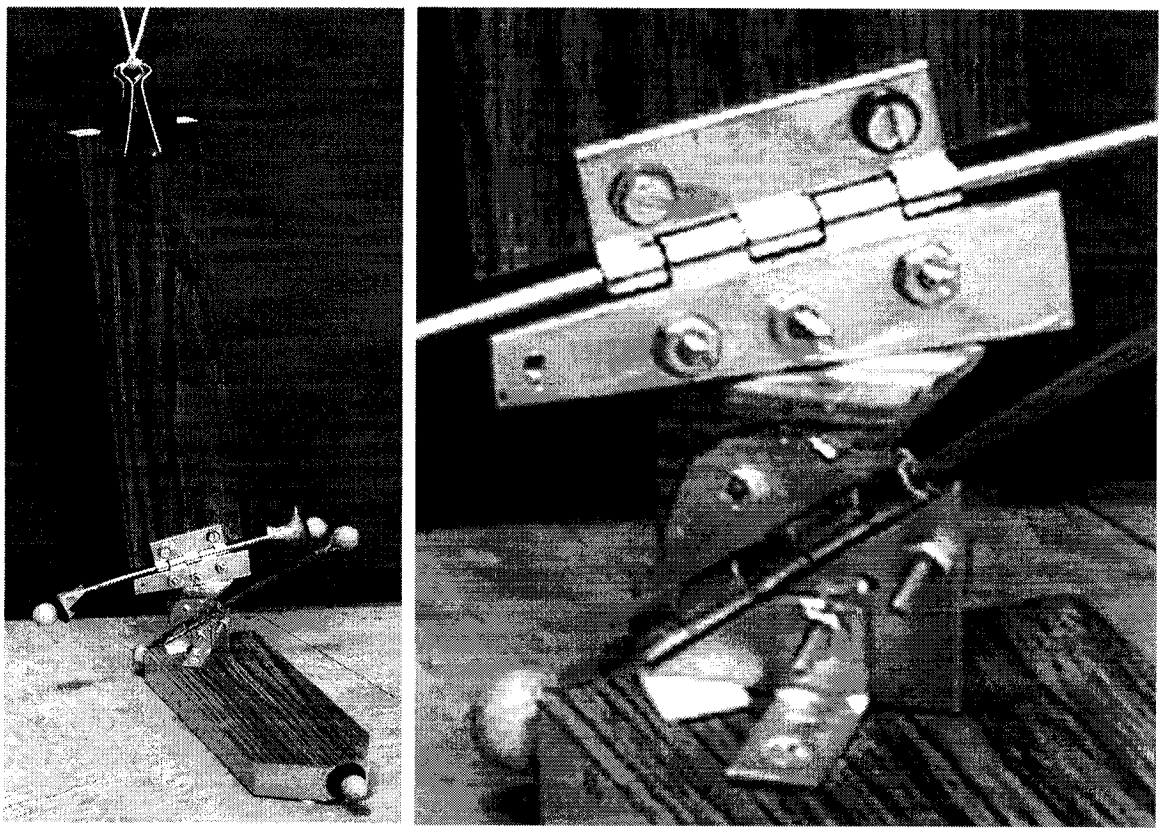

Figure 3.6 *(a) Model with subtalar and ankle joints; (b) Model enlarged*

The foot section of the models were secured to the floor by placing a strip of double-sided adhesive tape, on their plantar surface and adhering then to the floor. The x, y, and z coordinates of each of the markers on each of the models, were measured with the Qualisys system, as the models were rotated about their respective axes. The models were moved by a length of string attached to the proximal end of the tibial segment of the model (knee). The ends of the string were pulled to and fro, rotating the tibial segment about the joints, without obstructing the camera's view of the model.

The ***experimentally calculated*** locations and orientations of the joint axes were compared with the ***measured*** locations and orientations. The experimentally calculated orientation was derived by finding the direction of the vector between the markers of the Qualisys system, which had been placed at the ends of the rods through the hinge, while the measured locations and orientations were computed using the **JOINT AXIS DIRECTION AND LOCATION** method. To establish the accuracy of the method, the experimentally calculated locations and orientations of the axes were then compared to the measured values for the models. As an entire data set was collected in about 10 seconds, twenty estimates of the joint locations and directions were calculated in order to investigate the reliability and repeatability of the method.

Following this, the method was repeated on a human subject. Having precisely located and marked the locations of the bony landmarks of the lower leg and foot with a magic marker, Qualisys markers were then attached to each of the locations. Markers were first placed at the ankle joint only, as placing the markers defining the subtalar joint at the same time, caused interference, Figure 3.7.

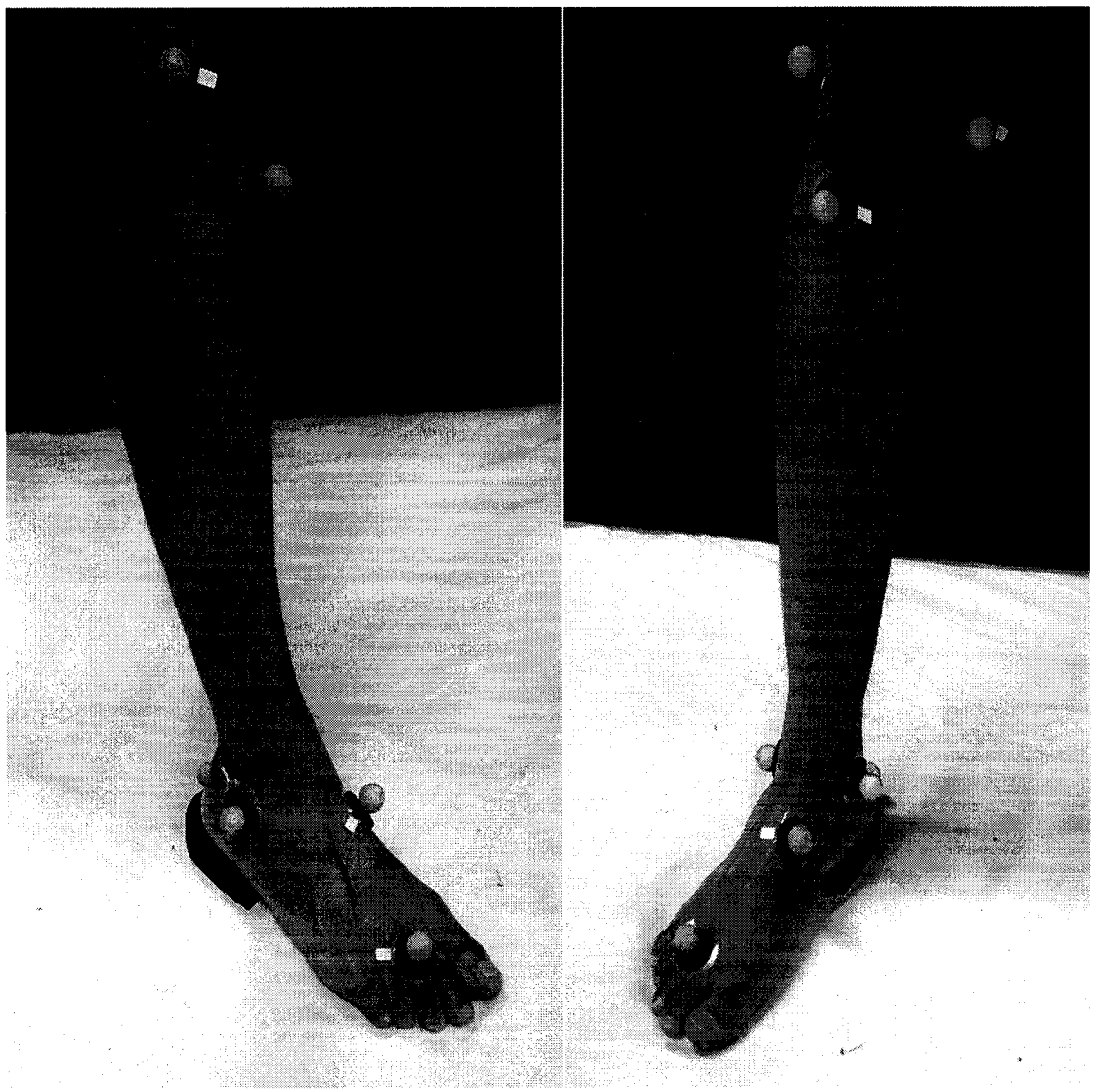

Figure 3.7 *Placement of joint markers too close to allow accurate Qualisys readings; a) lateral view; b) medial view*

A rubber heel was placed under the foot to allow the foot to move as it would in a shoe with a heel of average height. The landmarks of the lower leg and foot, which were required to determine an initial joint location and orientation, were located on the navicular, heel (calcaneus), and medial and lateral malleoli. The direction vector between the navicular and heel markers determined the initial estimate of the subtalar axis. As determined by Inman,[27] the ankle axis was assumed to pass 5±3 mm distal to the tip of the medial malleolus, and on the lateral side, 3±2 mm distal to, and 8±5 mm anterior to the distal tip of the lateral malleolus. An initial estimate of the location of each of the joints, was taken as the mid-point between each of the axis end points. Markers were also placed on the toe (between the base of the second and third toes, along the midline of the foot), on the tibial tuberosity, and the lateral tibial plateau in order to create a more complete picture of the leg and foot. Several test trials were then made with the subjects' leg moving with motion about the ankle joint alone (anterior/posterior motion), and subsequently about the subtalar joint alone (medial/lateral motion). The data from the marker attached to the medial tibial plateau (MTP) was used to determine the approximate joint center, as previously described. As was done with the model, the subject rotated the foot about each of the axes with as much independence of axes as possible. In order to reduce the interference between the markers defining the joint axes, the cameras of the Qualisys system were placed as close to the subject as possible, and only the markers representing a particular joint were placed on the subject when defining that joint, Figures 3.8 and 3.9.

(a) (b)

Figure 3.8 *Subject with markers along ankle joint as defined by Inman[27]; a) lateral view; b) medial view*

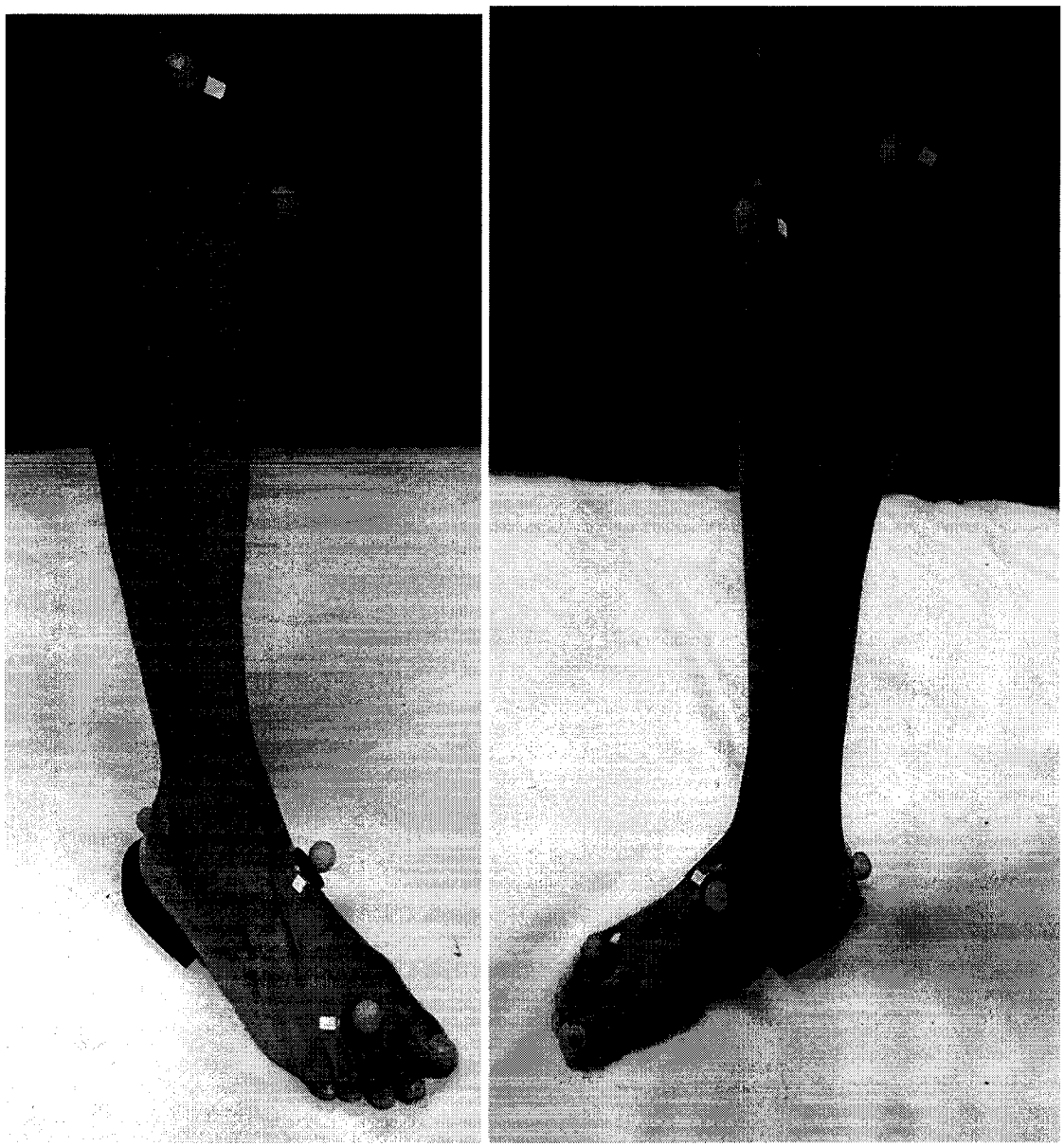

(a) **(b)**

Figure 3.9 *Subject with markers along subtalar joint defined as running through medial neck of talus and posterolateral tuberosity of calcaneus; a) lateral view; b) medial view*

Figure 3.10 shows the relative locations of the optical markers as detected by the Qualisys system for the range measurements of motion about the ankle joint that were used to calculate the axis location and orientation. The total range of motion was from MED 1 to MED 2, however the points used in the calculation of the joint orientation, ranged from START to END. This range was used because the change in values, particularly time, was the largest here.

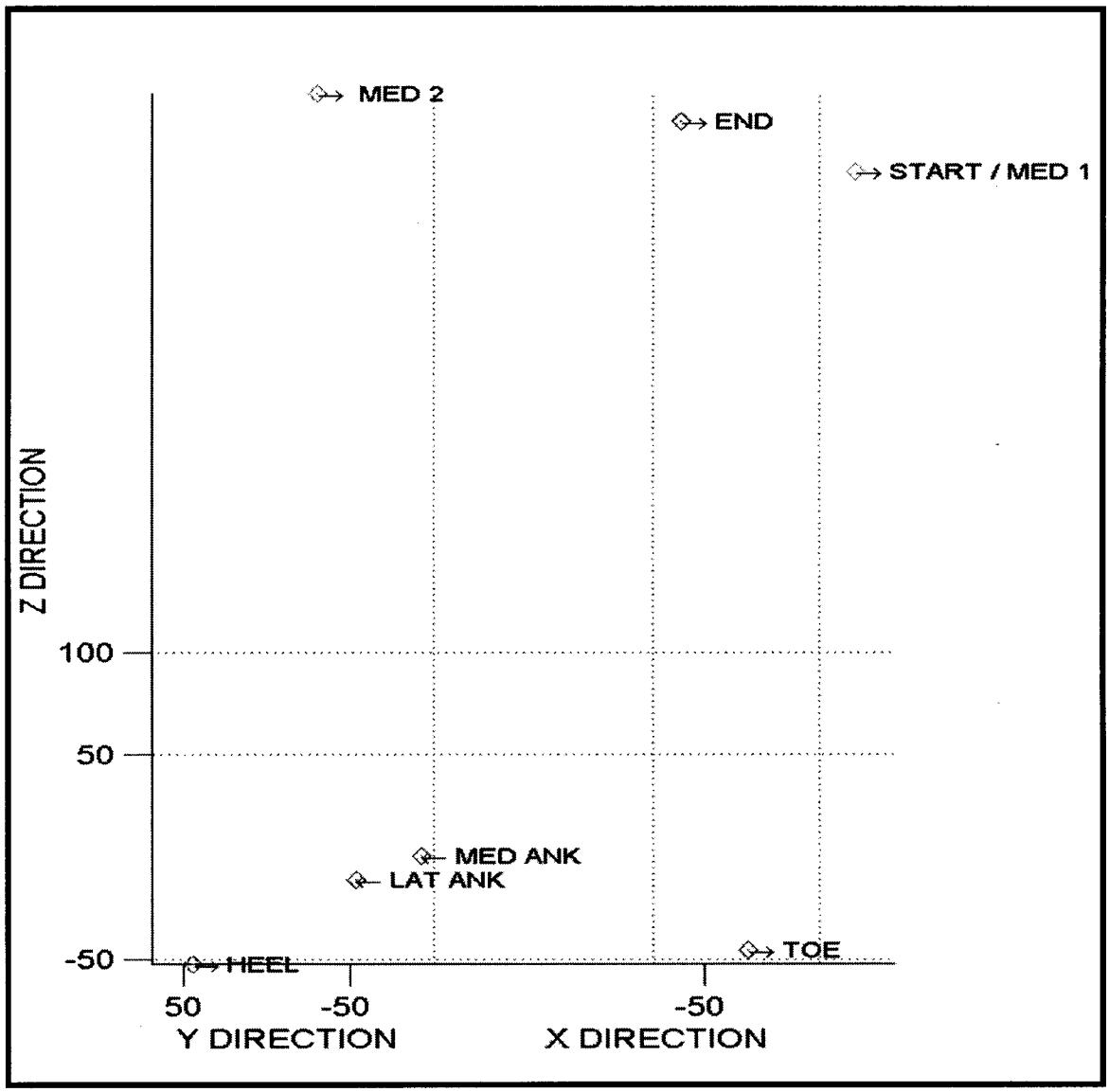

Figure 3.10 *Total range of motion, and range used in calculation of ankle joint orientation and location (lateral view)*

Figures 3.11 shows the relative locations of the optical markers as detected by the Qualisys system for the range of measurement of motion about the subtalar joint that were used to calculate the axis location and orientation. The total range of motion was from MED 1 to MED 2, however, the points used in the calculation of the joint location and orientation, ranged from START to END. This range is in the middle of the total range of motion, and gives the best representation of subtalar motion. At either extreme, the foot also tended to rotate on the floor, introducing noise.

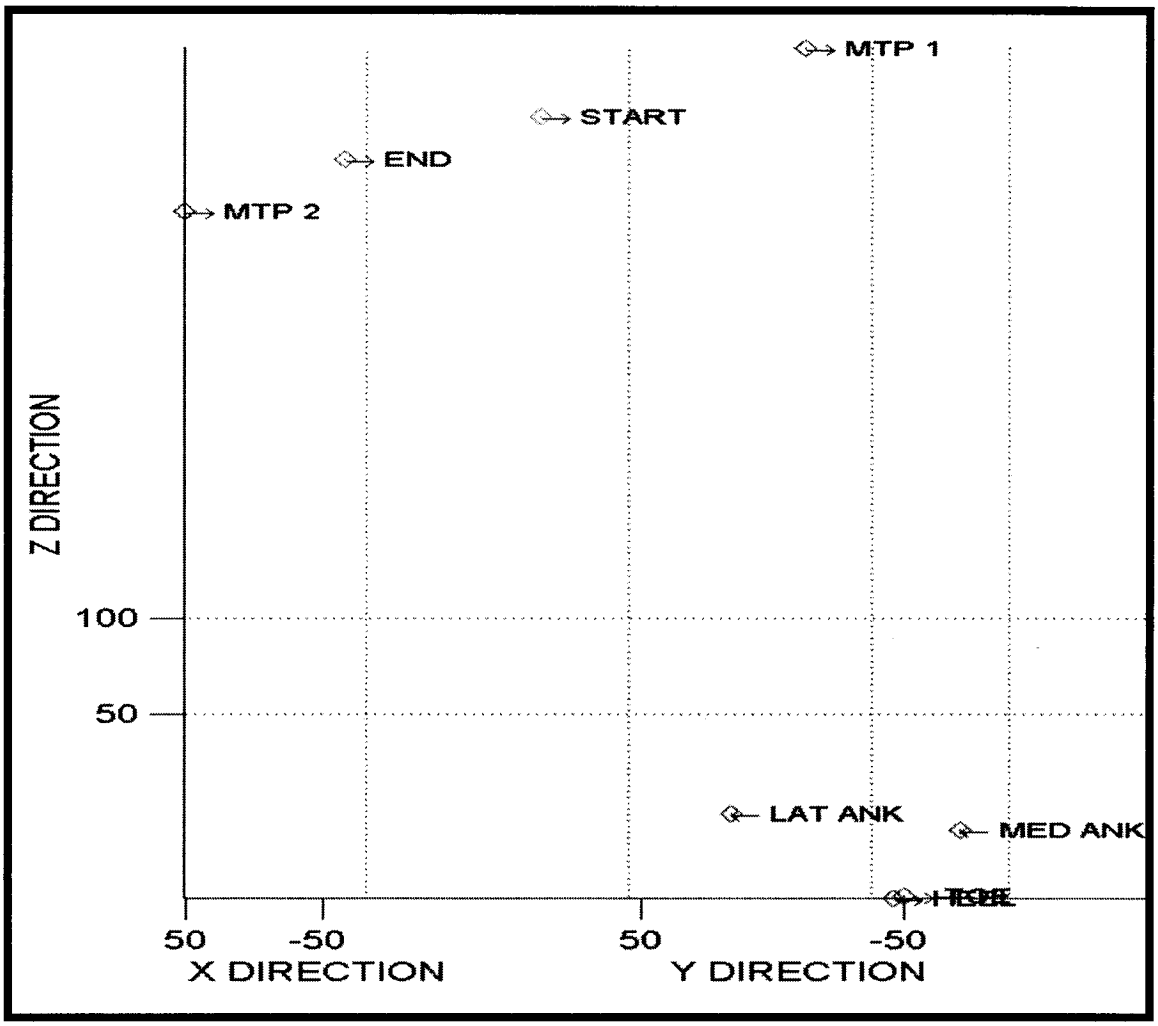

Figure 3.11 *Total range of motion, and range used in calculation of subtalar joint orientation and location, lateral view*

The measurement data from the Qualisys system was imported into Microsoft Excel, and the MATLAB programs developed for the project were then used to calculate the location and center of the ankle and subtalar joints, respectively.

In order to determine which measurement values were acceptable, ***Chauvenet's criterion*** was applied to each of the data sets. The standard deviation of the data set was calculated as:

$$\sigma = [\Sigma(x_i - x_m)^2/(n-1)]^{1/2} \qquad (3.10)$$

and Chauvenet's criterion[25] was applied. Chauvenet's criterion states that a measurement may be eliminated if the probability of obtaining a particular deviation from the mean is less than ½ n, where n is the sample size. The mean and standard deviations are calculated including all of the data points, and the deviations of each point is then compared to the standard deviation, where, **R**, the ratio of the maximum acceptable deviation to the standard deviation of the measurement sample (d_{max}/σ) is given by:

$$\mathbf{R = (sqrt(2))*erfinv(2*P)} \qquad (3.11)$$

where P = (0.5-1/4*n) and **erfinv** is the inverse of the error function. Thus, if there are 10 readings, the maximum acceptable ratio is 1.96, and if there are 20 readings, the maximum acceptable ratio is 2.414. If the standard score[29] (normalized value of the measurement), **z**, is defined to be:

$$\mathbf{z = [x - (mean\ of\ x)]/\ \sigma} \qquad (3.12)$$

then each of the normalized measurement values that exceeds the corresponding Chauvenet's value are considered as erroneous and discarded.

When the ankle and subtalar joint locations and orientations (relative to the Qualisys global reference system) were calculated with the MATLAB programs, they then had to be transformed to a local coordinate system, relative to the leg. To accomplish this, white circular paper markers were placed on the leg on each of the Qualisys landmark locations described above. Optical scans of the lower leg and foot were then acquired with the VA Lower Limb and Pedorthics Optical Digitizer. The scan measurements were then imported into the VA Prosthetics-Orthotics-Pedorthics CAD/CAM system, where they were converted into cylindrical coordinates for a solid body, and then exported into a MATPAB m-file. The system was designed to allow prosthetists-orthotists to design and/or modify the digital shape of patients' limb segments for use in design of prosthetic sockets, orthotic cuffs, and pedorthic Lasts and insoles. The three-dimensional contour of the outer surface of the leg is digitized, graphically displayed, and digitally modified. The resulting data may then be sent to a CNC milling machine, which produces a positive model of the socket, cuff, or Last. Scanning the leg, the system produced 128 points uniformly distributed around each 360 degree transverse cross section, at each of the 410 latitudes scanned along the length of the leg. For the foot, the system produced 512 points around each 360 degree transverse cross section, at each of the 231 latitudes scanned. The respective scan files of the leg and foot, one with 128 x 410 data points, and the other with 512 x 231 data points were concentrated and used to provide a composite surface shape of the leg and foot respectively. Two scans were performed with the laser beam in the leg scan moving

circumferentially around the long axis of the leg, while the scan of the foot was done with the circumferential laser beam moving longitudinally along the axis of the foot, toe to heel, rather than from the ankle to the plantar surface of the foot to allow the contour of the bottom of the foot to be exact. A MATLAB program was written to convert the 1 x (512*231) foot scan data set into a 512 x 231 matrix (n x k matrix), and then searching the data of the k^{th} slice to find where (360/512)*n was equal to the theta value of the landmark. The resulting values obtained were then converted into X, Y, and Z coordinates, respectively. The same was done to find the X, Y, Z coordinates of the landmarks of the leg, which was used as a check, as an accurate transformation of the data into the new coordinate system would result in the corresponding landmarks from the foot and leg scans overlaying each other.

As the foot scan, leg scan, ankle joint plot, and subtalar joint plot each had their own local orthogonal coordinate system, within their own global coordinate systems, it was necessary to find a way to determine their orientation and location with respect to each other, so the data could be superimposed. Transformation matrices for each of the systems were calculated so that the respective coordinate systems could be transformed to a common origin. As the respective local systems were generated separately, in order to be aligned correctly they had to be rotated. For two coordinate systems, O_{XYZ} and O_{xyz}, the latter can be considered to be a rotation of the former about the origin, Figure 3.12.

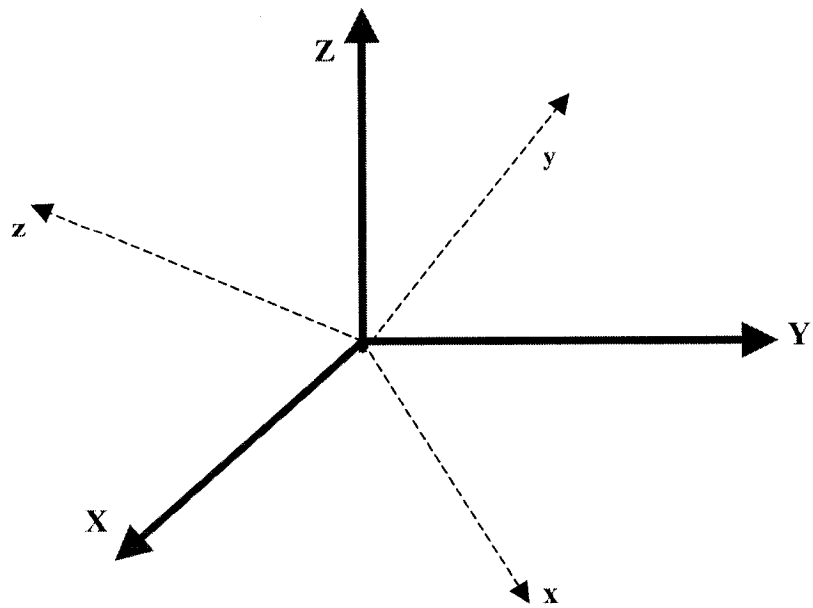

Figure 3.12 *Rotation of coordinate system about origin*

If a_{ij} is the cosine of the angle between the i*th* and j*th* coordinate axes, then the transformation matrix between the two systems is given by:

$$\mathbf{R} = \begin{bmatrix} a_{11} & a_{12} & a_{13} \\ a_{21} & a_{22} & a_{23} \\ a_{31} & a_{32} & a_{33} \end{bmatrix} \qquad (3.13)$$

where **X = [R]x,** thus if, **P**, is a point in the initial coordinate system,

then a point, $\mathbf{P_1}$, in the rotated coordinate system is given by:

$$[P] = [\cos_{Xx}, \cos_{Xy}, \cos_{Xz}; \cos_{Yx}, \cos_{Yy}, \cos_{Yz}; \cos_{Zx}, \cos_{Zy}, \cos_{Zz}][P_1]' \qquad (3.14)$$

where $[R]^T[R] = [I]$, and if R is orthogonal, $[R]^T = [R]^{-1}$.

To align (match up) the leg and foot scans so that a composite model of the leg and foot containing the ankle and subtalar joint axes could be viewed, four markers were placed on the lower leg, at medial, lateral, anterior, and posterior locations. The leg scan captured down to a location just below these four matching markers, while the foot scan captured up to a location just above these markers. A coordinate system was then defined as follows, Figure 3.13, and Figure 3.14, with the center, O, equidistant from all four markers:

X_DIRECTION = ANTERIOR MARKER LOCATION - POSTERIOR MARKER LOCATION *(3.15)*

Y_DIRECTION = MEDIAL MARKER LOCATION - LATERAL MARKER LOCATION *(3.16)*

Y_DIRECTION = Y_DIRECTION – dot (X_ DIRECTION, Y_DIRECTION)*X_ DIRECTION / dot (X_ DIRECTION, X_ DIRECTION) *(3.17)*

Z_DIRECTION = CROSS (X_DIRECTION, Y_DIRECTION) *(3.18)*

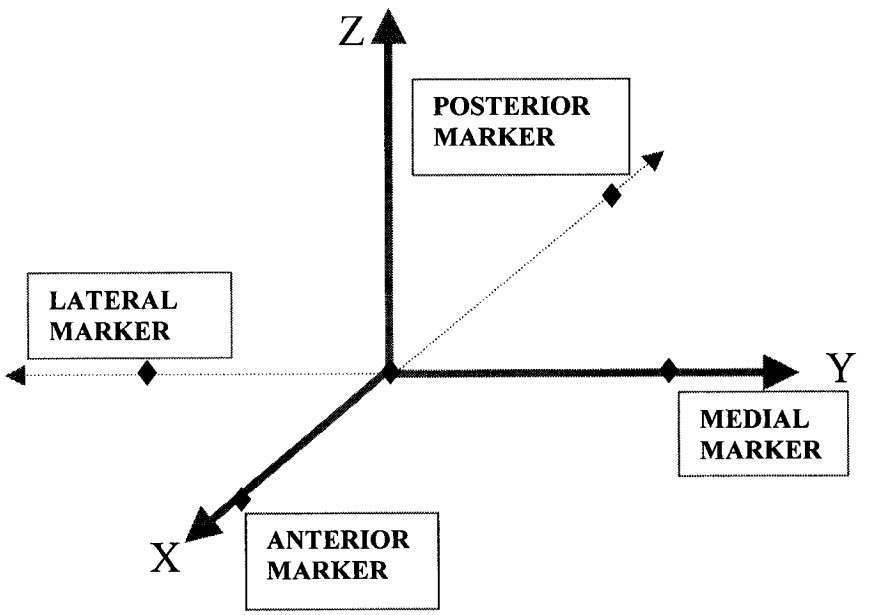

Figure 3.13 *The coordinate system (right foot) used to align all four coordinate systems*

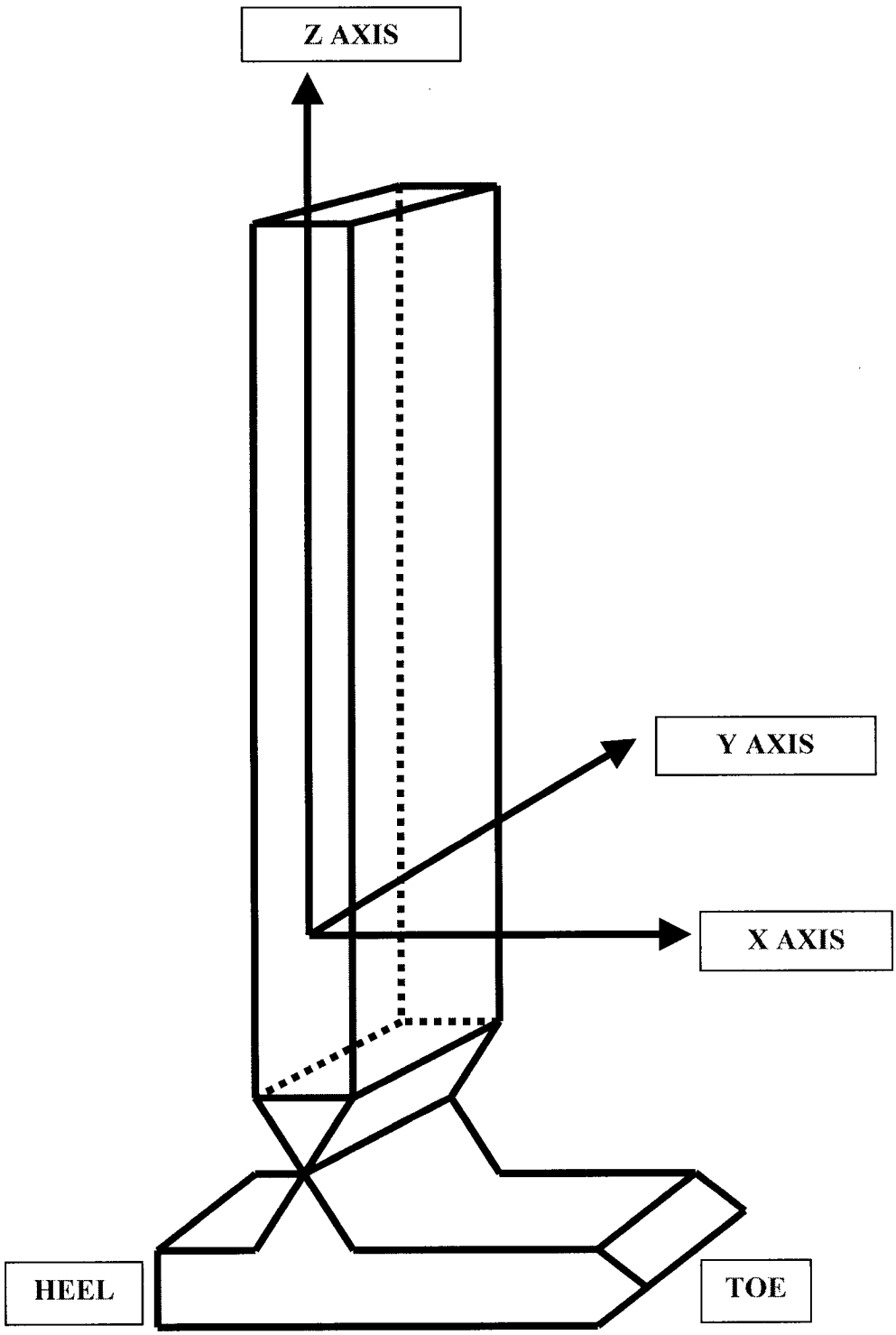

Figure 3.14 *The coordinate system (right foot) used to align all four measurement coordinate systems of the leg and foot shown with model of leg/foot*

Each of the vectors was normalized to a unit vector, and the Y-direction was made perpendicular to the X-direction, within the same XY plane in order to ensure that the coordinate system was orthogonal. The Y-direction was redefined using the Gram-Schmidt process[86], which creates a set of orthogonal vectors from a set of linearly independent vectors.

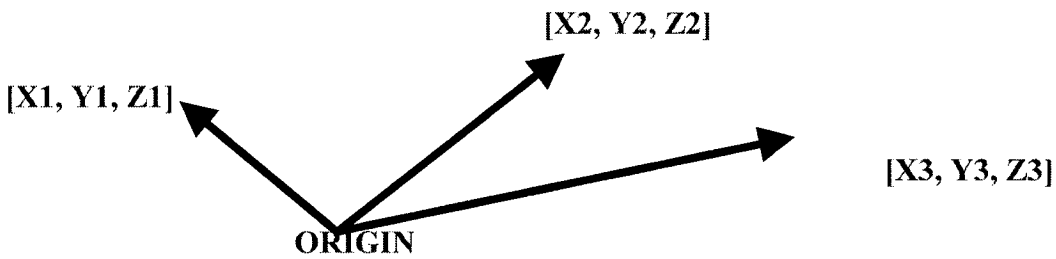

Figure 3.15 *Three linearly independent vectors*

A basis in R^3, Figure 3.15, must have three linearly independent vectors, for which it is necessary that

$$\mathbf{c_1*[X1, Y1, Z1] + c_2*[X2, Y2, Z2] + c_3*[X3, Y3, Z3] = 0} \qquad \textit{(3.19.1)}$$

Therefore,

if $\mathbf{v_1 = u_1 = [X1, Y1, Z1]}$, $\mathbf{u_2 = [X2, Y2, Z2]}$, **and** $\mathbf{u_3 = [X3, Y3, Z3]}$,

Then, since u_1 and u_2 are independent, they span the same vector space as v_1 and u_2. A vector, v_2, perpendicular to v_1, where v_2 is a member of the span of u_1 and u_2 is then defined. Therefore, v_2 is a member of the span of v_1 and v_2, thus

$$\mathbf{v_2 = c_1*v_1 + c_2*u_2 \text{ and } \langle v_1, v_2 \rangle = 0} \qquad \textit{(3.19.2)}$$

Therefore,

$$\langle v_1, c_1*v_1 + c_2*u_2\rangle = \langle v_1, c_1*v_1\rangle + \langle v_1, c_2*u_2\rangle \qquad (3.19.3)$$

$$= c_1\langle v_1,v_1\rangle + c_2\langle v_1,u_2\rangle = 0$$

If $c_2 = 1$, then

$$c_1 = -\langle v_1,u_2\rangle/\langle v_1,v_1\rangle = -\langle v_1,u_2\rangle/\|v_1\|^2 \qquad (3.19.4)$$

And

$$v_2 = c_2*u_2 + c_1*u_1 = u_2 - \langle v_1,u_2\rangle*v_1/\|v_1\|^2 \qquad (3.19.5)$$

The third vector v_3, Figure 3.16, is then defined as the cross product of the first two vectors.

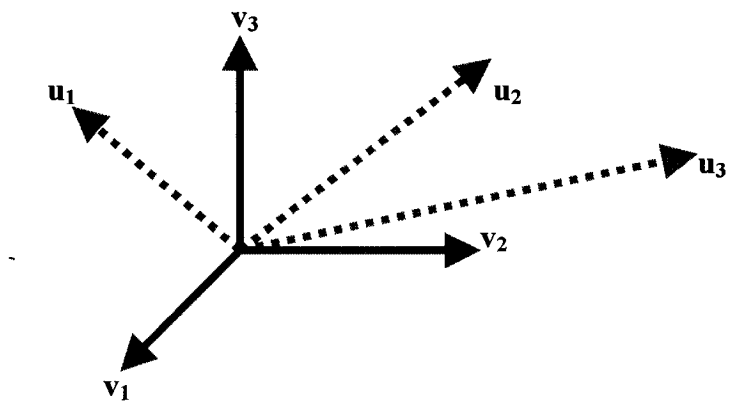

Figure 3.16 *Orthogonal coordinate system (v1, v2, v3) from non-orthogonal basis (u1, u2, u3)*

Defining a general XYZ coordinate system as:

$$X = [1,0,0],\ Y = [0,1,0],\ Z = [0,0,1]$$

the transformation matrix between the local coordinate systems defined by the four matching markers common to each data set and the general coordinate system, was found

for the leg and the foot, using a MATLAB program. In order to increase the speed of the analysis within MATLAB, the data were **'vectorized'**, which was more efficient than using two nested '**for**' loops. For this process, code that usually operates as scalars, is transformed into code that operates as vectors. Vectorized statements are performed with optimized binary code, rather than with scalar code. The data from the foot and leg scan was then also transformed into the new coordinate system in order to create a single foot-leg model. The origin of the leg coordinate system was taken as the point at the center of the four 'matching markers', using the facts that; (1) if the midpoints of the consecutive sides of any quadrilateral are connected by straight lines, the resulting quadrilateral is a parallelogram and; (2) the diagonals of a parallelogram bisect each other Figure 3.17.

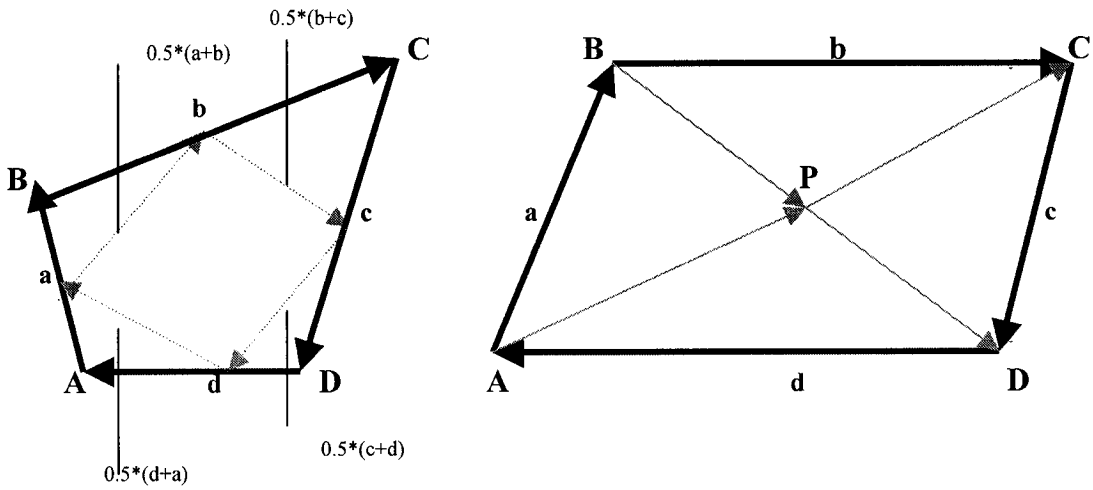

A = anterior marker location **B = lateral marker location**

C = posterior marker location **D = medial marker location**

Figure 3.17 *Determination of center of coordinate systems*

Markers were also placed at these same locations when recording data with the Qualisys system, and the ankle and subtalar axes transformed into the corresponding local coordinate systems. This was done so that the four systems could then be superimposed onto each other, with an accurate preservation of their orientations, with respect to each other.

The locations of the points of intersection of the subtalar and ankle axes with the foot scan were found by writing another MATLAB program. The program searched the plot of the superimposed joint axes and foot scan data, along the axes, for their (the axes) intersection with the foot scan, to an accuracy of 1 mm (distance between the intersecting axis and scan points). A MATLAB program was then written to find the distance between each of the points of intersection and three of the closest landmarks on the foot, Table 3.1.

Table 3.1 *Marker locations used to determine distances between points of intersection and landmarks*

INTERSECTING POINT	LANDMARKS USED TO DETERMINE POINT ON FOOT
Medial Ankle Axis	**Medial malleolus, Medial matcher, Anterior matcher**
Lateral Ankle Axis	**Lateral malleolus, Lateral matcher, Anterior matcher**
Anterior Subtalar Axis	**Lateral malleolus, Posterior matcher, Lateral matcher**
Posterior Subtalar Axis	**Navicular, Toe, Medial malleolus**

3.2.5). ***Construction of a prototype, articulated, dual axis, ankle-foot orthosis***

A negative mold using plaster-of-Paris bandage, was made of the test subject's right foot and tibial limb segment. The locations of the Qualisys landmarks, as well as the landmarks used to define the local coordinate system of the leg, as described in Section 3.2.3, were preserved on the leg and foot, and transferred to the plaster cast with indelible ink. Dental plaster was poured into the cast and a positive mold of the lower leg and foot was made. The plaster-of-Paris wrap bandage was peeled off, leaving the positive mold of the leg with the locations of the landmarks intact. The points of intersection of the ankle and subtalar joint axes with the foot were then located and marked, having calculated the distance of each of these intersections from at least three of the landmarks. Holes were then drilled through the cast along the ankle and subtalar axes, and a length of brass rod inserted through the holes along the respective axes, Figure, 3.18.

Figure 3.18 *(a) Medial, (b) lateral, and (c) frontal views. Positive plaster model of the experimental subject's right foot and ankle, with location of ankle and subtalar axes marked with brass rods*

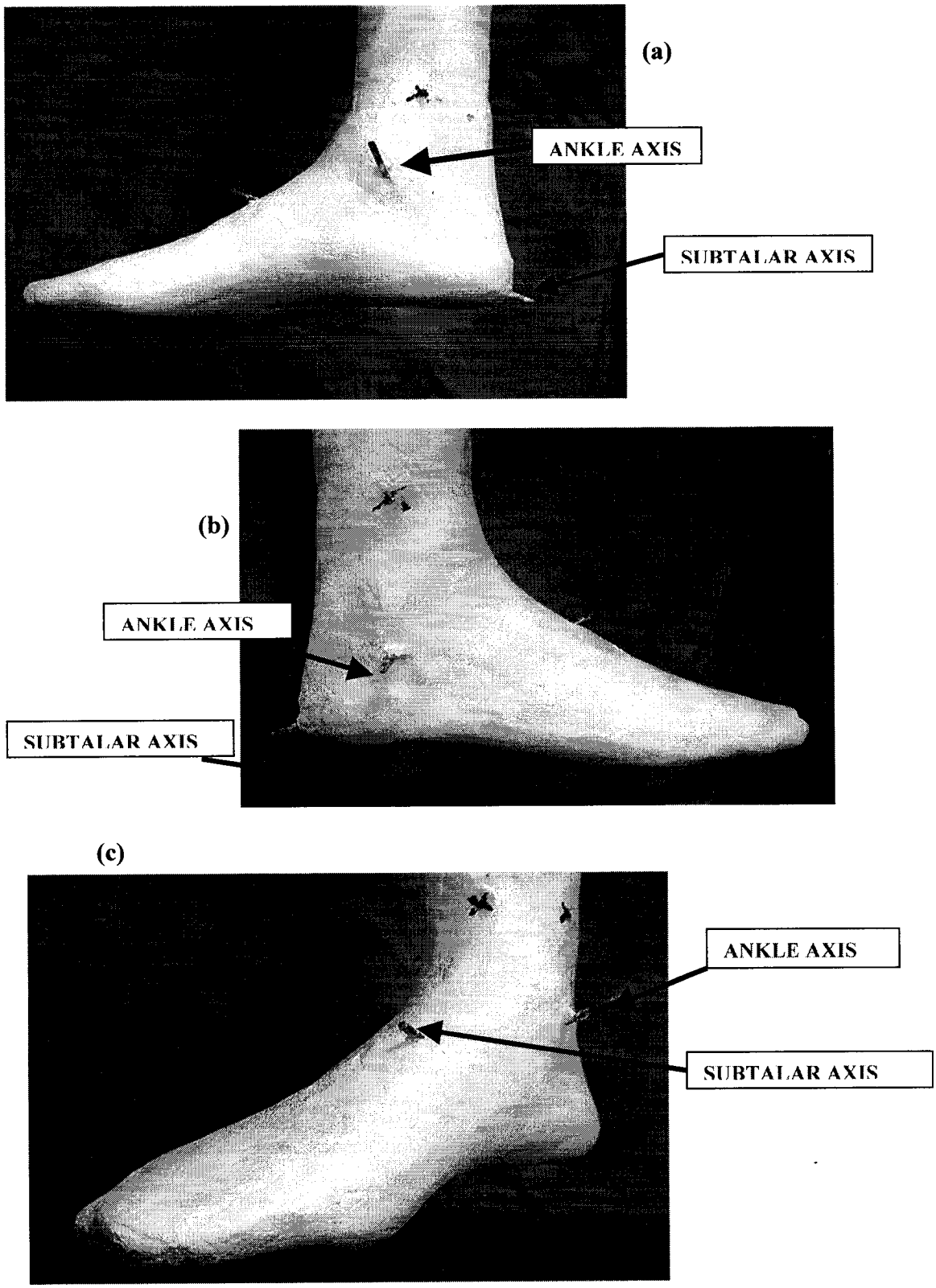

A design for a dual axis ankle-foot orthosis was formulated, consisting of a shoe attachment stirrup with an articulated subtalar joint, supporting a floating yoke with an articulated ankle joint, with or without dorsiflexion/plantar flexion stops and spring assists. Matte board patterns for the respective component pieces for the orthosis were made and adjusted to fit on the plaster model, and then fabricated out of metal. The brass yoke and supporting back strut, Figure 3.19, were made out of 0.125" thick, machinable, alloy 360 leaded brass stock, composed of 60–63% copper, 32.95 – 37.15 % zinc, 2.5-3.7% lead, and 0.35% iron, with a yield strength of 44,000-52,000 psi, and Rockwell hardness 25–85 B. This alloy was chosen because of its strength and ductility, which permitted cold working. The shape and dimensions of the yoke design were checked with the Matte board pattern on the plaster cast to ensure it fit about the joint axes and there was adequate space on all sides, to allow the yoke to rotate about the subtalar and ankle axes without binding and without impinging on the subject's foot/ankle. The yoke was designed to interface with conventional dorsiflexion/plantar flexion spring-assisted ankle joints and to have adjustable limit stops.

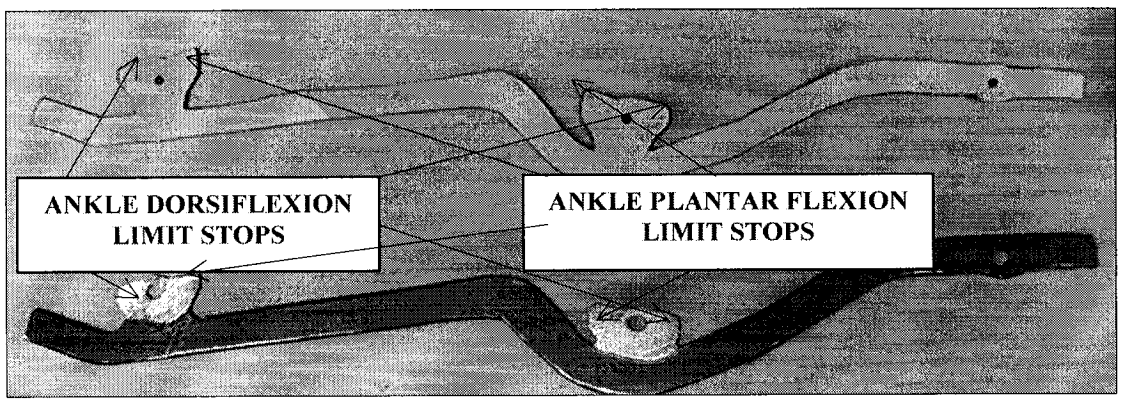

Figure 3.19(a) *Matte board pattern and corresponding brass prototype of orthosis ankle yoke*

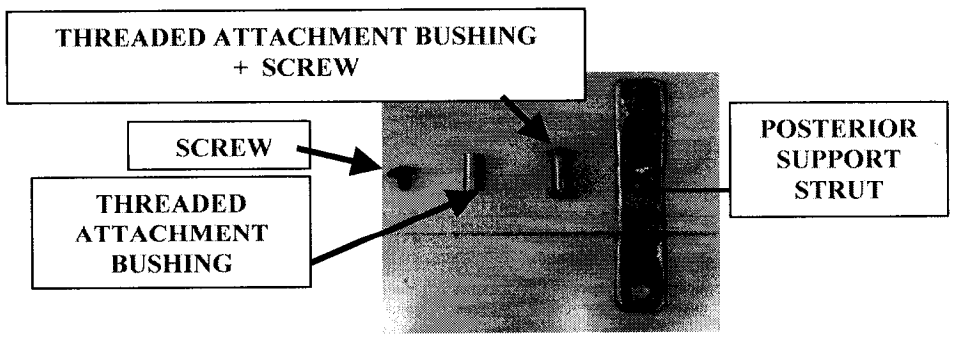

Figure 3.19(b) *Posterior yoke support strut, with attachment bushing and screws used to connect it to the posterior subtalar joint of the orthosis*

The posterior strut was designed to support the yoke and connect it to the posterior subtalar joint attachment with two 8-32, 0.25 inch long machine screws and an 8-32, 0.5 inch long, stainless steel, internally threaded bushing, with a 0.25 inch outer diameter, Figure 3.19 (b). The outside surfaces of the attachment bushing, which had an external diameter of 0.25 inches were filed down approximately 0.0002 inches in order to fit into the subtalar joint attachment holes, which also had a diameter of 0.25 inches.

To attach the ankle yoke to the subtalar joint and secure the orthosis to the subjects' shoe, a stirrup with an anteromedial strut and posterior flange, Figure 3.20, was made from 0.125 inch thick, aluminum Alloy 6061, composed of 0.4-0.8% silicon, 0.7% iron, 0.15-0.4% copper, 0.15% manganese, 0.8-0.12% magnesium, 0.04-0.35%chromium, 0.25% zinc, 0.15% titanium, with aluminum making up the remaining percentage, with yield strength of 40 ksi and 95 Brinell hardness. 21/32 inch holes were drilled into the posterior flange and the end of the anteromedial strut of the stirrup. Steel ball joints with 21/32 inch external diameter, 0.25 inch internal diameter, and 11/32 inch thick, were press fit into the respective holes in the stirrup for the subtalar joint. The holes

were made using drills of gradually increasing diameter in order to minimize chatter, and consequent elliptical deviation from a true circular hole during drilling. Reduced shank (1/2 inch shank) stainless steel drill bits with diameters of 0.1015" (#38), 0.1695" (#18), 0.2340" (A), 7/16", 0.5", 17/32", 9/16, 19/32", 5/8", 41/64", and 21/32" were used. Three 0-80 holes were drilled and tapped in the outer borders of the stirrup around the holes, into which 0.125 inch long, 0-80 set screws were inserted to secure the ball joints. A center-line was drawn down the center of the base plate of the stirrup to facilitate alignment with the subtalar joint axis of the foot, when it was attached to the shoe.

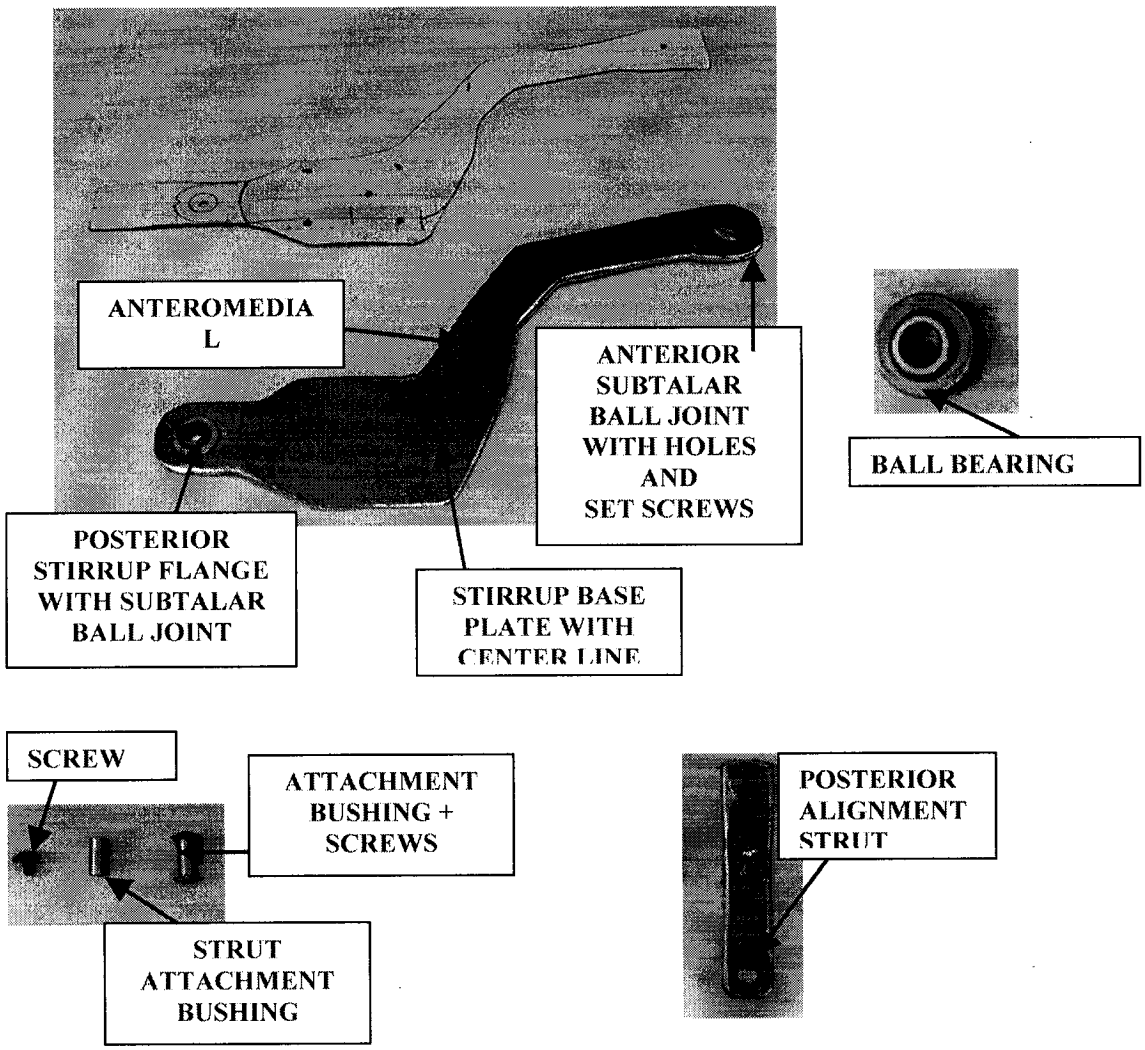

Figure 3.20 *Shoe attachment stirrup and components*

The Klenzak joints were then attached to the aluminum uprights, and secured with screws, Figure 3.21.

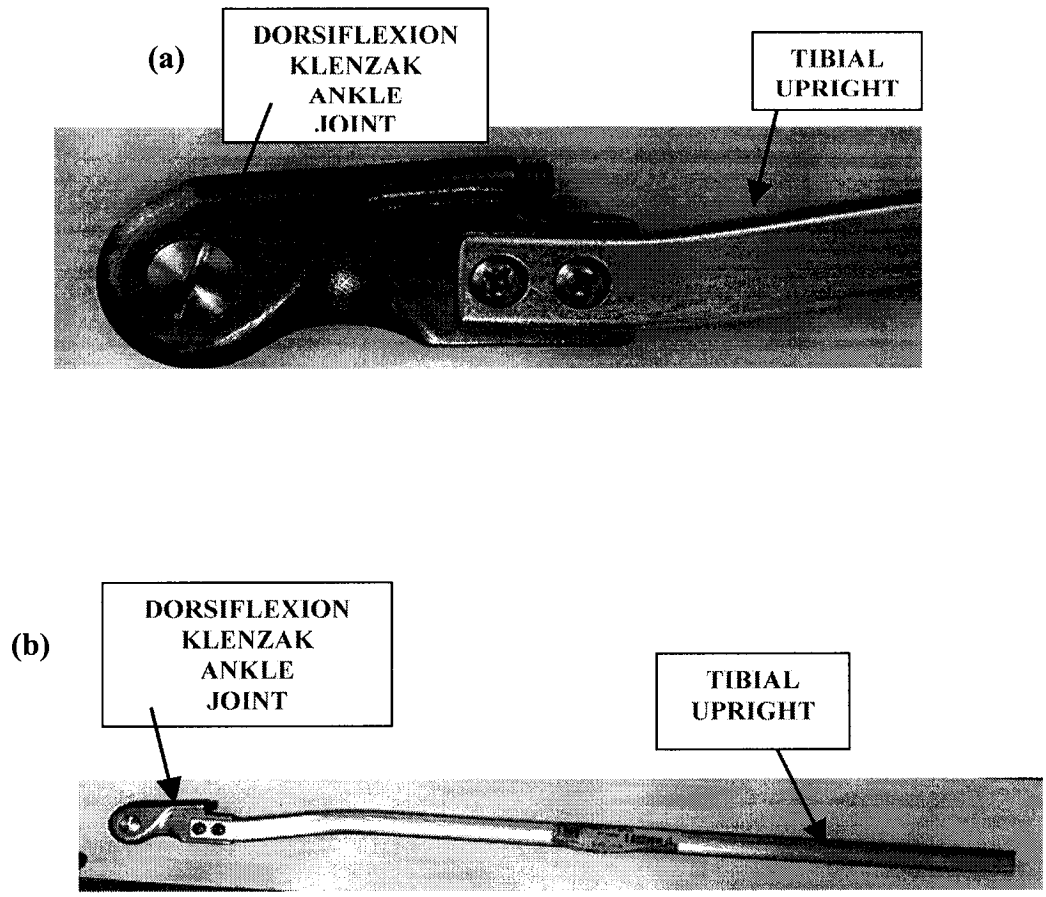

Figure 3.21 *Klenzak dorsiflexion assist ankle joint with tibial upright*

Using bending irons, the stirrup, yoke, and back strut were bent about the cast so that the anatomical joints, as indicated on the cast, coincided with the joint centers of the brace components, Figure 3.22. The distance between the inner and outer surfaces of the base of the shoe was measured, and the base of the flat surface of the stirrup was kept at that distance from the bottom surface of the foot of the cast.

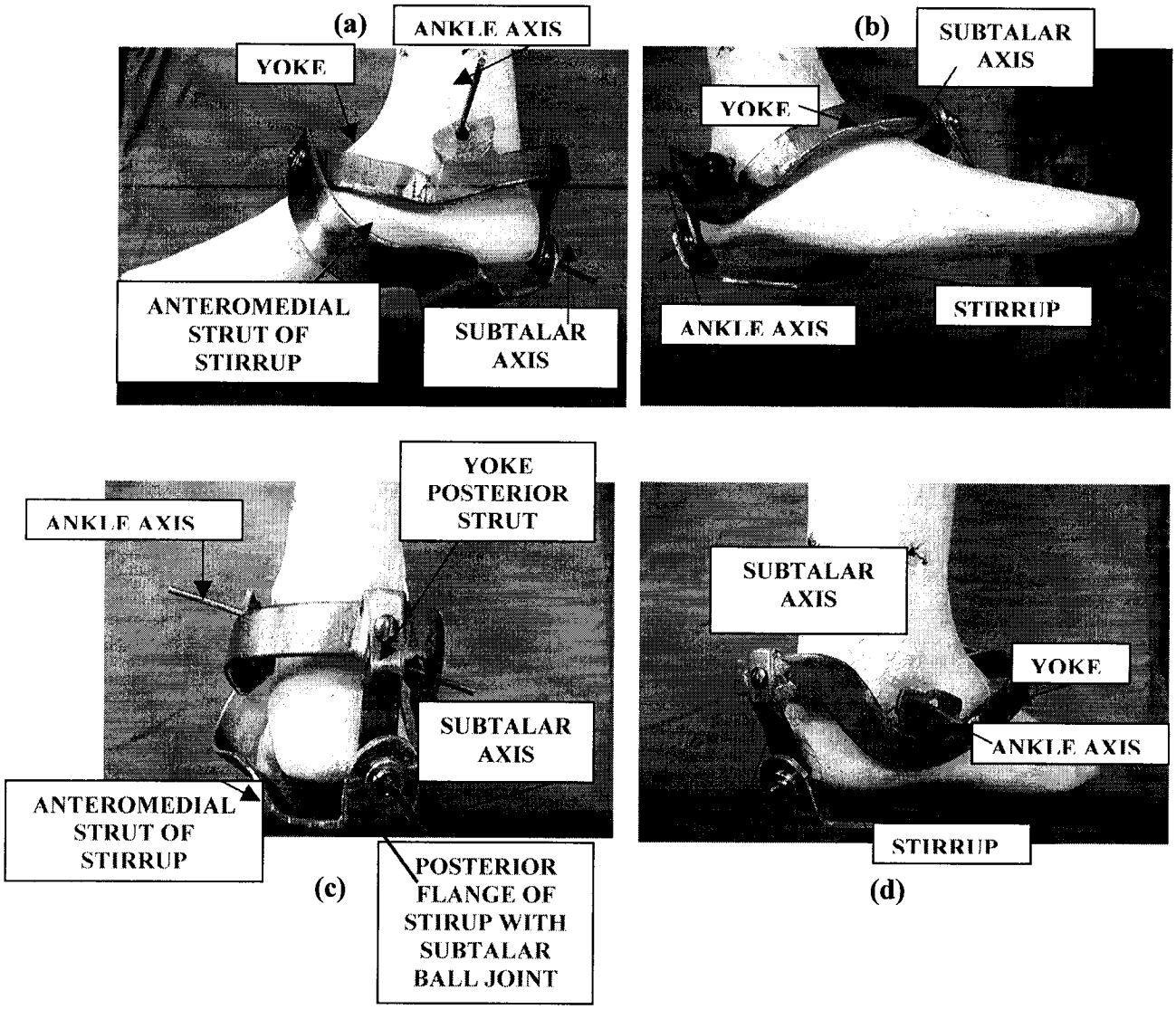

Figure 3.22 *Ankle-foot assembly of the Dual-Axis AFO fit on the cast of the subjects' leg to ensure: (1) coincidence of the orthosis joint axes with the anatomical axes of the foot and ankle; (2) adequate clearance of the orthosis components was maintained at all phases of stance and gait to avoid impingement upon the subjects foot and/or ankle. (a) medial view; (b) anterolateral view; (c) posterior view; (d) posterolateral view*

The joint faces of the ankle joint and the subtalar joint were made parallel to each other, Figure 3.23, by placing the respective joint faces of the yoke in an alignment jig[12], and torqueing them until they were exactly aligned, as previously shown in Figure 2.17.

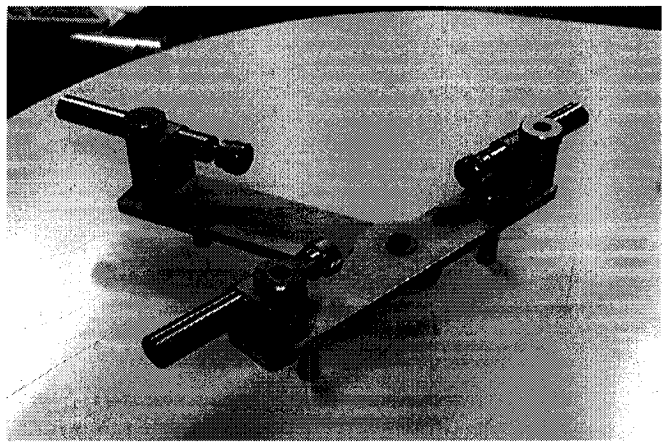

Figure 3.23 *Alignment fixture* [12]

The proximal part of the orthosis was designed to be a conventional PTB type cuff, supported by dual aluminum uprights. This would allow varying degrees of weight bearing to be achieved with the orthosis depending upon how tight the cuff closure straps were pulled when the orthosis was donned. To fabricate the cuff, the cast was smoothed and a plaster ridge 6 inches distal to where the MTP of the cuff was expected to be, was added to prevent gradient stresses and chaffing of the leg. Plaster was also added to the cast along the tibial crest, and at the back of the knee, to create an "access window" for the leg to easily enter and exit the orthosis. A polyethylene foam liner was cut, heated, and thermoformed on the cast to fit inside the cuff. A sheet of Surelyn® was cut and heated in a convection oven to 300 °F. when it reached glass temperature, it was carefully removed from the oven, and quickly drape molded over the knee and upper leg on the

cast under vacuum, with the two ends pressed together to form a longitudinal seam along the posterolateral border of the cast.

After the cuff was thermoformed, the plastic was allowed to cool and sit for 24 hours so the strains introduced during molding could equilibrate. The cuff was then cut off the cast, and the borders sanded to the PTB trimlines and smoothed. A tongue running the length of the posterolateral seam of the cuff was cut out of 1 mm thick polyethylene, heated with a heat gun, and pressed against the inside of the cuff over the seam. It was then glued in place. With the cuff and liner, and the ankle-foot assembly (yoke, posterior strut, and stirrup) positioned on the cast, the two aluminum uprights were bent so they matched the contour of the leg as closely as possible from the ankle joint to the cuff. Two Dacron Velcro closure straps were then sown and holes punched in them, so that they could be mounted on the cuff, and rivets inserted through the cuff and upright, cut off, and hammered over to secure the cuff firmly to the uprights, Figure 3.24.

Lines were then drawn along the mid-line of the bottom of the shoe, and along the projection of the subtalar joint axis. The stirrup was aligned with the mid-line of the base plate coincident with the projection of the subtalar axis onto the sole of the shoe and secured to the shoe with four 6-32, 0.5 inch screws. A heel was cut out of shoe sole leather, and glued in place so that the heel height matched that of the contralateral (left) shoe.

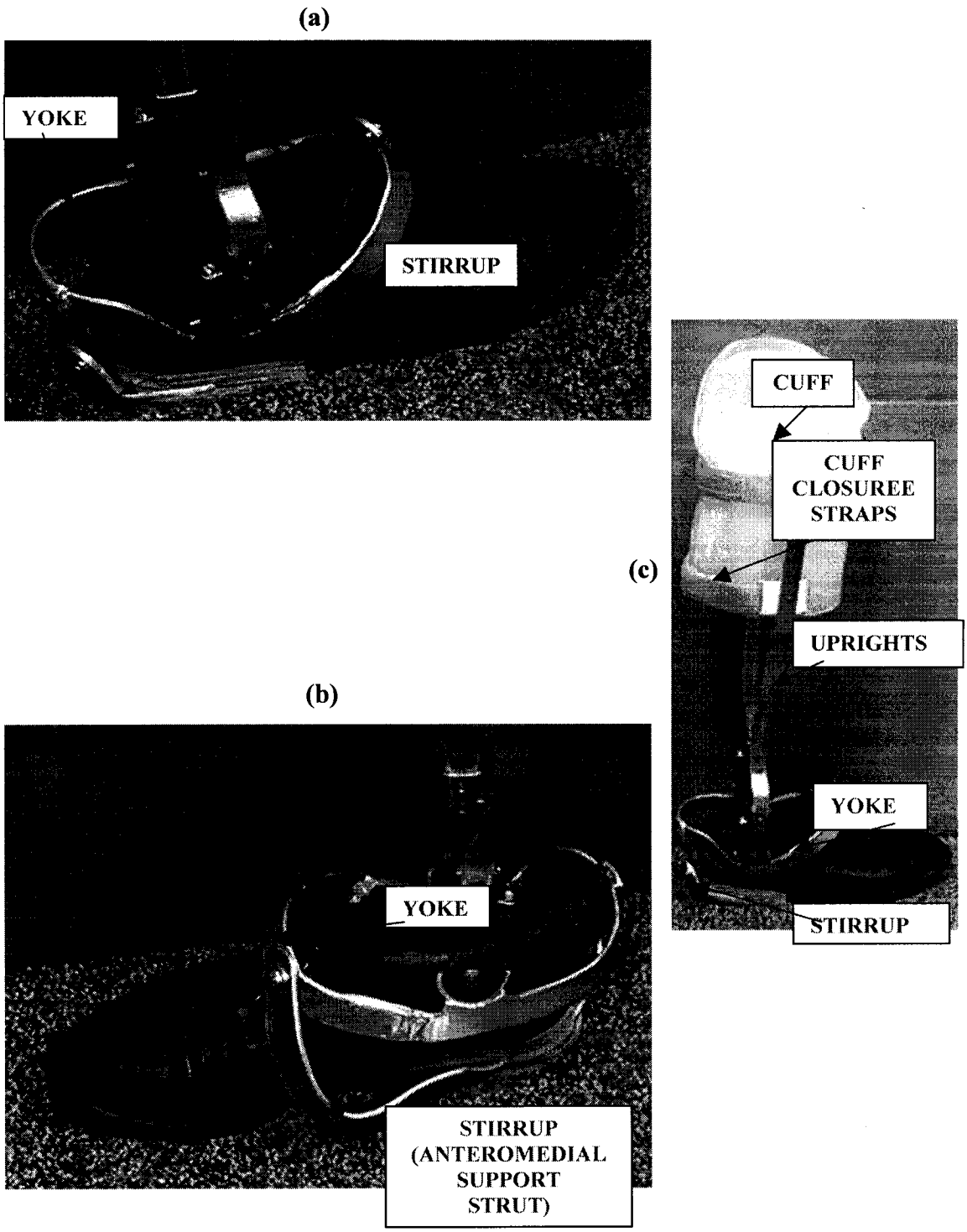

Figure 3.24 *Completed prototype of the Dual Axis AFO orthosis. (a) lateral view;and (b) medial close-up views; and (c) full lateral view*

3.2.6). *Testing and biomechanical analysis of prototype dual axis orthosis*

The functionality of the dual axis ankle-foot orthosis was measured and its performance analyzed in instrumental laboratory gait trials with an experimental subject. Results were compared to those achieved with a conventional plastic, non-articulated, posterior leaf spring AFO, Figure 3.25, and a single degree of freedom, articulating ankle, dorsiflexion assist AFO, Figure 3.26.

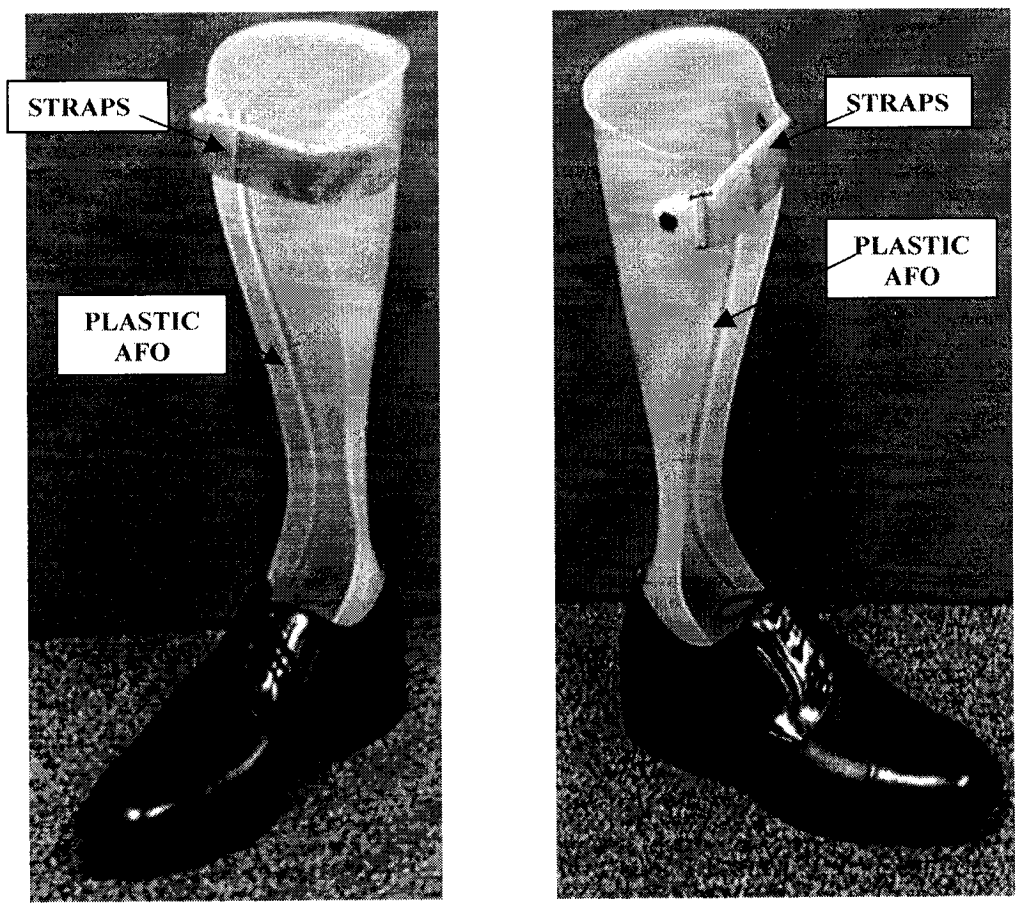

(a) (b)

Figure 3.25 *PAFO (a) medial; and (b) lateral views*

The single degree of freedom, articulated ankle joint AFO incorporated Klenzak spring actuated dorsiflexion assist ankle joints, Figure 3.26. The springs are compressed during the heel strike to foot flat phases of flat, aiding in the control of plantar flexion. They return energy from foot flat to mid-stance as the springs decompress. The mechanical stop on the anterior of the joint prevents excessive dorsiflexion of the ankle as the forefoot is loaded from mid-stance to toe-off, and the springs prevent plantarflexion (toe-drop) during the swing phase of gait.

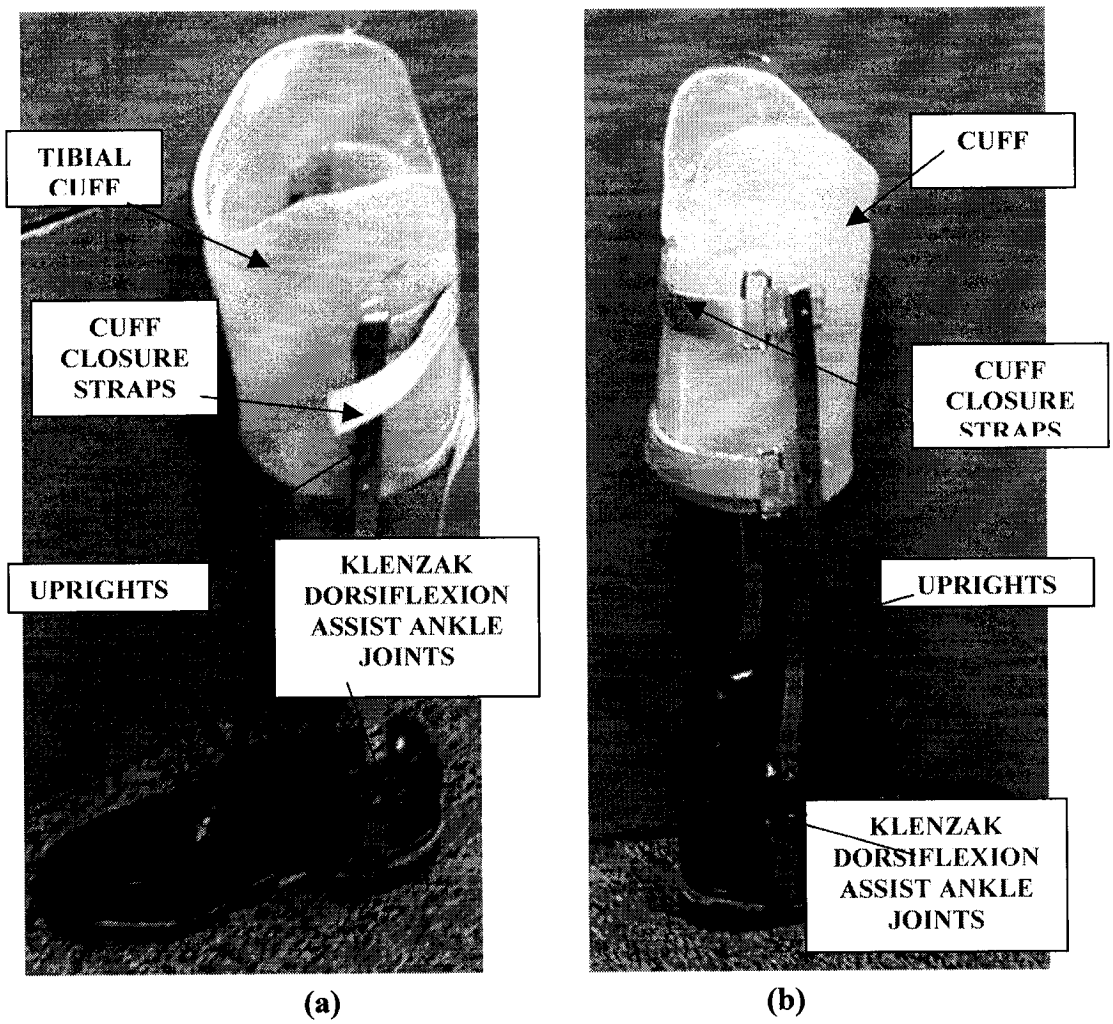

Figure 3.26 *Single degree of freedom articulated ankle AFO with Klenzak joints; (a) medial; and (b) lateral views*

The alignment of the anatomical ankle and subtalar joints with the joints of the orthosis was examined, in addition to the location and magnitude of resulting forces, using the procedure and instrumentation described below. The total and regional normal stresses incurred at the foot-orthosis or foot-orthosis-shoe interface were measured, as were gait timing and load durations, and toe, ankle, and knee velocities and accelerations, with the Vicon Motion Analysis System, the Tekscan Fscan Plantar Stress Measurement System, and the CIR Systems Gait-Rite Electronic Walkway, see Section 4.3.

4. RESULTS AND DISCUSSION

4.1). *Results for wood model*

4.1.1). *Experimentally calculated and conceptual model measured ankle axis locations*

Tables 4.1 and 4.2 show the Davidon experimentally predicted estimates and theoretical ankle axis locations, for twenty data sets of measurements acquired with the Qualisys Motion Analysis system. Each data set was comprised of four MTP (medial tibial plateau) locations, which were equidistant from each other.

Table 4.1. *Experimentally calculated ankle joint location (mm)*

DATA SET	x	y	z	DATA SET	x	y	z
1	-728.8395	291.1540	27.6725	11	-729.1835	291.1553	27.2987
2	-728.9272	291.1622	27.6003	12	-729.0465	291.0113	27.3090
3	-728.9395	291.1420	27.5730	13	-729.2012	291.0973	27.2010
4	-728.9002	291.1228	27.5030	14	-728.9835	290.9530	26.9223
5	-728.9545	291.0807	27.5152	15	-728.8443	290.8148	26.9930
6	-728.9050	291.0540	27.4393	16	-728.8553	290.8433	26.9808
7	-728.8913	291.0288	27.4298	17	-729.0353	290.9973	26.7905
8	-729.0968	291.1005	27.2698	18	-729.2663	291.0640	27.0090
9	-729.1877	291.1173	27.3247	19	-729.2768	291.0505	27.0520
10	-729.1555	291.1735	27.2490	20	-729.2603	291.1343	26.9793

MEAN ANKLE AXIS LOCATION = [-729.0375 291.0628 27.2556]
STANDARD DEVIATION = [0.1533 0.1000 0.2564]

Using the detection method described in the ***Methods*** section 3.2, the estimate obtained with the tenth measurement set, shown with **, did not adhere to Chauvenet's criterion, with a standard score of **[4.1060, 2.0848, 3.7867]**, and was therefore eliminated.

Table 4.2. *Measured model ankle joint location (mm)*

DATA SET	x	y	z	DATA SET	x	y	z
1	-723.0125	298.0238	24.3842	11	-715.2044	302.9013	24.6026
2	-723.3669	298.2991	24.4718	12	-720.6396	298.0199	25.5444
3	-723.9806	297.7448	24.8839	13	-724.2263	295.8417	25.7294
4	-729.4877	293.0835	27.0217	14	-724.4132	295.9572	25.3854
5	-723.1859	296.7720	25.2199	15	-723.8279	295.7197	25.1967
6	-724.0240	296.1249	25.5078	16	-725.3554	294.6875	25.6860
7	-712.3165	291.4491	25.1368	17	-724.6952	294.0397	25.6239
8	-721.0020	296.7626	25.3068	18	-722.9390	299.0258	24.9082
9	-724.3713	296.5606	25.8606	19	-723.2109	298.9235	25.2210
10	-662.5584	302.8491	20.2844 **	20	-724.0266	298.0031	25.5280

REVISED MEAN ANKLE AXIS LOCATION = [-722.8045 296.7337 25.3273]
STANDARD DEVIATION = [3.6788 2.4946 0.5894]

4.1.2). *Experimentally calculated and measured model ankle axis directions*

Tables 4.3 and 4.4 show the experimentally calculated and measured model directions of the ankle joint axis for the model, for each of the twenty data sets. Each data set was comprised of three MTP locations.

Table 4.3. *Experimentally calculated ankle joint direction (UNIT VECTOR)*

DATA SET	x	y	z	DATA SET	x	y	z
1	-0.8442	-0.5163	0.1439	11	-0.8448	-0.5162	0.1409
2	-0.8444	-0.5162	0.1436	12	-0.8443	-0.5170	0.1411
3	-0.8444	-0.5163	0.1431	13	-0.8450	-0.5160	0.1406
4	-0.8442	-0.5165	0.1431	14	-0.8447	-0.5169	0.1392
5	-0.8443	-0.5166	0.1426	15	-0.8442	-0.5176	0.1394
6	-0.8445	-0.5163	0.1419	16	-0.8441	-0.5178	0.1392
7	-0.8442	-0.5168	0.1421	17	-0.8450	-0.5166	0.1380
8	-0.8447	-0.5163	0.1409	18	-0.8452	-0.5161	0.1392
9	-0.8449	-0.5159	0.1414	19	-0.8453	-0.5159	0.1394
10	-0.8450	-0.5159	0.1407	20	-0.8453	-0.5158	0.1393

MEAN ANKLE JOINT AXIS DIRECTION = [-0.8446 -0.5165 0.1410]
STANDARD DEVIATION = [0.0004 0.0005 0.0017]

The last of the measured model data set values was eliminated, since it did not satisfy Chauvenet's criterion, with a standard score of **[3.0052, 0.6418, 0.5864],** and was therefore assumed to be erroneous.

Table 4.4. *Measured model ankle joint direction (UNIT VECTOR)*

DATA SET	x	y	z	DATA SET	x	y	z
1	-0.8482	-0.5197	0.1028	11	-0.8437	-0.5296	0.0872
2	-0.8475	-0.5206	0.1036	12	-0.8463	-0.5230	0.1012
3	-0.8471	-0.5209	0.1054	13	-0.8470	-0.5211	0.1052
4	-0.8484	-0.5110	0.1385	14	-0.8466	-0.5271	0.0734
5	-0.8466	-0.5130	0.1421	15	-0.8475	-0.5226	0.0929
6	-0.8460	-0.5061	0.1677	16	-0.8485	-0.5206	0.0953
7	-0.8466	-0.5010	0.1796	17	-0.8483	-0.5209	0.0949
8	-0.8462	-0.5077	0.1620	18	-0.8500	-0.5191	0.0898
9	-0.8479	-0.5061	0.1581	19	-0.8505	-0.5204	0.0765
10	-0.8480	-0.5052	0.1601	20	-0.8540	-0.5112	0.0971**

REVISED MEAN ANKLE JOINT AXIS DIRECTION = [-0.8474 -0.5166 0.1177]
STANDARD DEVIATION = [0.0015 0.0081 0.0340]

Figure 4.1 shows the mean of the twenty experimentally calculated values of the orientation of the ankle joint axis, with respect to the measured orientation of the conceptual model's ankle axis.

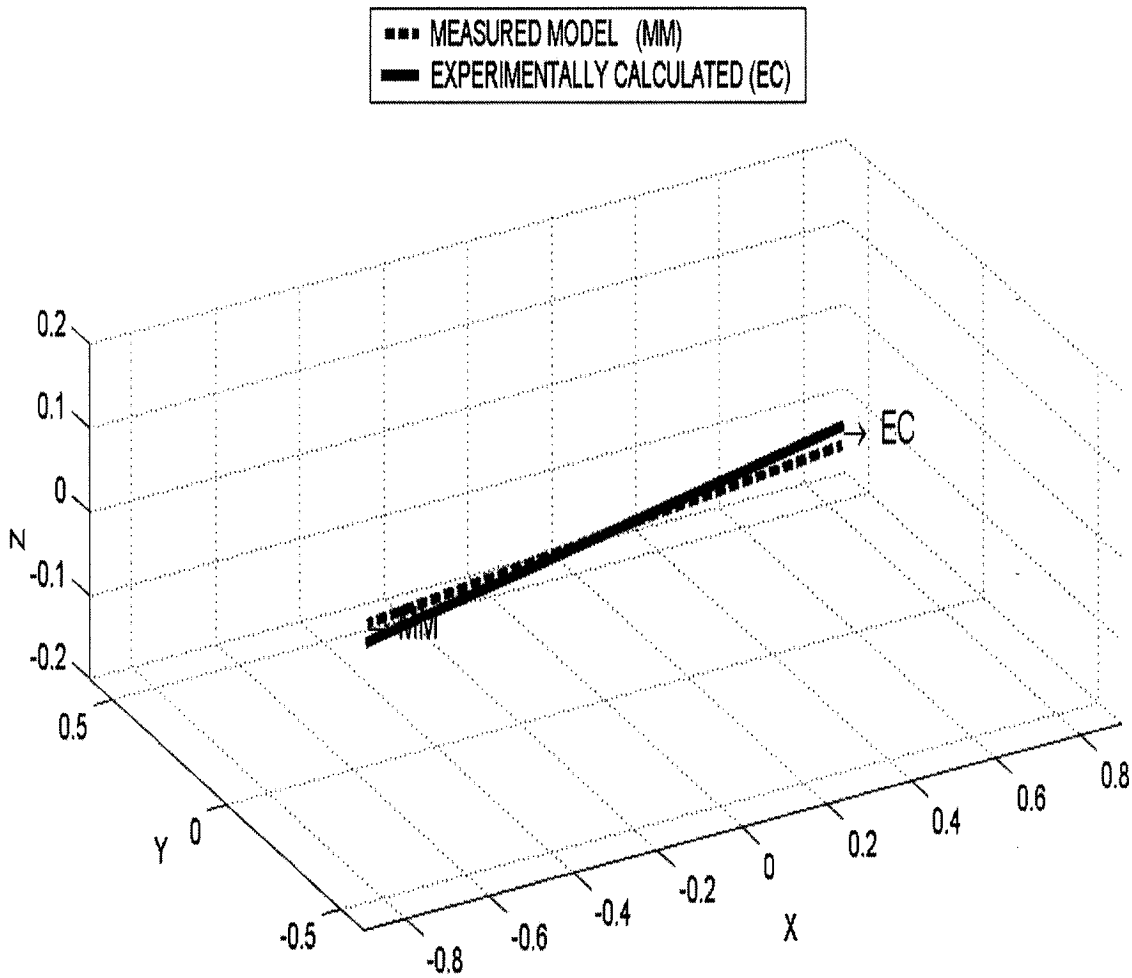

Figure 4.1 *The experimentally calculated and conceptual model measured orientation of the ankle joint axis*

Figure 4.2 shows the orientation of the experimentally calculated and measured model ankle joint axes within the global coordinate system, relative to the first location of the medial tibial plateau (MTP).

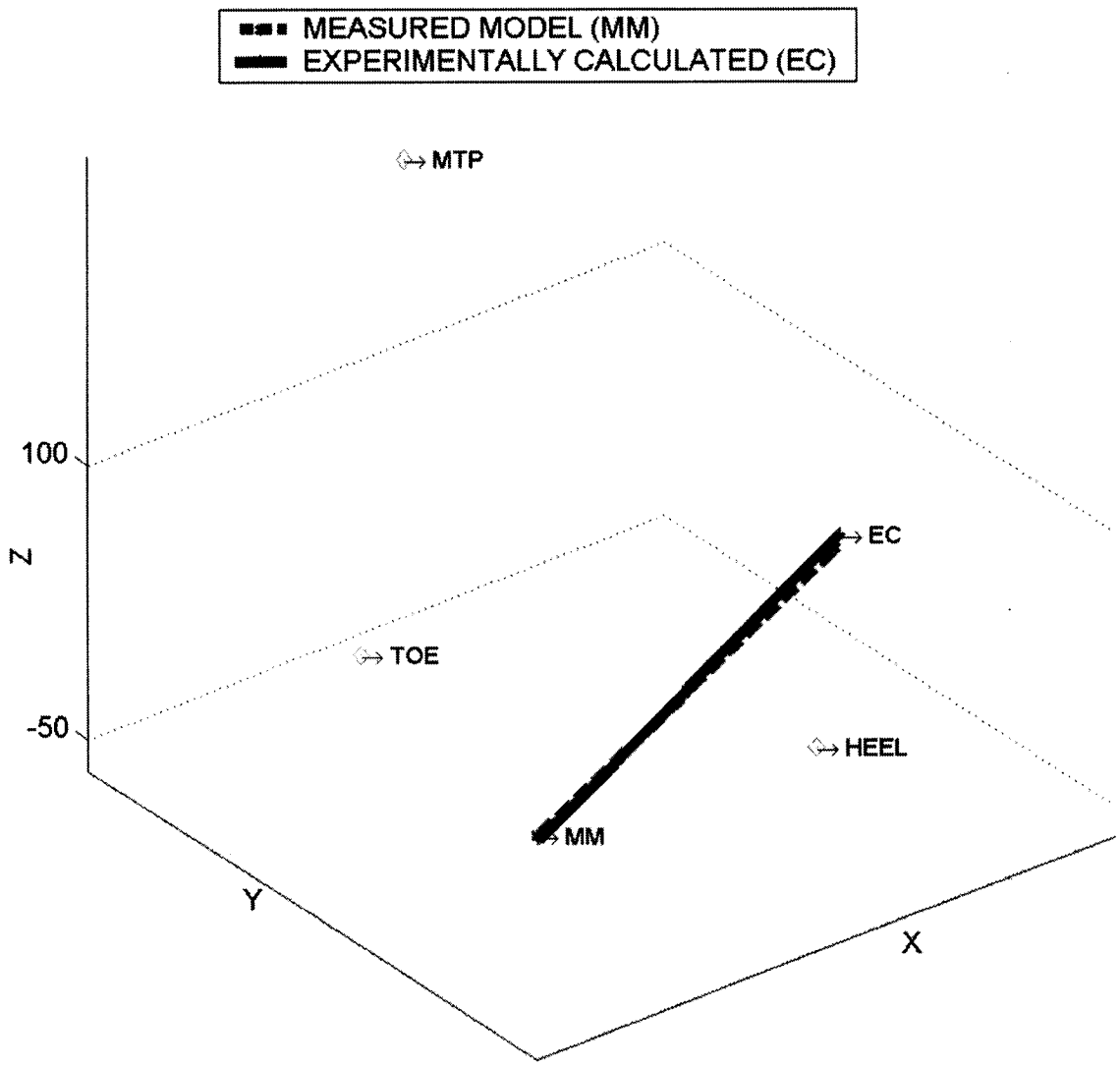

Figure 4.2 *Location and orientation of the experimentally calculated and measured model ankle joint axes in relation to the first MTP location, and the model foot, heel, and toe locations*

4.1.3). *Experimentally calculated and measured model subtalar axis locations*

Tables 4.5 and 4.6 show the location of the experimentally calculated values (midway between the heel and navicular markers) and the measured model subtalar axis. Each data set was comprised of four equidistant MTP locations.

Table 4.5. *Experimentally calculated subtalar joint location (mm)*

DATA SET	x	y	z	DATA SET	x	y	z
1	-677.5760	367.2193	-4.3855	11	-677.3690	367.0780	-4.0884
2	-677.4789	367.2214	-4.5492	12	-677.3273	367.1654	-4.0972
3	-677.5154	367.2328	-4.4429	13	-677.2880	367.2417	-4.2501
4	-677.5396	367.1598	-4.3778	14	-677.3156	367.2279	-4.1605
5	-677.5235	367.1814	-4.4144	15	-677.3189	367.2806	-4.2977
6	-677.5740	367.1519	-4.3745	16	-677.2970	367.3296	-4.2821
7	-677.6025	367.1213	-4.3952	17	-677.4413	367.2549	-4.2746
8	-677.6102	367.1349	-4.4521	18	-677.4094	367.2347	-4.3233
9	-677.3819	367.1882	-4.1541	19	-677.2764	367.1545	-4.0294
10	-677.3804	367.1727	-4.1744	20	-677.4081	367.2295	-4.3014

MEAN SUBTALAR JOINT AXIS LOCATION = [-677.4317 367.1990 -4.2912]
STANDARD DEVIATION = [0.1128 0.0592 0.1386]

Table 4.6. *Measured model subtalar joint location (mm)*

DATA SET	x	y	z	DATA SET	x	y	z
1	-683.8837	364.8531	-4.7552	11	-681.0996	364.2370	-4.4767
2	-683.0116	367.5349	-4.6814	12	-677.3484	367.0745	-4.0718
3	-682.9774	366.6825	-4.7072	13	-679.6453	359.1669	-4.8673
4	-679.6516	362.3659	-5.0197	14	-679.0545	368.8958	-4.0861
5	-679.1985	361.2872	-5.1096	15	-679.1734	369.0061	-3.9111
6	-680.7351	367.6771	-4.4667	16	-677.3146	367.3270	-4.2873
7	-677.8350	362.2965	-4.6385	17	-677.2804	367.3498	-4.2741
8	-681.8299	371.8835	-3.9717	18	-681.3259	364.8809	-4.5743
9	-680.7179	367.8447	-4.2941	19	-680.9969	368.8110	-4.3189
10	-678.2170	362.4894	-4.7819	20	-681.3665	367.7169	-4.0872

MEAN SUBTALAR JOINT AXIS LOCATION = [-680.1332 365.9690 -4.4690]
STANDARD DEVIATION = [1.9850 3.1662 0.3499]

4.1.4). *Experimentally calculated and measured model subtalar joint axis directions*

Tables 4.7 and 4.8 show the experimentally calculated and measured model directions of the subtalar joint axis. Each data set was comprised of three equidistant MTP locations.

Table 4.7. *Experimentally calculated subtalar joint direction (unit vector)*

DATA SET	x	y	z	DATA SET	x	y	z
1	-0.7124	0.3027	0.6332	11	-0.7104	0.3042	0.6347
2	-0.7121	0.3023	0.6337	12	-0.7109	0.3042	0.6341
3	-0.7117	0.2991	0.6357	13	-0.7101	0.3037	0.6352
4	-0.7130	0.2962	0.6355	14	-0.7125	0.3059	0.6314
5	-0.7137	0.2921	0.6366	15	-0.7123	0.3056	0.6319
6	-0.7114	0.3015	0.6349	16	-0.7142	0.3035	0.6307
7	-0.7111	0.3016	0.6351	17	-0.7142	0.3033	0.6308
8	-0.7105	0.3017	0.6358	18	-0.7140	0.3031	0.6311
9	-0.7107	0.3047	0.6341	19	-0.7144	0.3040	0.6303
10	-0.7104	0.3046	0.6345	20	-0.7143	0.3034	0.6307

MEAN SUBTALAR JOINT AXIS DIRECTION = [-0.7122 0.3024 0.6335]
STANDARD DEVIATION = [0.0015 0.0033 0.0021]

Table 4.8. *Measured model subtalar joint direction (unit vector)*

DATA SET	x	y	z	DATA SET	x	y	z
1	-0.7434	0.3128	0.5912	11	-0.7578	0.3160	0.5708
2	-0.7264	0.2967	0.6199	12	-0.7090	0.2720	0.6506
3	-0.7070	0.2902	0.6449	13	-0.7326	0.3188	0.6014
4	-0.7182	0.2904	0.6323	14	-0.7127	0.2665	0.6489
5	-0.7366	0.3108	0.6008	15	-0.7308	0.2963	0.6150
6	-0.6991	0.2739	0.6605	16	-0.7061	0.2719	0.6538
7	-0.7750	0.3232	0.5431	17	-0.7118	0.2799	0.6441
8	-0.7190	0.2757	0.6380	18	-0.7191	0.3007	0.6265
9	-0.6923	0.2609	0.6728	19	-0.7610	0.3195	0.5646
10	-0.7066	0.2793	0.6502	20	-0.7066	0.2793	0.6502

MEAN SUBTALAR JOINT AXIS DIRECTION = [-0.7237 0.2917 0.6239]
STANDARD DEVIATION = [0.0220 0.0198 0.0352]

Figure 4.3 shows the experimentally calculated orientation of the subtalar joint axis, with respect to the measured conceptual model orientation of the ankle axis, as defined by the axis markers.

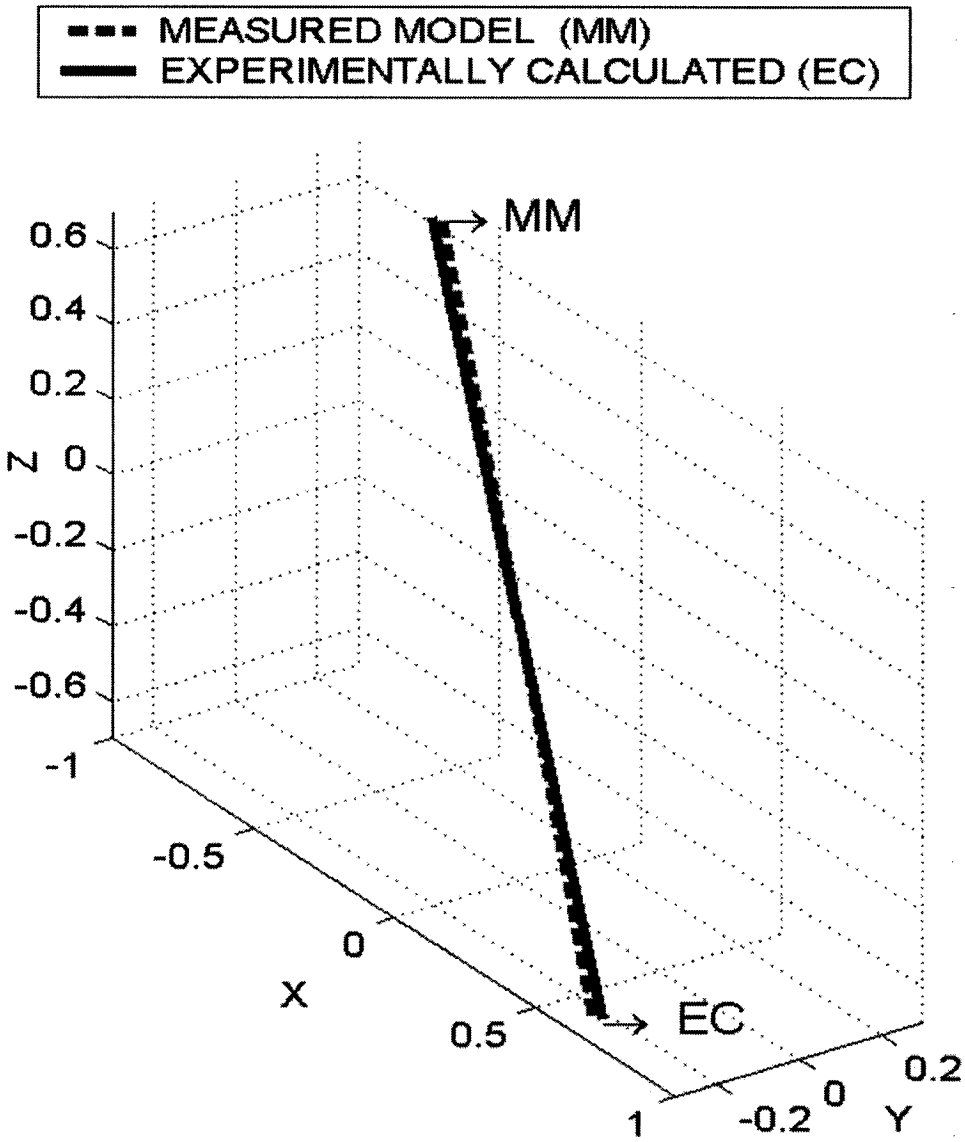

Figure 4.3 *The experimentally calculated and conceptual model measured orientation of the subtalar joint axis*

Figure 4.4 shows the orientation of the subtalar joint axes (experimentally calculated and measured model) within the global coordinate system, in relation to the first location of the medial tibial plateau (MTP)

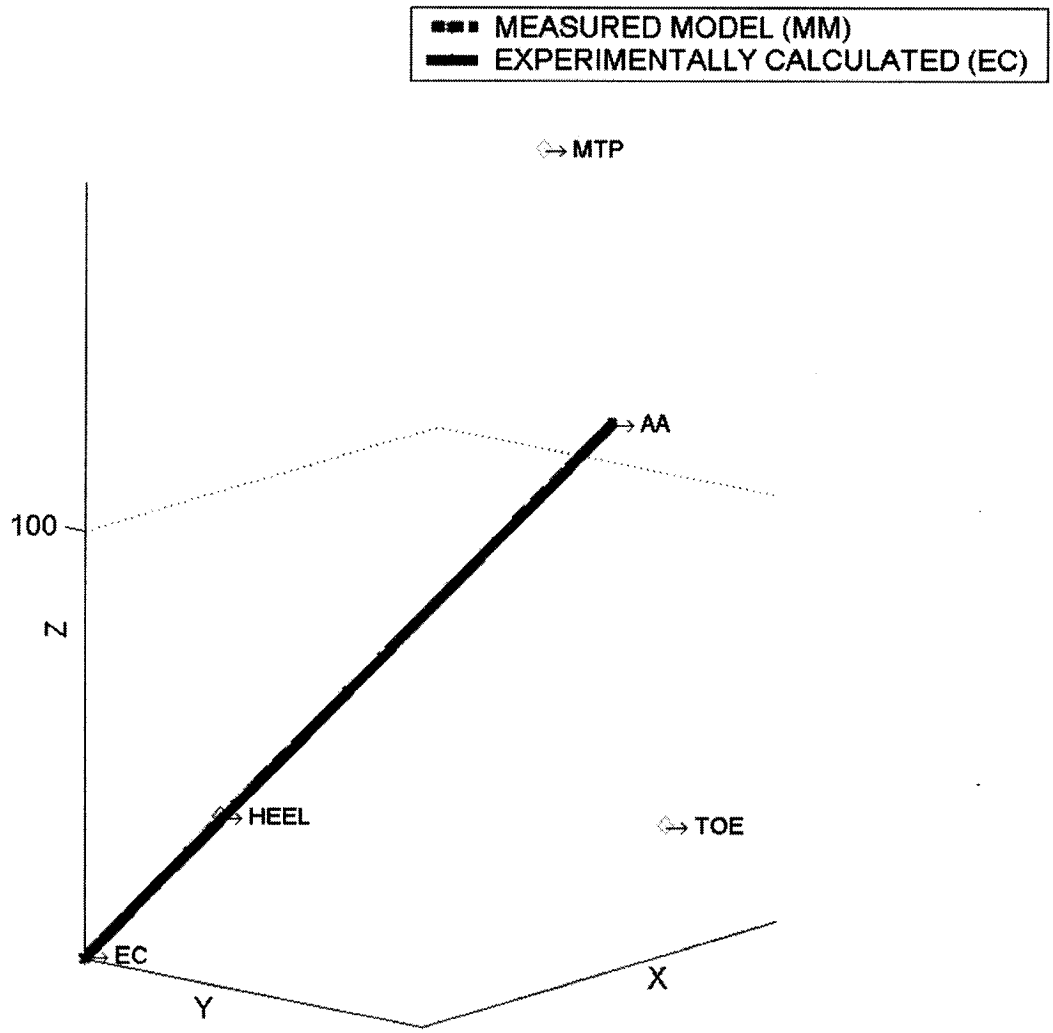

Figure 4.4 *Location and orientation of the experimentally calculated and measured model subtalar joint axes in relation to the first MTP location and the model foot, heel, and toe locations*

4.1.5). ***Variation in experimental data set measurement incremental distances***

Table 4.9 shows the incremental distances that exist between successive MTP (model marker) measurement locations for each of the data sets used to calculate ankle joint location and axis orientation in Tables 4.2 and 4.4, respectively. The same data set was previously used in the calculation of the axis location and orientation. The MTP values (locations) were selected, so that the distances between successive values were very close in magnitude, since this proved to afford the best results. The performance metric, $\Delta\mathbf{d}$, is defined as the distance between the experimentally calculated ankle joint location of each data set, (x_i, y_i, z_i), and the mean measured model ankle joint location, (x_m, y_m, z_m) that is, Figure 4.5:

$$\Delta d = [\,(x_i - x_m)^2 + (y_i - y_m)^2 + (z_i - z_m)^2\,], \text{ where} \qquad (4.1)$$

$$\mathbf{L1 \cong L2}$$

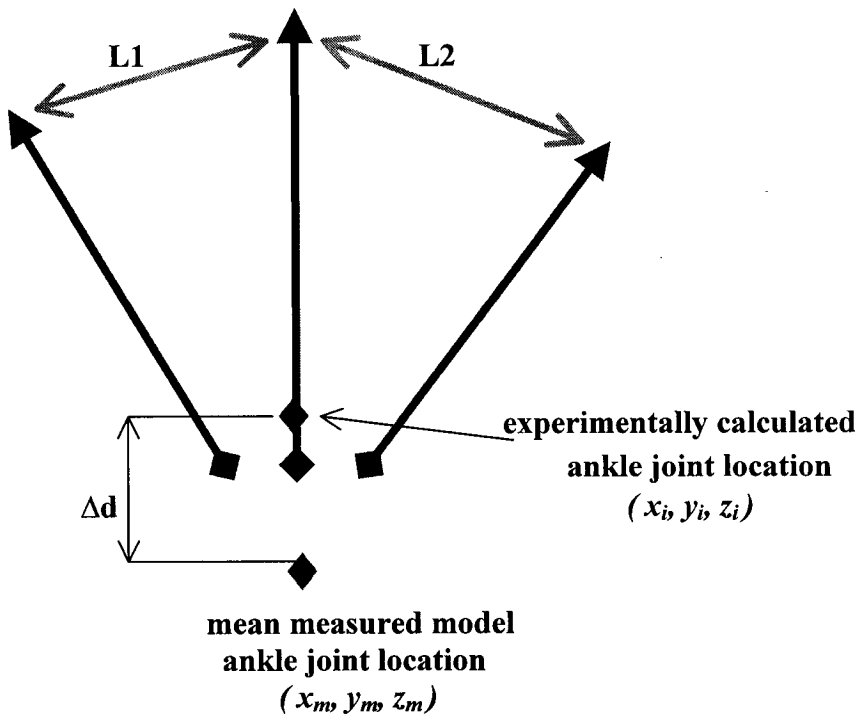

Figure 4.5 *Defining the performance metric, Δd*

Table 4.9. *Effect of variations in experimental data set MTP measurement incremental distances in calculation of ankle joint location and axis orientation*

DATA SET	DISTANCES L1 & L2 (mm)	Δd	DATA SET	DISTANCES L1 & L2 (mm)	Δd
1	64.8920		11	65.0038	
	58.5385	8.5472		60.9480	8.7004
2	65.2694		12	65.2392	
	58.6070	8.5846		60.7924	8.6969
3	65.1824		13	64.9155	
	58.7654	8.5993		61.4391	8.7292
4	65.0074		14	64.9012	
	59.3484	8.5659		61.5466	8.6105
5	64.8595		15	64.9754	
	59.7420	8.6351		61.9250	8.6190
6	64.8497		16	63.9580	
	60.1772	8.5986		62.1662	8.6048
7	64.9853		17	64.1801	
	60.1086	8.6032		62.3093	8.5948
8	64.3954		18	63.8443	
	60.6360	8.6659		62.3781	8.7594
9	65.1824		19	63.7581	
	58.7654	8.7339		62.5796	8.7843
10	65.0074		20	63.4095	
	59.3484	8.6570		62.743	8.7040

The performance metric, Δd, shows that the distance between the experimentally calculated value and the mean measured value was essentially equal for all data sets. The necessity for the distances to be about the same is illustrated by considering three adjacent MPT points with very different distances between them. With distances between adjacent MTP locations of 17.0479 mm and 105.8327 mm, the resulting axis direction was [0.7951, 0.5890, 0.1442]. With adjacent distances of 6.8064mm and 116.4565mm, the resulting axis direction was [0.8182, 0.5714, 0.0640]. These values were quite different from the original mean measured value of [-0.8474 -0.5166 0.1177].

Table 4.10 shows the effect of variations in the distances between the MTP marker locations selected for the data sets used to calculate subtalar joint location and axis direction, in calculating the subtalar axis direction. The marker locations were again chosen, so that the distances between the markers were very close in magnitude.

Table 4.10. *Effect of variations in experimental data set MTP measurement incremental distances in calculation of subtalar joint location and axis orientation*

DATA SET	DISTANCES L1 & L2 (mm)	Δd	DATA SET	DISTANCES L1 & L2 (mm)	Δd
1	43.2010		11	44.3537	
	43.2763	2.8477		45.4572	3.0026
2	49.6896		12	56.9575	
	49.5743	2.9360		57.2211	3.0729
3	59.9497		13	40.1313	
	59.3150	2.9070		38.6909	3.1246
4	50.1469		14	32.3336	
	50.1329	2.8553		31.7158	3.1014
5	55.5114		15	30.6700	
	56.3310	2.8781		31.3580	3.1097
6	43.9879		16	33.3490	
	44.2207	2.8209		31.3580	3.1512
7	55.6575		17	52.0448	
	54.2403	2.7816		54.2403	2.9896
8	44.0942		18	54.9777	
	43.3184	2.7794		53.2132	3.0071
9	24.7399		19	54.4264	3.1241
	24.8769	3.0258		54.7424	
10	52.0448		20	29.9874	3.0072
	54.2403	3.0189		26.2110	

Here again, the performance metric, Δd, shows that the distance between the experimentally calculated value and the mean measured value was essentially equal for all data sets. To illustrate the necessity of using adjacent points with almost equal distances, points with distances of 8.2983 mm and 55.5114 mm were used. The axis direction that resulted was [0.8699, -0.3459, -0.3516]. With distances of 4.3563 mm and 49.6896 mm, the axis direction was [0.7708, -0.3111, -0.5559]. These results were quite different from the mean measured value of [-0.7237 0.2917 0.6239].

DISTANCE

Table 4.11 shows the distances from the medial tibial plateau (MTP) to the experimentally calculated ankle joint location, as predicted from the respective data set, MTP and ankle marker locations. Each distance shown is the average of the measured values for each of the four MTP markers relative to the joint axis, for each of the twenty data sets.

Table 4.11. *Experimentally calculated distances from the medial tibial plateau to the predicted location of the ankle joint axis*

DATA SET	DISTANCE (mm)	DATA SET	DISTANCE (mm)
1	287.8905	11	287.6930
2	287.9053	12	287.7080
3	287.8376	13	287.665
4	287.8905	14	287.844
5	287.9164	15	287.849
6	287.9264	16	287.762
7	287.8917	17	287.8715
8	287.8418	18	287.5206
9	287.8267	19	287.5099
10	287.8007	20	287.5919

DISTANCE FROM MTP LOCATION TO EXPERIMENTALLY PREDICTED MEAN ANKLE JOINT AXIS LOCATION = 287.7892 mm

STANDARD DEVIATION = [0.1299]

Table 4.12 shows the distances from the medial tibial plateau (MTP) to the measured ankle joint axis for the conceptual model. Each distance represents the average of the distance from each of the four MTP measured (marker) locations to the predicted (measured) joint axis location. W_i and W_f represent the values of the minimized equation (by Davidon's method), demonstrating the degree to which the equation was minimized.

Table 4.12. *Distance from the conceptual model medial tibial plateau to the measured ankle joint axis*

DATA SET	MEAN	DAVIDON MINIMIZATION COSTS	
	DISTANCE (mm) (MTP TO ANKLE AXIS)	INITIAL COST, W_i	FINAL COST, W_f
1	289.318	9.6714	1.9156
2	289.083	9.7157	1.9011
3	288.7357	8.8041	2.0345
4	287.7501	7.9906	3.6815
5	288.6970	7.9360	2.2948
6	288.554	7.1374	2.4986
7	290.3159	6.6826	2.6124
8	288.468	8.3146	2.8492
9	287.984	8.0730	2.9600
10	298.6223	10.7973	2.1327
11	288.0206	10.7450	3.1147
12	287.8501	10.1219	2.7831
13	288.0239	6.9507	2.4492
14	288.2848	7.1142	2.3590
15	288.5023	9.2354	2.5473
16	288.1592	7.7014	2.7441
17	288.3589	6.7596	2.7642
18	287.9980	12.1298	1.8448
19	287.7656	11.4920	1.8754
20	287.6714	9.6761	2.0513

DISTANCE FROM DATA SET MEAN MTP LOCATION TO MEAN MEASURED ANKLE JOINT AXIS LOCATION= 288.9081 mm

STANDARD DEVIATION = [2.3720]

Table 4.13 shows the distances from the measured MTP (marker) locations to the measured location of the markers on the subtalar joint axis of the conceptual model. The distances shown are the average values of the MTP-to-subtalar axis for the four MTP marker locations, for each of the twenty measurement data sets.

Table 4.13. *Distance from the conceptual model medial tibial plateau to the experimentally calcuated subtalar joint axis*

DATA SET	DISTANCE L1 & L2 (mm)	DATA SET	DISTANCE L1 & L2 (mm)
1	310.1641	11	309.9423
2	310.2068	12	310.3393
3	310.0192	13	310.1334
4	310.2969	14	309.8095
5	310.0963	15	309.9976
6	310.1827	16	309.9693
7	310.2274	17	309.9470
8	310.0013	18	309.8110
9	310.1939	19	309.8697
10	309.7231	20	310.3064

MEAN DISTANCE FROM MTP TO SUBTALAR JOINT AXIS = 310.0619 mm
STANDARD DEVIATION = [0.1796]

Table 4.14 shows the distances from the measured MTP (marker) locations to the subtalar joint axis, as defined by the model joint axis markers. Each distance represents the average of the distance from each of the four MTP locations in the data set to the subtalar joint axis.

Table 4.14. *Distance from the measured medial tibial plateau markers to the subtalar joint axis markers in the conceptual model*

DATA SET	DISTANCE (mm)	W_i	W_f
1	308.7699	3.5208	0.0113
2	308.5325	3.5442	0.7448
3	308.4882	1.4840	0.7736
4	310.5742	5.1983	0.1750
5	310.6738	8.0908	0.2363
6	309.1738	1.3837	0.7600
7	310.5744	1.4607	0.0116
8	308.2356	3.8767	0.8449
9	309.1797	0.6398	0.4016
10	309.1859	3.4057	0.2682
11	309.8894	3.3613	1.1689
12	311.0542	14.5166	0.0139
13	309.4035	6.2045	1.7052
14	308.9913	4.3354	1.4540
15	309.9844	0.5911	0.3760
16	309.9700	0.5924	0.4130
17	308.9530	1.8657	0.4742
18	308.6411	0.6307	0.6092
19	308.5260	2.0114	1.0631
20	310.5455	1.8652	0.0054

MEAN DISTANCE FROM MTP TO SUBTALAR JOINT AXIS = 309.4673 mm
STANDARD DEVIATION = [0.8716]

The perpendicular distance between the experimentally calculated ankle and subtalar joint axes was computed and compared to the perpendicular distance between the measured ankle and subtalar joint axes markers in the conceptual model, Figure 4.6.

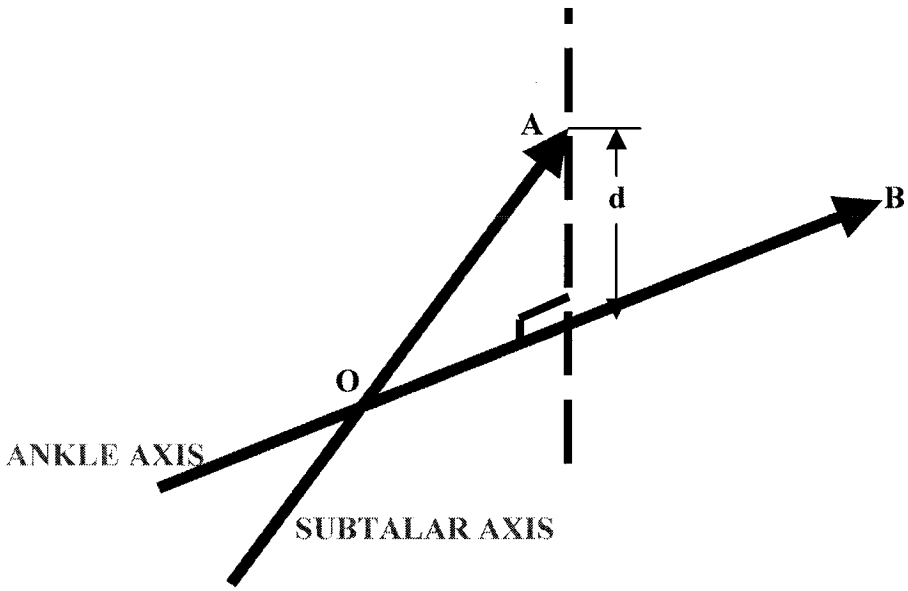

Figure 4.6 *The perpendicular distance between axes*

The perpendicular distance was then calculated:

$$\textbf{DISTANCE, d} = |\textbf{dot(AB\_vect, vect\_3)}|/|\textbf{vect\_3}| \qquad \textit{(4.2)}$$

where AB_vect is a vector between two points A (a point on the ankle axis) and B (a point on the subtalar axis), and vect_3 is the cross product of the direction vectors of the two axes (ankle and subtalar). The distance between the experimental ankle and subtalar axes was 39.97mm (1.57 inches), while the distance between the two theoretical axes was 39.82mm (1.57 inches).

An important feature of the program developed is to eliminate data values that are too far off from the average of the rest of the data. Although this was not the case with the above data set, in such an event, that particular value would be eliminated and the average recalculated, using Chauvenet's criterion, as described in the ***Methods*** section.

4.2). *Results for human subject*

4.2.1). *Experimentally calculated and approximate anatomized ankle axis locations*

Tables 4.15 and 4.16 show the experimentally predicted and approximate anatomical ankle axis locations, determined from ten data sets, acquired from Qualisys System measurements of an experimental subject. Each data set was comprised of four MTP locations, which were equidistant from each other. Ten data sets were compiled and used, instead of the twenty used in tests of the wooden models, as the speed of rotation about the joint was greater for the human subject than for the model, to keep the motion as smooth and as natural as possible. The eighth measurement data set value was eliminated from the approximate anatomical set of values because the estimate exceeded Chauvenet's criterion.

Table 4.15. *Experimentally calculated ankle joint axis location (mm)*

DATA SET	x	y	z	DATA SET	x	y	z
1	-125.2215	2.6031	-5.4225	6	-124.8879	2.6009	-5.4601
2	-124.7486	2.5251	-5.4251	7	-124.8532	2.5565	-5.4417
3	-124.7515	2.5158	-5.4229	8	-124.6554	2.5336	-5.4613
4	-124.6606	2.5546	-5.4186	9	-124.7864	2.5556	-5.4295
5	-124.8276	2.5511	-5.4404	10	-124.6283	2.5594	-5.5110

MEAN ANKLE AXIS JOINT LOCATION = [-124.8021 2.5556 -5.4433]
STANDARD DEVIATION = [0.1712 0.0286 0.0282]

Table 4.16. *Approximate anatomical ankle joint axis location (mm)*

DATA SET	x	y	z	DATA SET	x	y	z
1	-125.1636	2.5401	-5.4579	6	-124.8541	2.5458	-5.4927
2	-124.7014	2.4567	-5.4628	7	-126.0253	-0.2078	-7.2410
3	-124.8527	-2.9048	-8.6660	8	-129.2309	-5.6647	-10.7298**
4	-124.6105	2.4892	-5.4556	9	-125.5999	1.3629	-6.2467
5	-124.7727	2.4857	-5.4776	10	-125.3724	-3.5428	-9.3194

MEAN ANKLE JOINT AXIS LOCATION = [-125.1058 2.2818 6.5355]
STANDARD DEVIATION = [0.4758 2.4605 1.5229]

4.2.2). *Experimentally calculated and approximate anatomical ankle axis directions*

Tables 4.17 and 4.18 show the experimentally calculated and approximate anatomical predicted values of the ankle axis directions, determined from each of the ten respective data sets.

Table 4.17. *Experimentally calculated ankle joint axis direction*

DATA SET	x	y	z	DATA SET	x	y	z
1	-0.8162	-0.5569	-0.1539	6	-0.8160	-0.5582	-0.1499
2	-0.8161	-0.5587	-0.1475	7	-0.8162	-0.5582	-0.1491
3	-0.8161	-0.5589	-0.1473	8	-0.8162	-0.5589	-0.1469
4	-0.8167	-0.5582	-0.1464	9	-0.8160	-0.5586	-0.1487
5	-0.8163	-0.5582	-0.1484	10	-0.8165	-0.5583	-0.1468

MEAN ANKLE JOINT AXIS DIRECTION = [-0.8162 -0.5583 -0.1485]
STANDARD DEVIATION = [0.0002 0.0006 0.0022]

Table 4.18. *Approximate anatomical ankle joint axis direction*

DATA SET	x	y	z	DATA SET	x	y	z
1	-0.7780	-0.5127	-0.3631	6	-0.7259	-0.6878	0.0026
2	-0.7176	-0.6953	-0.0408	7	-0.7606	-0.5628	-0.3237
3	-0.7295	-0.6840	- 0.0097	8	-0.7542	-0.6330	-0.1749
4	-0.7684	-0.6096	-0.1945	9	-0.7610	-0.6095	-0.2223
5	-0.7643	-0.5572	-0.3247	10	-0.7544	-0.5249	-0.3942

MEAN ANKLE JOINT AXIS DIRECTION = [-0.7514 -0.6077 -0.1964]
STANDARD DEVIATION = [0.0201 0.0675 0.1604]

Figure 4.7 shows the experimentally calculated orientation of the ankle axis, in comparison to the approximate anatomically predicted orientation of the ankle axis.

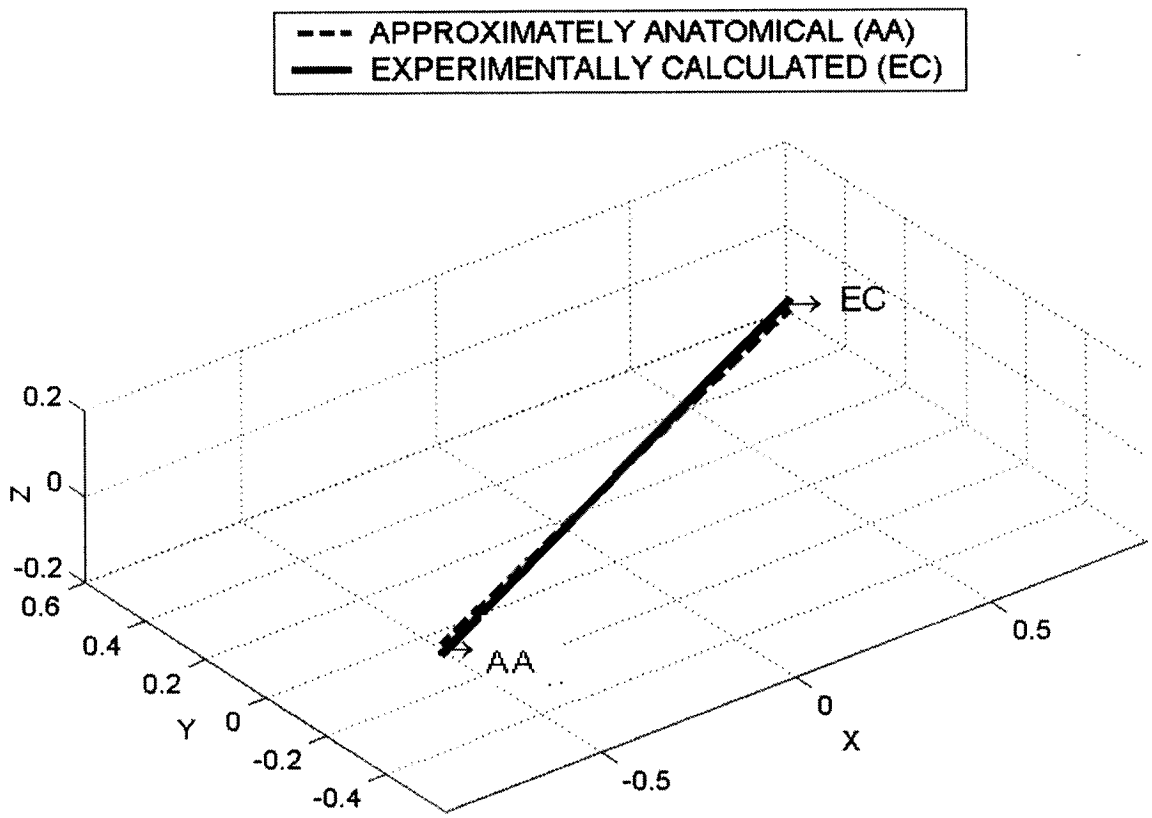

Figure 4.7 *Experimentally calculated and approximate anatomical ankle joint axes*

Figure 4.8 shows the experimentally calculated and anatomically predicted orientations of the ankle axis within the global coordinate system, relative to the leg medial tibial plateau (MTP) and the foot, heel, and toes.

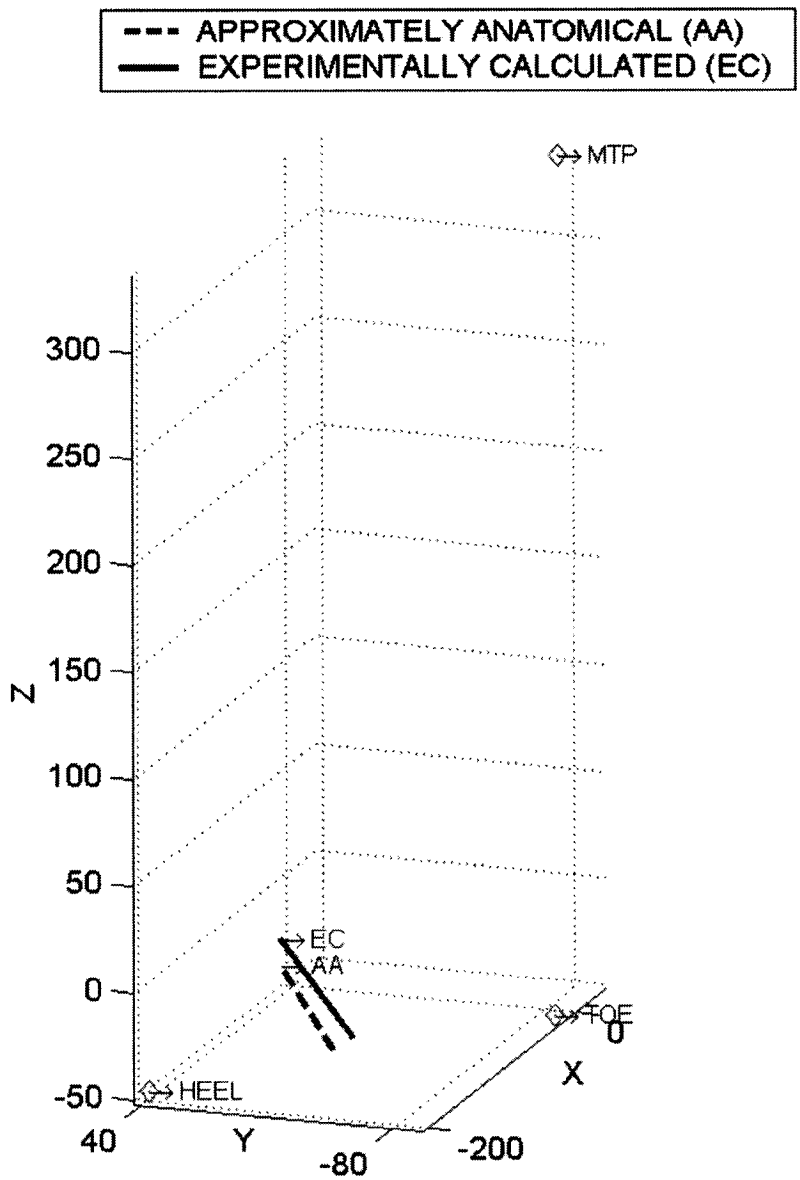

Figure 4.8 *Experimentally calculated and measured locations and orientations of the ankle joint axes in relation to the leg MTP and foot, heel, and toe locations*

4.2.3). *Experimentally calculated and approximate anatomical subtalar joint axis locations*

Tables 4.19 and 4.20 show the experimentally calculated and approximate anatomically predicted (midway between the calcaneal and navicular markers) subtalar joint axis locations, for the ten respective data sets. Each data set was comprised of four equidistant MTP locations. Here the seventh approximate anatomical data set and predicted joint location was eliminated using Chauvenet's criterion.

Table 4.19. *Experimentally calculated subtalar joint location (mm)*

DATA SET	x	y	z	DATA SET	x	y	z
1	-83.7432	-60.6631	-24.3233	6	-84.9661	-61.5875	-24.3518
2	-83.8664	-60.7906	-24.4025	7	-84.7044	-61.3028	-24.4763
3	-84.5934	-61.1775	-24.5034	8	-84.2349	-60.8336	-24.4229
4	-84.2259	-60.8273	-24.3959	9	-83.9084	-60.8593	-24.4322
5	-84.1441	-60.6887	-24.4771	10	-83.8593	-60.8293	-24.4561

MEAN SUBTALAR JOINT AXIS LOCATION = [-84.2246 -60.9560 -24.4241]
STANDARD DEVIATION = [0.4104 0.2999 0.0573]

Table 4.20. *Approximate anatomically predicted subtalar joint axis location (mm)*

DATA SET	x	y	z	DATA SET	x	y	z
1	-80.1817	-54.1451	-28.1487	6	-78.2279	-52.1084	-28.7747
2	-79.9348	-53.9127	-28.5233	7	-85.7445	-61.3488	-25.5830**
3	-80.0128	-53.5057	-28.5608	8	-79.0809	-52.2332	-29.3272
4	-79.2769	-52.7782	-28.9843	9	-78.0450	-50.9979	-29.9789
5	-77.9432	-51.4980	-29.6971	10	-77.5867	-51.6557	-28.8827

MEAN SUBTALAR JOINT AXIS LOCATION = [-78.9211 -52.5372 -28.9864]
STANDARD DEVIATION = [0.9966 1.1167 0.5873]

4.2.4). *Experimentally calculated and approximate anatomical subtalar axis directions*

Tables 4.21 and 4.22 show the directions of the experimentally calculated and approximate anatomical subtalar joint axes for the ten data sets, Table 4.21. Each data set was comprised of three MTP locations.

Table 4.21. *Experimentally calculated subtalar joint axis direction (UNIT VECTOR)*

DATA SET	x	y	z	DATA SET	x	y	z
1	-0.9256	0.2199	-0.3080	6	-0.9207	0.2265	-0.3179
2	-0.9254	0.2189	-0.3093	7	-0.9222	0.2241	-0.3150
3	-0.9225	0.2235	-0.3148	8	-0.9247	0.2194	-0.3112
4	-0.9246	0.2191	-0.3115	9	-0.9250	0.2198	-0.3099
5	-0.9248	0.2192	-0.3109	10	-0.9247	0.2199	-0.3107

MEAN SUBTALAR JOINT AXIS DIRECTION = [-0.9240 0.2210 -0.3119]
STANDARD DEVIATION = [0.0016 0.0027 0.0030]

Table 4.22. *Approximate anatomically predicted subtalar joint axis direction (UNIT VECTOR)*

DATA SET	x	y	z	DATA SET	x	y	z
1	-0.7936	0.3120	-0.5223	6	-0.7555	0.2673	-0.5981
2	-0.7187	0.1978	-0.6666	7	-0.7860	0.3300	-0.5228
3	-0.6611	0.1434	-0.7364	8	-0.7482	0.2645	-0.6085
4	-0.7084	0.2015	-0.6764	9	-0.7545	0.2765	-0.5952
5	-0.7222	0.2303	-0.6522	10	-0.7576	0.2652	-0.5964

MEAN SUBTALAR JOINT AXIS DIRECTION = [-0.7406 0.2489 -0.6175]
STANDARD DEVIATION = [0.0392 0.0563 0.0672]

Figure 4.9 shows the experimentally calculated orientation of the subtalar joint axis, in comparison to the approximate anatomically predicted orientation of the subtalar axis.

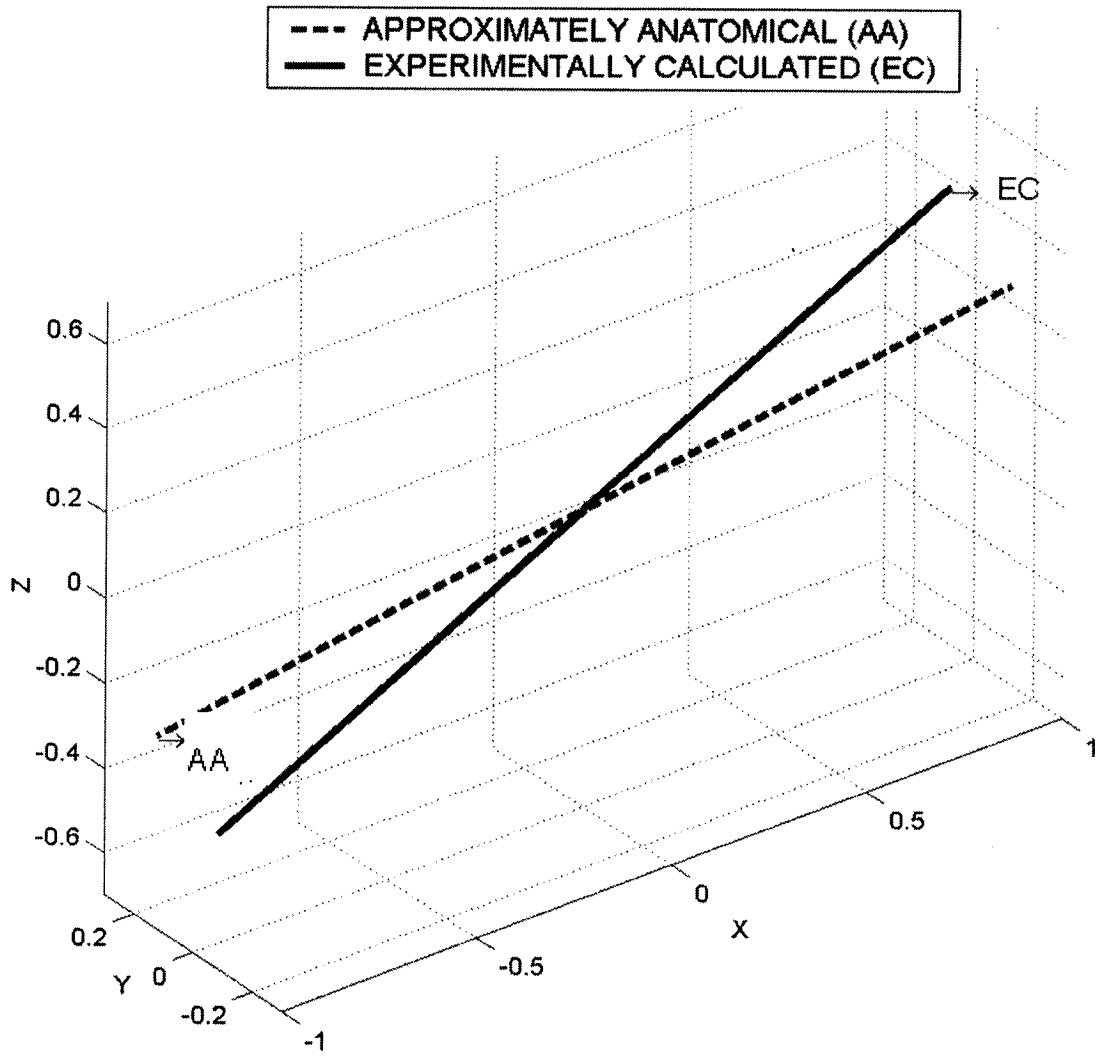

Figure 4.9 *The orientations of the experimentally calculated and approximate anatomical subtalar joint axis*

Figure 4.10 shows the experimentally calculated and approximate anatomical orientations of the subtalar joint axis directions the global coordinate system, in relation to the medial tibial plateau (MTP), and foot, heel, and toe.

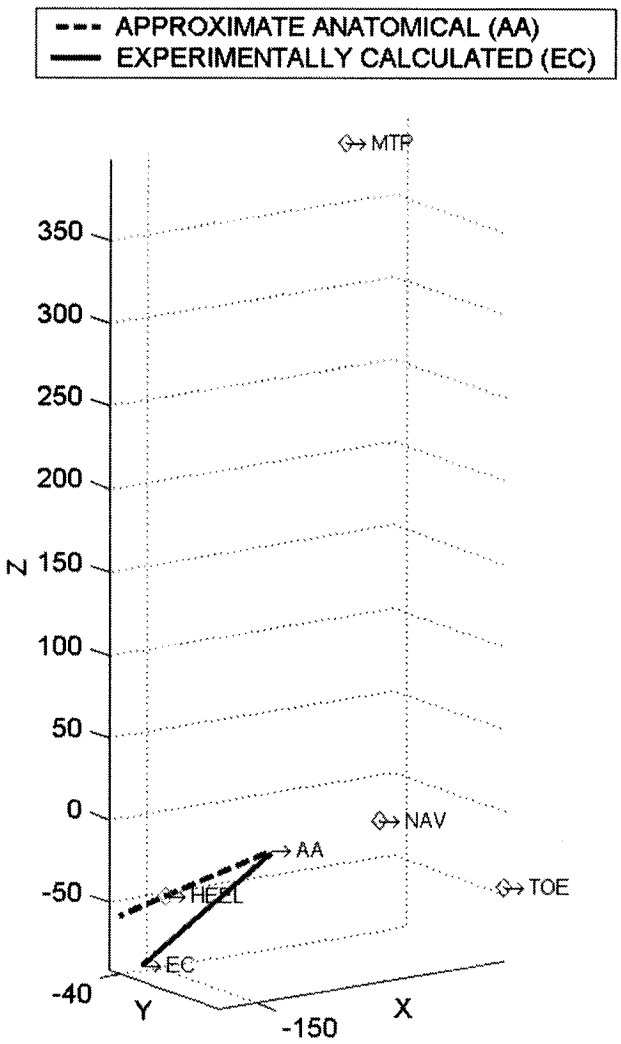

Figure 4.10 *Experimentally calculated and approximate anatomically orientations of the subtalar joint axes in relation to the leg MTP and foot, heel, and toe locations*

4.2.5). *Effect of variations in distances between data set measurements*

Tables 4.23 and 4.24 show the variations in the distances between successive MTP measurements in the data sets used to calculate the ankle axis and subtalar axis locations and directions. The measurements were again chosen, so that the distances between successive values were very close in magnitude, and the respective distances between the MTP and ankle/subtalar joints were equal within the given data set.

Table 4.23. *Variation in distances between successive MTP measurement locations for the data sets used to calculate ankle joint location and orientation*

DATA SET	DISTANCES L1 & L2 (mm)	Δd	DATA SET	DISTANCES L1 & L2 (mm)	
1	32.6285		6	34.6501	
	28.2334	11.9629		32.5771	12.0018
2	33.9035		7	36.1875	
	34.0447	11.9684		34.2996	11.9831
3	33.4912		8	34.7089	
	35.5925	11.9659		34.7090	12.0078
4	32.2854		9	33.0918	
	31.0682	11.9655		32.6438	11.9724
5	37.0750		10	32.7938	
	34.2996	11.9821		32.5772	12.0592

The performance metric, Δd, shows that the distance between the experimentally calculated value and the mean measured value was almost the same for all data sets. With distances of 32.62 mm and 8.43 mm between adjacent MTP locations, the axis direction that resulted was [0.0120, -0.4899, 0.8717]. With distances of 33.90 mm and 9.04 mm, the axis direction that resulted was [-0.1461, 0.3904, -0.9090]. Both results would be quite different from the mean measured value of [-0.7514 -0.6077 -0.1964].

Table 4.24. *Variation in distances between successive MTP measurement locations for the data sets used to calculate subtalar joint location and orientation*

DATA SET	DISTANCES L1 & L2 (mm)	Δd	DATA SET	DISTANCES L1 & L2 (mm)	Δd
1	64.3573		6	17.4611	
	61.9750	10.5370		20.1758	11.8292
2	33.8727		7	46.6233	
	36.8443	10.6577		49.7769	11.4290
3	38.4245		8	42.3671	
	37.1116	11.2662		43.0342	10.8578
4	27.1712		9	23.1668	
	26.8691	10.8599		26.9179	10.7177
5	40.9447		10	25.2152	
	37.474	10.6799		25.7249	10.6615

Here again, the performance metric, Δd, shows that the distance between the experimentally calculated value and the mean measured value was essentially the same for all data sets. With distances between adjacent MTP locations of 69.0479 mm and 2.6757 mm, the axis direction was [-0.6867, 0.6150, 0.3876]. With distances of 112.8862 mm and 12.9591mm, the axis direction was [-0.0596, 0.4568, 0.8876]. These would have been quite far from the original measured mean measured value of [-0.7406, 0.2489, -0.6175].

DISTANCE

Tables 4.25 and 4.26 show the experimentally calculated and approximate anatomical measured distances from the medial tibial plateau (MTP) to the ankle joint axis. The values shown are the average distance from each of the four MTP measured markers to the joint axis, for each of the ten data sets. $\mathbf{W_i}$ and $\mathbf{W_f}$ represent the initial and final values of the minimized equation (by Davidon's method), demonstrating the degree to which the equation was minimized.

Table 4.25. *Mean distance from the measured MTP marker location to the experimentally calculated ankle joint axis*

DATA SET	DISTANCE (mm)	DATA SET	DISTANCE (mm)
1	386.3058	6	385.8832
2	385.8466	7	385.9299
3	385.9886	8	385.9759
4	385.8152	9	385.8313
5	385.9087	10	386.0447

MEAN DISTANCE FROM MTP TO ANKLE JOINT AXIS = 385.9530 mm
STANDARD DEVIATION = [0.1442]

Table 4.26. *Mean distance from the measured MTP marker locations to the approximate anatomical ankle joint axis*

DATA SET	DISTANCE (mm)	W_i	W_f
1	386.3097	1.1250	0.5608
2	385.853	0.4254	0.1740
3	388.251	0.9935	0.0775
4	385.820	0.4290	0.2452
5	385.913	0.3311	0.2572
6	385.893	0.2208	0.1256
7	387.649	0.4955	0.2449
8	391.444	0.7375	0.0501
9	386.722	0.3837	0.2888
10	388.9687	0.8827	0.0547

MEAN DISTANCE FROM MTP TO ANKLE JOINT AXIS = 387.2826mm
STANDARD DEVIATION = [1.8404]

Tables 4.27 and 4.28 show the experimentally calculated and approximate anatomical distances from the measured MTP marker location respective to the subtalar joint axis. Each distance represents the average of the distances for the four MTP values in each of the ten data sets.

Table 4.27. *Experimentally calculated distance from the measured MTP marker locations to the experimentally calculated subtalar joint axis*

DATA SET	DISTANCE (mm)	DATA SET	DISTANCE (mm)
1	402.7259	6	402.7975
2	402.9528	7	402.9789
3	403.1944	8	402.9813
4	402.9702	9	403.0391
5	402.9127	10	402.9191

MEAN DISTANCE FROM MTP TO SUBTALAR JOINT AXIS = 402.9472 mm
STANDARD DEVIATION = [0.1272]

Table 4.28. *Mean distance from the measured MTP marker locations to the approximate anatomical subtalar joint axis*

DATA SET	DISTANCE (mm)	W_i	W_f
1	403.9119	2.4698	0.0041
2	404.0627	2.6874	0.0325
3	403.9800	2.2927	0.0437
4	404.0482	3.5157	0.0579
5	403.2858	4.9779	0.0311
6	404.1263	1.0011	0.9286
7	404.0030	3.5615	0.0176
8	404.1571	4.6391	0.0912
9	403.2737	0.6398	0.4016
10	403.9386	4.8803	0.1822

MEAN DISTANCE FROM MTP TO SUBTALAR JOINT AXIS = 403.8787 mm
STANDARD DEVIATION = [0.3248]

4.2.6). *Finding the ankle and subtalar joint locations on the body*

Figures 4.13 (a) and (b) show the local coordinate systems of the ankle and subtalar joint systems superimposed onto the local coordinate system of the foot (and leg) scans. The figures show the alignment of the respective systems. One of every five digitized cross-sections is plotted, Figure 4.11 (a), in order to allow the axes to seen clearly.

(a)

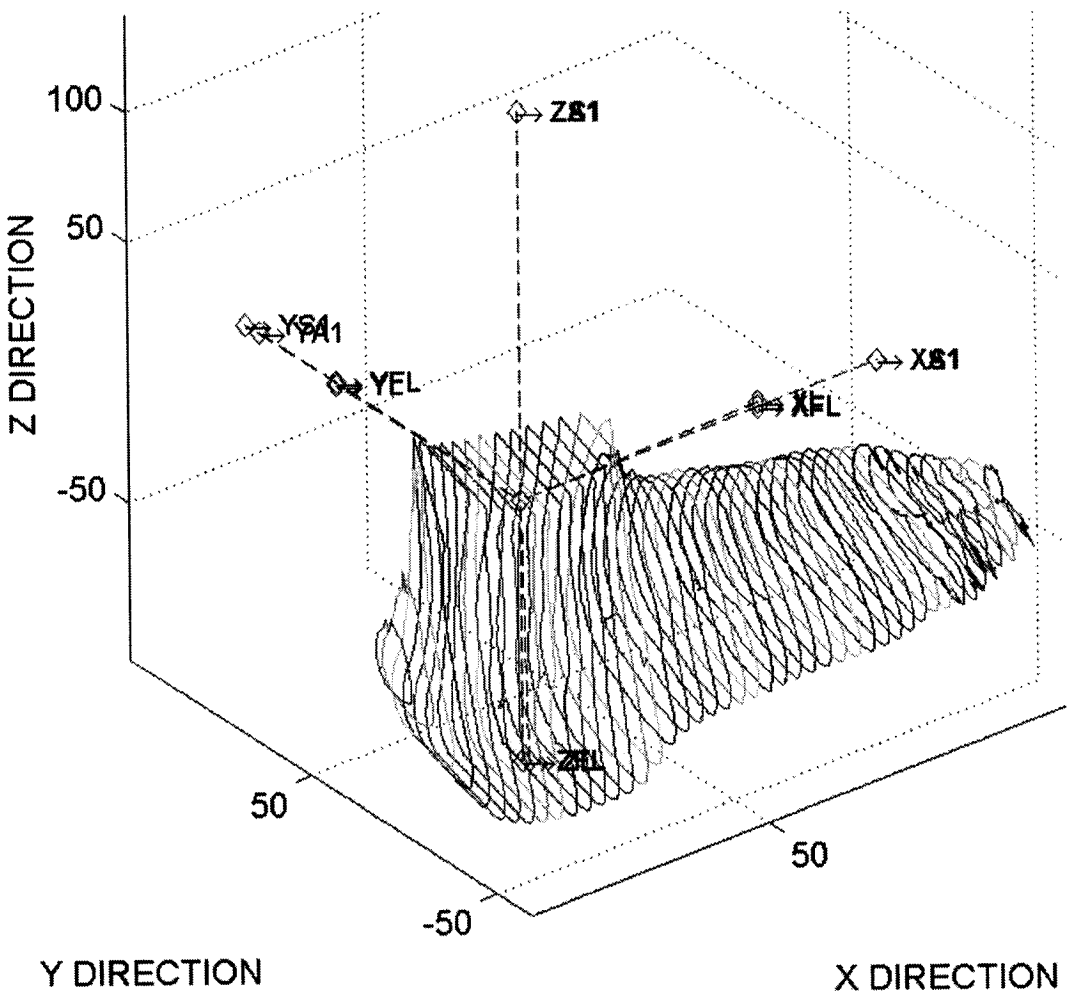

Figure 4.11 (a) *Superimposed, rotated, and translated coordinate systems (foot)*

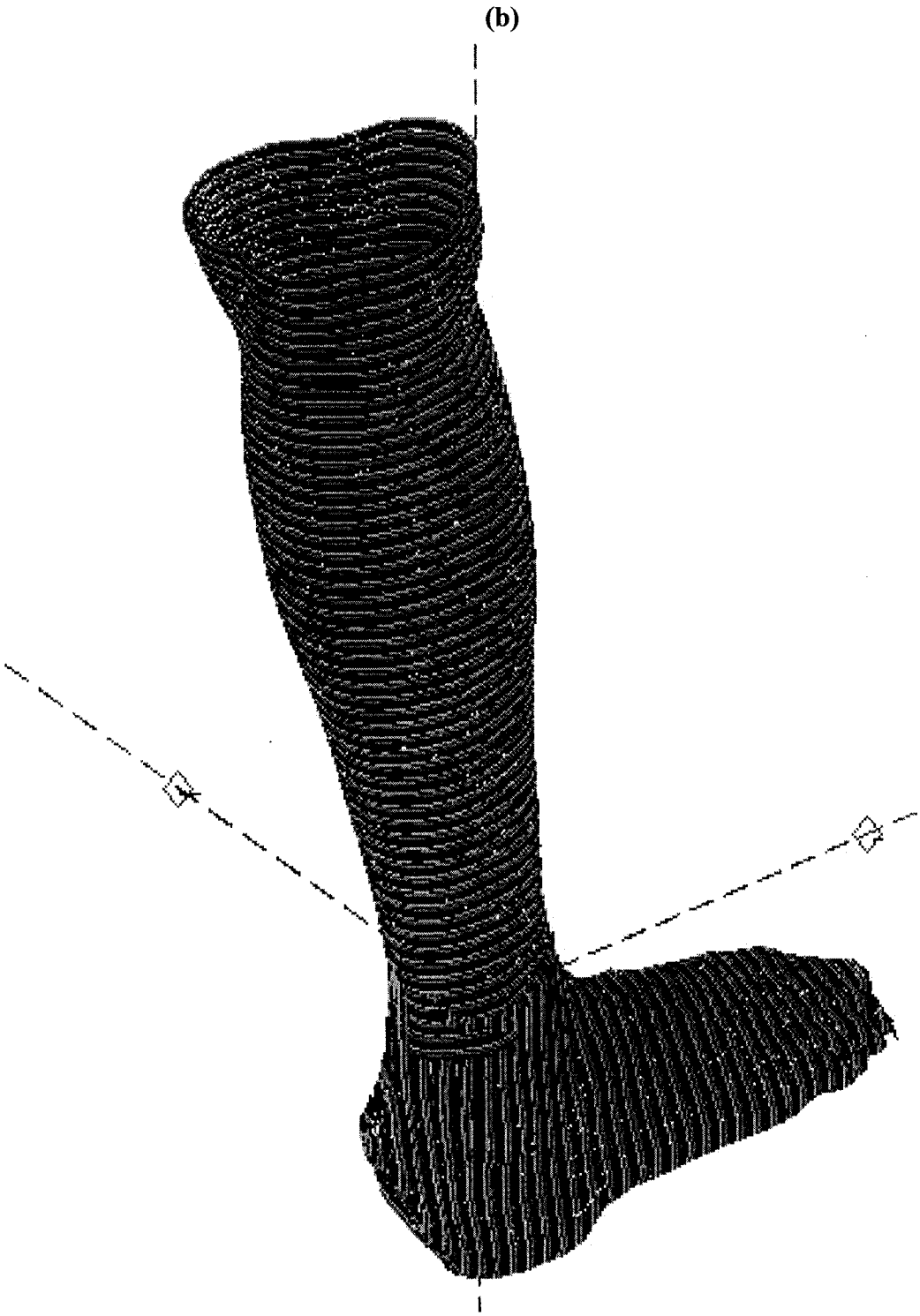

Figure 4.11 (b) *Superimposed, rotated, and translated coordinate systems (leg and foot)*

Figures 4.12 and 4.13 show the approximate anatomically predicted ankle and subtalar joint axes superimposed onto the scans of the foot and leg. The figure also demonstrates the alignment of the systems.

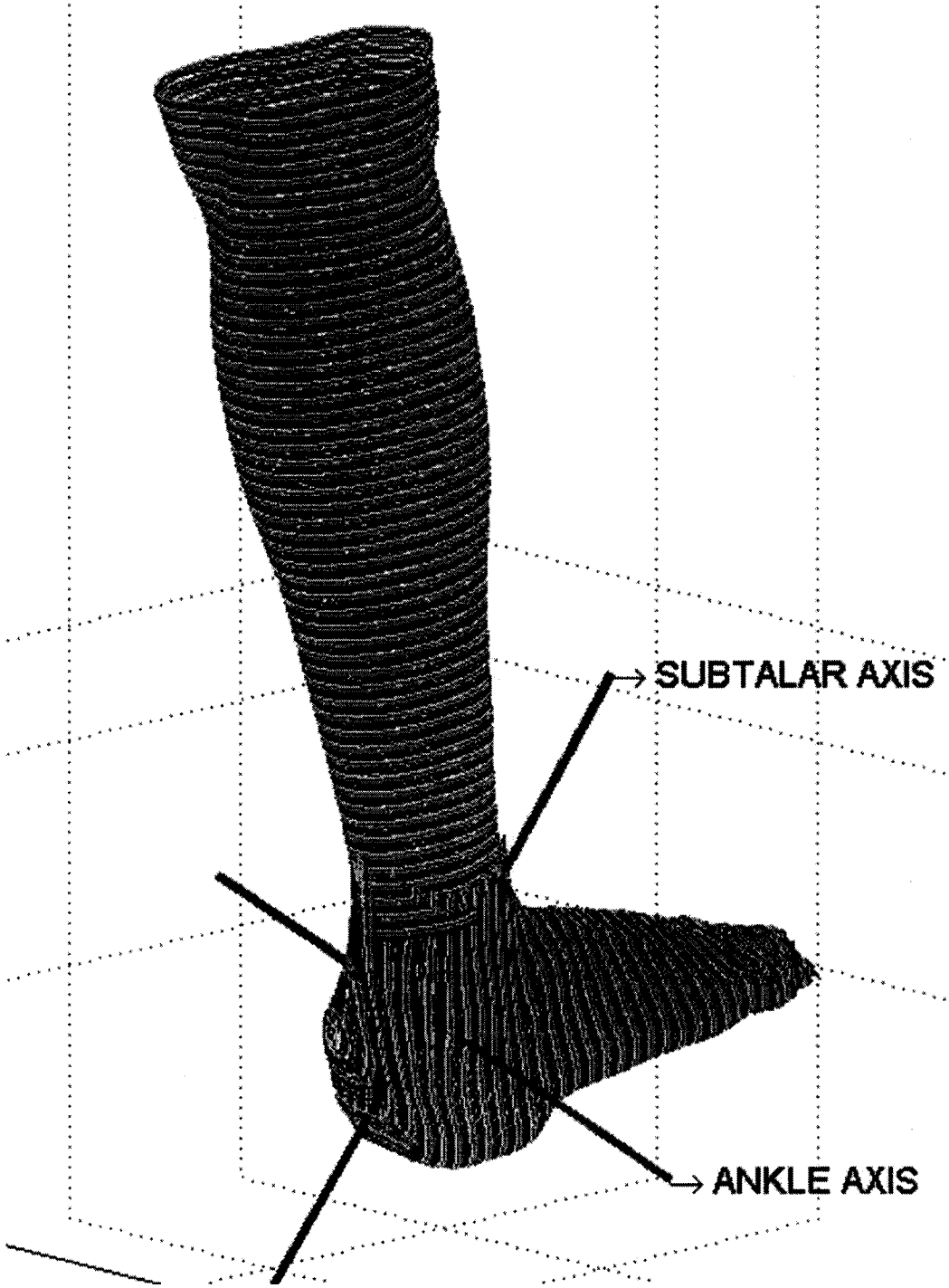

Figure 4.12 *Approximate anatomically predicted ankle and subtalar joint axes superimposed onto foot and leg*

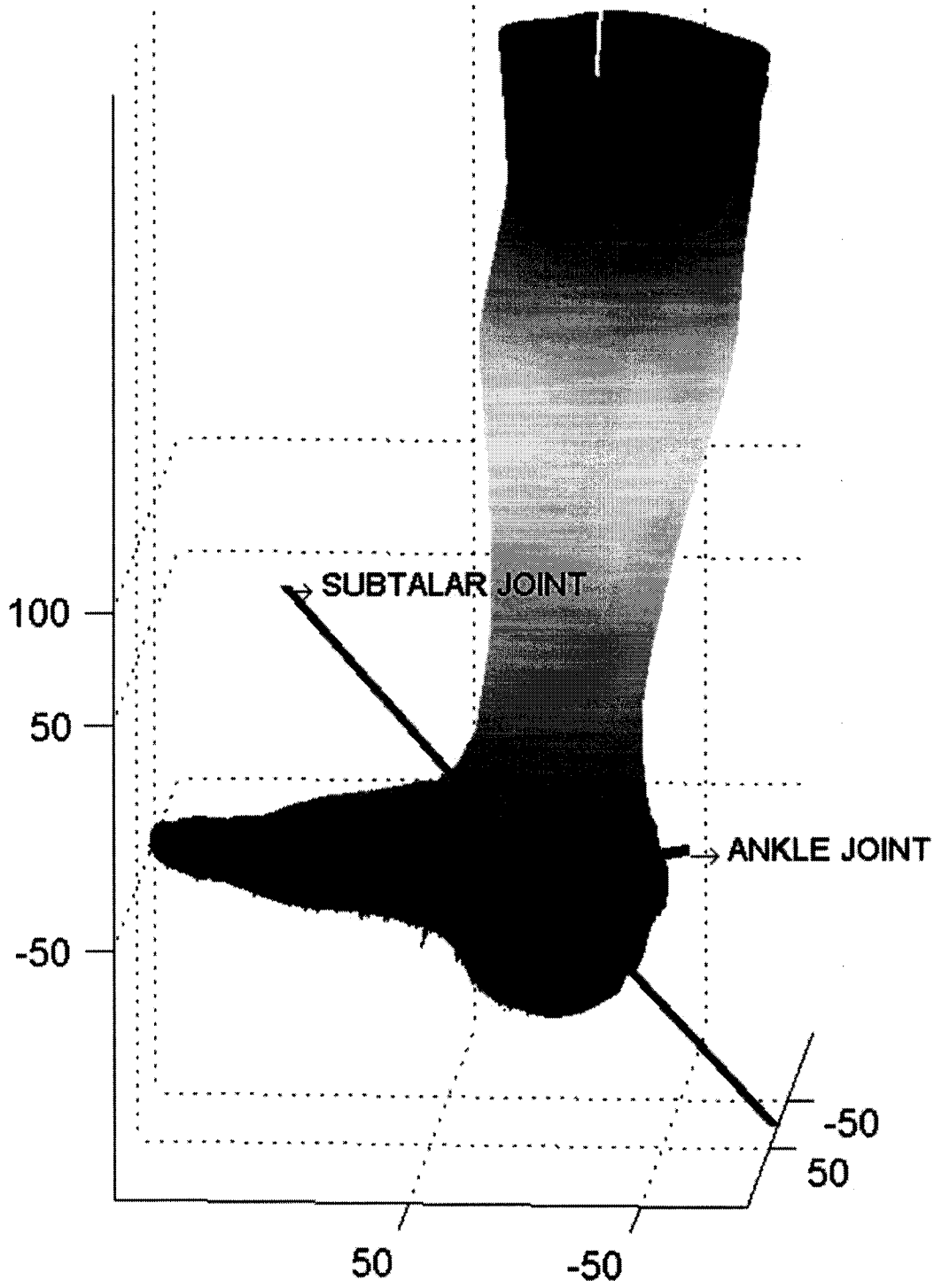

Figure 4.13 *Posteromedial view of approximate anatomically predicted ankle and subtalar joint axes superimposed onto foot and leg*

Figure 4.14 shows the set of ankle joint axes (red dotted lines), along with the average ankle axis orientation and its location.

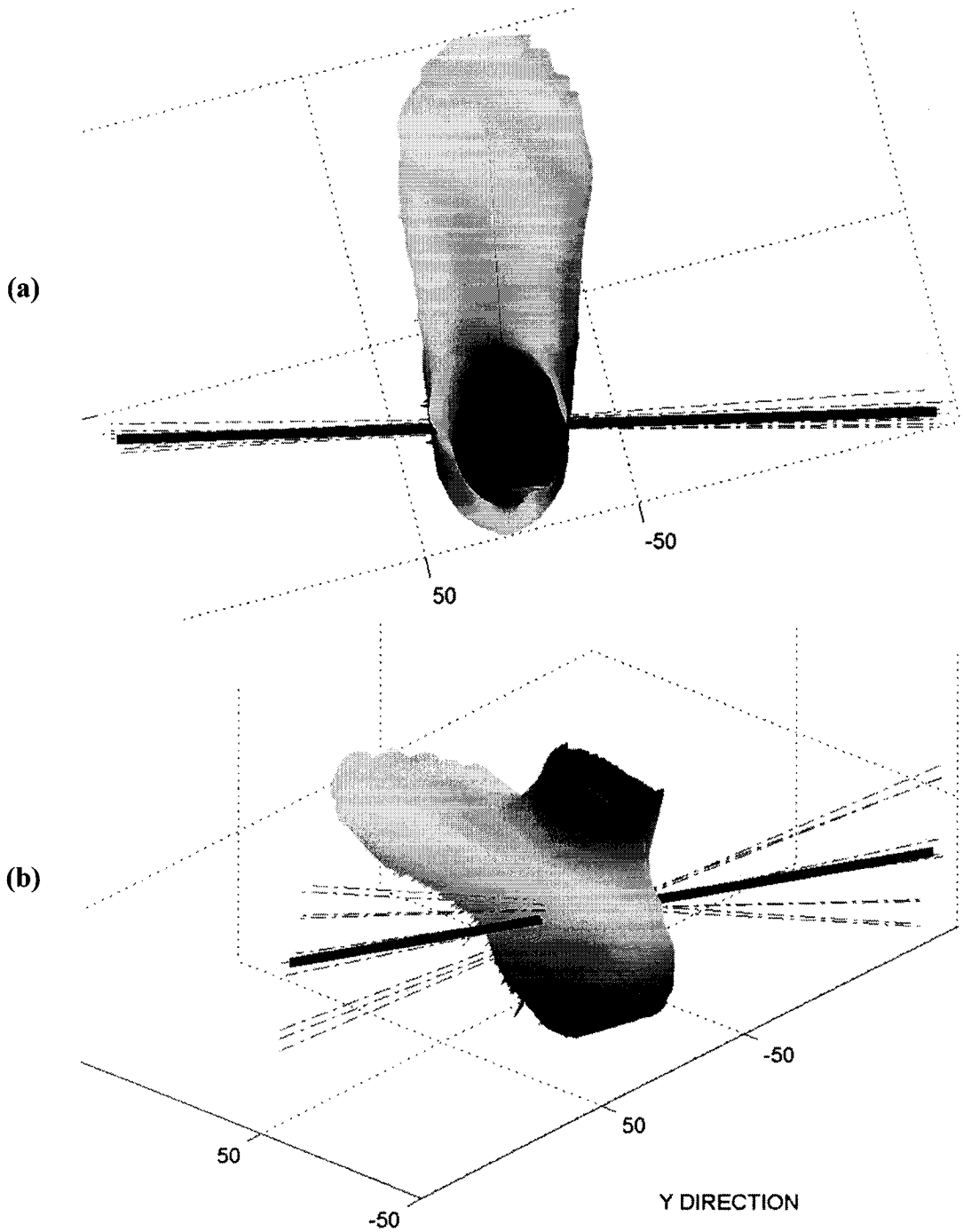

Figure 4.14 *Ankle axis projected onto scan; (a) proximal view; (b) posteromedial view*

Figure 4.15 shows the set of subtalar axes (red dotted lines), along with the average subtalar axis orientation and its location.

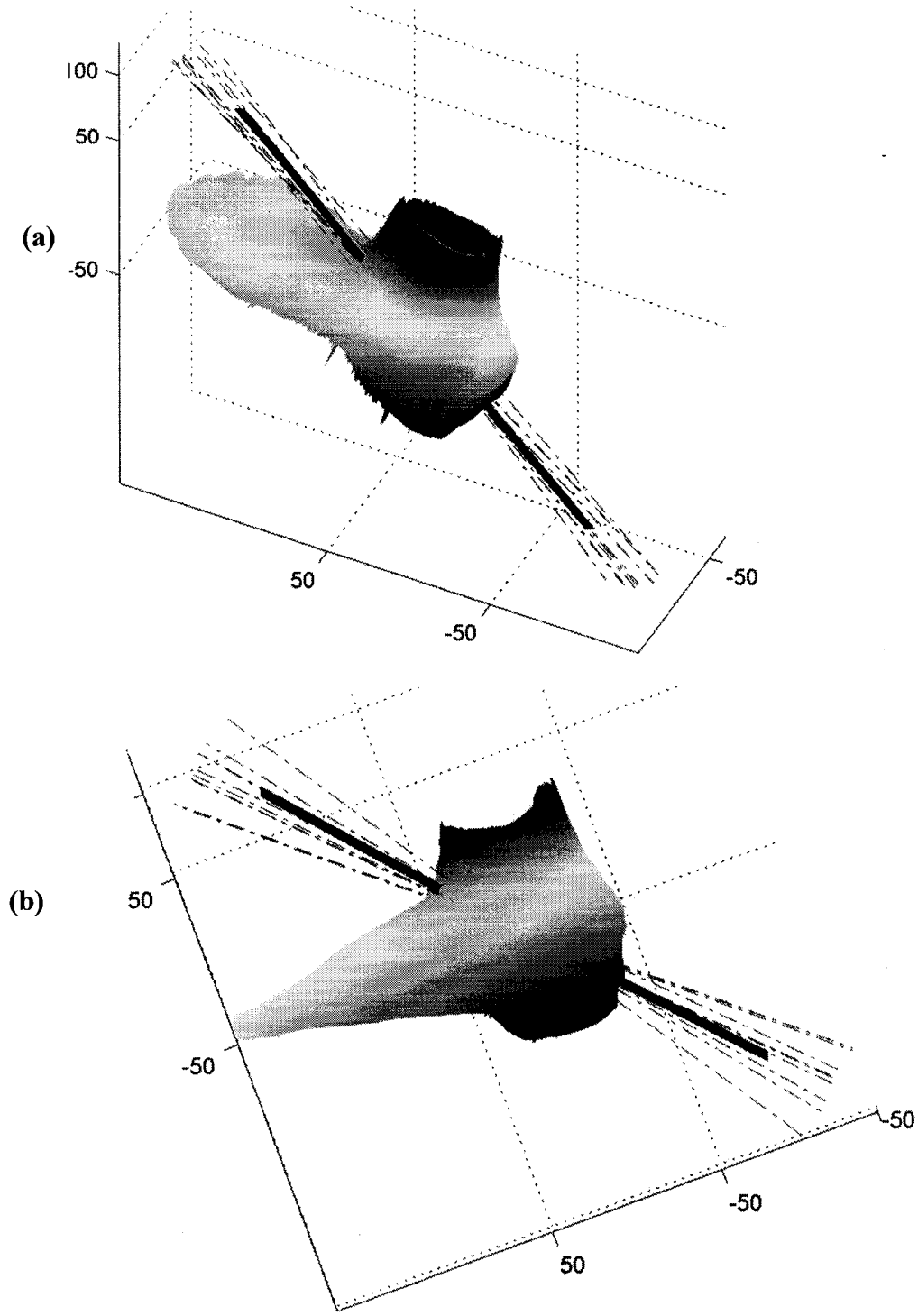

Figure 4.15 *Subtalar axis superimposed onto scan; (a) posteromedial; (b) medial view*

Figure 4.16 shows the points of intersection between the scan and the superimposed ankle and subtalar axes.

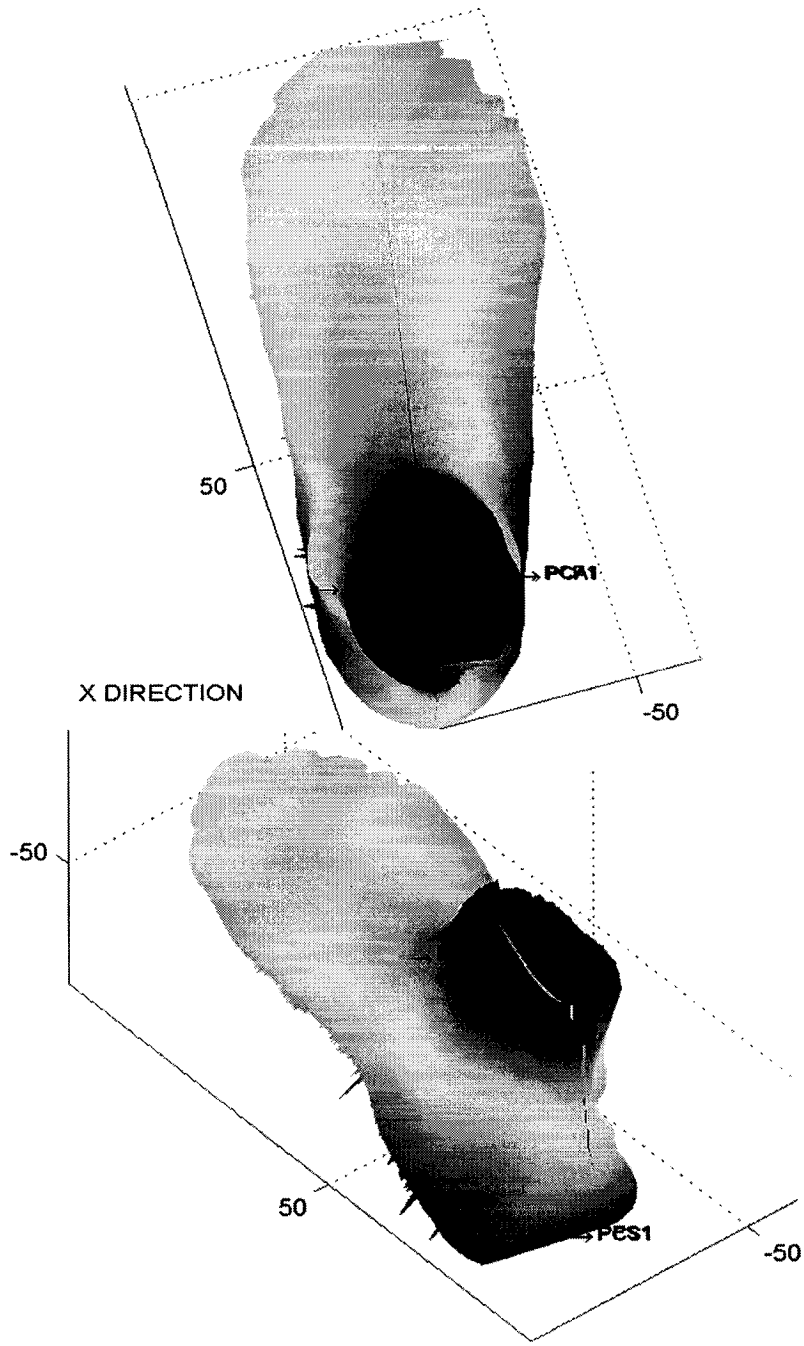

Figure 4.16 *Points of intersection between (a) ankle joint axis and foot scan; (a) subtalar joint axis plot and foot scan*

The points of intersection between the scan of the foot and the superimposed axes were also found to be very close to each other, Table 4.29, as they were found to be within 1 mm of each other, see Figure 4.19 (a) and (b).

Table 4.29. *Points of intersection between scan of foot and superimposed approximate anatomical axes*

LOCATION OF INTERSECTION	LOCATION OF POINT OF INTERSECTION ON SCAN OF FOOT(x, y, z)	LOCATION OF POINT OF INTERSECTION ON SUPERIMPOSED AXES (x, y, z)	DISTANCE BETWEEN SCAN AND SUPERIMPOSED AXES (mm)
Medial Ankle axis	[5.9537 30.8857 -46.9564]	[5.8066 30.7939 -46.0569]	0.9043
Lateral Ankle axis	[-6.6872 -26.8728 -54.0831]	[-7.0104 -27.3310 -54.7926]	0.9161
Anterior Subtalar axis	[43.2642 10.0125 -7.9087]	[42.7977 9.3612 -8.2759]	0.6864
Posterior Subtalar axis	[-33.2411 7.2020 -89.9269]	[-32.7463 7.4995 -90.2983]	0.8813

The coordinate system used to transfer the joint axes to the leg was used because it was the most convenient, since the locations of the markers had to be captured by both of the scanners. These locations were the most convenient locations, as markers placed too low or too high would not be captured by both scanners. The International Society of Biomechanics (ISB), recommended coordinate system, defined by bony landmarks of the lower leg and foot, Figure 4.20, is expected to become a widely recognized coordinate system. In the future, all points may be referred to in this coordinate system, as it may be more convenient. The definition of the local coordinate system was proposed by the Standardization and Terminology Committee (STC) of the International Society of Biomechanics, as shown below, Figure 4.17.

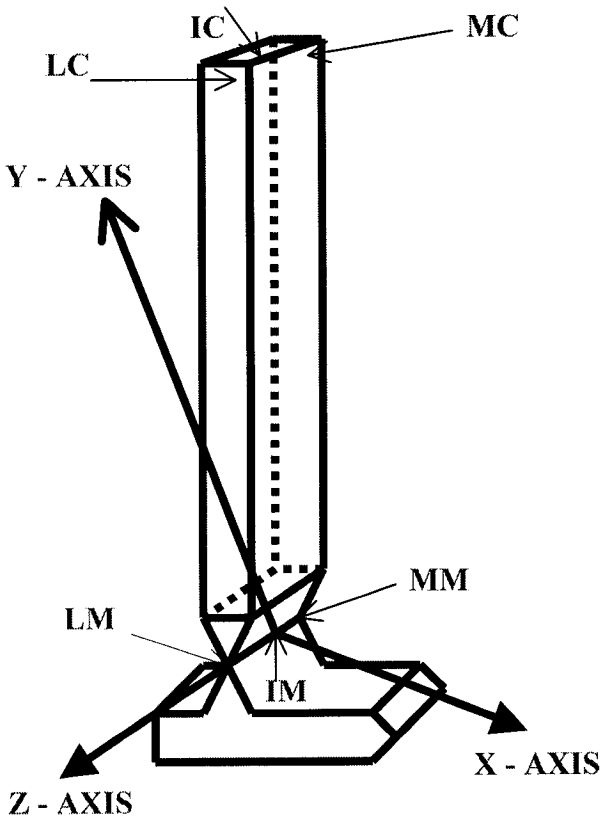

MM: The tip of the medial malleolus.
LM: The tip of the lateral malleolus.
MC: The most medial point on the border of the medial tibial condyle.
LC: The most lateral point on the border of the lateral tibial condyle.
TT: Tibial tuberosity.
IM: The inter-malleolar point located midway between the tips of the MM, and LM.
IC: The inter-condylar point located midway between the tips of the MC, and LC.
Torsional plane: The plane containing the points IC, MM, and LM.
O: The origin coincident with IM.
Z: The line connecting MM and LM, and pointing to the right.
X: The line perpendicular to the torsional plane of the tibia/fibula, and pointing anteriorly.
Y: The common line perpendicular to the X- and Z- axes.

Figure 4.17 *The ISB recommended definition of the tibia/fibula coordinate system (right foot)*

Also of interest is the array of ankle and subtalar joint axes found when the entire range of motion of the joints was considered, Figures 4.18 (a) – (d) and 4.19 (a) – (d). In calculating the axis direction, there was found to be variation in axis direction, depending on where in the cycle of rotation, the joint was currently at. Figure 4.18 demonstrates a finding similar to that of Lundberg et al.,[46] in that it shows the axis of rotation of the ankle to rotate from a downward and medial to a downward and lateral inclination, when the entire cycle of rotation was considered. Wang, et al.,[94] also proposed that the centers of rotation of the ankle joint lie close to each other within the body of the talus.

In addition, Figure 4.19 shows a similar finding for the subtalar joint, with the axis of rotation varying from a downward and anterior to a downward and posterior position. This idea was also put forward by Siegler et al.,[81] who suggested that the ankle and subtalar joints do not act as ideal hinge joints with a fixed axis of rotation.

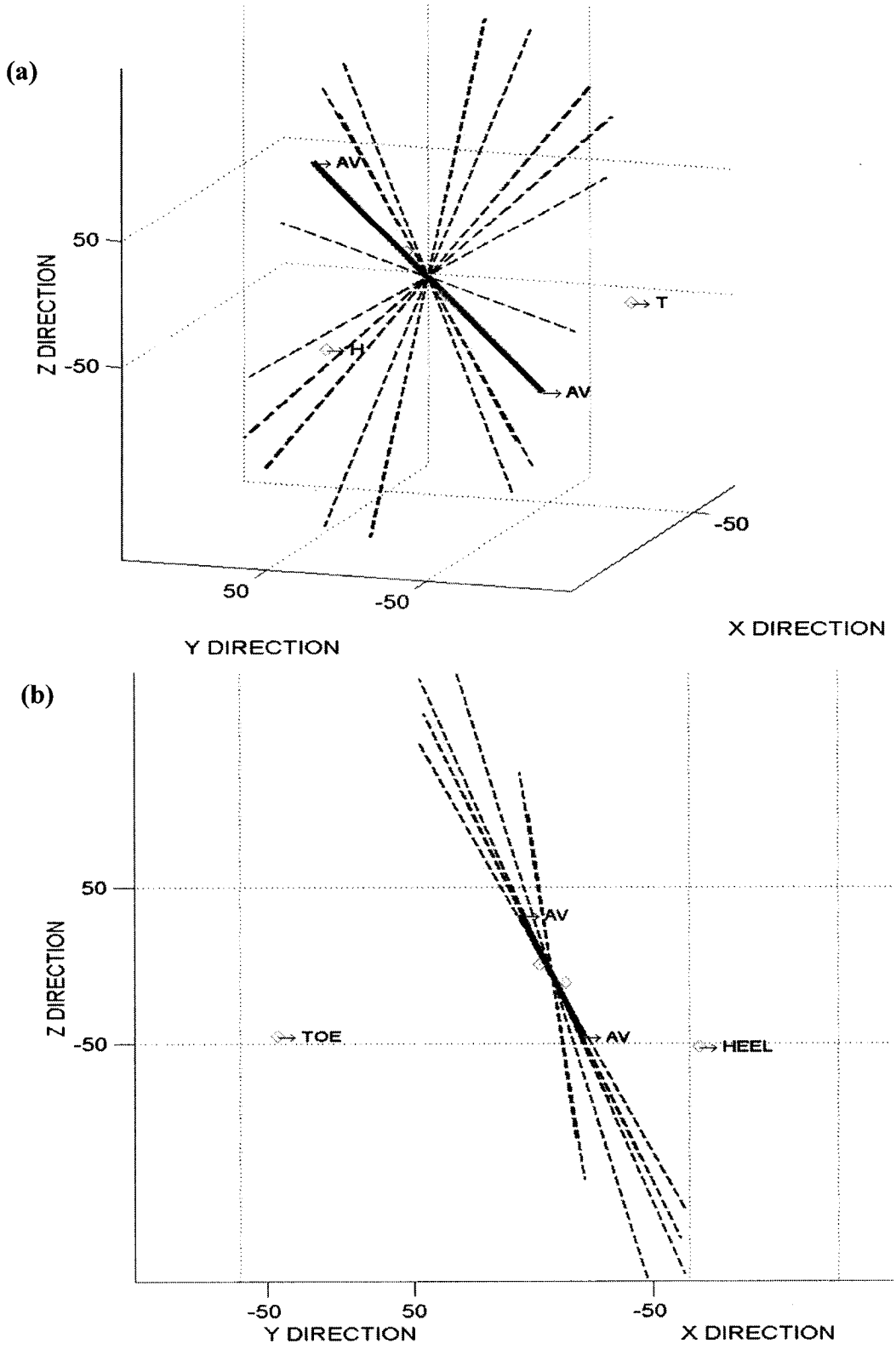

Figure 4.18 (a,b) *Range of ankle joint axis;(a) isometric; (b) medial views*

(c)

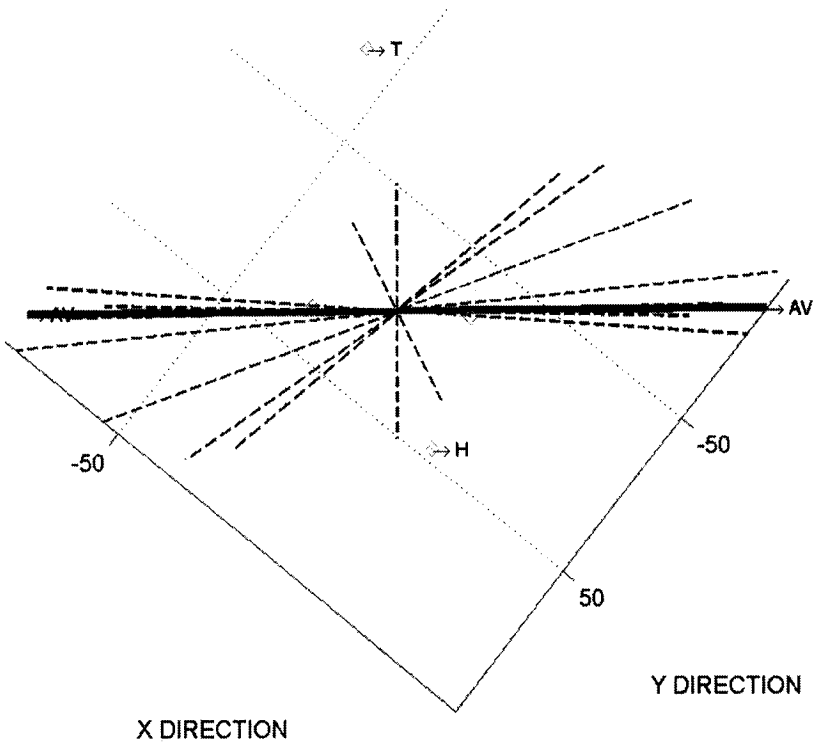

(d)

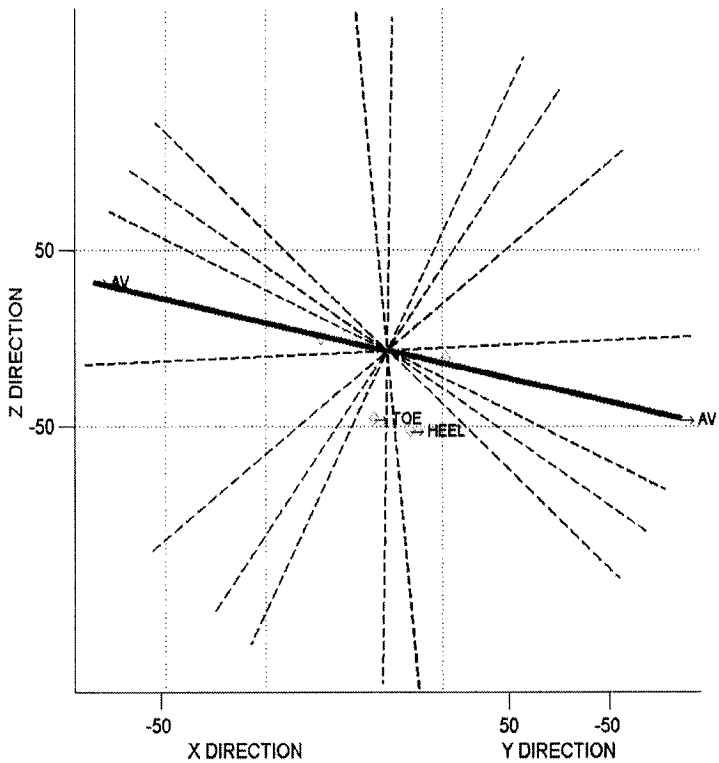

Figure 4.18 (c,d) *Range of ankle joint axis; (c) rear; (d) top views*

(a)

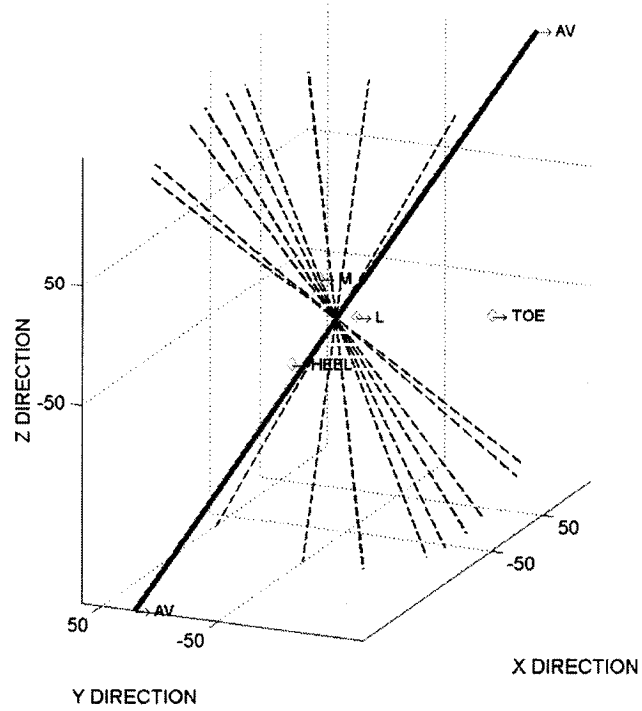

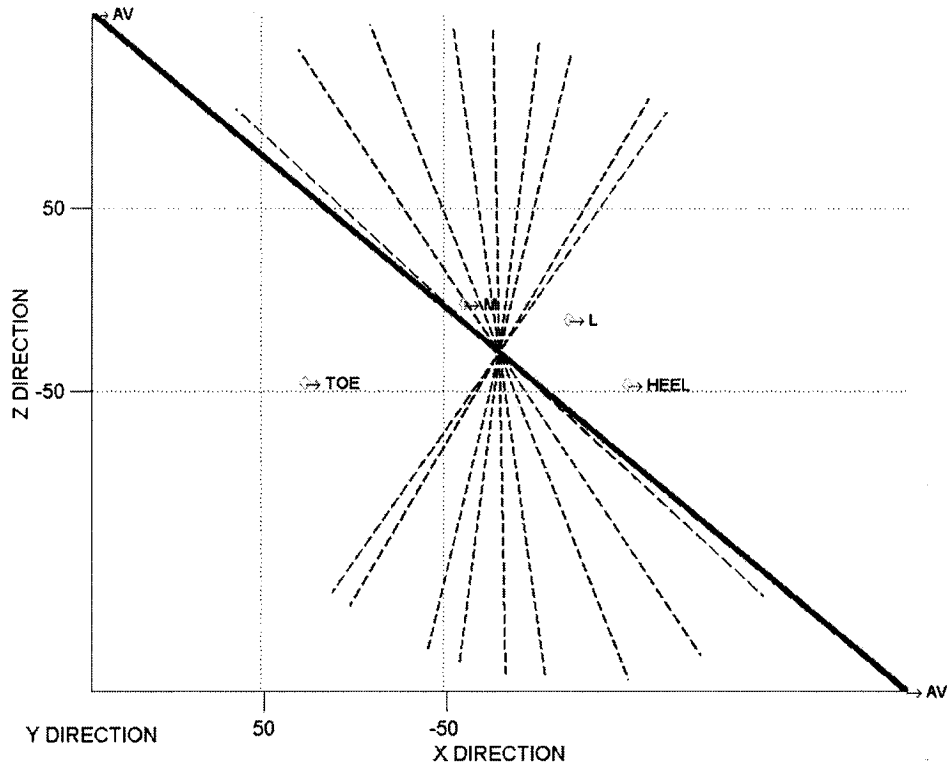

Figure 4.19 (a,b) *Range of subtalar joint axis;(a) isometric, lateral view; (b) medial view*

(c)

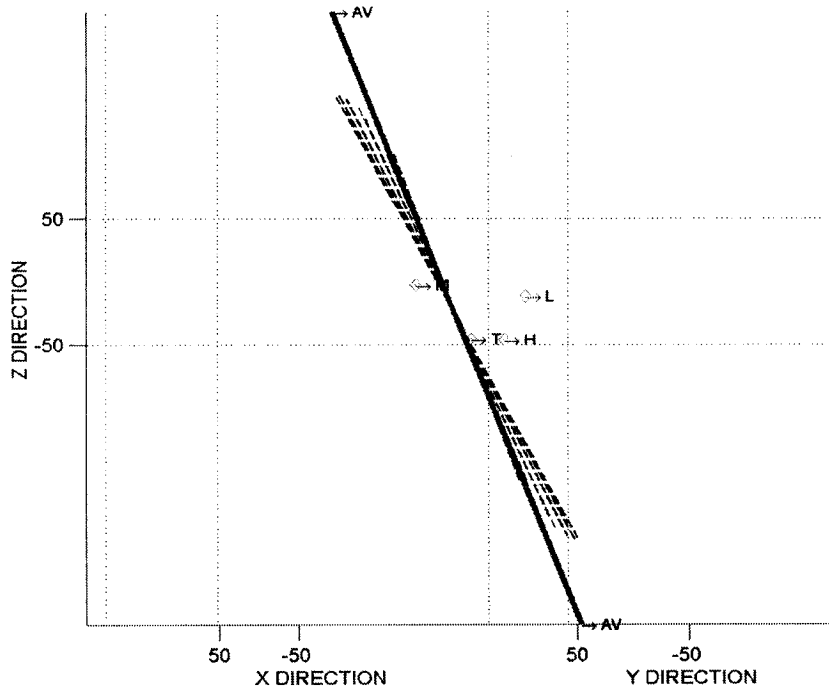

(d)

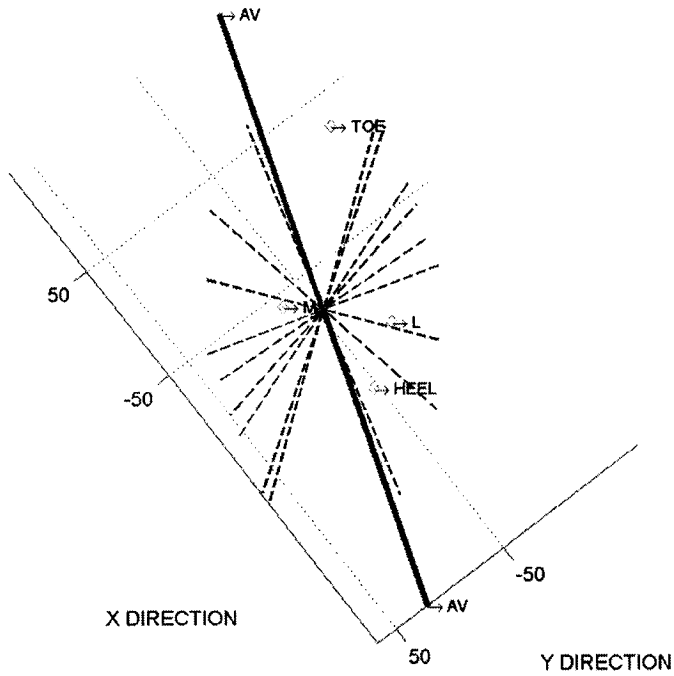

Figure 4.19 (c,d) *Range of subtalar joint axis; (c) rear; (d) top views*

4.3). *Comparison of methods of solving equations*

The system of equations defining the joint location is very sensitive, therefore, for example, when Broyden's method was employed for the second, third, and seventh ankle data sets (subject), the four distances, between the MTP and ankle joint center, and the corresponding joint center locations were, Table 4.30:

Table 4.30 *Distances and joint centers (Broyden)*

Data Set No.	Distances (mm)	Joint center locations (x,y,z)
2	L1 = 385.6888 L2 = 386.1555 L3 = 385.6785 L4 = 385.6747 Mean = 385.7994	[-120.6860 20.5415 -42.0727]
3	L1 = 437.2399 L2 = 437.2399 L3 = 437.2399 L4 = 437.2399 Mean = 437.2399	[-74.4903 72.6315 -60.3954]
7	L1 = 385.7201 L2 = 386.3774 L3 = 385.5585 L4 = 385.8543 Mean = 385.8776	[-99.1536 100.0866 -157.6534]

As shown in Table 4.31, although the distances were, in fact, equal within each data set, the method did not zero in on any specific point for the joint center location, as the three points are rather far apart. This was the case even though the gradients and s values did decrease a great deal. The number of iterations, initial and final gradients (g_i and g_f), and initial and final correcting value (s_i and s_f), where $s = -A_k^{-1}F(x^{(k)})$, were, Table 4.31:

Table 4.31 *Gradients and s values (Broyden)*

Data Set No.	No. of iterations	Gradient(x, y, z, L)		s(x, y, z, L)	
		g_i	g_f	s_i	s_f
2	7	-0.8178 0.3496 -1.7959 -3.0697	1.0e-11 *[0.1365 -0.0654 0.4039 0.4320]	167.3971 197.5690 -85.3534 41.9845	1.0e-007 * [-0.4760 -0.1066 -0.6865 0.4618]
3	8	-1.2652 0.5435 -2.7423 -2.0054	1.0e-10*[0.0630 -0.0818 0.2594 0.2797]	45.4323 63.3859 -49.7004 37.5434	1.0e-007 * [0.0959 0.2708 -0.3041 0.3246]
7	9	-0.5168 0.2419 -1.0336 -1.1792	1.0e-010 *[0.1766 -0.2226 0.7134 0.7685]	18.6582 71.0673 -111.0535 104.5794	1.0e-009 *[-0.1019 0.0891 0.2174 -0.1463]

With the Steepest Descent method applied to the second, third, and seventh ankle (subject) data sets, the four distances and the corresponding joint center locations were, Table 4.32:

Table 4.32 *Distances and joint centers (Steepest Descent)*

Data Set No.	Distances (mm)	Joint center locations (x,y,z)
2	L1 = 385.7145 L2 = 385.7612 L3 = 385.6513 L4 = 385.8075 Mean = 385.7336	[-122.8163 0.4990 -6.3936]
3	L1 = 385.9656 L2 = 385.8214 L3 = 385.5874 L4 = 385.7669 Mean = 385.7853	[-122.0252 -0.1879 -6.7363]
7	L1 = 385.8320 L2 = 386.0024 L3 = 385.5726 L4 = 386.1960 Mean = 385.9007	[-123.1765 0.835 -6.3387]

The four distances are just about equal and the joint center locations are within 1 mm of each other. The gradients and h values also near zero, Table 4.33, where,

$$h(x_1, x_2, x_3, x_4) = \Sigma [f_i(x_1, x_2, x_3, x_4]^2 \qquad (3.5)$$

Table 4.33 *Gradients and h values (Steepest Descent)*

Data Set No.	No. of iterations	Gradient (x, y, z, L)		h	
		g_i	g_f	h_i	h_f
2	8	-0.8178 0.3496 -1.7959 -2.0054	-0.0044 0.0048 0.0031 -0.0002	0.4254	0.0134
3	8	-1.2652 0.535 -2.7423 -3.0697	-0.0062 0.0046 0.0037 -0.0000	0.9935	0.0733
7	20	-0.5168 0.2419 -1.0336 -1.1792	-0.0043 0.0043 0.0046 -0.0012	0.4955	0.1943

Unlike the Steepest Descent method, the Continuation method gives varying values for the distances between the different data sets, and the joint center locations also vary dramatically, Table 4.34.

Table 4.34 *Distances and joint centers (Continuation)*

Data Set No.	Distances (mm)	Joint center locations (x,y,z)
2	L1 = 420.8653 L2 = 420.8648 L3 = 420.8651 L4 = 420.8657 Mean = 420.8652	[-120.6934 20.5102 -42.0097]
3	L1 = 437.0976 L2 = 437.0961 L3 = 437.0964 L4 = 437.0975 Mean = 437.0969	[-74.6099 72.4648 -60.2648]
7	L1 = 539.7027 L2 = 539.7019 L3 = 539.7007 L4 = 539.7058 Mean = 539.7028	[-99.3685 99.2783 -156.3958]

The gradients and h values, however, approach zero, which was quite unexpected considering the difference in the joint center locations and distances between the joint centers and MTP locations, Table 4.35.

Table 4.35 *Gradients and h values (Continuation)*

Data Set No.	Gradient (x, y, z, L)		h	
	g_i	g_f	h_i	h_f
2	-0.8178 0.3496 -1.7959 -2.0054	-0.7356 0.4032 -1.8203 -2.0054	0.4254	4.2817e-004
3	-1.2652 0.5435 -2.7423 -3.0697	-0.3205 0.3902 -1.3000 -1.3972	0.9935	0.1220
7	-0.5168 0.2419 -1.0336 -1.1792	-0.3311 0.3921 -1.3583 -1.4537	0.4955	0.1321

Using Newton's method, the distances again varied dramatically between data sets, as did the joint center locations, Table 4.36:

Table 4.36 *Distances and joint centers (Newton)*

Data Set No.	Distances (mm)	Joint center locations (x,y,z)
2	L1 = 420.9263 L2 = 420.9263 L3 = 420.9263 L4 = 420.9263 Mean = 420.9263	[-120.6860 20.5415 -42.0727]
3	L1 = 437.2399 L2 = 437.2399 L3 = 437.2399 L4 = 437.2399 Mean = 437.2399	[-74.4903 72.6315 -60.3954]
7	L1 = 541.0550 L2 = 541.0550 L3 = 541.0550 L4 = 541.0550 Mean = 541.0550	[-99.1536 100.0866 -157.6534]

However, the gradients and h values again approach zero for the data sets, Table 4.37.

Table 4.37 *Gradients and h values (Newton)*

Data Set No.	Gradient (x, y, z, L)		h	
	g_i	g_f	h_i	h_f
2	-0.8178 0.3496 -1.7959 -2.0054	-0.0091 0.0046 -0.0249 -0.0270	0.4254	1.0300e-013
3	-1.2652 0.5435 -2.7423 -3.0697	-0.1272 0.1657 -0.5371 -0.5773	0.9935	5.6807e-010
7	-0.5168 0.2419 -1.0336 -1.1792	-0.0050 0.0064 -0.0215 -0.0230	0.4955	6.0892e-014

Thus, even though the gradients and h values suggest that an accurate solution had been reached, the varying distances calculated for the Broyden, Continuity, Steepest Descent methods demonstrate the sensitivity of the equation set. Thus, a more reliable, more robust method was required.

Using Davidon's method, for the first ankle data set (subject), the values of **s = -U*gradient**, which determines the direction of the step, and the component of that direction gradient (gradient) after the first and second iterations were, Table 4.38:

Table 4.38. *Gradients and s values for modified initial matrix, first data set*

Data set No.	Gradient (x, y, z, L)		s(x, y, z, L)	
	g_i	g_f	s_i/1.0e+004	s_f
3	1.0235 -0.305 2.8041 3.0046	-0.0634 0.0632 0.0351 -0.0000	-0.0001 0.0000 -0.0003 -1.5023	0.0579 -0.0631 -0.0353 0.0217

Thus for the first data set, all of the components of the s vector had fallen below 0.1, therefore there were no more iterations, as this was the criterion for termination. However, had the unit matrix been used, the values of s = -U*gradient and the gradient and after the first and second iterations would have been, Table 4.39:

Table 4.39. *Gradients and s values for unit matrix, first data set*

Data set No.	Gradient (x, y, z, L)		s(x, y, z, L)	
	g_i	g_f	s_i/1.0e+004	s_f
1	1.0235 -0.305 2.8041 3.0046	-0.0640 0.0632 0.0328 -0.0023	-0.0001 0.0000 -0.0003 -1.5023	-12.3699 0.1970 -0.5884 38.3595

Thus, the approach to termination would have been much slower, requiring many more iterations.

For the third data set, the values of the gradient and **s** after the first, second and twentieth iterations were, Table 4.40:

Table 4.40. *Gradients and s values for modified initial matrix, third data set*

Data Set No.	Gradient (x, y, z, L)			s(x, y, z, L)		
	g_1	g_2	g_{20}	s_1/1.0e+004	s_2	s_{20}
3	-1.2652 0.5435 -2.7423 -3.0697	-0.1008 0.1034 0.0560 0.0000	0.0220 0.0406 02772 0.2580	0.0001 -0.0001 0.0003 1.5348	0.0001 -0.0001 0.0003 1.5348	0.0064 -0.7692 -0.4585 0.6132

However, had the unit matrix been used initially, there would have been no further improvement, Table 4.41.

Table 4.41. *Gradients and s values for unit initial matrix, third data set*

Data Set No.	Gradient (x, y, z, L)			s(x, y, z, L)		
	g_1	g_2	g_{20}	s_1	s_2	s_{20}
3	-1.2652 0.5435 -2.7423 -3.0697	-0.0987 0.1025 0.0604 0.0049	-0.0987 0.1025 0.0604 0.0049	1.2652 -0.5435 2.7423 3.0697	-32.9301 0.5550 -1.4515 102.2027	-32.9301 0.5550 -1.4515 102.2027

The axis directions were calculated using a separate MATLAB program, with the input data taken from a separate file containing ten sets of three practically equally spaced MTP locations. The distances between consecutive points were not necessarily exactly the same, in order to demonstrate that the result was close to the expected answer as long as the points were not too far apart. For the first measurement, the axis direction was found to be:

x	y	z
[-0.7780	**-0.5127**	**-0.3631]**

and the distance between the first and second markers was **32.6285** mm, while that between the second and third markers was **28.2334** mm. For the second data set, the axis direction was found to be:

x	y	z
[-0.7176	**-0.6953**	**0.0408]**

and the distances between the first and second markers was **33.9035** mm, while that between the second and third markers was **34.0447** mm. However, when the distances were no longer almost equal, but were in fact rather far apart, the result was quite different. When the first set of input MTP locations was changed so that the distances between the markers were **32.6285** mm and **8.6522** mm, the axis direction changed to:

x	y	z
[-0.2694	**0.2799**	**-0.9215]**

Additionally, when the second set of MTP locations were changed so that the distances between the markers were **67.8924** and **3.3313**, the axis direction was found to be:

x	y	z
[-0.1556	**-0.5648**	**0.8105]**

which is also quite different from the direction found when the points were equally or almost equally spaced.

In applying Chauvenet's criterion to the first data set of ankle joint directions (subject), the standard scores, *z*, were, Table 4.42:

Table 4.42 *Standard scores for the ankle axis direction data*

DATA SET	x	y	z
1	**1.3261**	**1.4071**	**1.0692**
2	**1.6828**	**1.2982**	**1.1116**
3	**1.0904**	**1.1301**	**1.3218**
4	**0.8495**	**0.0292**	**0.0715**
5	**1.2679**	**1.1871**	**1.3696**
6	**0.4567**	**0.6644**	**0.8028**
7	**0.1387**	**0.3747**	**0.2039**
8	**0.4773**	**0.0272**	**0.1170**
9	**0.6427**	**0.7481**	**0.8094**
10	**0.1501**	**1.2269**	**1.2800**

where the x values were compared to the other x values, and similarly for the y and z values. The highest standard score occurs amongst the x values, with a value of **1.6828**, which is substantially lower than that specified by Chauvenet's criterion for ten data inputs, which has a value of **1.96**.

When the standard scores were computed for the subtalar axis directions, Table 4.43, the highest value was **2.0292** (third data set), which is slightly higher than the recommended value of 1.96. However, as there was only a difference of **0.0692**, the value was considered acceptable.

Table 4.43 *Standard scores for the subtalar axis direction data*

DATA SET	x	y	z
1	1.3541	1.1223	1.4161
2	0.5581	0.9074	0.7299
3	2.0292	1.8736	1.7698
4	0.8217	0.8409	0.8766
5	0.4698	0.3302	0.5169
6	0.3807	0.3281	0.2881
7	1.1587	1.4425	1.4086
8	0.1943	0.2783	0.1344
9	0.3554	0.4905	0.3314
10	0.4355	0.2903	0.3145

Table 4.44 shows the standard scores for the averages of the ankle axis locations. The eighth location was eliminated from the calculation of the average as the x value, **2.6913**, was far above the accepted value of 1.96, while the y value was slightly above it.

Table 4.44 *Standard scores for the ankle axis location data*

DATA SET	x	y	z
1	0.2572	0.0570	0.7659
2	0.5922	0.1166	0.7634
3	0.4826	0.2032	0.8754
4	0.6581	0.0934	0.7670
5	0.5405	0.0959	0.7558
6	0.4815	0.0530	0.7481
7	0.3675	1.7213	0.1463
8	2.6913	2.1726	1.9312**
9	0.0591	0.8971	0.3623
10	0.1058	0.6584	1.2096

Table 4.45 shows the standard scores for the subtalar axis location. The x, y, and z values are all above the accepted value of 1.96, thus the seventh location was eliminated from the calculation of the average.

Table 4.45 *Standard scores for the subtalar axis location data*

DATA SET	x	y	z
1	0.2457	0.2440	0.4109
2	0.1408	0.1660	0.1014
3	0.1739	0.0293	0.0705
4	0.1387	0.2149	0.2795
5	0.7054	0.6447	0.8684
6	0.5845	0.4398	0.1063
7	2.6094	2.6623	2.5308**
8	0.2220	0.3979	0.5628
9	0.6622	0.8126	1.1012
10	0.8569	0.5918	0.1955

The accuracy of the method was demonstrated by the use of the wooden model, for which the orientation and location of the ankle and subtalar axes are known. Figures 4.2 and 4.3 show the near alignment of the theoretical and experimental axes of rotation. The value of the Davidon's minimized equation also decreased rapidly. For example, the eleventh and twelfth values of Table 4.12, show the value decreasing from **6.7596** to **2.7642**, and from **12.1298** to **1.8448** respectively. Considering the sensitivity of the equation set, this was a rather considerable decrease. Similarly, for the subtalar joint, the value decreased from **3.5208** to **0.0113** for the first data set, and from **4.3354** to **1.4540** for the fourteenth data set. The result for the human subject showed the same trend, although the initial values of minimized equation were quite low. For example, for the third ankle data set, the initial value was **0.9935**, however this value decreased to **0.0775**. For the subtalar joint axis location calculations, the first data set shows a decrease from **2.4698** to **0.0041**.

It was previously noted, that more accurate results were obtained when the difference in the distances between markers of the same data set was not too great. For example, the second data set for the ankle results (human subject) resulted from distances of **33.9035mm** and **34.0447mm** between the consecutive marker locations. Similarly, the fifth data set was obtained with markers having distances of **37.0750mm** and **34.2996mm** between consecutive locations, with an axis direction of **[-0.7643 -0.5572 -0.3247]**. However, when the MTP locations were adjusted so that the distances were instead **23.9817mm** and **8.6522mm**, the direction then changed dramatically to **[0.2694 -0.2799 0.9215].** When the locations were then changed so that the distances were **70.3023mm** and **9.7149mm**, the direction, once again, changed to

[-0.2209 -0.6056 0.7645]. Thus, there appears to be a marked increase in accuracy of the method, when distances that are similar in magnitude are used.

The accuracy of the method was also shown through the calculation of the distances between the calculated and theoretical ankle and subtalar axes of the model. The distance between the experimental and subtalar axes was 39.9727mm (1.5737 inches), while the distance between the two theoretical axes was 39.8158mm (1.5676 inches). As the difference between the two distances was 0.1569 mm, the accuracy of the method was again proven.

4.4). ***Testing the brace***

In order to test the effectiveness of the braces, Vicon, F/Scan, and GaitRite systems were utilized. A vertical ground reaction force pattern was extracted from the data and examined for each of the braces and compared to the ground reaction force pattern, which resulted when no brace was worn.

The ***FScan Pedal Plantar Stress Measurement System (Tekscan Inc., South Boston, MA, USA)***, is used to measure total and regional pedal plantar interface pressures. FScan measurements of pedal loading and gait event timing combined with GaitRite step spatial and temporal information can be used to calculate how pedal center of pressure is related to approximate body center of gravity location relative to pedal base of support. The FScan sensor is an ultra-thin (0.11 mm), two-layer mylar sheet in the shape of a shoe insole, with 960 evenly distributed (4 mm^2), pressure sensing elements (sensels) in area. The sensor can be cut to the shape of an individual test subject's feet, or to a prescribed shoe size, by following the pre-outlined contours. The sensels are made of electrically conductive silver oxide ink printed on the Mylar sheets, in rows and columns. Parallel rows of electrodes on the top Mylar layer face parallel columns of electrodes on the bottom layer. Where the rows and columns overlap they produce the resistance/conductivity, which varies in accordance with the magnitude of the pressure with which they are squeezed together, which in turn changes the electrical signal output from the sensor to the computer. Each sensel can be sampled at user selected rates up to 165 times per second in user selectable steps. Each of the sensels in an FScan sensor is calibrated using a servo controlled pneumatic calibration fixture. Each individual sensel's input/output performance is tabulated in a "lookup" table, which is used to process

subsequent measurements to an accuracy of 5% full scale or better. The FScan system measurement acquisition can be triggered to operate in synchrony with other external devices and systems, viz., the Vicon Motion Analysis System, GaitRite Electronic Walkway, and Kistler Force Platforms. Recorded data from the FScan system may be displayed in interface pressure versus time graphs, peak pressure versus time or per gait cycle plots, or in graphs of total and regional pressure profiles. A movie of the sequentially collected data frames from a walking trial can also be displayed to show pedal plantar load distribution with time.

The ***Gait-Rite Electronic Walkway (CIR Systems Inc., Clifton, NJ, USA)*** is a 24 foot long by 24 inch wide, instrumenting carpet, containing six local area networks (LAN) of 2304 sensors, each arranged in a 48 x 48 grid pattern. Each (LAN) sensor network is independently controlled by the PC server that the system is connected to. The networks are independently activated when the subject steps into the LAN's sensor grid. Communication between the PC server and the LAN being walked on is via high-speed network data transmission. The GaitRite Walkway is used to measure spatiotempral parameters of gait that can be measured with the Gait Rite System include the duration of step, gait cycle, swing, stance, single, and double support, time, step and stride lengths, base of support width, degree of toe-in and toe-out, cadence, stride velocity, and event times of contact, last contact, and foot flat. The FScan system was used to determine the times at which the different phases of gait occurred.

In the comparative laboratory tests of the dual axis ankle-foot orthosis, Figure 4.20, the subject walked at a normal speed along a thirty foot walkway wearing the dual axis AFO, the plastic posterior leaf spring AFO, and the single degree of freedom

articulated ankle joint AFO. Results were compiled and comparatively analyzed for each orthosis.

Figure 4.20 *Laboratory test of the dual axis AFO using the Vicon, GaitRite, and FScan systems; Right foot; (a) heel contact; (b) foot flat; (c) mid-stance; (d) heel rise; (e) toe off*

(a) **(b)**

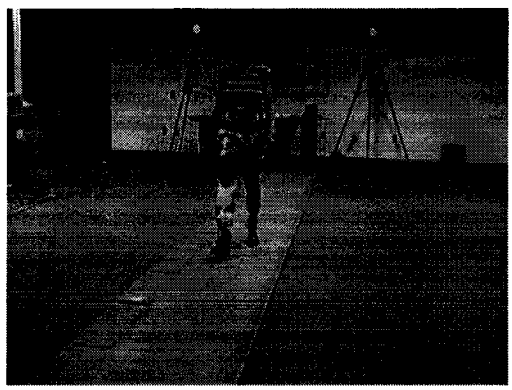

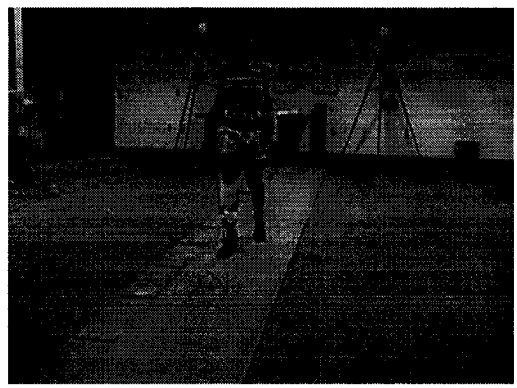

(c) (d)

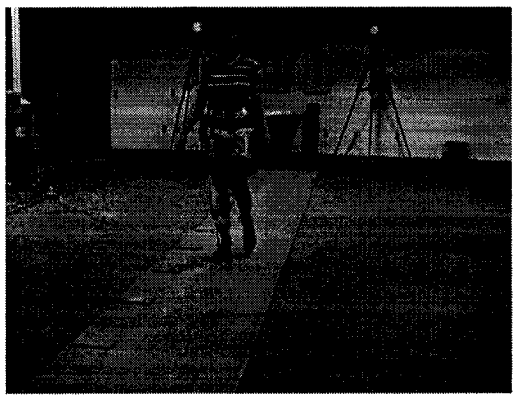

(e)

A normal vertical ground reaction force pattern has two peaks, representing approximately 110% of the body weight and a valley, representing about 80% of body weight, Figure 4.21, depending on the amount of weight transferred to the foot at each point.

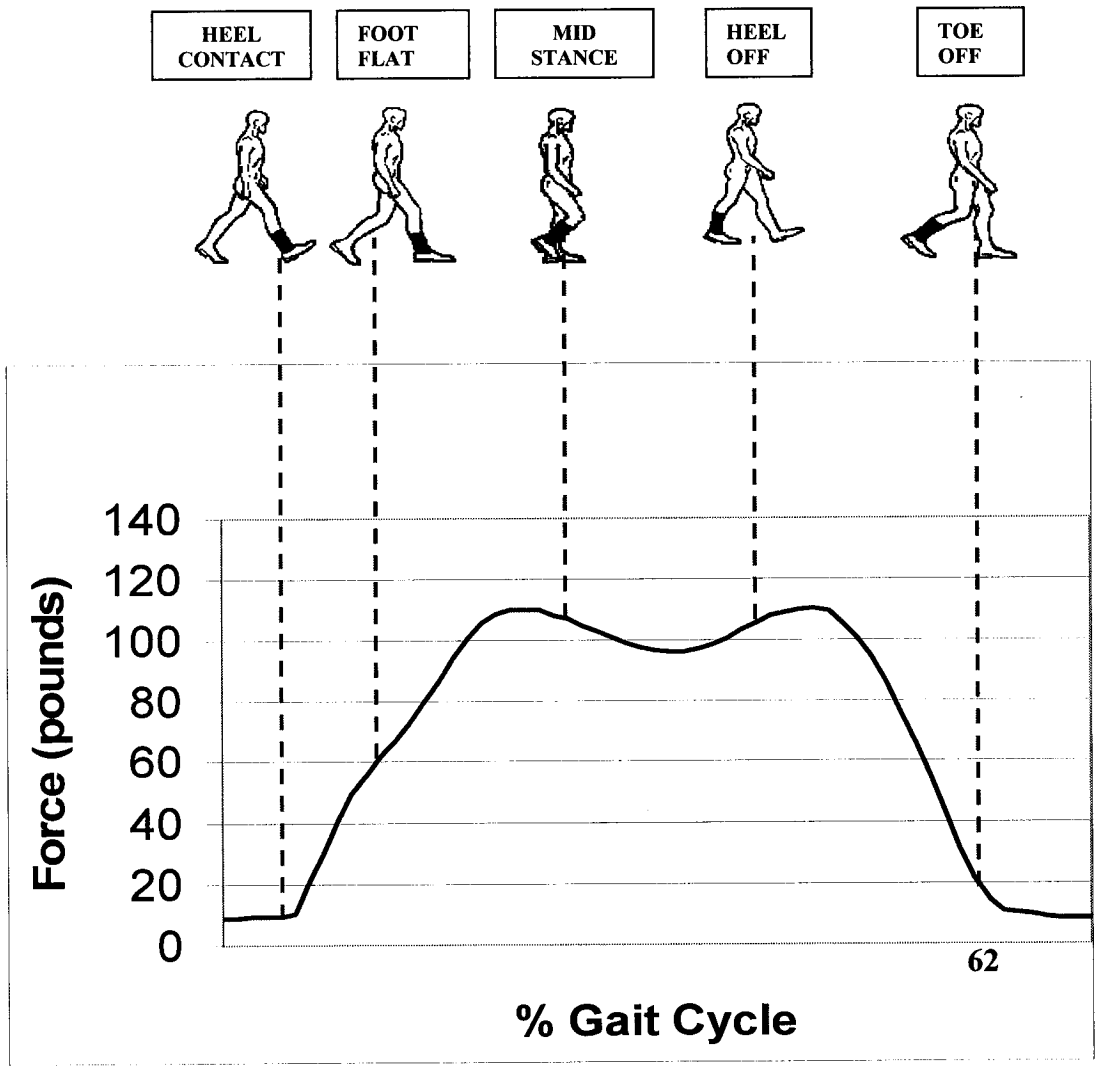

Figure 4.21 *Normal vertical ground reaction force pattern*

Figure 4.22 shows the total vertical ground reaction and regional force distribution for the toe, forefoot, midfoot, and heel of the subjects' left and right feet, while walking at a normal pace without an orthosis, wearing sneakers. The main differences between the profiles of the right and left feet are seen in the heel, toe, and midfoot sections of the foot, with a slightly lower maximum force being experienced in the toe area of the left foot. All regions showed only minor differences between the right and left feet. That is, the profiles are almost identical.

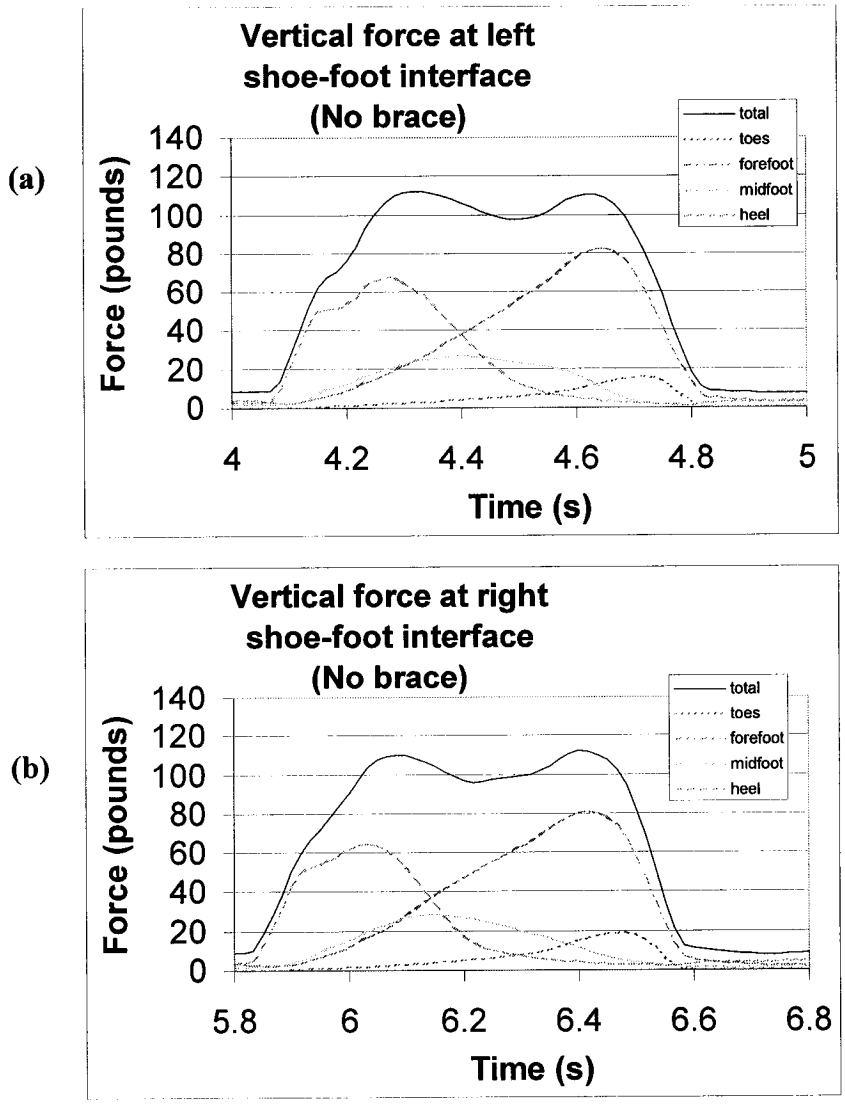

Figure 4.22 *Vertical force at shoe-foot interface for the stance phase of a typical gait cycle (no brace); (a) left foot; (b) right foot*

Figure 4.23 shows that there was a slight difference in the degree of pedal load duration of the right and left feet for all regions, except for the toes of the right foot. There was a tendency to push off a little more with the left foot than with the right foot.

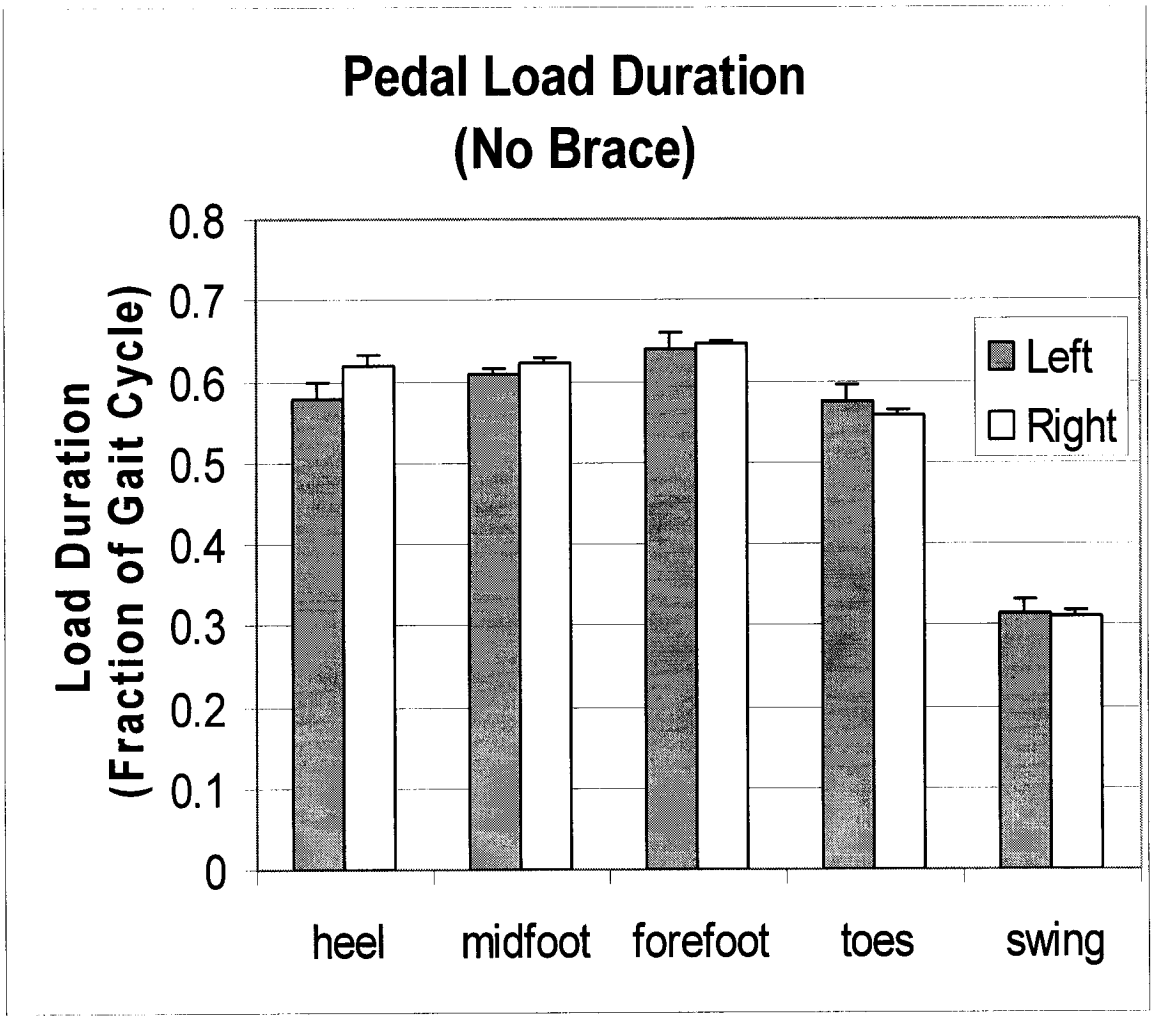

Figure 4.23 *Pedal loading (no brace)*

Figure 4.24 shows the vertical force distributions for the total plantar surface of the foot, and for the toes, forefoot, midfoot, and heel sections of the subjects' left and right feet, while wearing in-shoe, the non-articulated "posterior leaf spring" AFO shown in Figure 3.25 on the right foot, with a matching shoe on the left foot. The maximum forces experienced by the right foot, were considerably greater than the forces experienced by the left. The force experienced at the heel during heel contact through foot flat, was approximately the same for both feet, except at the moment of heel contact. This was to compensate for the large knee flexion moment, which resulted from the rigidity of the PAFO. This also resulted in larger forces in the right forefoot. For a hemiplegic, this would cause unsteadiness in gait, because of the weakened musculature, which would not allow the individual to compensate for the added moments quite as readily.

(a)

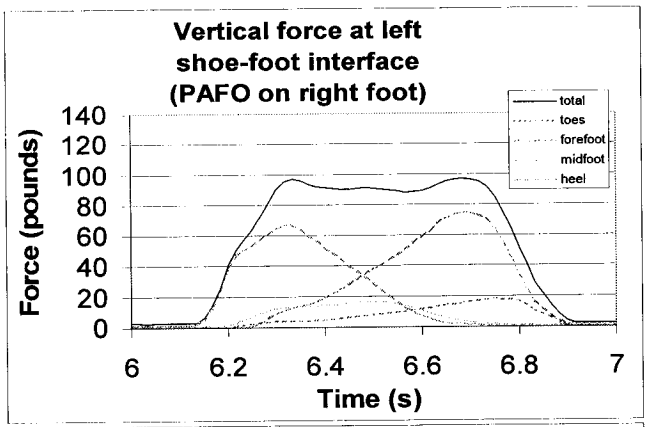

(b)

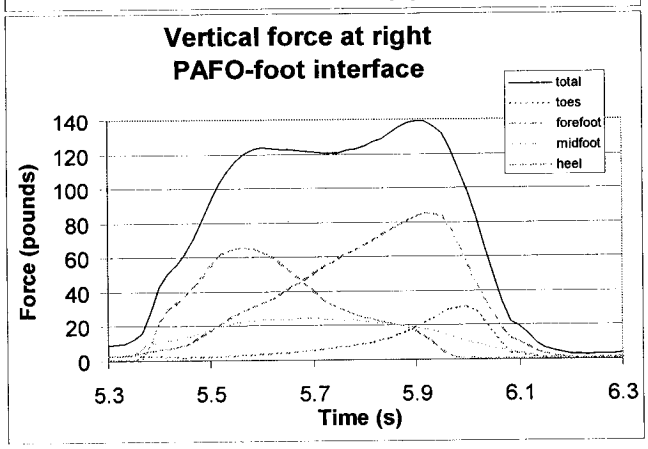

Figure 4.24 *Force at PAF0-foot interface; (a) left foot; (b) right foot*

Differences in pedal load durations, Figure 4.25, were seen in the heel and midfoot, when walking in the PAFO. The subject was forced to walk with more of a festinating gait to compensate for a large knee flexion moment at heel contact. The load duration for the left foot was therefore much shorter for the midfoot, than was experienced when no brace was worn. It was, however, very similar to the load durations for the forefoot, when no brace was worn. When walking with the PAFO , the subject had strive to carefully maintain her balance, due to the unexpectedly large knee flexion moments.

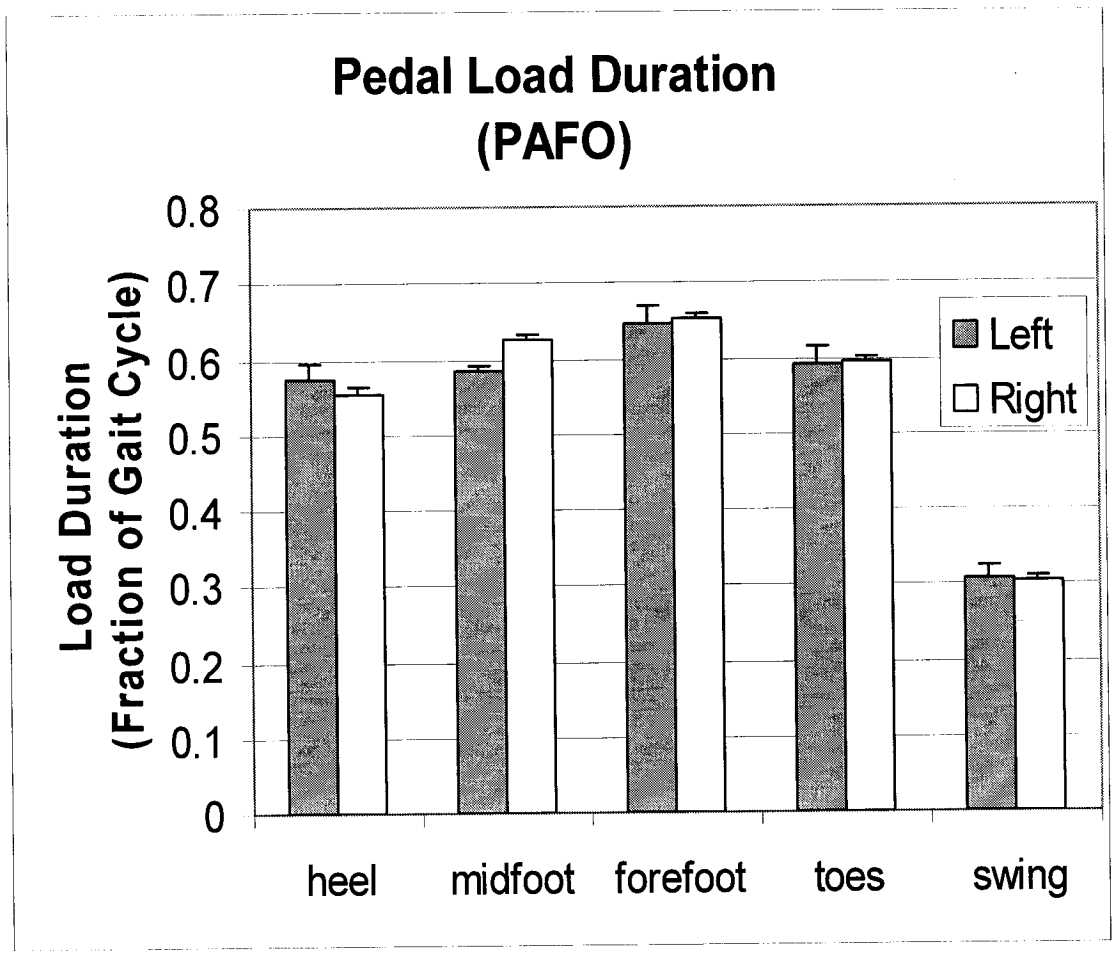

Figure 4.25 *Pedal loading (PAFO)*

Figure 4.26 shows the vertical ground reaction force and regional load distribution for the toes, forefoot, and heel sections of the subjects' left and right feet, respectively, while wearing the single-of-degree-of-freedom, articulated, dorsiflexion assist AFO, shown in Figure 3.26, with a matching shoe on the left foot. The initial slopes for both force profiles are about the same, implying that the onset of loading at heel contact is similar for both, unlike for the PAFO, for which there was little or no force at heel contact.

(a)

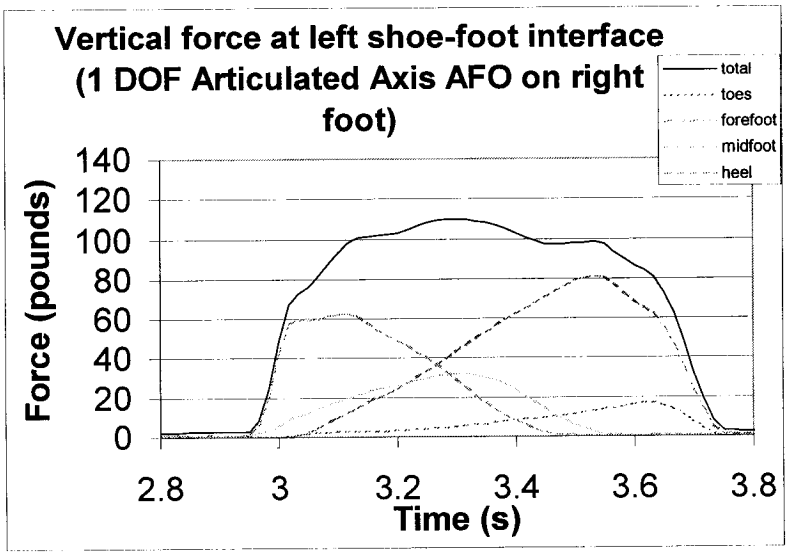

(b)

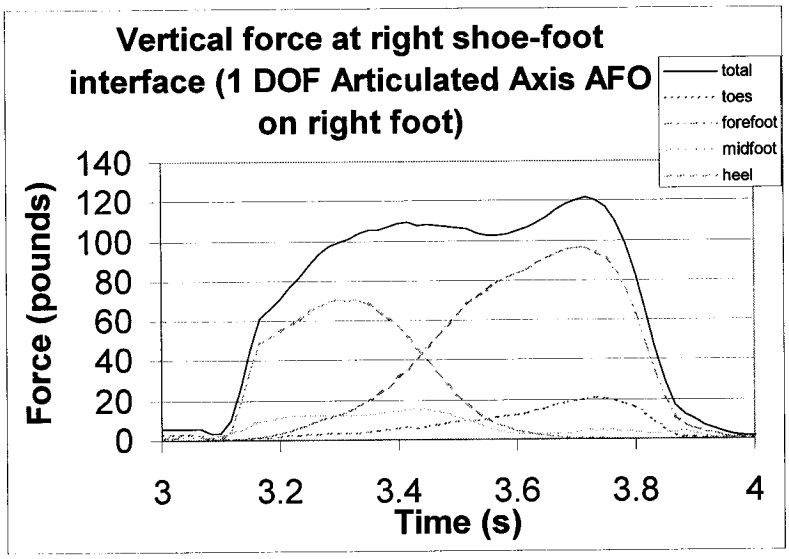

Figure 4.26 *Force at shoe-foot interface (1 DOF brace); (a) left foot; (b) right foot*

There were also differences in the heel force profile, with the right foot, on which the brace was worn, experiencing a larger peak force than the left foot, as a result of the added force due to the compression of the joint springs. The decompression of the springs resulted in the development of a large knee flexion moment, causing the knee to buckle as mid stance was approached. There was also the chance that the rising center of gravity could cause hyperextension. From foot flat to toe off, the total force was high because of the decompression of the springs. Additionally, the dorsiflexion stop was hit too soon, causing the delay of heel rise. The maximum force in the midfoot was also much greater for the non-braced foot, in addition to there being a significant difference in the second peak forces, with the braced foot experiencing the larger force, as the springs were decompressed. These effects would be very much felt by a hemiplegic, who would have to exert great amounts of excess energy to maintain balance. Additionally, the onset of loading at heel contact is more normal than with the PAFO, which impeded heel contact due to its rigidity.

There were greater differences in pedal regional load durations, Figure 4.27, with the one-degree-of-freedom, articulated ankle joint, than with the PAFO. The load durations for the heel, midfoot, and forefoot were shorter here than for the PAFO. This was also the case for all sections, except the toes, when no brace was.

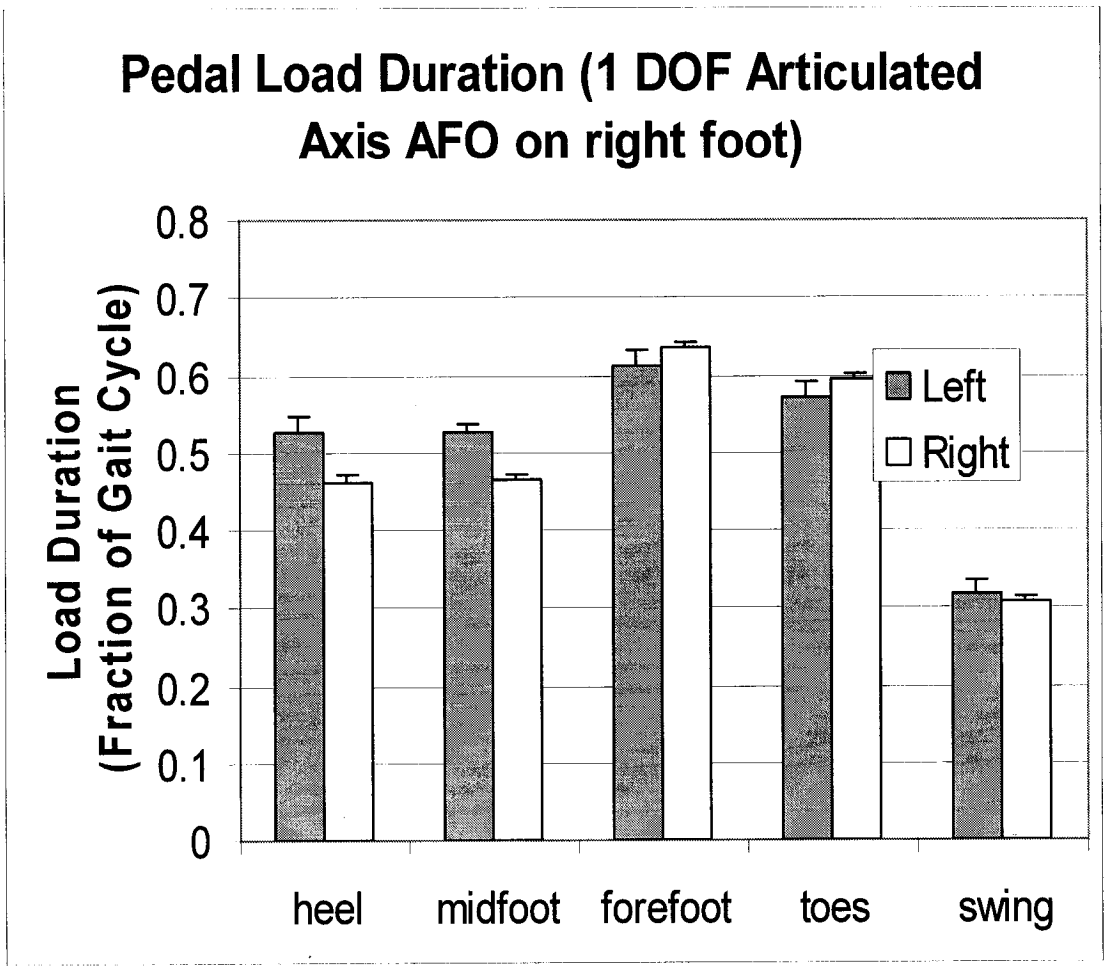

Figure 4.27 *Pedal loading (1 DOF brace)*

Figure 4.28 shows the vertical ground reaction force and regional load distributions for the toes, forefoot, midfoot, and heel of the subjects' left and right feet respectively, while wearing the articulated dual axis dorsiflexion assist AFO on the right foot, with a matching shoe on the left foot.

(a)

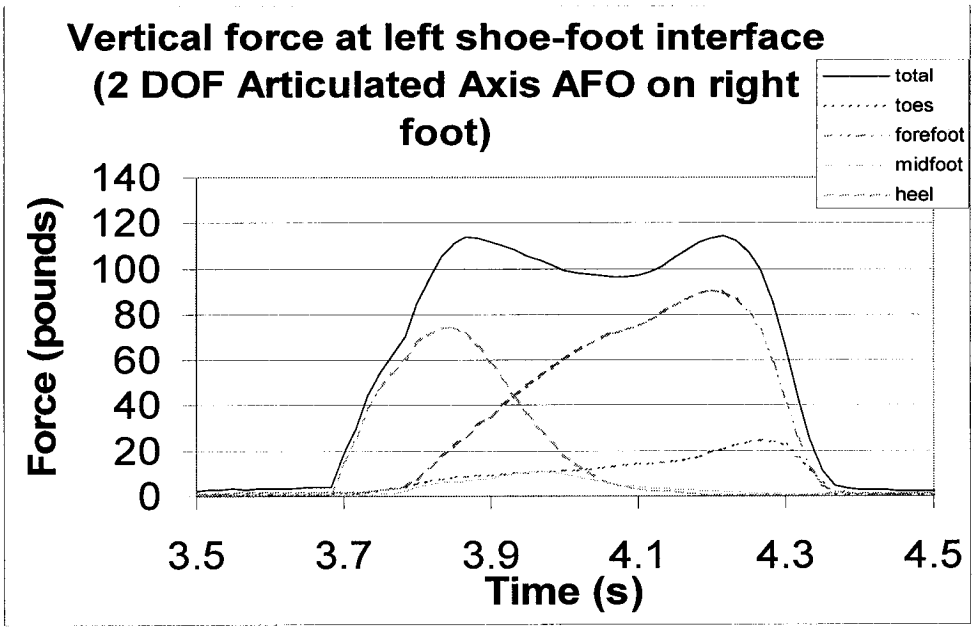

(b)

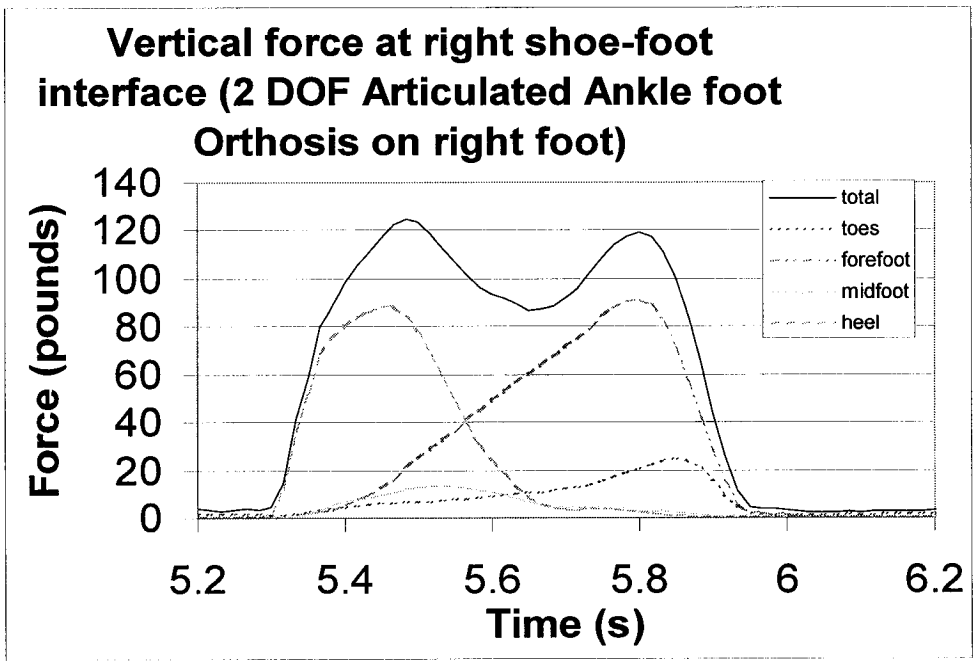

Figure 4.28 *Force at shoe-foot interface (2 DOF brace);* (a) *left foot;(b) right foot*

The forces experienced in the right and left feet were similar, in most regions. The overall reaction force profile was similar to that for the no brace case. The slope at heel contact was about the same for both feet, implying that its onset was fairly symmetrical. Moreover, there was no contribution from the forefoot and midfoot early on. The dual axis brace therefore permitted normal function.

The pedal load duration values for the left foot, Figure 4.29, were about the same as those for the normal, no brace, case. The values for the right foot also mimic those for the normal, no brace cases, although they are uniformly smaller, which implies that there was some limping. As the forces and moments were also similar to the case in which no brace was worn, a hemiplegic would not have to struggle to maintain balance. The subject reported that walking with the dual axis brace was quite similar to walking without it, as there was no struggle with unfamiliar outside forces and moments.

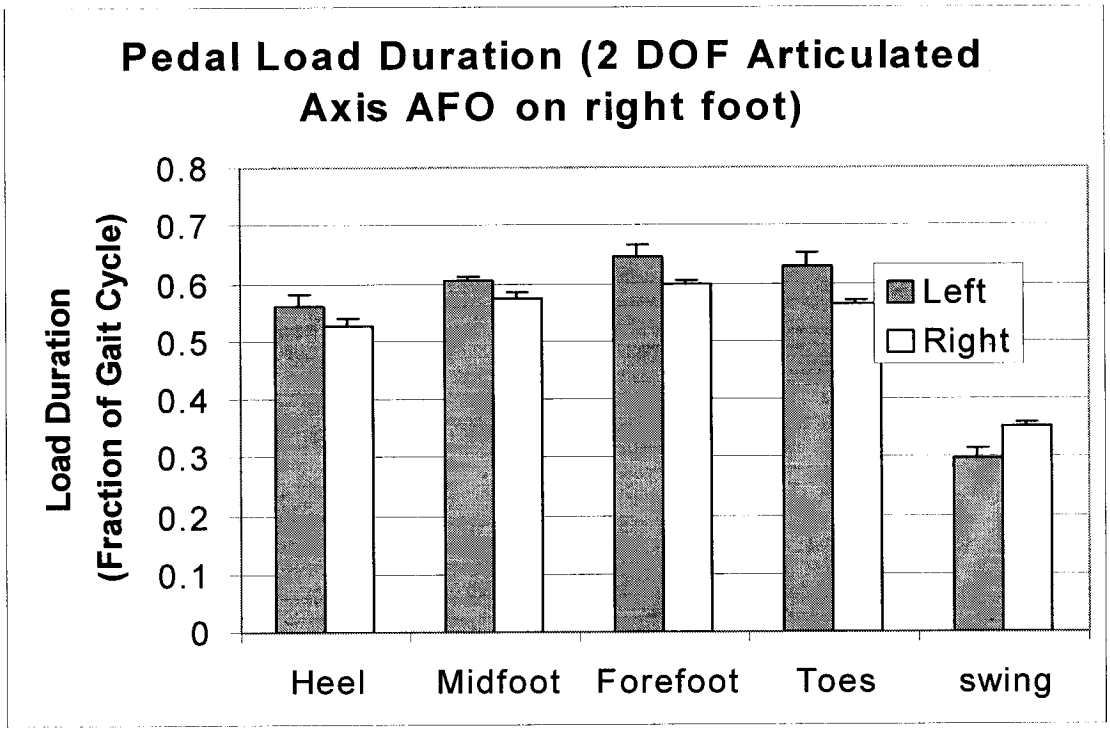

Figure 4.29 *Pedal loading (2 DOF brace)*

Figure 4.30, shows the profiles of the vertical force at the shoe-left foot interface for all tests. Wearing the brace on the right foot clearly affected the left, except for the case in which the dual axis orthosis was worn.

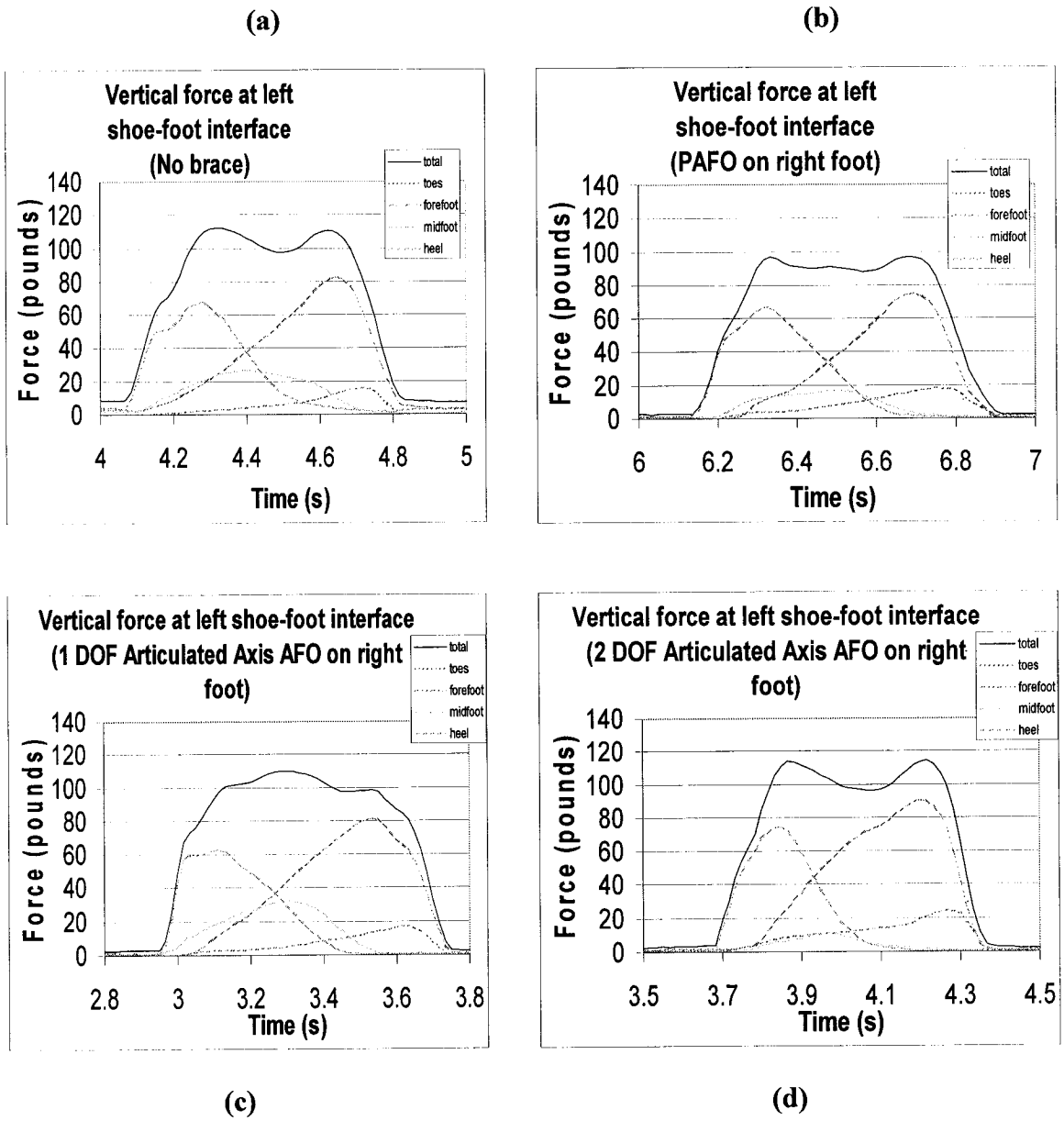

Figure 4.30 *Vertical force at left shoe-foot interface (all cases)*

Figure 4.31 shows the profiles of the right foot for all tests. The similarity between the force profiles of the individual foot sections (toe, forefoot, midfoot, and heel), for Figures 4.31 (a) and (d), (no brace and dual axis AFO case) is very striking, and illustrates how well the brace works. The major difference between the two profiles occurred in the heel section of the foot, which experienced larger forces, resulting in an increase in the first peak of the force profile when the brace was worn.

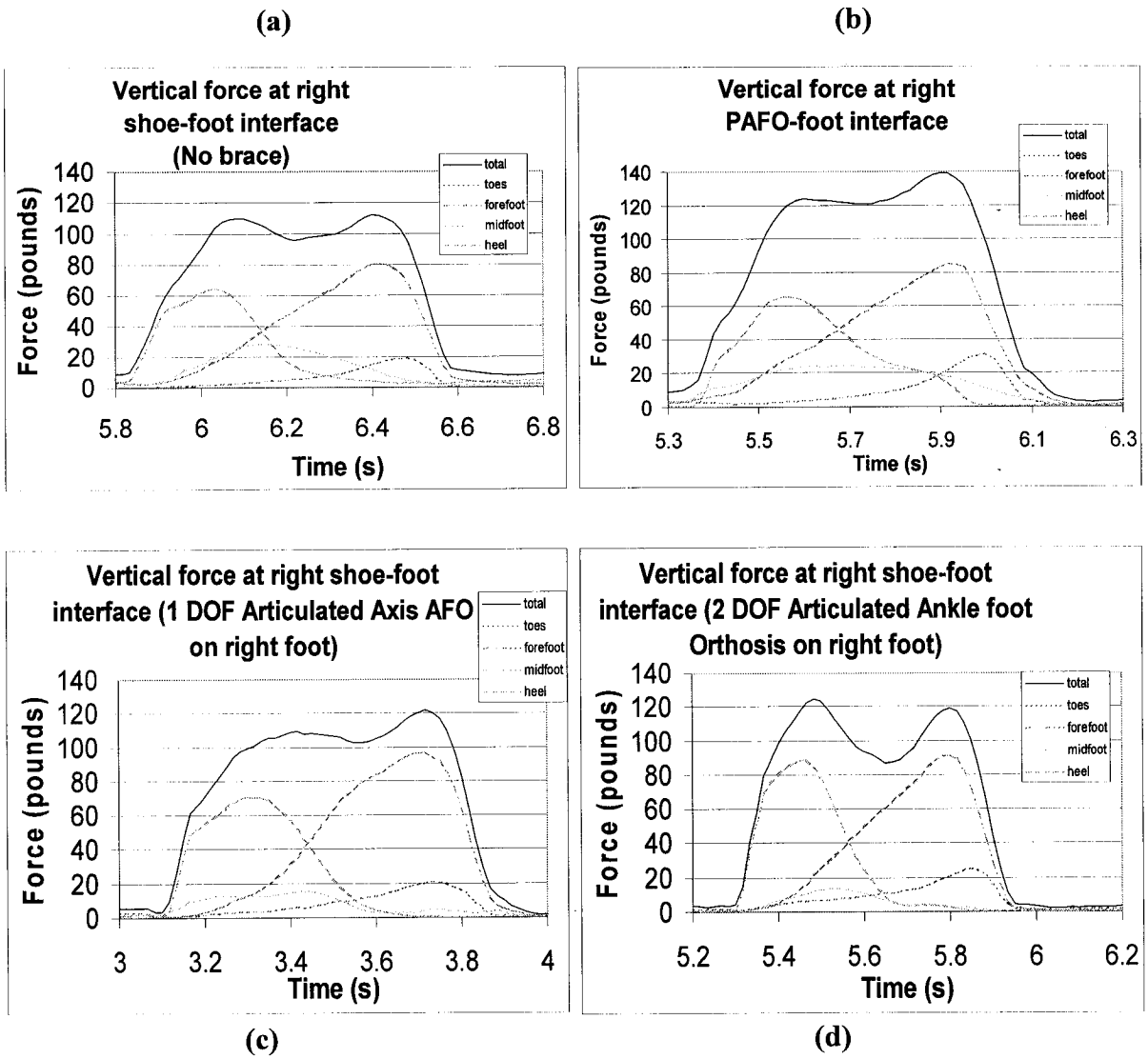

Figure 4.31 *Vertical force at right shoe-foot interface*

Figures 4.32–4.35 shows the velocity profiles of the right and left toes. The velocity and acceleration at the knee and ankle are presented in Appendix B.

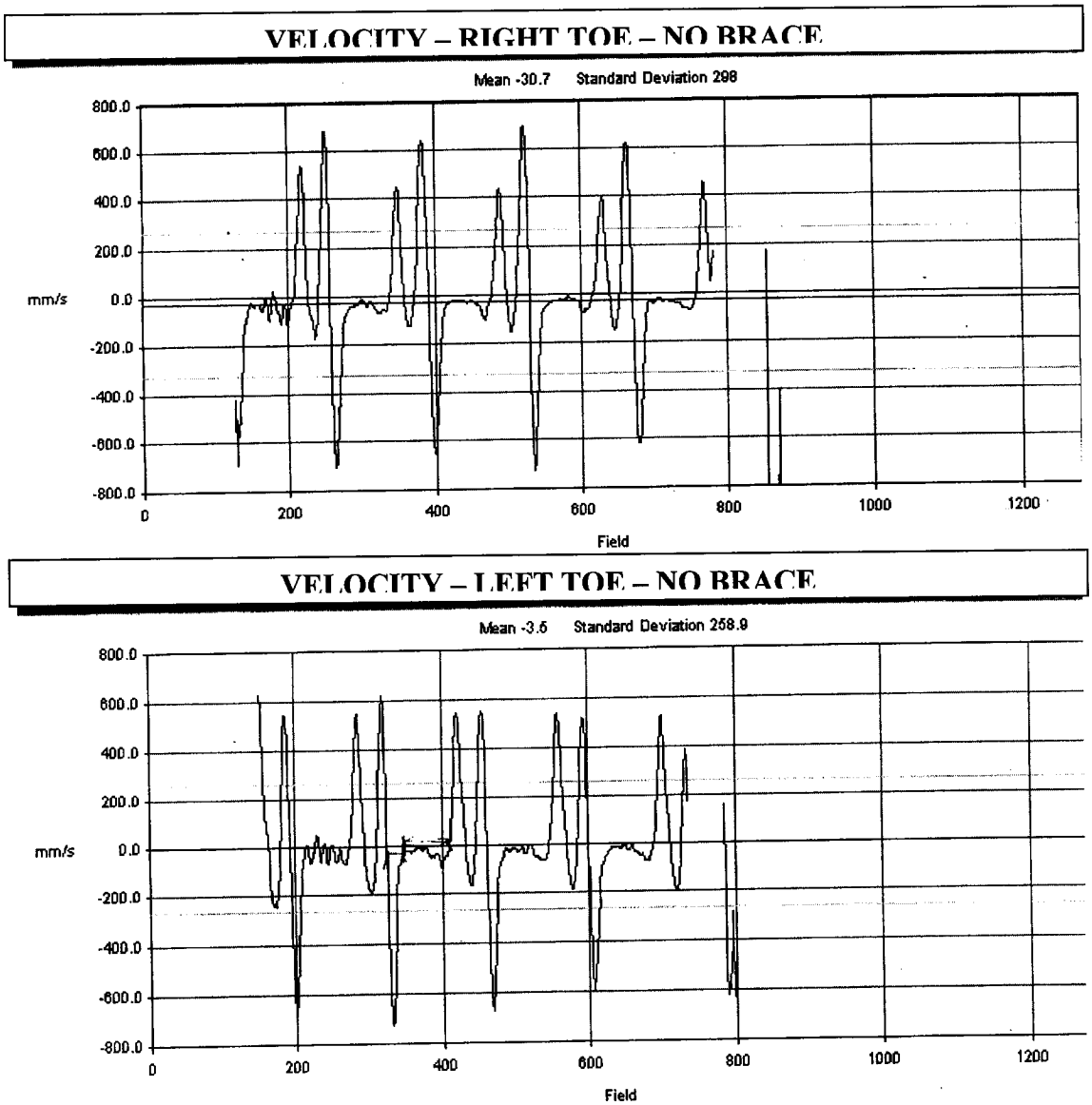

Figure 4.32 *The velocity profile of the right and left toes, wearing no brace*

As the right foot nears heel contact, Figure 4.32, the toe experiences a negatively increasing velocity, which falls to about –650 mm/s, and as foot flat is neared, there is a negatively decreasing velocity. In fact, at mid-stance, there is zero velocity. The velocity then increases negatively again, but only falls to about –50 mm/s, then negatively

decreases again, after heel off. It continues to negatively decrease, then positively increase through to toe-off, with a peak velocity of 400 mm/s. During swing, the velocity positively decreases, negatively increases and decreases, then positively increases until it reaches its peak velocity of 700 mm/s during mid-swing. The left toe follows a similar pattern, however the peak velocities at toe-off and mid-swing, are about the same. For both feet, heel contact is approached with a speed of about –600 mm/s.

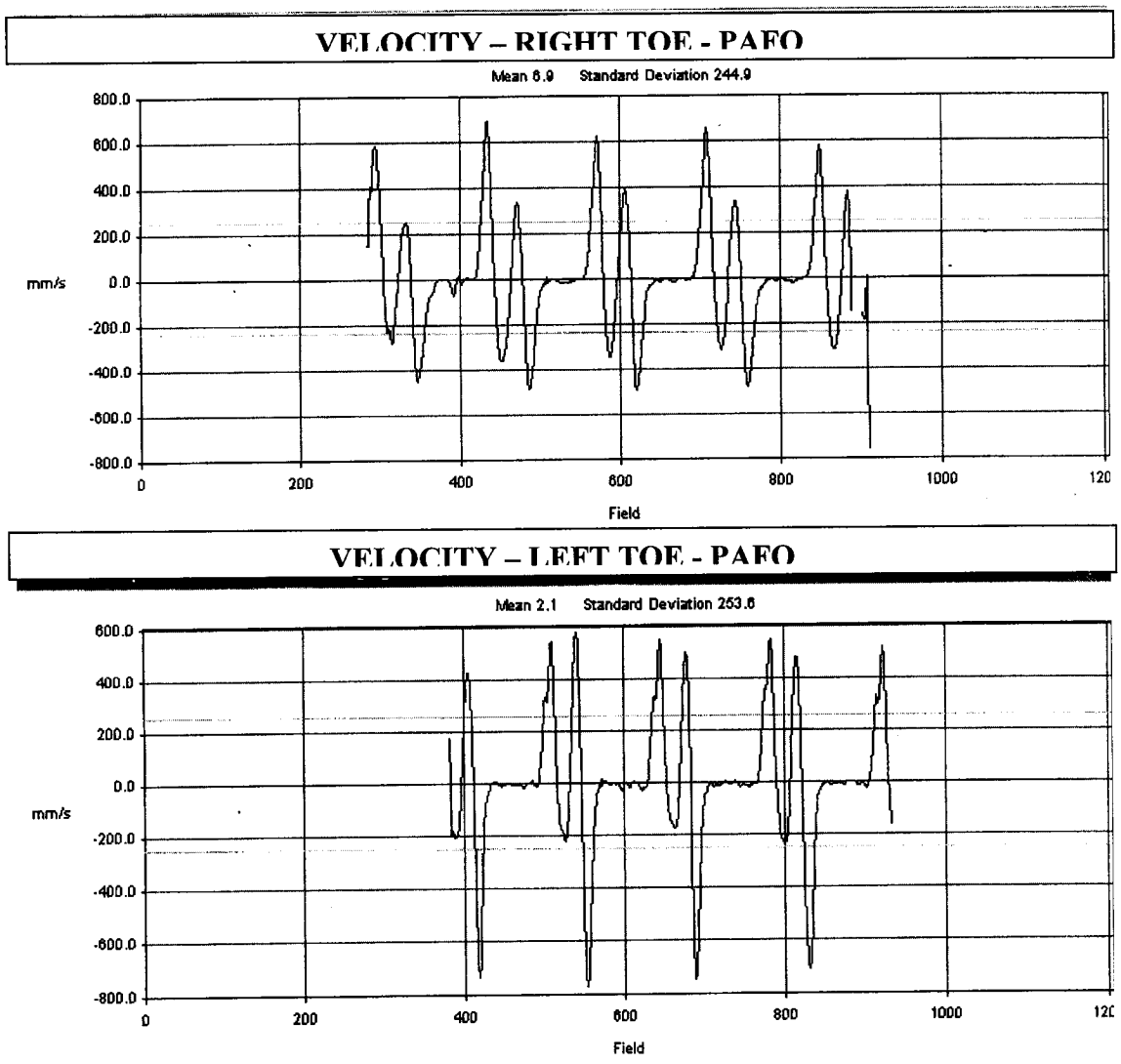

Figure 4.33 *The velocity profile of the right and left toes, wearing PAFO on right foot*

When the PAFO, is worn on the right foot, Figure 4.33, the peak velocity occurs at toe-off rather than at mid-swing, which is also a peak, but is substantially smaller. The peak velocity is again around 600 mm/s, occuring at toe-off, while the lesser peak at mid-swing varies between 200 mm/s and 400 mm/s. The velocity at heel contact is consistently about –400 mm/s. Heel off is not accompanied with a negatively increasing velocity, but the speed remains essentially constant from mid-stance to heel-off. During swing, the velocity positively decreases, followed by a negatively decreasing velocity, which reaches –300 mm/s at the lowest point, before it begins to rise again. The velocity profile of the left also changes, with heel contact occuring at speeds approaching –800 mm/s. As was the case with the left foot when no brace was worn, the peak forces at toe-off and mid-swing are about the same, around 500 mm/s.

When the one-degree-of-freedom AFO is worn, Figure 4.34, the peak velocities of the right foot at toe-off and mid-swing are about the same, 400 mm/s. The velocity at heel contact, however is about 600 mm/s, as was the case with the right foot when no brace was worn. Once again, there is no substantial change in velocity during heel-off, however, the velocity does reach about –200 mm/s during swing. For the left foot, the profile is about the same as when no brace was worn, although the maximum velocities are a little greater.

When the two-degree-of-freedom brace was worn, Figure 4.35, the peak velocities at toe-off and mid-swing are a little lower, in addition to the speed at toe-off being lower than the speed at mid-swing, unlike when no brace was worn. The velocity profile for the left foot is very similar to the profile of the left foot when no brace was worn.

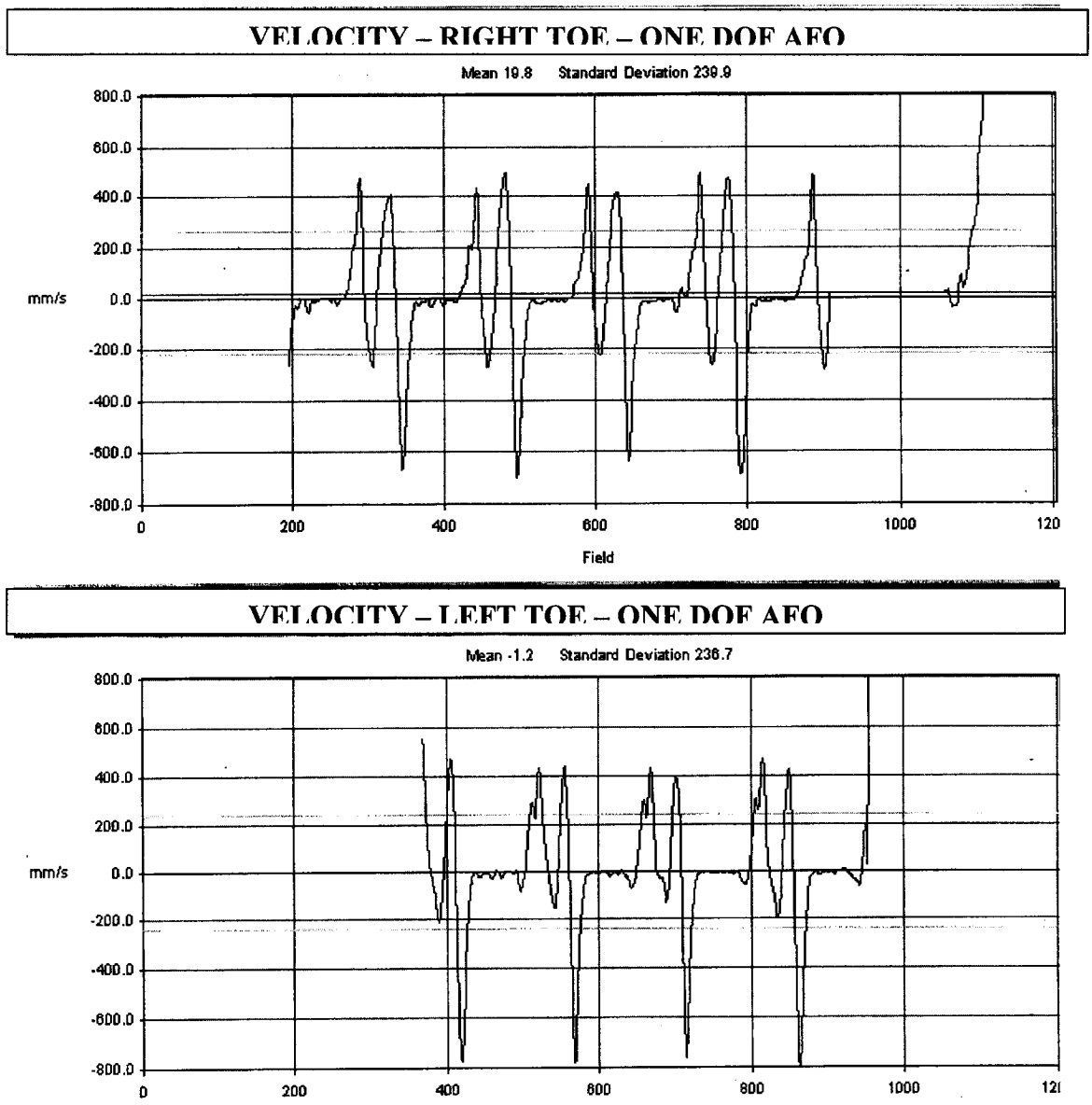

Figure 4.34 *The velocity profile of the right and left toes, wearing the one-degree-of-freedom AFO on right foot*

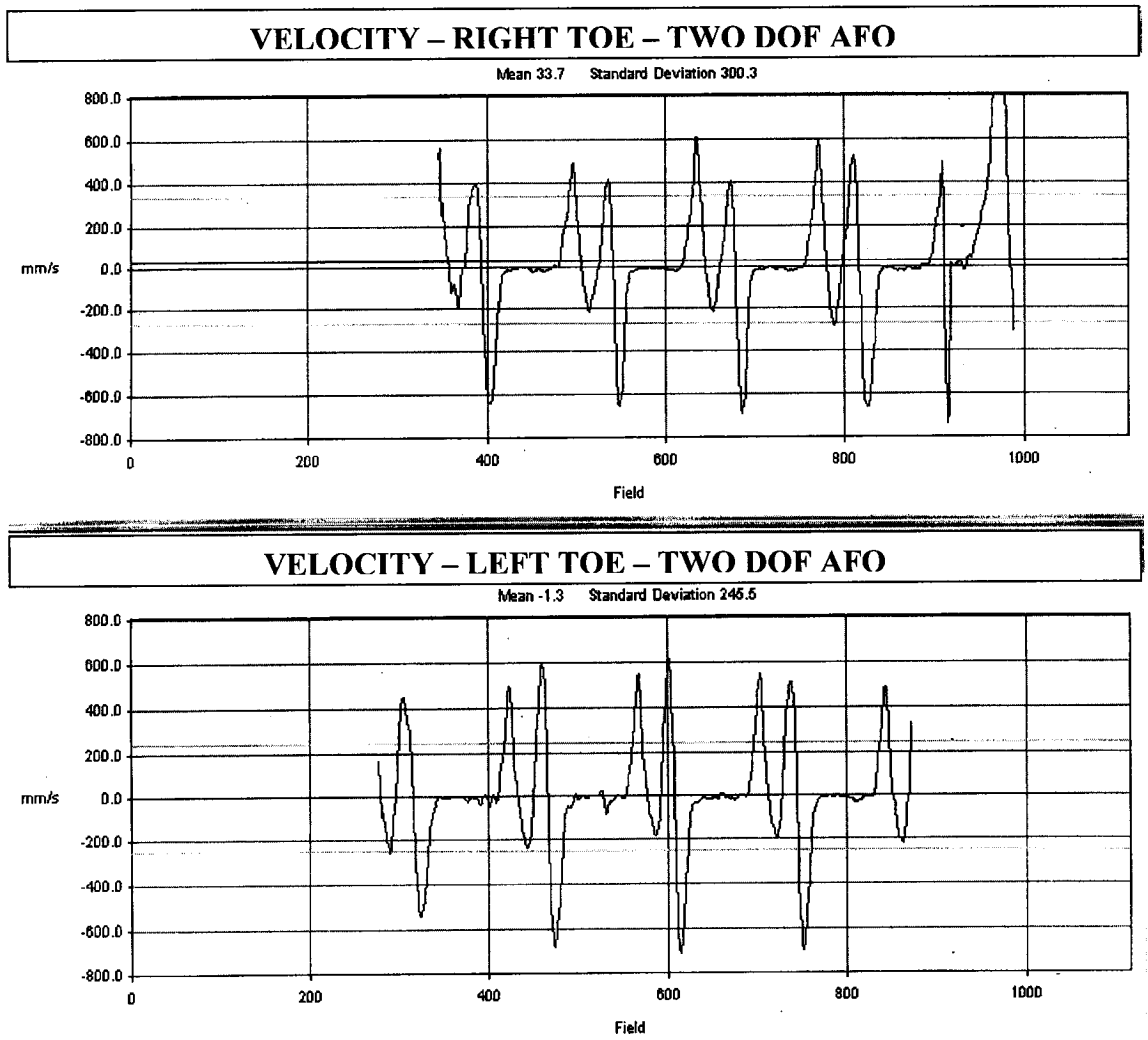

Figure 4.35 *The velocity profile of the right and left toes, with the two-degree-of-freedom AFO on right foot*

Figure 4.36 – 4.39 show the shows the acceleration profiles of the right and left toes.

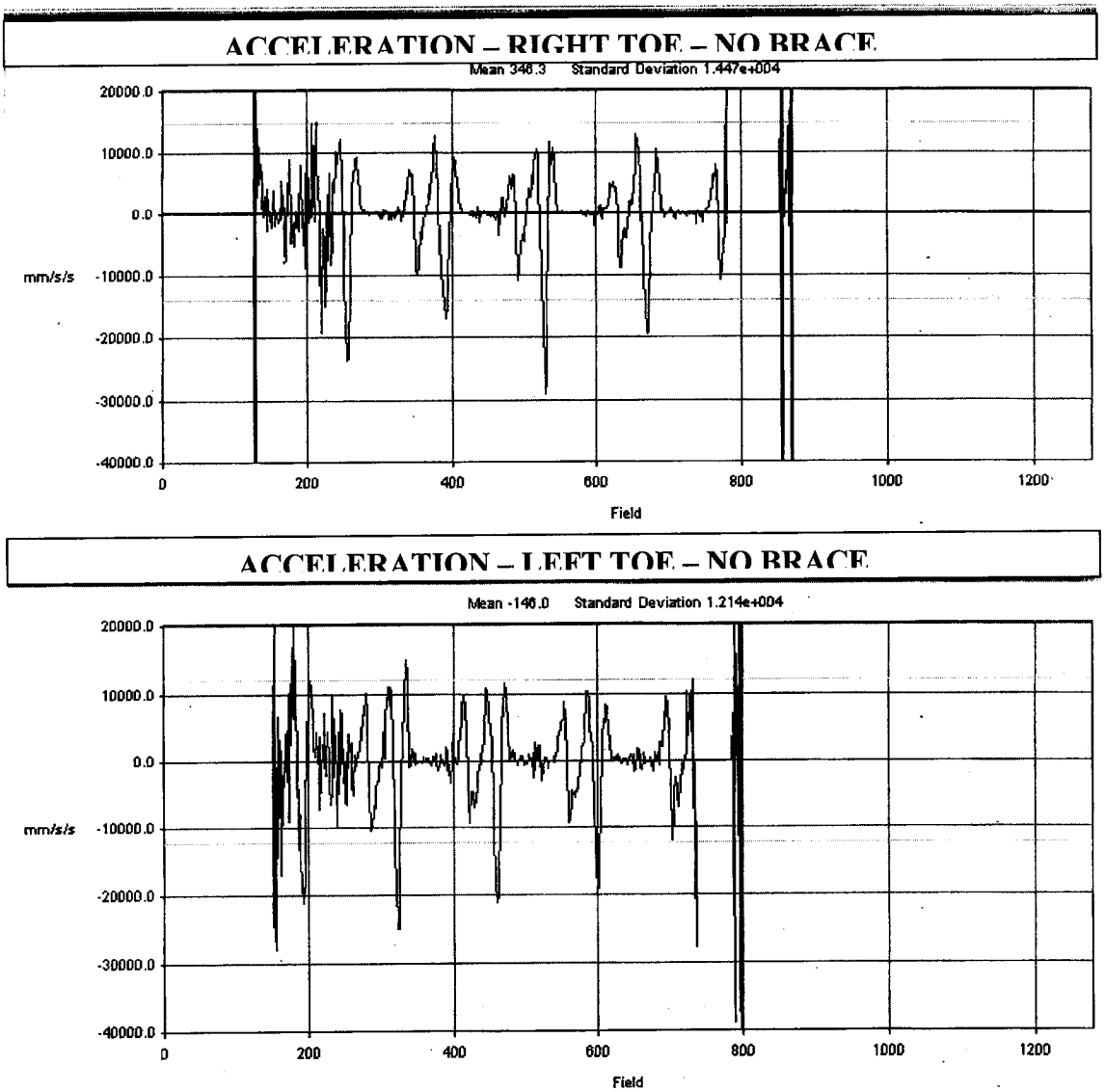

Figure 4.36 *The acceleration profiles of the right and left toes, with no brace*

Heel contact of the right foot was approached with an increasingly positive acceleration, which upon contact at about 1000 mm/s^2 began to positively decrease as foot flat was approached, Figure 4.36. The acceleration remained at zero until heel off, when it began to positively increase as toe-off was approached, occuring about 800 mm/s^2. The acceleration then positively decreased, negatively increased, then positively increased, during swing, and peaked at mid-swing (1000 mm/s^2), before plunging to –

3000 mm/s^2 at terminal swing, and negatively decreasing, then positively increasing, as the peak of heel contact was approached. The main difference between the right and left foot acceleration profiles is that the acceleration at toe-off is greater for the left foot (900 mm/s^2), than for the right foot (500 mm/s^2).

Use of the PAFO on the right foot, Figure 4.37, resulted in a marked in the acceleration at terminal stance, which occured at about -1000 mm/s^2, compared with the average of about –2500 mm/s^2 when no brace was worn on the right foot.

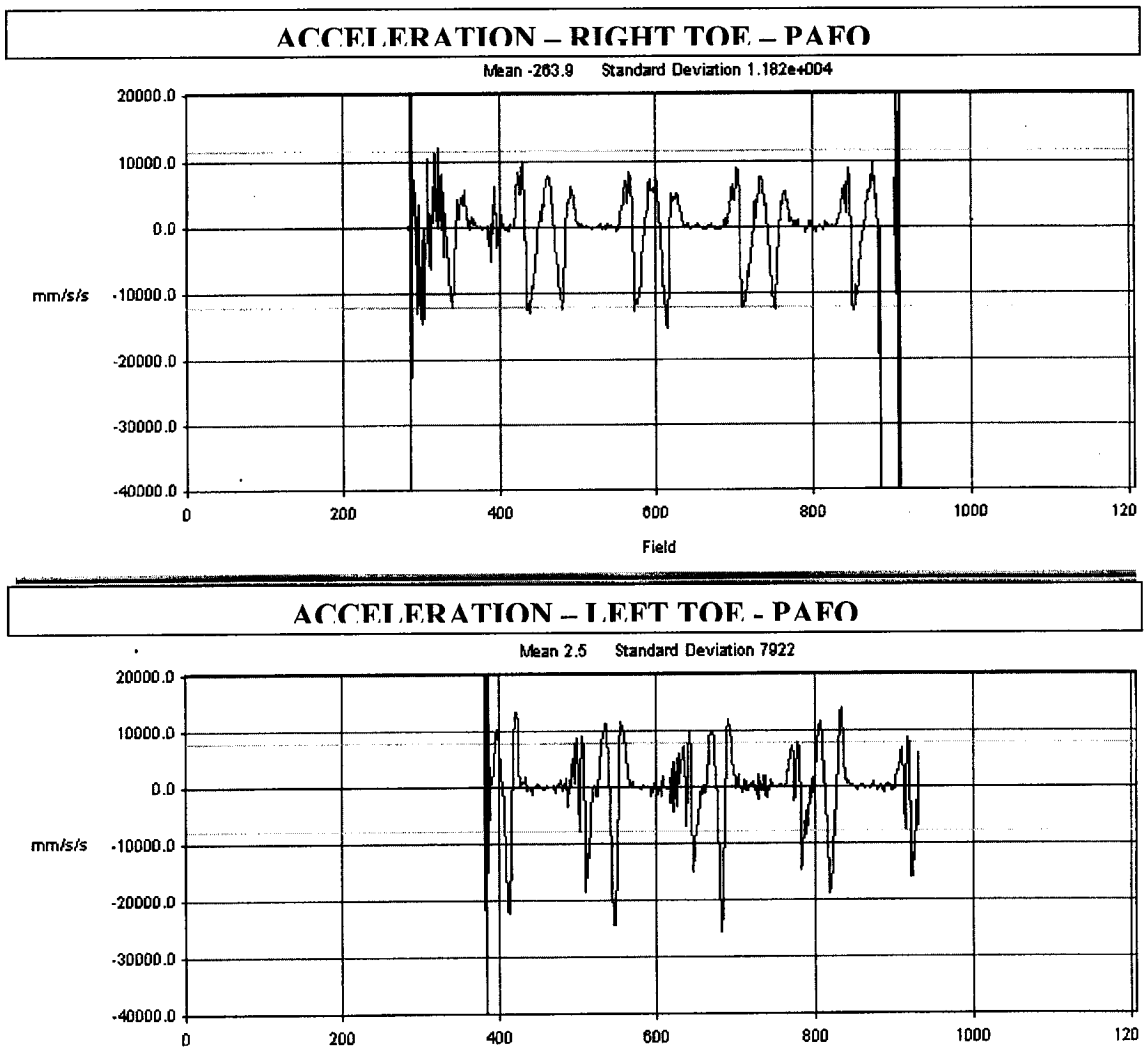

Figure 4.37 *The acceleration profiles of the right and left toes, with PAFO on right foot*

Additionally, the acceleration at med-swing also decreased, falling from about 1000 mm/s^2 to when no brace was worn, to about 500 mm/s^2 when the PAFO was worn on the right foot. The acceleration at heel contact was also lower (500 mm/s^2). The profile for the left foot remained essentially the same, as when no brace was worn on the right foot.

When the one-degree-of-freedom brace was worn on the right foot, Figure 4.38, the acceleration at mid-swing again was smaller (500 mm/s^2) than when no brace was worn, as was the magnitude of the negative acceleration at terminal stance.

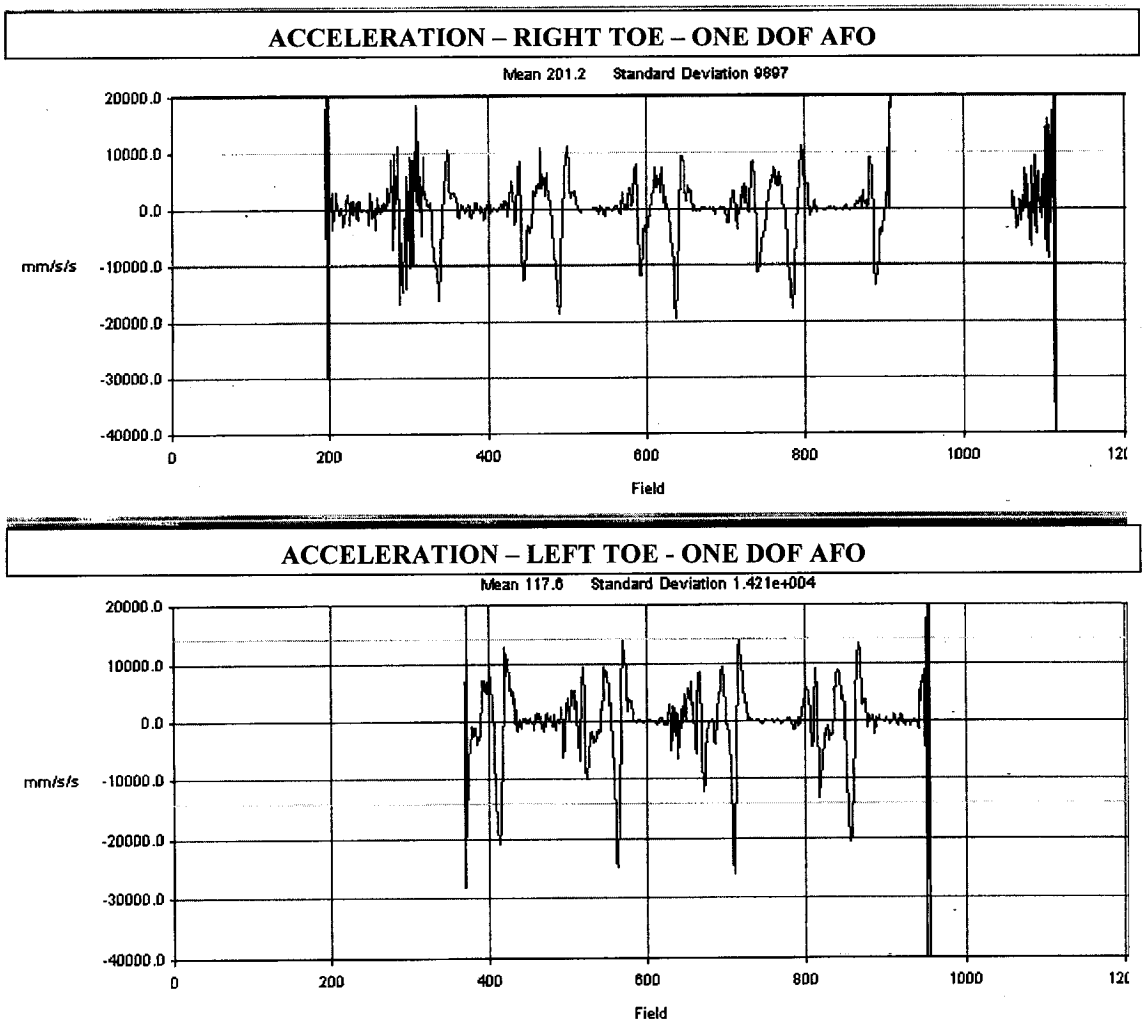

Figure 4.38 *The acceleration profiles of the right and left toes, with one-degree-of-freedom AFO on right foot*

For the left foot, however, the acceleration at heel contact generally increased.

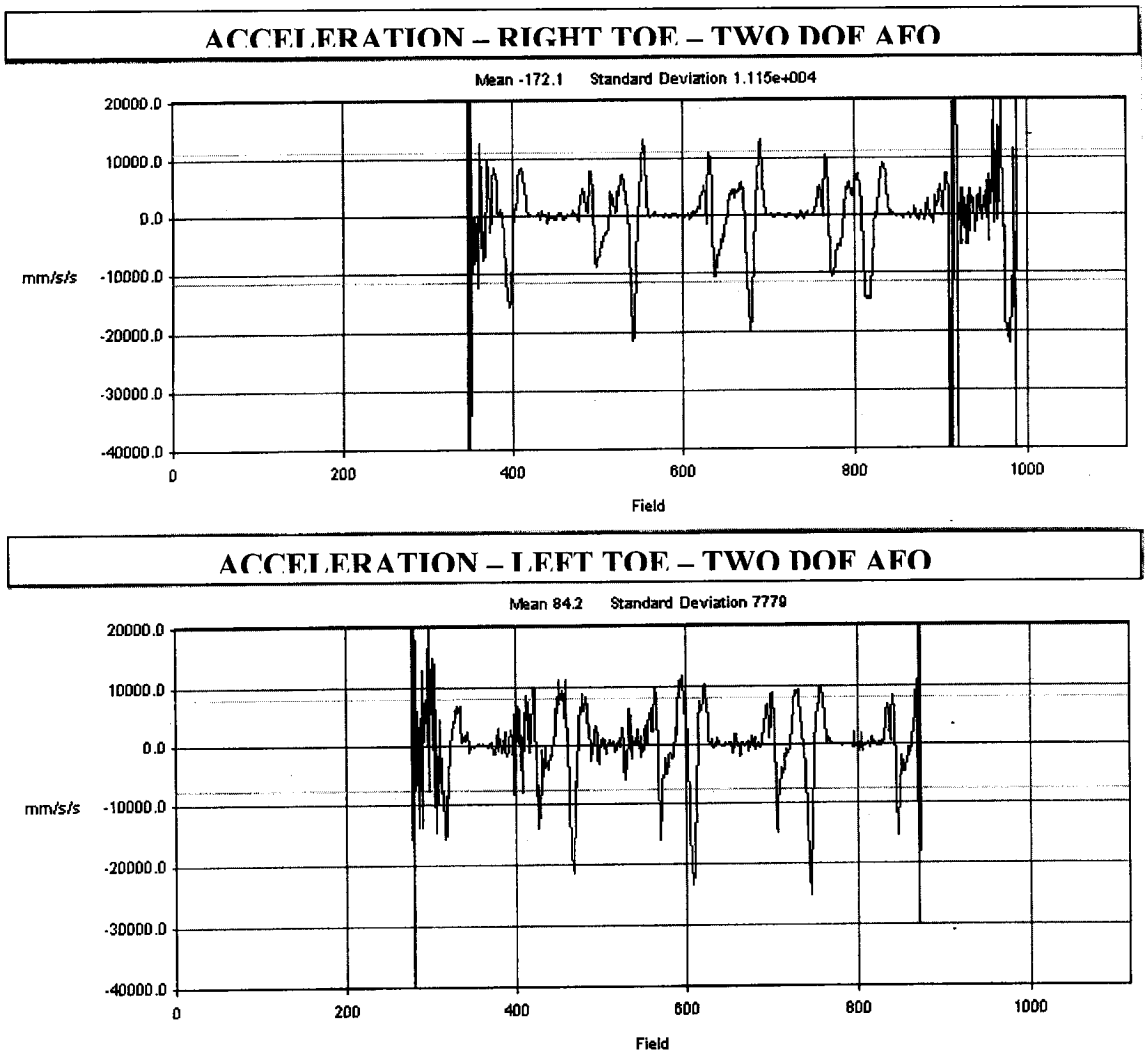

Figure 4.39 *The acceleration profiles of the right and left toes, with two-degree-of-freedom AFO on right foot*

For the two-degree-of-freedom AFO, Figure 4.39, the maximum negative acceleration at terminal stance was slightly smaller. The acceleration at mid-swing, however was much lower, and was in fact lower than the peaks associated with toe-off

and heel contact, unlike when no brace was worn. The acceleration at mid-swing when no brace was worn was about 1000 mm/s^2, while when the two-degree of freedom brace was worn, it decreased to about 500 mm/s^2. The profile for the left foot was very similar to the case in which no brace was worn.

5. CONCLUSION

The **JOINT AXIS DIRECTION AND LOCATION** method developed in this thesis, is an in vivo semi-automatic numerical method that utilizes 3-D optical images to determine the "best" (least mean square error) equivalent joint location. It improves upon previous methods of determining joint orientations and locations. The **JOINT AXIS DIRECTION AND LOCATION** method requires input of the (x, y, z) coordinates of four data points, obtained by measuring the respective locations of patients' tibia, ankle, and foot while rotated about the respective joints with independent joint axis motion, to calculate the effective joint location and direction. The method utilizes the mathematically robust Davidon Variable Metric Minimization Method to find the "best" (least mean square error) joint location. This method was chosen because in deciding upon a method of solution, it was necessary to determine whether a deterministic or stochastic approach should be taken. As the signal to noise ratio was high and the measurement data set size was limited, it was decided that a deterministic method would be best. A stochastic method would have required a large number of data sets, which would be inpractical in a clinical setting, in which most of the patients would not have the stamina or strength to go through the required data collections precedures. More specifically, a Non-Linear Optimization Method was the method of choice as; the ankle and subtalar joints are not perfect hinge joints; the system of equations was non-linear; there was measurement noise from movement of optical markers on the body, and optical and electrical noises in the system; and there was computational numerical round-off error due to the four unknowns, (x, y, z, and L) being very different in magnitude. Davidon's Variable Metric Method for Minimization, which utilizes a symmetric, non-

negative metric, was chosen as its rate of convergence and accuracy of the method is enhanced by initially defining the metric as a diagonal matrix, the diagonal elements of which are the mean-square uncertainties for each variable, and the solution matrix is improved upon with each consecutive iteration.

Although other methods, such as those proposed by Reuleux, Halvorsen, and Gamage, also take into consideration the fact that each patient is anatomically unique, use of the **JOINT AXIS DIRECTION AND LOCATION** method is more convenient, as it is robust, simple, and fast. The other methods are cumbersome, difficult to understand, and prone to error. The method was applied and used to find the effective locations and orientations of the ankle and subtalar joints in the subject's leg for fabrication of a two-degree-of-freedom, dual axis, ankle-foot orthosis. The method is very efficient in that it allowed both ankle and subtalar joint axes to be found using the same principles. As demonstrated with the conceptual, wooden model, the method proposed in this thesis work locates the joint axes and locations accurately, and is not too computationally and experimentally involved. In addition, by finding the distances between the experimentally calculated and the measured ankle and subtalar joint axes of the model, and showing them to be equal, the validity of the method was proven.

In order to locate the joint axes of rotation on the subject's foot, the local coordinate systems of a foot scan, leg scan, ankle axis, and subtalar axis, were defined and superimposed onto each other. Thus, by finding a local coordinate system, specific to a patient, it becomes possible to determine the location of the joint axes of the individual with respect to their own anatomical landmarks. Having performed the procedure on the individual once, it would not be necessary to go through the time-consuming process of

finding the joint axes, every time an orthosis is fabricated for that particular person. Thus, the time spent in future fitting procedures will also be drastically cut.

One of the problems associated with some orthoses is the fact that the sizes are usually standardized. The patient is simply given the size that provides the best fit. This often means that the anatomical joint axes will not be as closely aligned with any existing joint axes of the brace, as is necessary for the patient to have a comfortably fitted orthosis. Having the anatomical and mechanical joint axes aligned, allows the foot/ankle to function more naturally. Thus, the patient is less likely to develop related physical problems, which occur when the anatomy is unnaturally positioned. As the anatomical joint axes are aligned with the joint axes of the dual axis AFO, there is also decreased discomfort due to chaffing caused by the calf band moving along the leg.

Application of the **JOINT AXIS DIRECTION AND LOCATION** method in the fabrication of the orthosis increased the level of comfort experienced by the wearer, as unwanted torques, which occur with other braces, such the PAFO, were eliminated. Unlike other orthoses, which can introduce unnatural forces and torques to the gait of an individual, causing discomfort and even pain, the dual axis orthosis allows for movement about the subtalar and ankle anatomical joints, rather than about the ankle joint alone. The dual axis orthosis was tested in comparison with a plastic leaf spring orthosis, single-degree-of-freedom orthosis, in addition to the case in which no brace was worn. The vertical ground reaction forces at the shoe-foot interface of the dual axis orthosis were found to be quite similar to the case in which no brace was worn. Thus, the wearer enjoyed a more stable, confident gait, due to the reduction in unwanted knee flexion moments, which were prevalent with the use of other types of orthoses.

Future work may entail seeking to incorporate the range of joint axes observed in Figures 4.18 and 4.19 into a single axis. As suggested by several other investigators, including Lundberg, the orientation of the ankle axis may vary as the foot moves through its entire range of motion. Thus a single joint, which allows this motion, may be investigated.

The method described here has clinical applications, with the possibility of using it to treat several biomedical pathologies, such as tendon transfers, in which case the location of the effective axis is unknown. If the tendon is incorrectly placed, the linkage is opposed, impeding movement, and may be especially troublesome, especially in growing children.

The dual axis AFO is economical, made of sturdy metal components, is used with standard shoes, and may be separated from the shoe, if desired, in order to be transferred to another pair. It has the potential to substantially reduce the amount of time spent in adjustment procedures, which becomes necessary when the joint axes are located using bony landmarks or by trial and error. When compared with off-the-shelf models, such as the PAFO, or even with single-degree-of-freedom models, the dual axis orthosis is well worth the time invested in its fabrication.

APPENDIX A

Davidon's Variable Metric Method for Minimization

List of variables

x^{μ}: $\mu = 1,.....,N$: the set of N independent variables

$f(x)$: the value of the function being minimized

$g_{\mu}(x)$: the derivative of $f(x)$ with respect to x^{μ}, at x

$h^{\mu\nu}$: a nonnegative symmetric matrix, used as a metric in the space of the variables

Δ: the determinant of $h^{\mu\nu}$

ε: fractional accuracy that f(x) is minimized to X 2

d: limiting value for minimum value of the function

K: number of times the variables are randomly interchanged

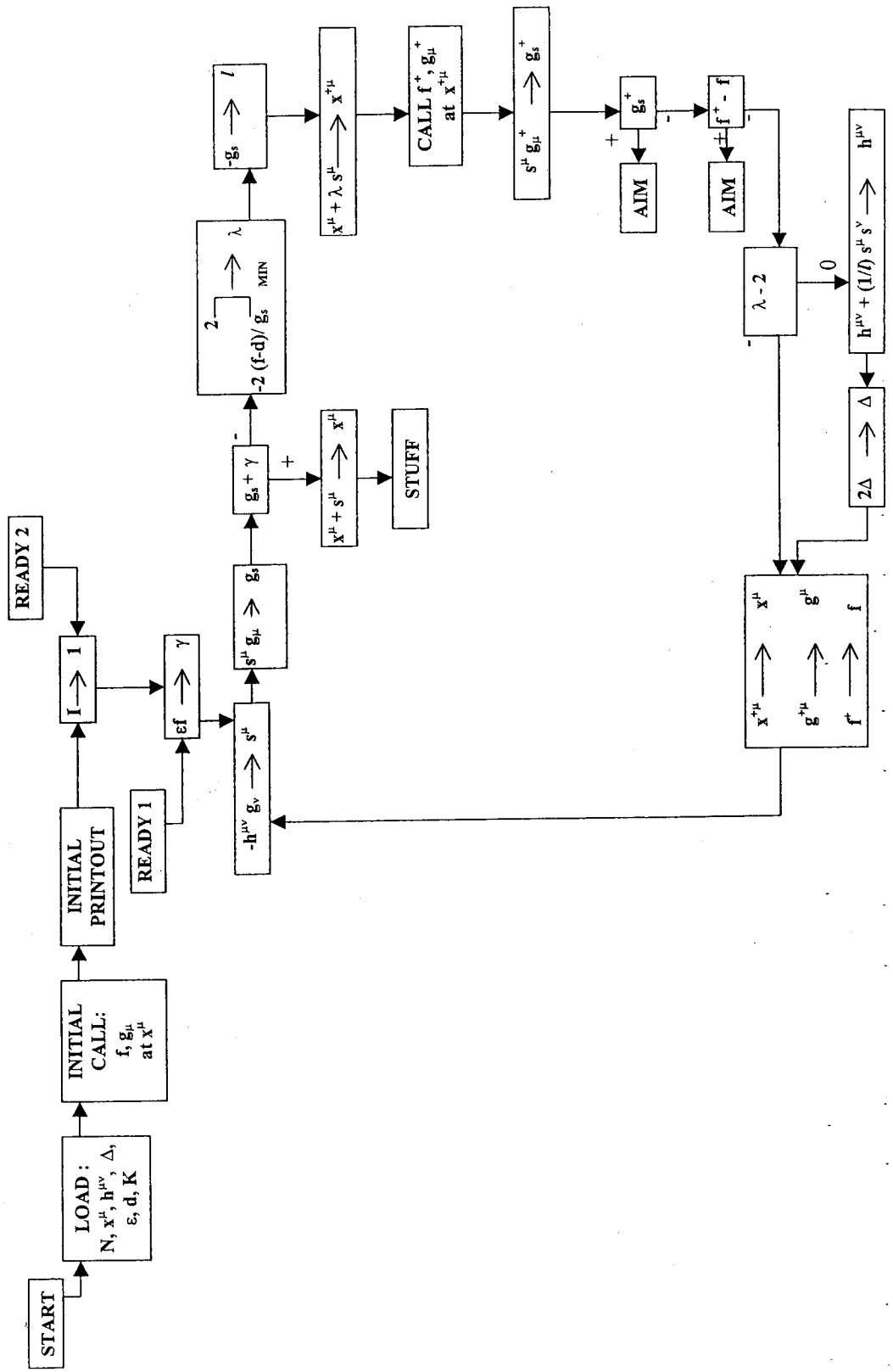

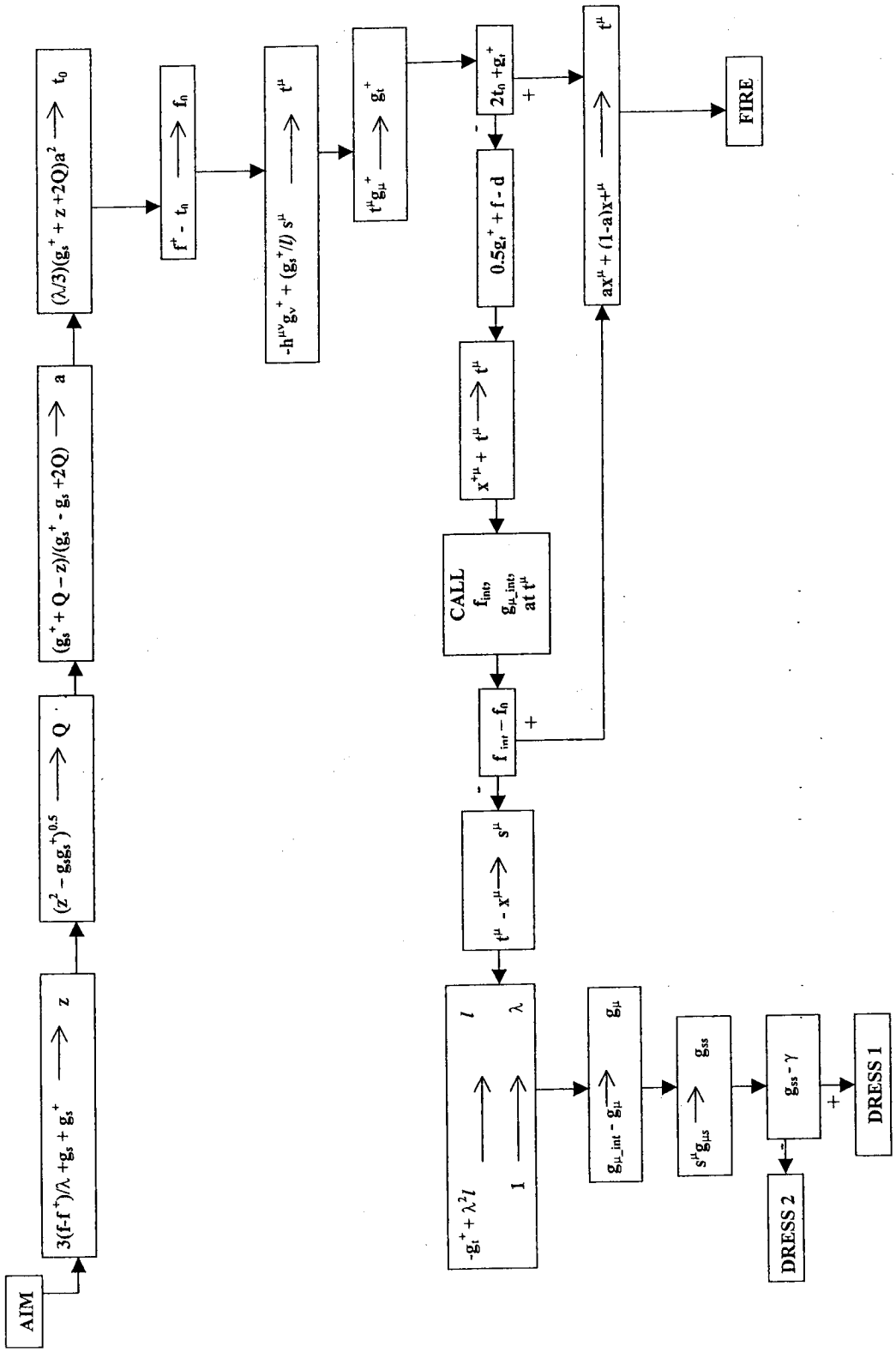

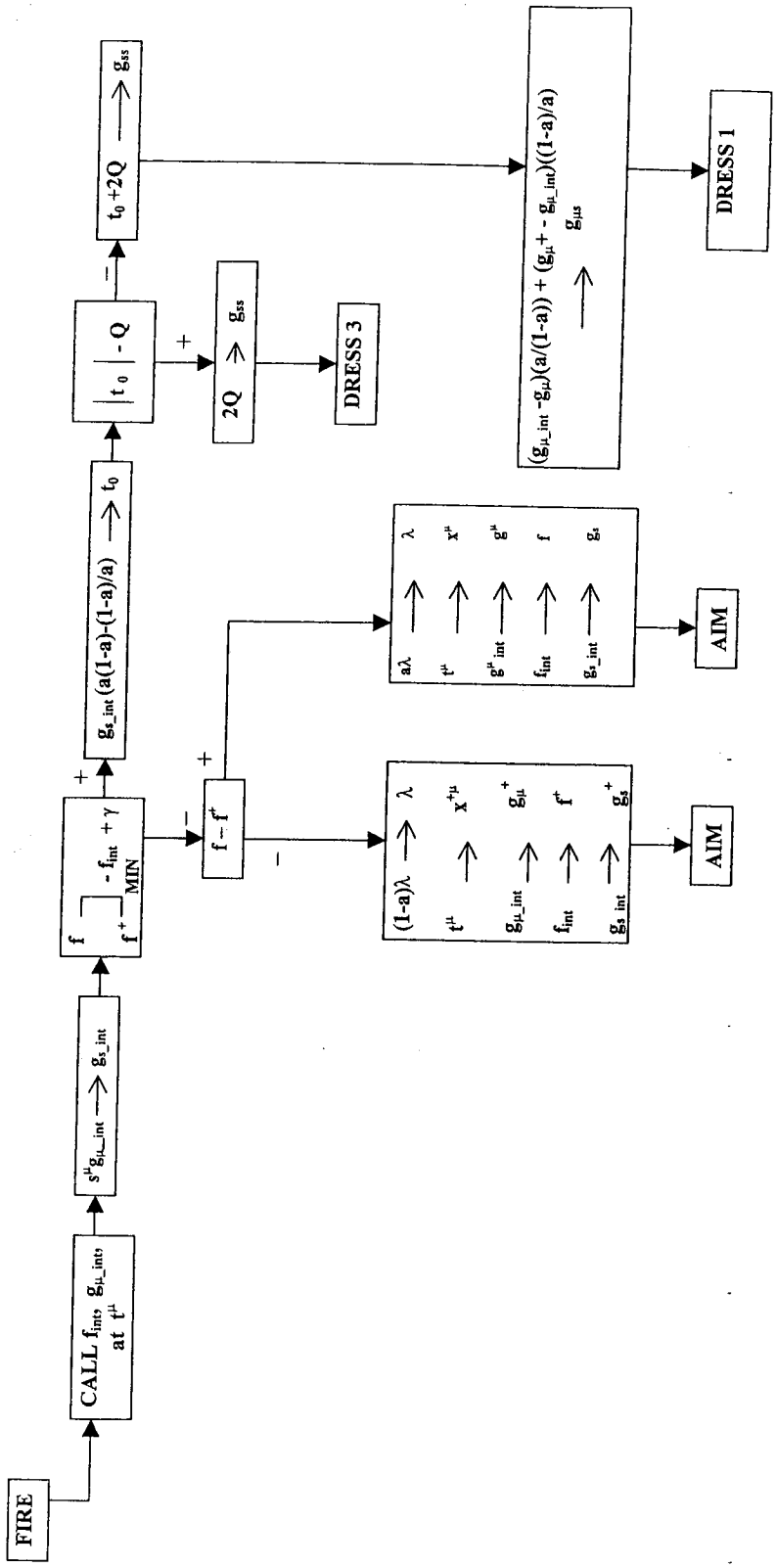

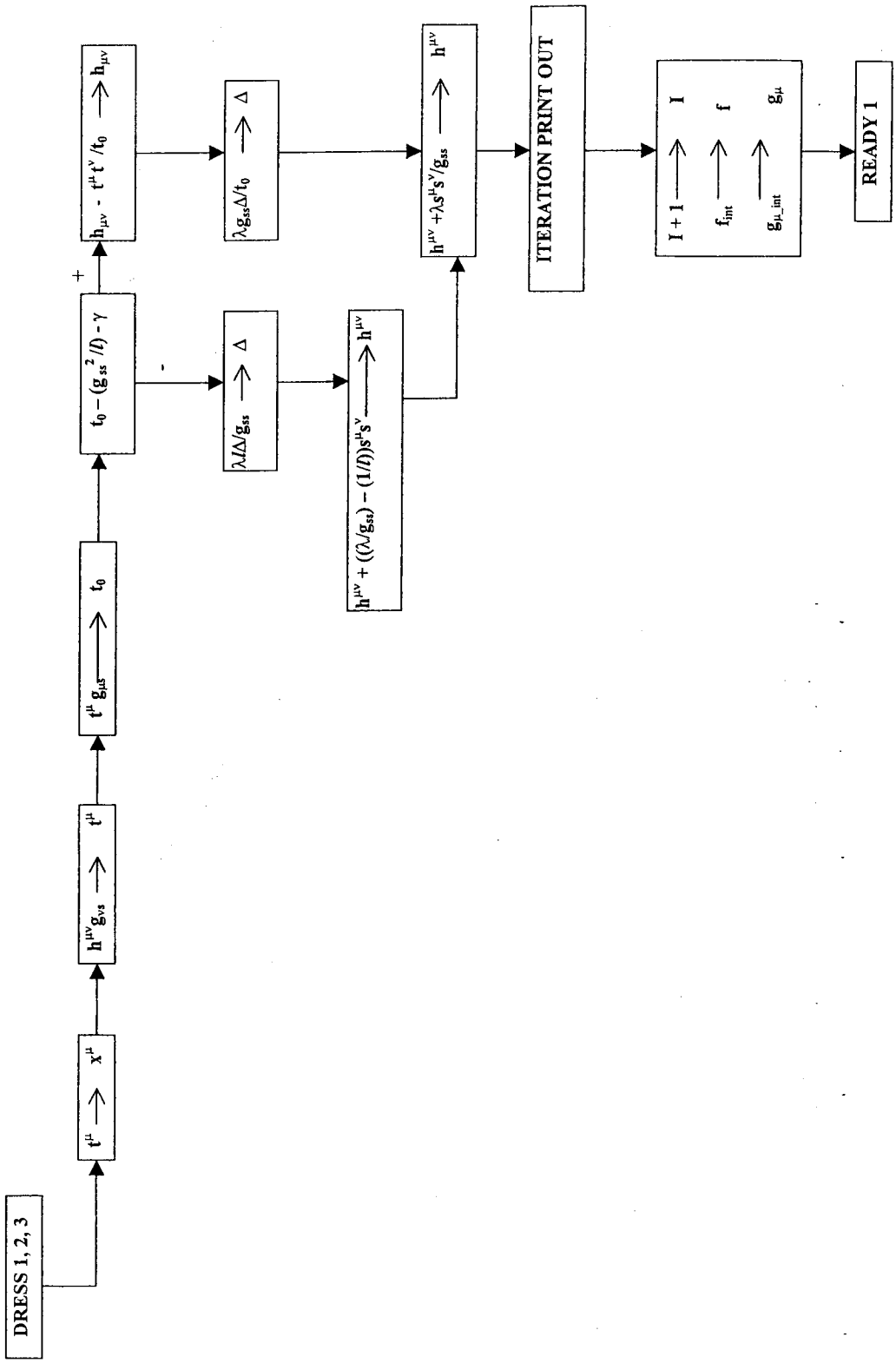

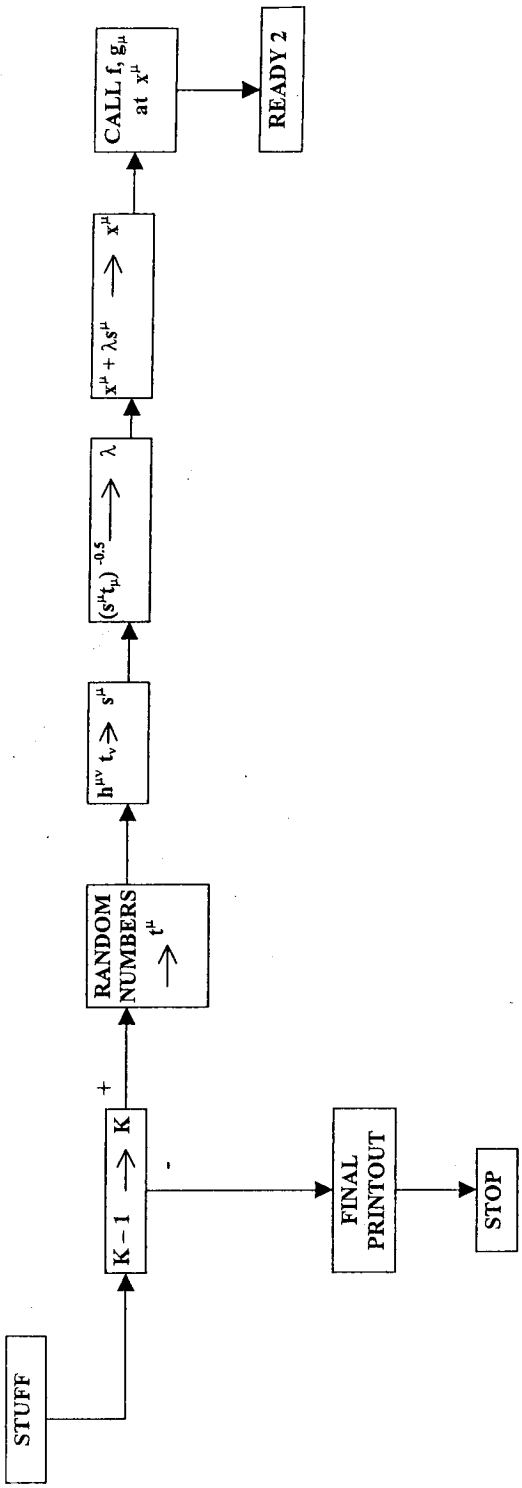

APPENDIX B

Figure B.1 *The velocity profiles of the right and left ankles, when no brace was worn*

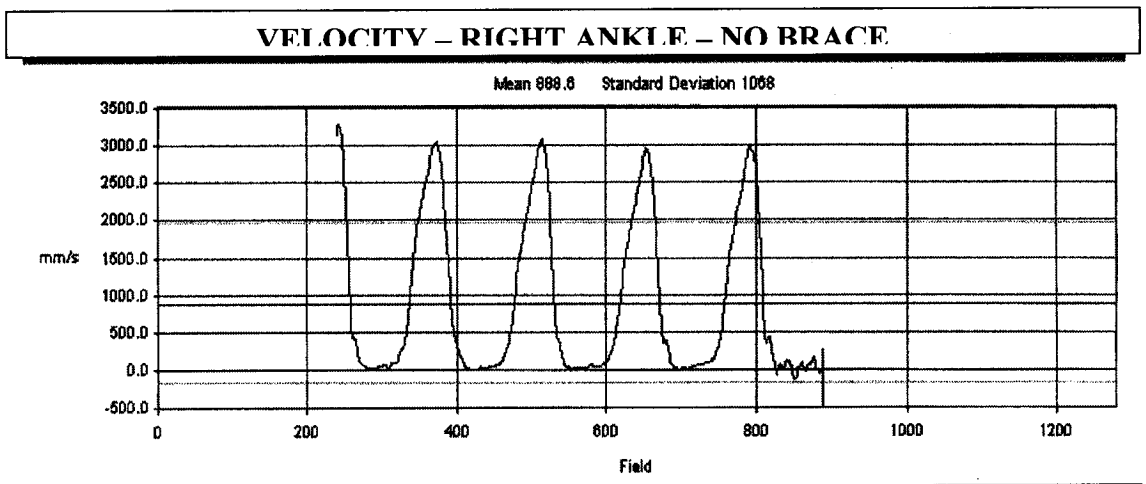

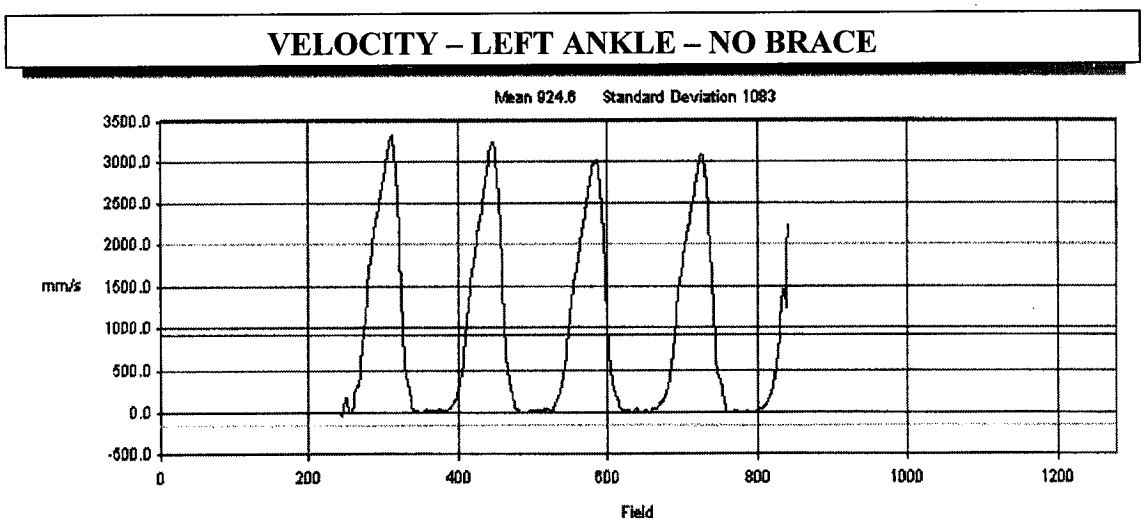

Figure B.2 *The velocity profiles of the right and left ankles, when a PAFO was worn*

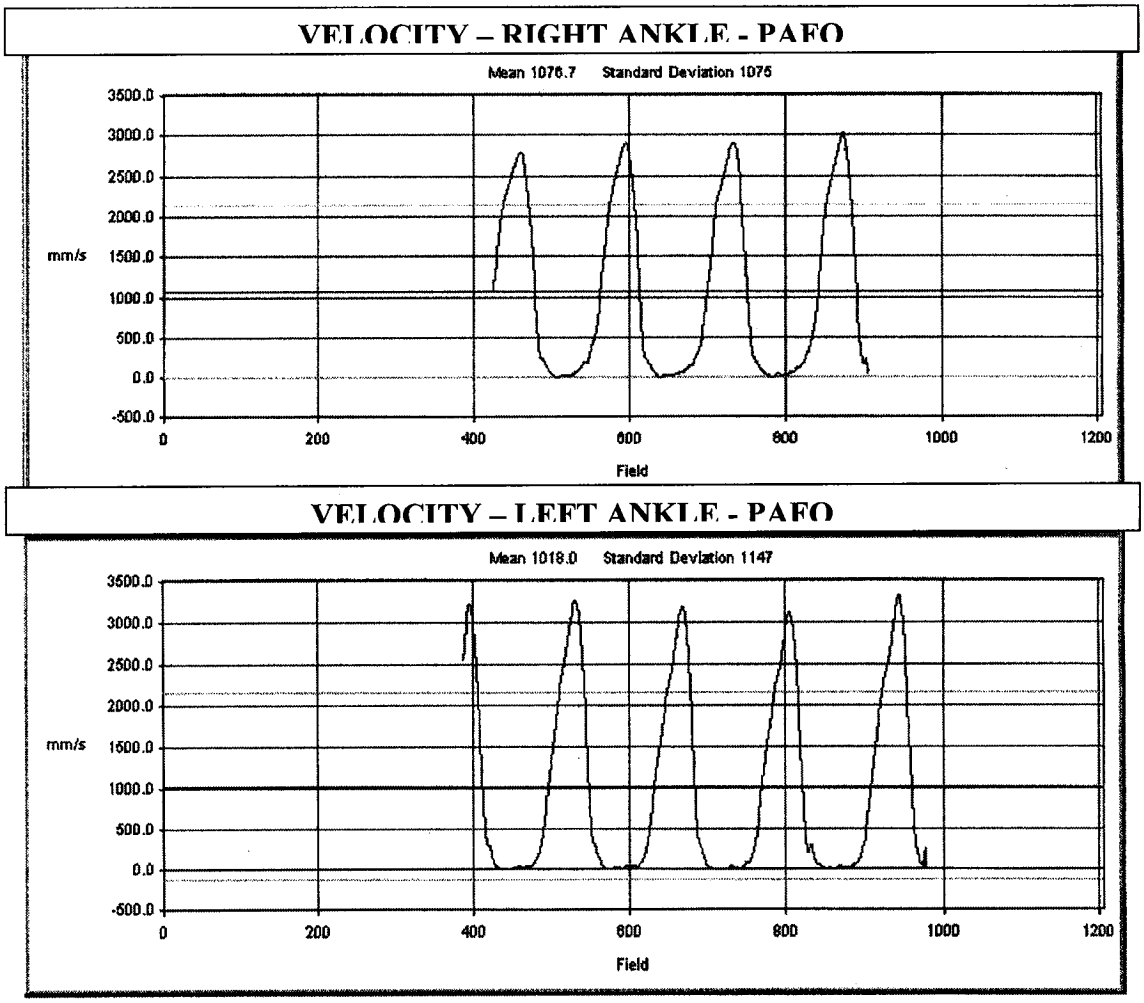

Figure B.3 *The velocity profiles of the right and left ankles, when a one-degree-of-freedom AFO was worn*

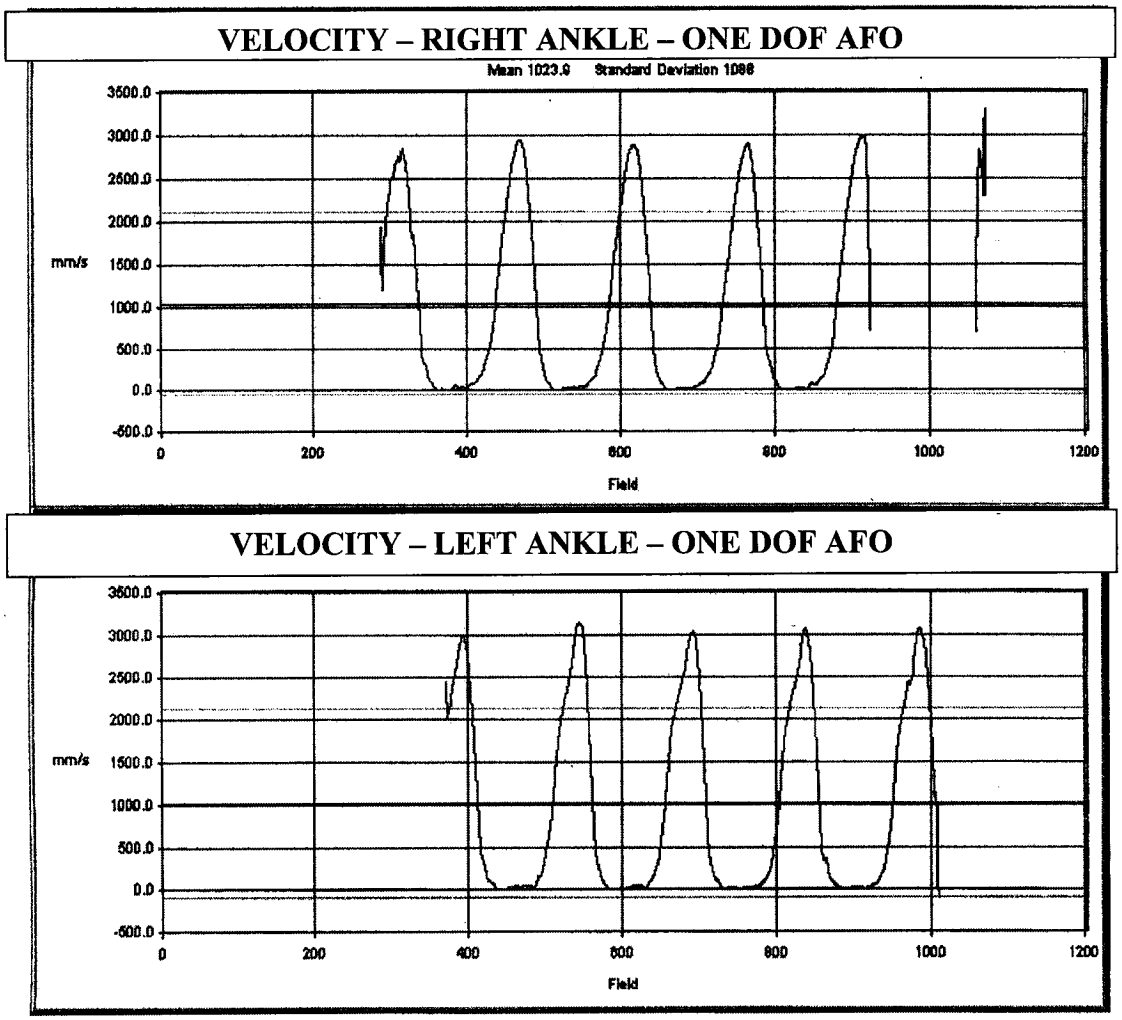

Figure B.4 *The velocity profiles of the right and left ankles, when a two-degree-of-freedom AFO was worn*

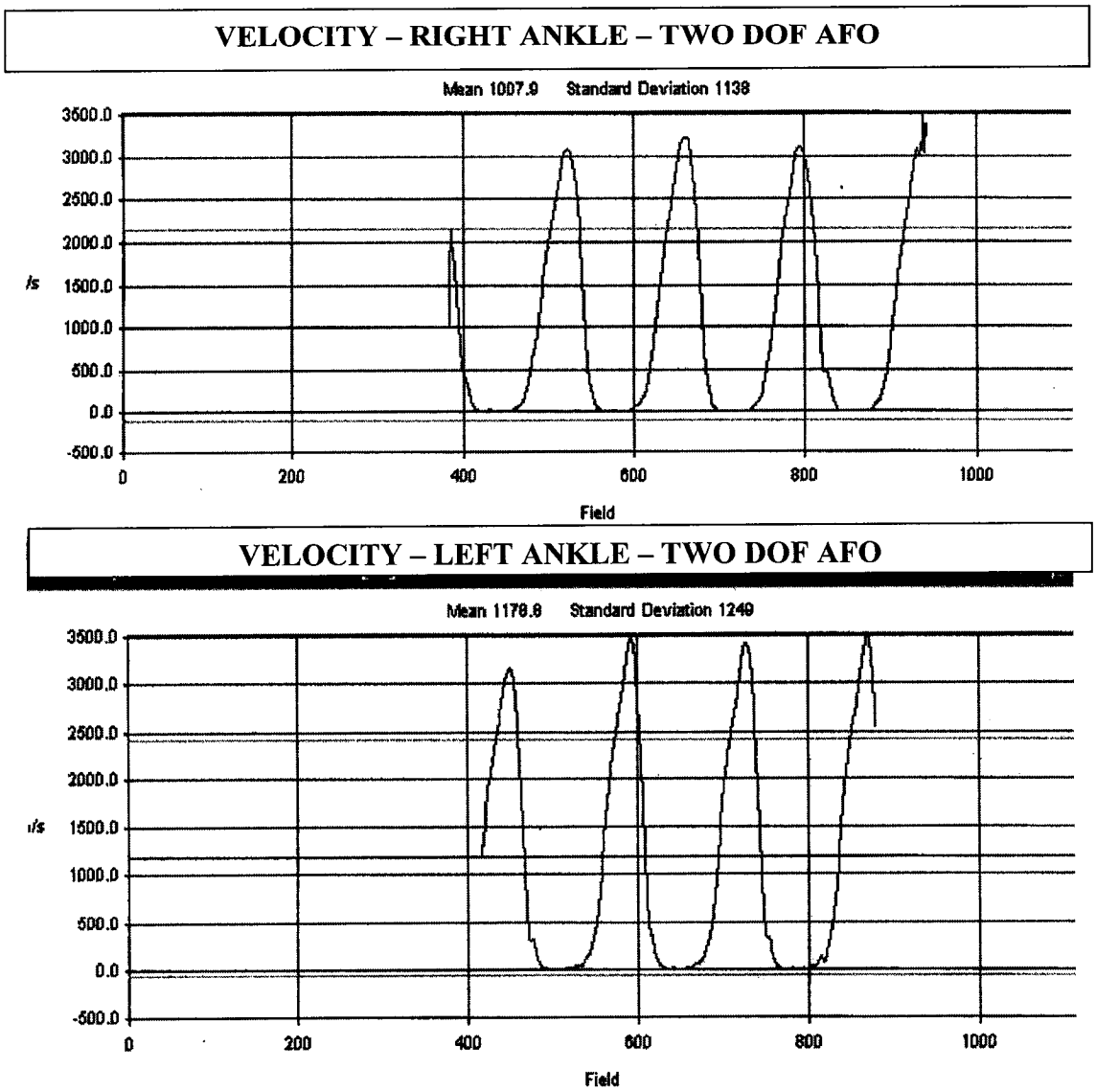

Figure B.5 *The acceleration profiles of the right and left ankles, when no brace was worn*

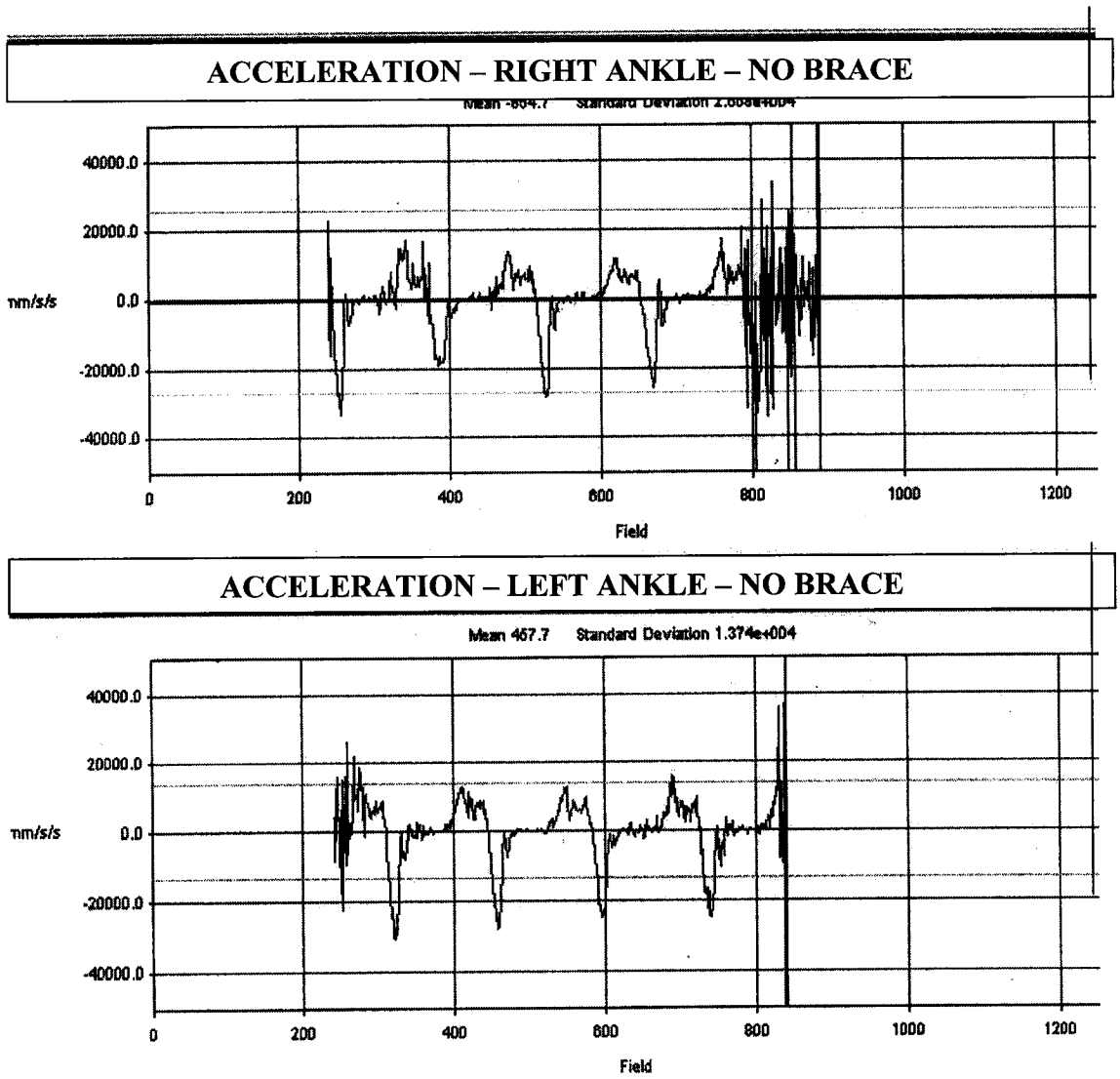

Figure B.6 *The acceleration profiles of the right and left ankles, when a PAFO was worn*

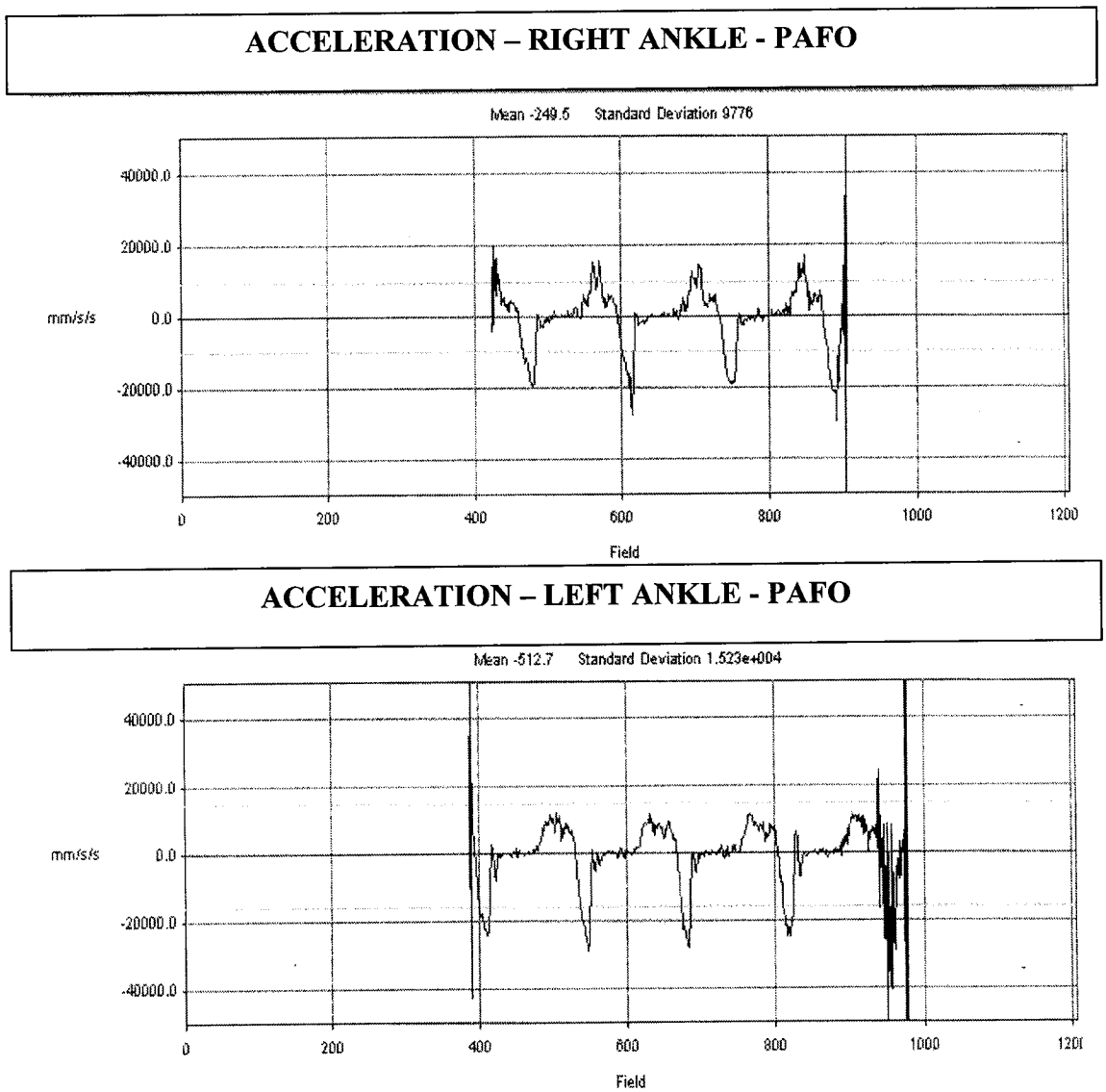

Figure B.7 *The acceleration profiles of the right and left ankles, when a one-degree-of-freedom AFO was worn*

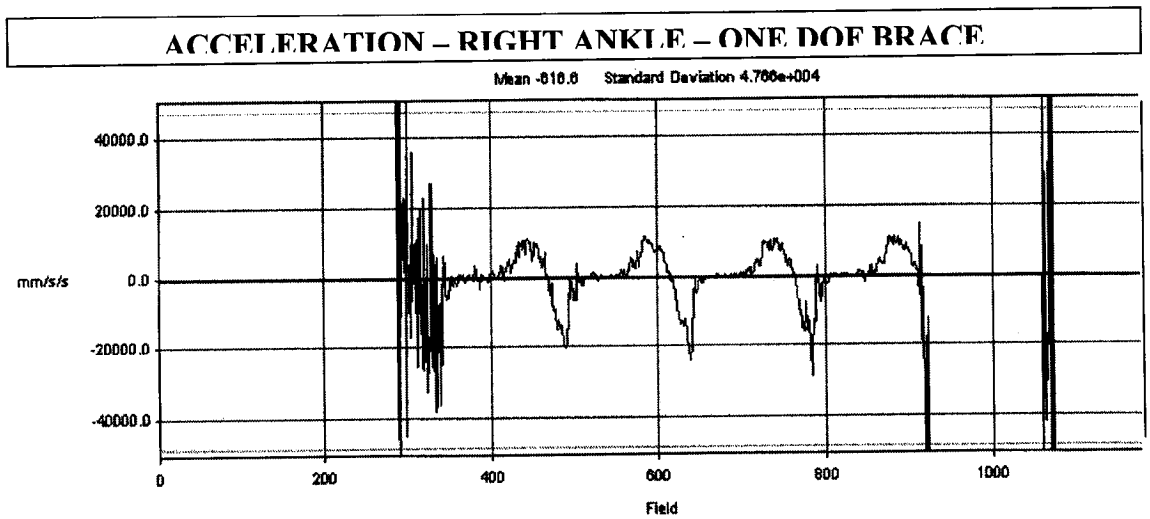

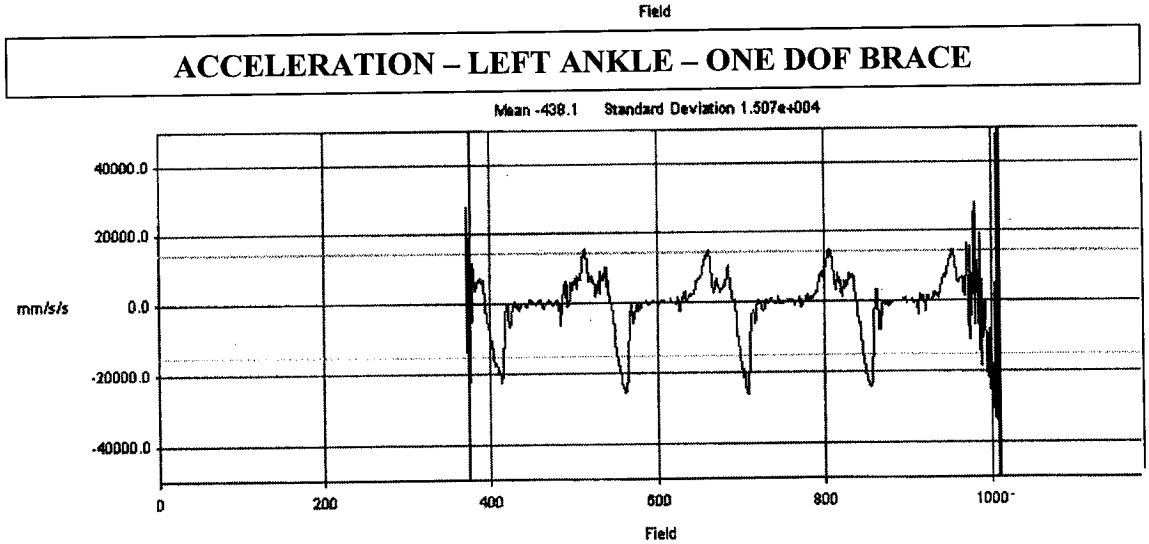

Figure B.8 *The acceleration profiles of the right and left ankles, when a two-degree-of-freedom AFO was worn*

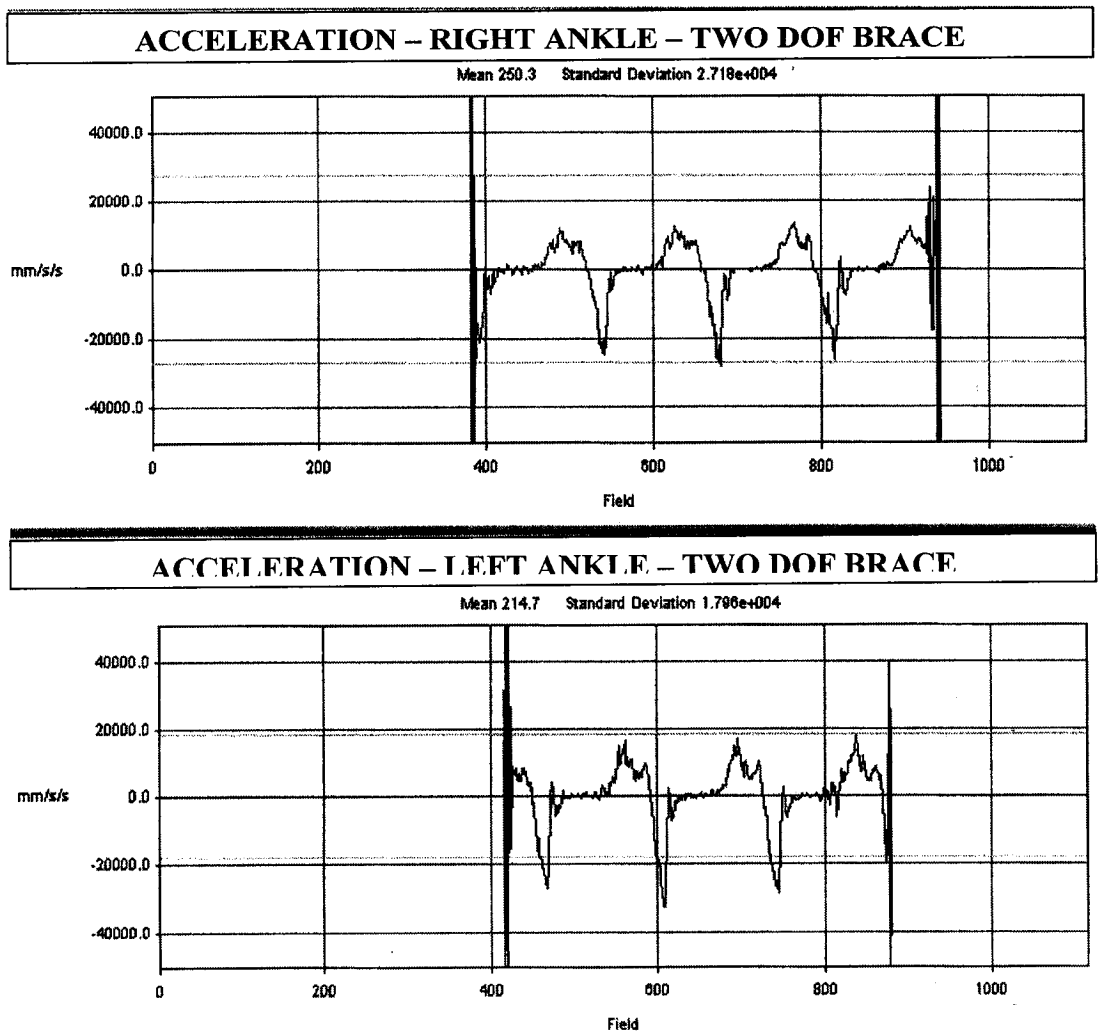

Figure B.9 *The velocity profiles of the right and left knees, when no brace was worn*

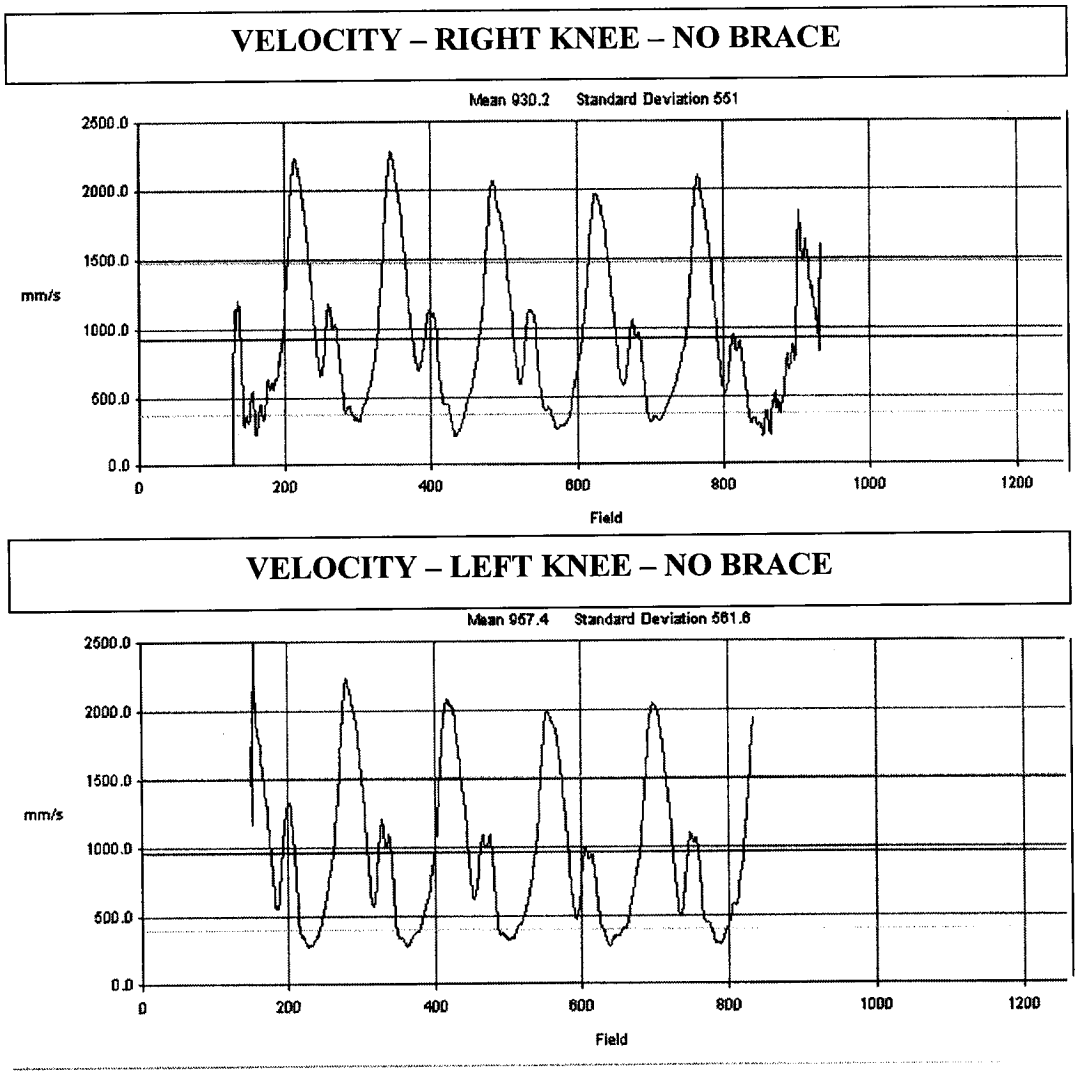

Figure B.10 *The velocity profiles of the right and left knees, when a PAFO was worn*

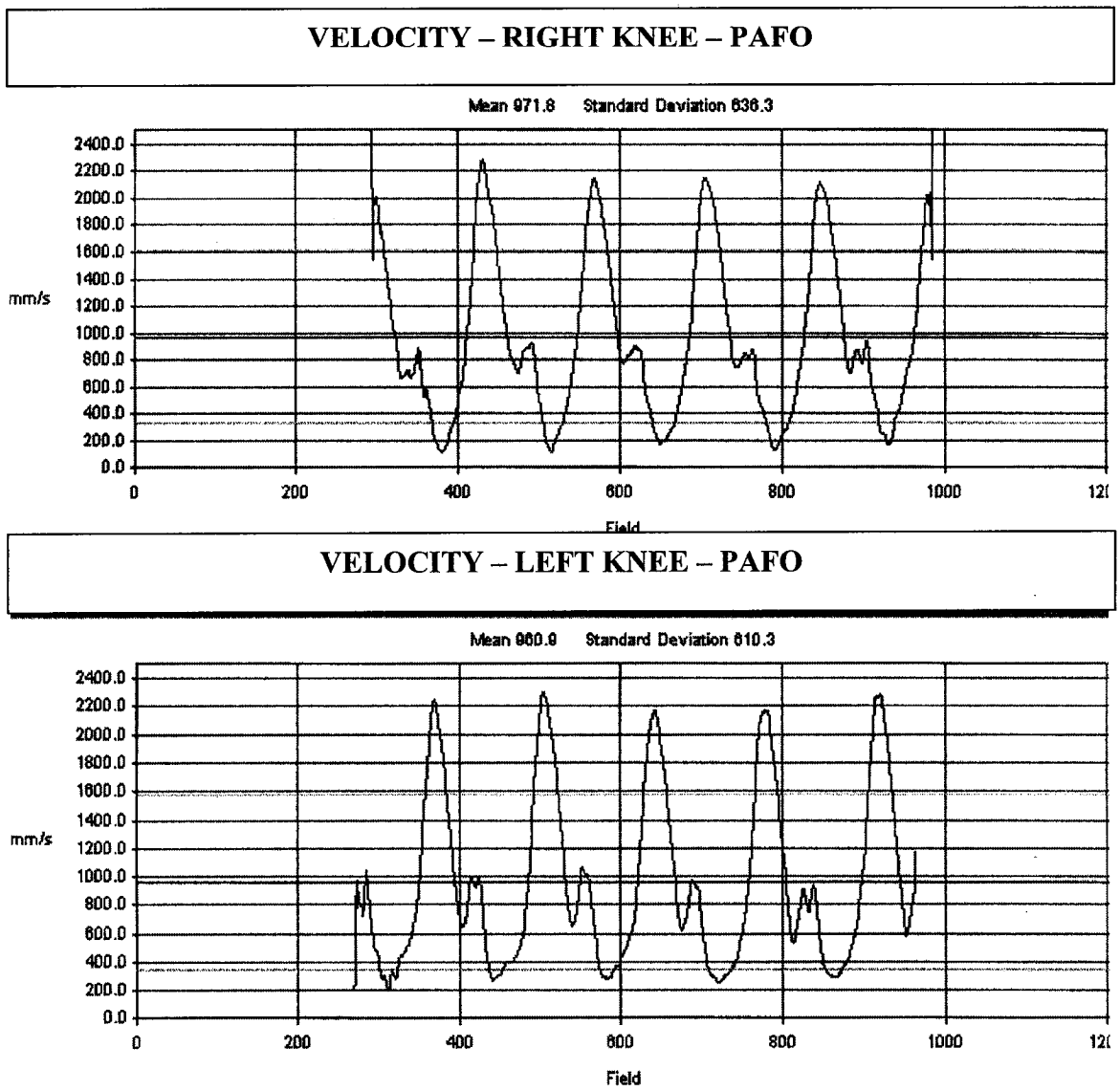

Figure B.11 *The velocity profiles of the right and left knees, when a one-degree-of-freedom AFO was worn*

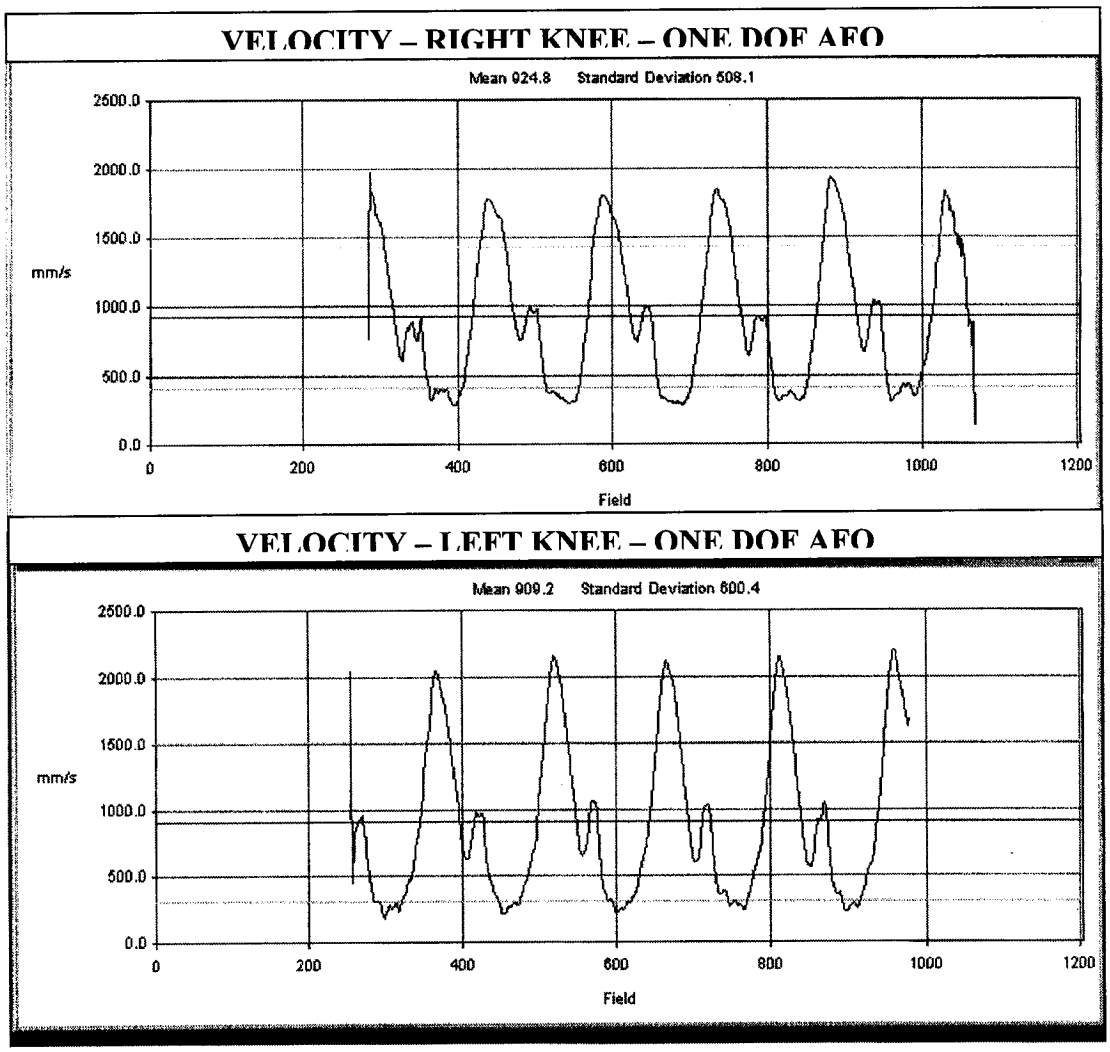

Figure B.12 *The velocity profiles of the right and left knees, when a two-degree-of-freedom AFO was worn*

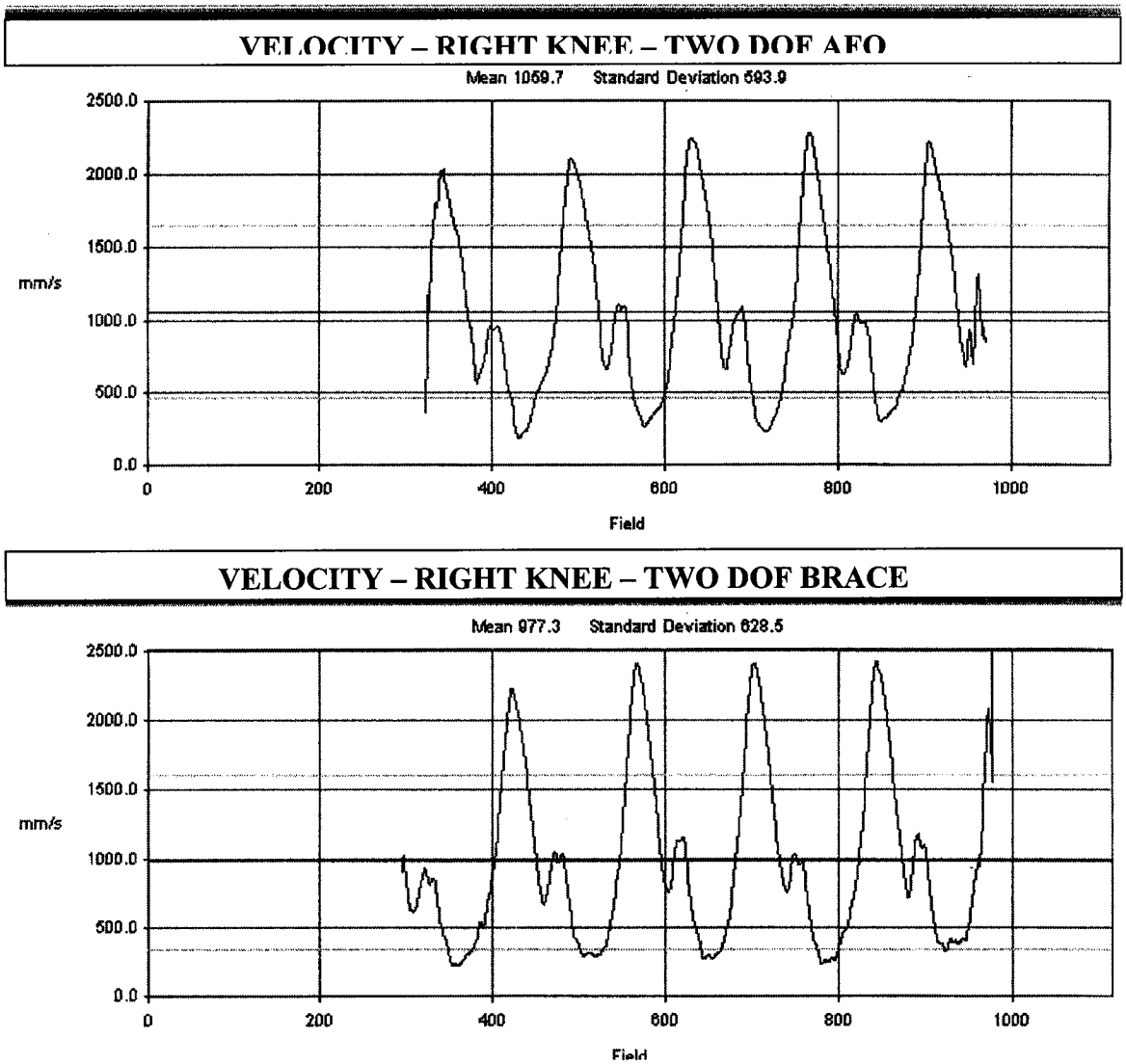

Figure B.13 *The acceleration profiles of the right and left knees, when no brace was worn*

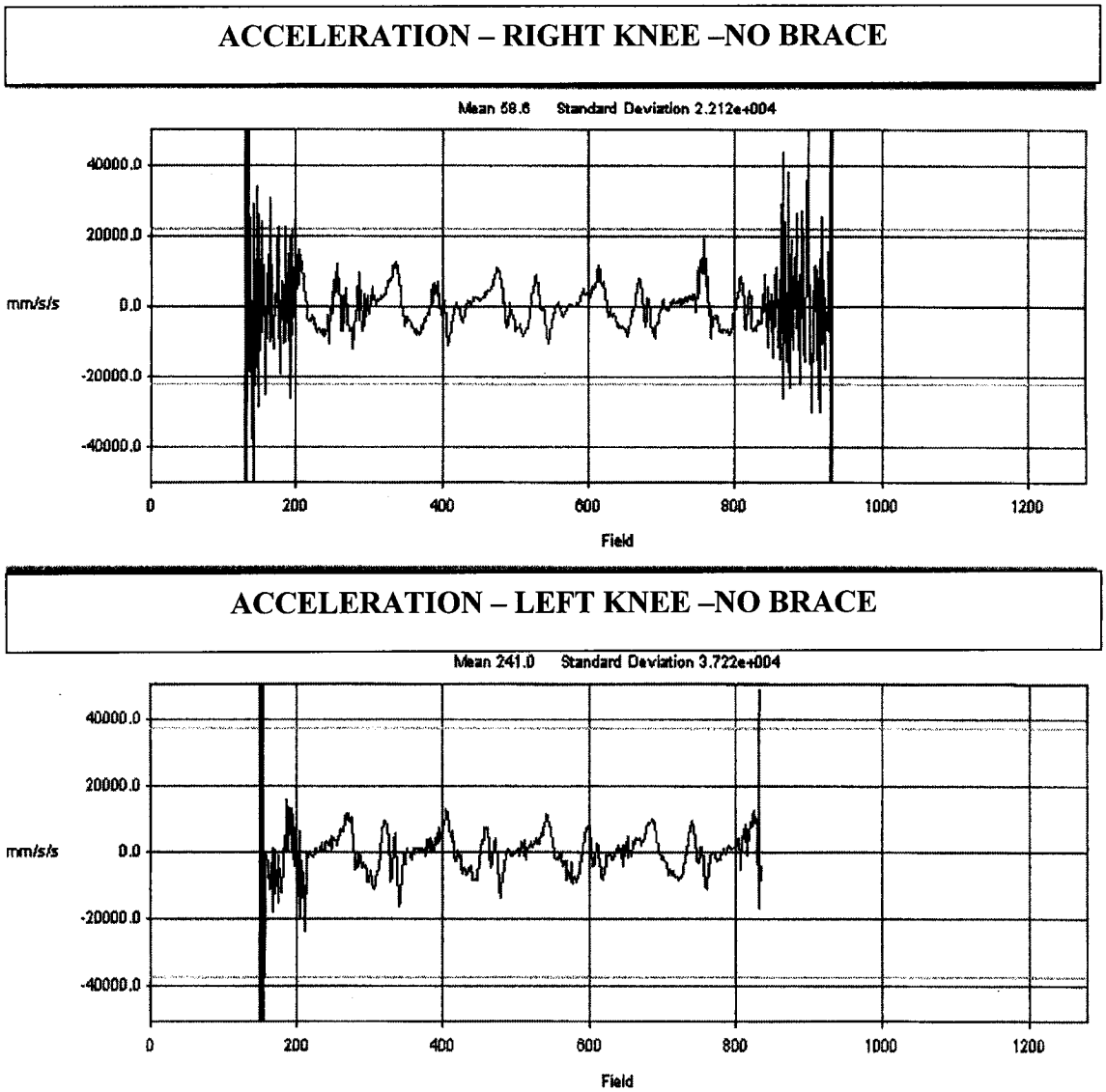

Figure B.14 *The acceleration profiles of the right and left knees, when a PAFO was worn*

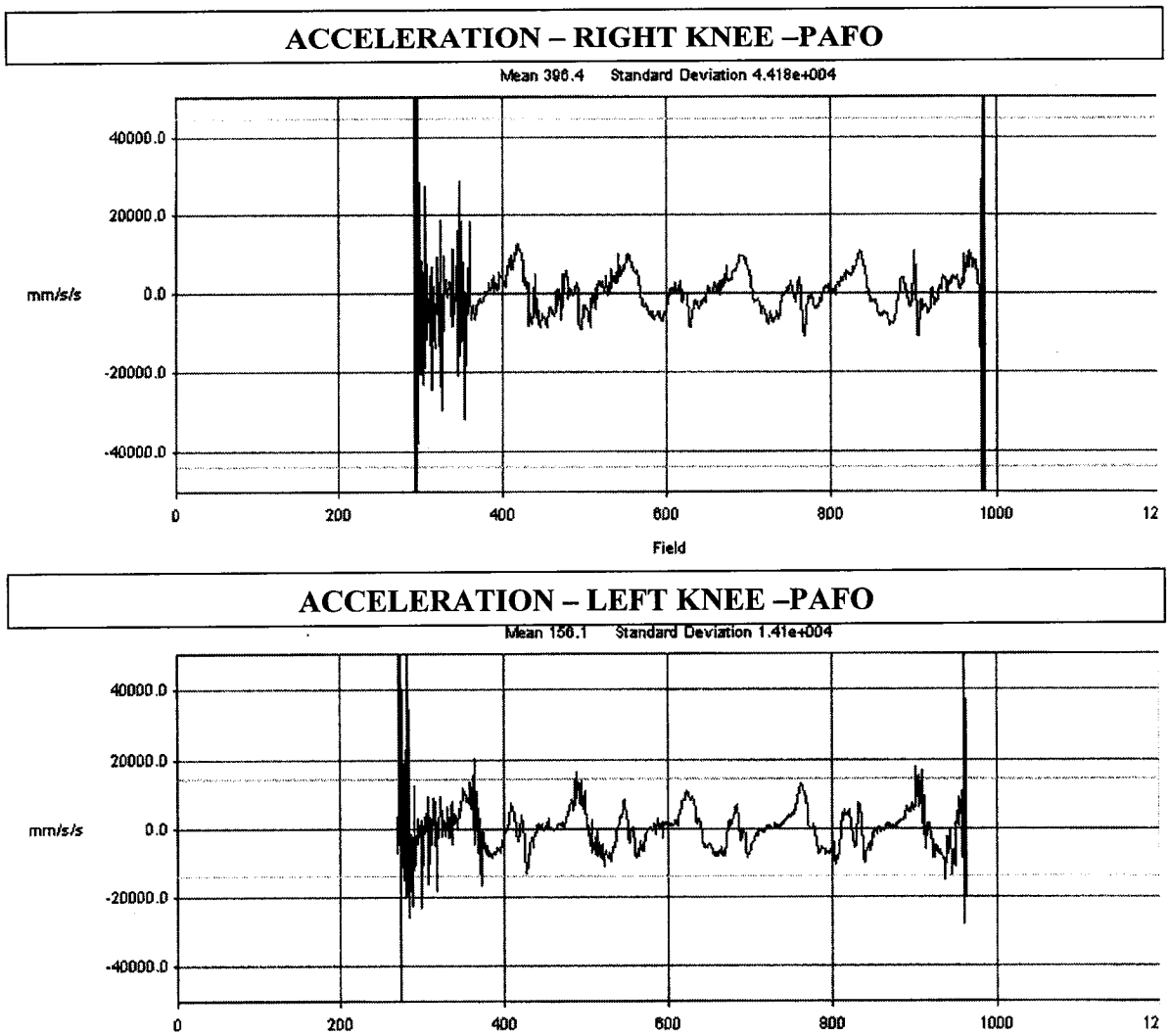

Figure B.15 *The acceleration profiles of the right and left knees, when a one-degree-of-freedom AFO was worn*

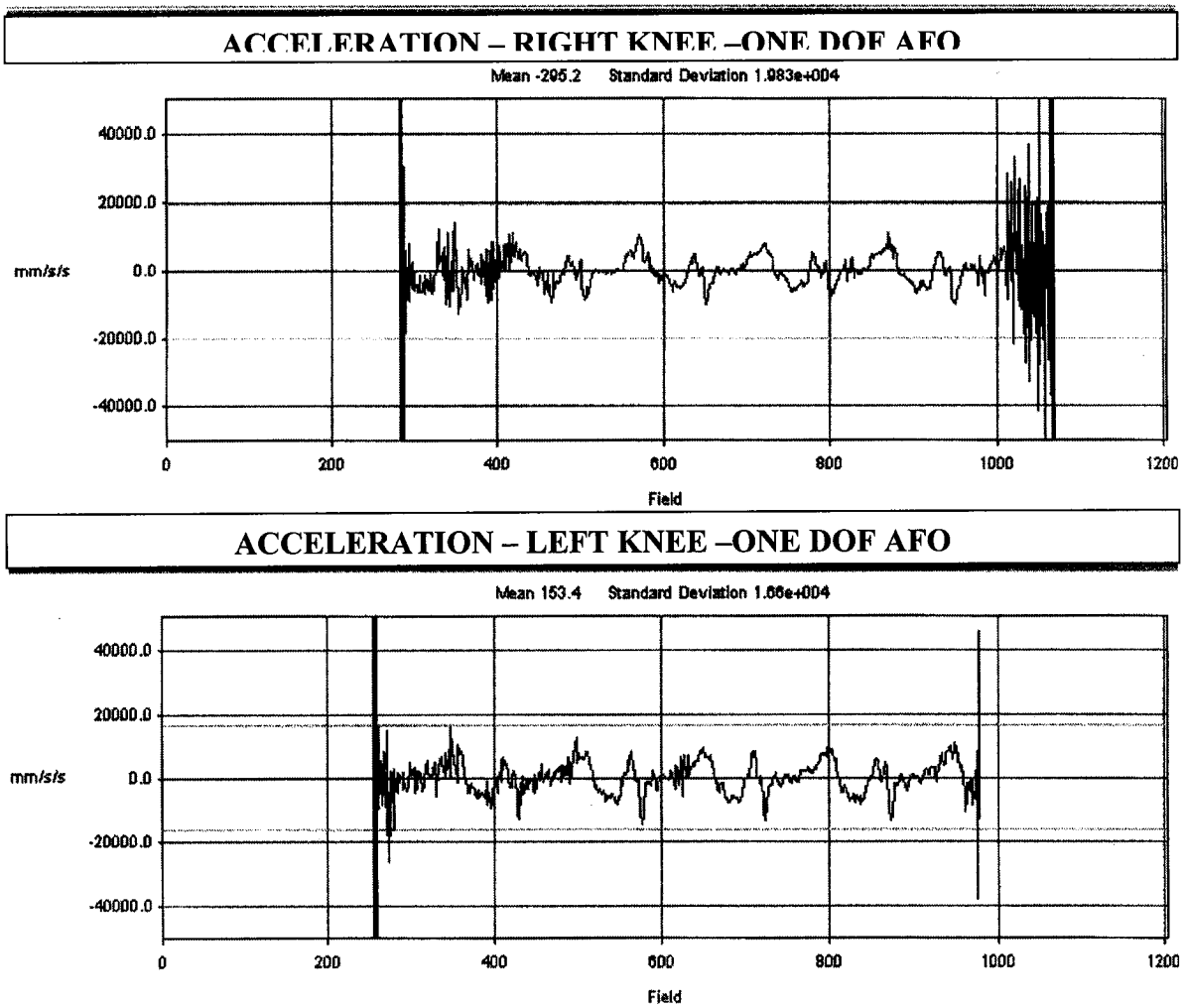

Figure B.16 *The acceleration profiles of the right and left knees, when a two-degree-of-freedom AFO was worn*

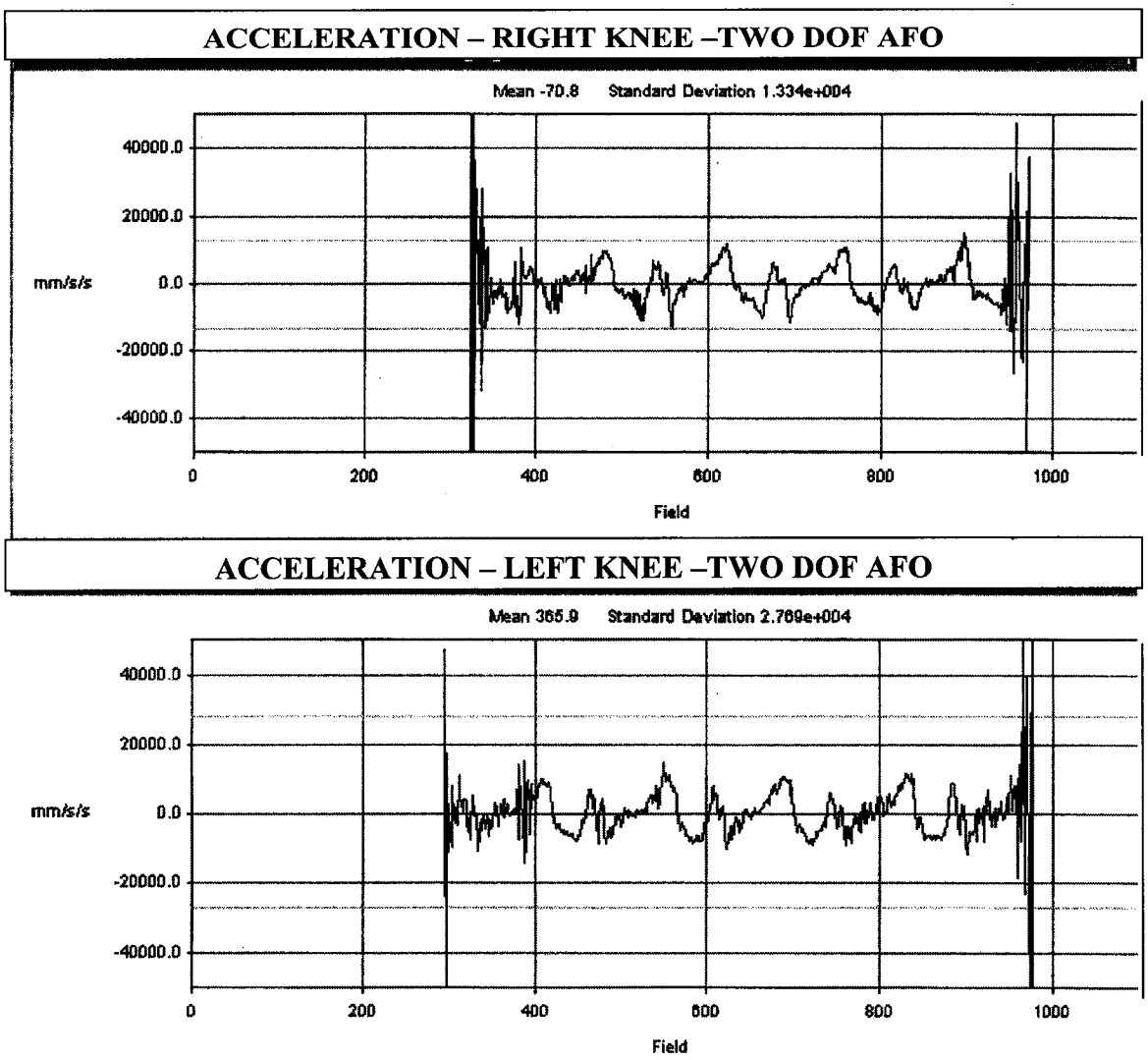

BIBLIOGRAPHY

1). Allinger, T., Ensberg, J., 1993. A method to determine the range of motion of the ankle joint complex, in vivo. Journal of Biomechanics. 26(1), 69-76.

2). American Association of Orthopaedic Surgeons, 1965. Joint Motion: Method of Measuring and Recording. 4'th reprint, 1969. E. & S. Livingstone Ltd., Edinburgh.

3). Baggett, B., Young, G., 1993. Ankle joint dorsiflexion. Establishment of a normal range. J Am Podiatr Med Assoc. 83(5), 251-4.

4). Bahr, R., Pena, F., Shine, J., Lew, W., Engebretsen, L., 1998. Ligament force and joint motion in the intact ankle: a cadaveric study. Knee Surg Sports Traumatol Arthrosc. 6(2), 115-21.

5). Balmaseda, M., Koozekanani, S., Fatehi, M., Gordon, C., Dreyfuss, P., Tanbonliong, E., 1988. Ground reaction forces, center of pressure, and duration of stance with and without an Ankle-Foot Orthosis. Arch Phys Med Rehabil. Vol. 69, 1009-10012.

6). Bates, B., Osternig, L., Mason, B., James, L., 1979. Foot orthotic devices to modify selected aspects of lower extremity mechanics. The American Journal of Sports Medicine. 7(6), 338-342.

7). Berger, N., Edelstein, J., Fishman, S., Hoffman, E., Krebs, D., Springer, W., 1986. Lower limb orthotics. Prosthetic-Orthotic Publications, NY, NY.

8). Van den Bogert, A., Smith, G., Nigg., 1994. In vivo determination of the anatomical axes of the ankle joint complex: an optimization approach. Journal of Biomechanics. 27 (12), 1277-88.

9). Boone, D., Azen, S., 1979. Normal range of motion of joints in male subjects. J Bone Joint Surg. 61-A, 756-759.

10). Calais-Germain, B., 1993. Anatomy of Movement. Eastland Press, Seattle, Washington, USA.

11). Caldarale, P., Scelfo, G., 1987. A mathematical model of the lower locomotor apparatus. Engineering Medicine. 16:147-61.

12). Campbell, J., Henderson, W., Patrick, D., 1969. UC-BL Dual Axis Ankle-Control System: Casting, alignment, fabrication, and fitting. Bulletin of Prosthetics Research. Spring.

13). Cass, J., Settles, H., 1994. Ankle instability: in vivo kinematics in response to axial load. Foot Ankle Int. 15(3), 143-40.

14). Chu, T., Narender, Reddy, N., 1995. Stress distribution in the Ankle-Foot Orthosis used to correct pathological gait. Journal of Rehabillitation Research and Development. 32(4), 349-360.

15). Chu, T., Feng, R., 1998. Determination of stress distribution in various Ankle-Foot Orthoses: Experimental stress analysis. Journal of Prosthetics and Orthotics 10(1), Winter.

16). Crowninshield, R., Brand, R., 1981. A physiologically based criterion of muscle force prediction in locomotion, Journal of Biomechanics. 14:793-801.

17). Le Damany, P., 1909. La torsion du tibia: normale, pathologique,experimentale. L Anat Physiol. 45:598.

18). Davidon. W., C., 1991. Variable metric method for minimization. Siam J Optimization, 1(1): pp 1-17.

19). Dezwart, D., Davidson, J., 1983. Rupture of the posterior tibial tendon associated with fractures of the ankle. Journal of Bone and Joint Surgery Am., 65:260.

20). Gamage, S., Lasenby, J., 2002. New least squares solutions for estimating the average center of rotation and the axis of rotation. Journal of Biomechanics, (35:87-93).

21). Gilchrist, L., Winter, D., 1996. A two-part, viscoelastic model for use in gait simulations. Journal of Biomechanics. 29(6), 795-798.

22). Hachisuka, K., Ogata, H., Tajima, F., Ohmine, S., 1998. Clinical evaluations of dorsiflexion assist controlled by spring ankle-foot orthosis for hemiplegic patients. J UOEH. 1(20), 1-9.

23). Halvorsen, K., Lesser, M., Lundberg, A., 1999. A new method for estimating the axis of rotation and the center of rotation. Journal of Biomechanics, (32:1221-1227).

24). Hinterman, B., Nigg, B., 1995. Influence of arthrodeses on kinematics of the axially loaded ankle complex during dorsiflexion/plantarflexion. Foot ankle Int. 16(10), 633-6.

25). Holman, J.P., 1966. Experimental Methods for Engineers, McGraw-Hill Inc, USA.

26). Hutter, C., Scott, W., 1949. Tibial torsion. J Bone Joint Surg. 31-A:511.

27). Inman, V., 1976. The Joints of the Ankle. The Williams & Wilkins Company, USA.

28). Jacob, S., Patil, M., 1999. Three-dimensional foot modeling and analysis of stresses in normal and early stage Hansen's Disease with muscle paralysis. Journal of Rehabilitation Research and Development. 36(3), 252-263.

29). Johnson, R., Kuby, P., 2000. Elementary Statistics, Eighth Edition. Duxbury, 511 Forest Lodge Road, Pacific Grove, CA, 93950, USA.

30). Kapandji, I., 1970. The philosophy of the joints: Lower Limb.Edinburgh, Scotland, Churchill Livingstone Inc. Vol.2,154-177.

31). Kidder, S., Abuzzahab, F., Harris, G., 1996. A system for the analysis of foot and ankle kinematics during gait. IEEE Transactions on Rehabilitation Engineering. 4(1), 25-32.

32). Komistek, R., Stiehl, J., Dennis, D., Paxson, Soutas-Little, R., 1998. Mathematical model of the lower extremity joint reaction forces using Kane's method of dynamics. Journal of biomechanics, 31, 185-189.

33). Lam, P., Reddy, N., 1987. One more step in redesigning the Ankle-Foot Orthotic. SOMA. April, No.39.

34). Lamoreaux, L., 1969. UC-BL Dual Axis Ankle-Control System: Engineering design. Bulletin of Prosthetics Research. Spring, 146 – 183.

35). Lamoreaux, L., 1971. Linematic measurements in the study of human walking. Bull Prosthet Res. 10(3), Spring.

36). Von Lanz, T., Wachsmuth, W., 1938. Praktische anatomie:Ein Lehr-und Hilfsbuch der anatomischen Grundlagen arztlichen Handelns. 1(4).

37). Leardini, A., O'Connor, J., Catini, F., Giannini, S., 1999. A geometric model of the human ankle joint. Journal of Biomechanics. Vol. 32, 585-591.

38). Leardini., A., O'Connor, J., Catani, F., Giannini, S., 1999. Kinematics of the human ankle complex in passive flexion; A single degree of freedom system. Journal of Biomechanics. Vol 32, 111-118.

39). Ledoux, W., Meaney, D., Hillstrom, H., 1999. A quasi-linear, structural model of the plantar soft tissue with frequency dependent damping properties. 23'rd Annual Meeting of the American Society of Biomechanics.

40). Ledoux, W., Camacho, D., Ching., R., Sangeorzan, B., 2000. The development and validation of a computational foot and ankle model. World Congress in Medical Physics and Biomedical Engineering.

41). Lehmann, J., 1970. Biomechanics of Ankle-Foot Orthoses: Prescription and design. Archives of Medical Rehabilitation, Vol 60, 200-207.

42). Lehmann, J., Esselman, P., Ko, M., Smith, J., deLateur, B., Dralle, A., 1983. Plastic ankle-foot orthoses: evaluation of function. Arch Phys Med Rehabil. 64(9), 402-7.

43). Lehmann, J., Condon, S., Price, R., deLAteur, B., 1987. Gait abnormalities in hemiplegia: Their correction by Ankle-Foot Orthoses. Arch Phys Med Rehabil. 68(11), 763-71.

44). Leone, D., 1987. A structural model for molded thermoplastic Ankle-Foot Orthoses. Journal of Biomechanical Engineering. Vol 109, 305-310.

45). Lindsjo, U., MD, PhD, Danckwardt – Lilliestrom. G., MD, PhD, Sahlstedt, B, MD, PhD, 1985. Measurement of the motion range in the loaded ankle. Clinical Orthopaedics and Related Research, (199:68-71).

46). Lundberg, A., Svensson, O., Nemeth, G., Selvik, G., 1989. The axis of rotation of the ankle joint. 71-B(1), 94-99.

47). Lundberg, A., Goldie, I., Kalin, B., Selvik, G., 1989. Kinematics of the ankle/foot complex: Plantarflexion and dorsiflexion. Foot & Ankle. 9(4), 194-200.

48). Lundberg, A., Svensson, O., Bylund, C., Selvik, G., Goldie, I.,1989. Kinematics of the Ankle/Foot Complex – Part 2: Pronation and supination. Foot & Ankle. 9(5), 248-253.

49). Lundberg, A., Svensson, O., Bylund, C., Selvik, G., 1989. Kinematics of the ankle/foot complex - Part 3: Influence of Leg rotation. Foot & Ankle. 9(6), 304-309.

50). Marsh, E., Sale, D., McComas, A., Quinlan, J., 1981. Influence of joint position on ankle dorsiflexion in humans. J Appl Physiol. 51(1), 160-7.

51). McCullough, C., Burge, P., 1980. Rotatory stability of the load-bearing ankle. An experimental study. J Bone Joint Surg Br. 62-B(4), 460-4.

52). Merriam Webster's Medical Dictionary, 1995. Merriam-Webster, Incorporated, USA.

53). Metz-Schimmerl, S., Bhatia., G., Vannier, M., 1994. Vizualization and quantitative analysis of talocrural joint kinematics. 18(6), 443-448.

54). Michelson, J., Mizel, M., Jay, P., Schmidt, G., 1998. Effect of medial displacement calcaneal osteotomy on ankle kinematics in a cadaver model. Foot Ankle Int. 19(3), 132-6.

55). Michelson, J., Ahn, U., Helgemo, S., 1996. Motion of the ankle in a simulated supination-external rotation fracture model. J Bone joint Surg Am. 78(7), 1024-31.

56). Milgrom, C., Giladi, M., Simkin, A., Stein, M., Kashtan, H., Margulies, J., Steinberg R., Aharonson, Z., 1985. The normal range of subtalar inversion and eversion in young males as measured by three different techniques. Foot and Ankle, 6(3):143 –5.

57). Morris, W., 1978. The American Heritage Dictionary of the English Language. Houghton Mifflin Company, Boston, Massechusettes, 02107.

58). Myerson, M., 2000. Foot and Ankle Disorders. W. B. Saunders Company, Philadelphia, PA, USA.

59). Nakamura, S., Crowninshield, R., Cooper, R., 1981. An analysis of soft tissue loading in the foot: A preliminary report. Bulletin of Prosthetics Research. 10-35(18);27-34.

60). Nigg, B., Fisher, V., Allinger T., 1992. Range of motion of the foot as a function of age. Foot and Ankle, 13:336.

61). Norkin, C., White, D., 1985. Measurement of joint motion:A guide to goniometry. F A Davis, Co., Philadelphia, PA, USA.

62). Nowak, M., Abu-Hasaballah, K., Cooper, P., 2000. Design enhancement of a Solid-Ankle-Foot Orthosis: Real-time contact pressures evaluation. Journal of Rehabilitation Research and Development. 37(3), 273-281.

63). Oatis, C., 1988. Biomechanics of the foot and ankle under static conditions. Physical Therapy. 68(12), 1815-1821.

64). Ounpuu, S., Bell, K., Davis, R., Deluca, P., 1996. An evaluation of the posterior leaf spring orthosis using joint kinematics and kinetics. J Pediatr Orthop. 16(3), 378-84.

65). Parenteau, C., Viano., D., Petit, P., 1998. Biomechanical properties of human cadaveric ankle-subtalar joints in quasi-static loading. Journal of Biomechanical Engineering. Vol.120, 105-111.

66). Patil, K., Babu, M., Oomen, P., Maliviya, G., 1996. On line system of measurement and analysis of standing and walking foot pressures in normals and patients with neuropathic feet. Innovations in Technol Biol Med. 17:401-408.

67). PATRAN Plus user manual, 1990. PDA Engineering Software Products Division. Costa Mesa, CA, USA.

68). Perry, J., Hilsop, H., 1967. Principles of Lower-Extremity Bracing. American Physical Therapy Association, NY, NY, USA.

69). Perry, J., 1992. Gait analysis, Normal and Pathological Function. McGraw-Hill, Incorporated, NY, NY.

70). Rao, N., Aruin, A., 1999. The effect of Ankle-Foot Orthoses on balance impairment: single-case study. Journal of Prosthetics and Orthotics. 11(1), 15-19.

71). Radtka, S., Skinner, S., Dixon, D., Johanson, M., 1997. A comparison of gait with solid, dynamic, and no ankle-foot orthoses in children with spastic cerebral palsy. Physical Therapy. 77(4), 395-409.

72). Reeck, J., Felten, N., McCormack, A., Kiser, P., Tencer, A, Sangeorzan, B., 1998. Support of the talus: A biomechanical investigation of the contributions of the talonavicular and talocalcaneal joints, and the superomedial calcaneonavicular ligament. Foot & Ankle International. 19(10), 674-682.

73). Reuleuax, F., 1875. Theoretische Kinematik, Braunschweig.

74). Roaas, A., Andersson, G., 1982. Normal range of motion of the hip, knee, and ankle joints in male subjects, 30-40 years of age. Acta Orthop Scand. 53(2), 205-8.

75). Schreppers, G., Sauren, A., Huson, A., 1990. A numerical model of the load transmission in the tibio-femoral contact area. Proceedings of the Institute of Mechanical Engineering. 204:53-59.

76). Scott, S., Winter, D., 1991. Talocrural and talocalcaneal joint kinematics and kinetics during the stance phase of walking. Journal of Biomechanics. 24(8), 743-752.

77). Seireg, A., Arvikar, R., 1975. The predication of muscular load sharing and joint forces in the lower extremities during walking. Journal of Biomechanics. 8:89-102.

78). Sell, K., Verity, T., Worrell, T., Pease, B., Wigglesworth., J., 1994. Two measurement techniques for assessing subtalar joint position: A Reliability Study. JOSPT. 19(3), 162-167.

79). Shiang, T., Cavanagh, P., 1992. Finite element analysis of the foot-shoe interface in diabetic patients. Proceedings of the Symposium on Biomedical Engineering in the 21'st Century. pp 1-7.

80). Shigley, 1980. Mechanical Engineering Design, McGraw Hill, USA.

81). Siegler, S., Chen, J., Schneck, C., 1988. The three-dimensional kinematics and flexibility characteristics of the human ankle and subtalar joints - Part 1:Kinematics. Transactions of the ASME. 110 (11), 364-373.

82). Silaghi, M., Plaenkers, R., Boulic, R., Fua, P., Thalmann, D., 1998. Local and global skeleton fitting techniques for optical motion capture. In: Magnenat-Thalmann, N., Thalmann, D. (Eds.), Modelling and Motion Capture Techniques for Virtual Environments, Lecture Notes in Artificial Intelligence, No. 1537. Springer, Berlin, pp. 26-40

83). Soames, R., 1985. Foot pressure patterns during gait. Journal of Biomedical Engineering. Vol.7, 120-126.

84). Sobel, E., Levitz, S., Casselli, M., 1999. Orthoses in the treatment of rearfoot problems. Journal of the American Podiatric Medical Association. 89(5), 220-233.

85). Spoor, C., 1992. Mechanical models of selected parts of the human musculoskeletal system (thesis). Eindhoven, The Netherlands: Einhoven University of Technology.

86). Staff of Research and Education Association, Dr. M. Fogiel, Director, 1994. The Advanced Calculus Problem Solver. Research and Education Association, 61 Ethel Road West, Piscataway, New Jersey, 08854.

87). Stahelin, T., Nigg, B., Stefanyshyn, D., Bogert, A., Kim, S., 1997. A method to determine bone movement in the ankle joint complex. Journal of Biomechanics. 30(5), 513-516.

88). Stefanyshyn, D., Engsberg, J., 1994. Right to left differences in the ankle joint complex range of motion. Med Sci Sports Excer 26:551.

89). Sumiya, T., Yoshita, S., Kashara, T., Ogata, H., 1997. Instantaneous centers of rotation in dorsi/plantarflexion movements of posterior-type Plastic Ankle-Foot Orthoses. Journal of Rehabilitation Research and Development 34(3), 279-285.

90). Tannous, R., Bandak, F., Toridis, T., Eppinger, R., 1996. A Three-Dimensional Finite Element Model of the Human Ankle:Development and Preliminary Application to Axial Impulsive Loading. Society of Automotive Engineers.

91). Thilman, A., Fellows, S., Ross, H., 1991. Biomechanical changes at the ankle joint after stroke. J Neurol Neurosurg Psychiatry. 54(2), 134-9.

92). User Manual (Report ARD 87-1), 1987. ADINA R&D, Inc. Watertown, MA, USA.

93). Vargerg, D., Purcell, E., 1992. Calculus with Analytic Geometry, Prentice-Hall, Inc, Englewood Cliffs, New Jersey, 07632.

94). Wang, C., Hang, Y., Liu, T., 1992. A dynamic study of the Ankle-Foot Complex. Journal of Formosan Medical Association. 91(4), 432-437.

95). Williams, P., 1998. Gray's Anatomy (38'th Edition). Churchill Livingstone, Kent, UK.

96). Winter, D., Quanbury, A., Hobson, D., Sidwall, H., Reimer, G., Trenholm, B., Steinke, T., Shlosser, H., 1974. Kinematics of normal locomotion – A statistical study based on T.V. Data. Journal of Biomechanics. 7:479.

97). Wiley, J., Nigg, B., 1996. The effect of an ankle orthosis on ankle range of motion and performance. J Orthop Sports Phys Ther. 23(6), 362-9.

98). Woodburn, J., 1991. Video joint angle position analysis of the effects of subtalar joint position on maximum ankle joint dorsiflexion. J Br Podiatr Med, 46:1.

99). Yamamoto, H., Yagishita, K., Ogiuchi, T., Sakai, H., Shinomiya, K., Muneta, T., 1998. Subtalar instability following lateral ligament injuries of the ankle. Injury. 29(4), 265-8.

100). Yamamoto, S., Ebina, M., Kubo, S., Hayashi, T., Atika, Y., Hayakawa, Y., 1999. Development of an Ankle-Foot Orthosis with dorsiflexion Assist, Part2: Structure and evaluation. Journal of Prosthetics and Orthotics 11(2), 24-28.